RELATIVE TIMING AND SIGNIFICANCE OF FOLDING IN THE WESTERN SKEENA FOLD BELT, NORTHWESTERN BOWSER BASIN, BRITISH COLUMBIA: INTERPRETATION OF STRUCTURAL AND SEISMIC REFLECTION DATA.

by

Katherine E. Bone

B.Sc. (Hons) University of London, 1998

A THESIS IN PARTIAL FULFILLMENT OF THE REQUIREMENTS FOR

THE DEGREE OF MASTER OF SCIENCE

in

THE FACULTY OF GRADUATE STUDIES

(Department of Earth and Ocean Sciences)

We accept this thesis as conforming to the required standard

THE UNIVERSITY OF BRITISH COLUMBIA

April 2002

In presenting this thesis in partial fulfilment of the requirements for an advanced degree at the University of British Columbia, I agree that the Library shall make it freely available for reference and study. I further agree that permission for extensive copying of this thesis for scholarly purposes may be granted by the head of my department or by his or her representatives. It is understood that copying or publication of this thesis for financial gain shall not be allowed without my written permission.

Department of Earth & Ocean Sciences

The University of British Columbia
Vancouver, Canada

Date April 22/2002

DE-6 (2/88)

ABSTRACT

The northwestern Bowser Basin overlies Mesozoic units of Stikine Terrane and encompasses deformation of the western Skeena Fold Belt. The region includes a portion of Lithoprobe SNORCLE Line 2A seismic reflection transect. The research has allowed detailed observation of the surface geology to be combined with high quality subsurface information.

Folds within the western Skeena Fold Belt are separated into three groups, based on fold trend. Northeast-trending folds are located in select areas through the region and exhibit transected cleavage that is northwest-striking. North- and northwest-trending folds comprise separate fold groups in the area. North-trending folds are observed in the central area of the region and are spatially associated with north- or northwest-striking cleavage. In the majority of cases northwest-trending folds are spatially associated with relatively axial-planar cleavage. The transected nature of folds in this region is interpreted to be the result of a temporal sequence of rotating fold orientation, with initial northeast-trending folds overprinted by north- then northwest-trending folds. This temporal sequence supports the work of *Evenchick* [2001] within the western Skeena Fold Belt.

Seismic reflection data for the area were post-stack migrated to produce a data set highlighting near surface structures. Near surface velocity variations were examined using forward modelling and 2-D tomographic inversion of first-break arrival data. The near surface velocities were used to produce a laterally varying velocity sequence for post-stack migration. Reflection data for the upper eight seconds contains the boundary between the Bowser Basin and Stikine Terrane. The Bowser Basin is observed to have a variable thickness, with the thickest sections caused by the structural stacking of units. The data set also indicates that below the Bowser Basin Stikine Terrane is involved in Skeena Fold Belt deformation, with faulting and overthrusting of Stikine Terrane on Bowser Basin units observable.

TABLE OF CONTENTS

LIST OF TABLES

LIST OF FIGURES

ACKNOWLEDGEMENTS

I wish to thank both my supervisors Lori Kennedy and Ron Clowes for their support and enthusiasm over the past few years. Through their work and trust I have been able to experience the ever expanding fields of earth science and had the chance to explore a very beautiful, not to mention geologically exciting part of the world.

I am indebted to Carol Evenchick, who enthusiastically supported this project and gave immensely useful insight and advice throughout. Her direction in the field and great knowledge of the area, which she shared very patiently is greatly appreciated. Within UBC this project would not have been completed without the patient work of Phil Hammer both in putting up with a great number of questions and fishing me out of confusion when entirely lost in the middle of computer codes. I am also indebted to John Amor for leading me through the murky world of unix systems and my fellow but vastly more advanced grad students Steve Israel and Kim Welford without whom my life would have been rather more haphazard and confusing over the last few years.

I wish to thank the Association of Commonwealth Universities for supporting me for two years and giving me the opportunity to study in Canada.

My great thanks go to Olwyn Bruce without whom a summer of mapping in northern BC would have been unimaginable and for the greatly appreciated support and friendship she offered through that time and since. [illegible]

I also wish to thank all my friends. In particular Scott Heffernan and Steve Israel who have taught me the very useful skills of skating with my head up and taking someone out in the corner. Steve Quane for teaching me (the hard way) that goalies don't always stay in the crease and Nancy Joyce without whose support and friendly competition I wouldn't have survived the last few months.

Lastly but not least I would like to thank all my friends in Britain who have looked on with amused concern at the many antics of their faraway friend and provided greatly appreciated support throughout the planning and completion of this project.

Dedicated to the memory of

Robert Bone and Harold Taylor

and

to my family

for letting me get on the plane

1 INTRODUCTION

1.1 CONTEXT OF STUDY

Seismic reflection data from a subsection of Lithoprobe Line 2A and detailed structural mapping of discrete areas near the seismic transect are used to investigate the geometry and kinematics of folding in the northwest Bowser Basin and the western Skeena Fold Belt. The region examined is an area of northern British Columbia crossed by the Stewart-Cassiar Highway, ~100 km south of Dease Lake (Figure 1.1). Along this highway the Lithoprobe Slave-Northern Cordillera Lithospheric Evolution (SNORCLE) Transect recorded the seismic reflection profile. The subset of seismic data interpreted within this investigation extends from the crossing of the Bell-Irving River (Bell II) in the south to Iskut in the north (Figure 1.1), a distance of ~100 km.

Geologically, the region studied encompasses the northwestern Bowser Basin, a Mesozoic sedimentary basin lying across the Palaeozoic and early Mesozoic Stikine Terrane. The Stikine Terrane is one of the largest accreted terranes along the margin of western North America (Figure 1.2). It records a Palaeozoic and Mesozoic island arc history outboard of North America, with accretion to the continent occurring within the middle Mesozoic [*Mihalynuk et al.*, 1994]. Accretion of Stikine Terrane was accompanied by the closure of the Cache Creek oceanic basin in the northern Cordillera. As this amalgamation occurred, an overlap basin, the 'Bowser Basin', formed across a large portion of northern Stikinia mainly as a result of sediment erosion from the uplifting of surrounding areas [*Gabrielse et al.*, 1992]. In the late Mesozoic the area was affected by a compressional/transpressional deformation event that produced a large-scale fold and thrust belt throughout northern Stikinia, the 'Skeena Fold Belt' [*Evenchick*, 1991a]. Structural fabric across the Skeena Fold Belt is characterised by northwest-trending folds and less common thrust faults [*Evenchick,* 1991a]. At the western edge of the fold belt, areas of northeast-trending folds are present, the origin and relationship of these areas of folds to the main trend of the fold belt is enigmatic. *Evenchick* [2001] proposed that the northeast-trending folds are the result of oblique, sinistral, plate convergence early in the history of the fold belt.

The main objectives of this thesis are to 1) identify the subsurface structure of the Bowser Basin using the reflection data, 2) document the kinematics and geometry of fold style in the western Skeena Fold Belt, and 3) discern relative timing constraints on the northeast and northwest-trending folds using both the structural data and the seismic reflection data.

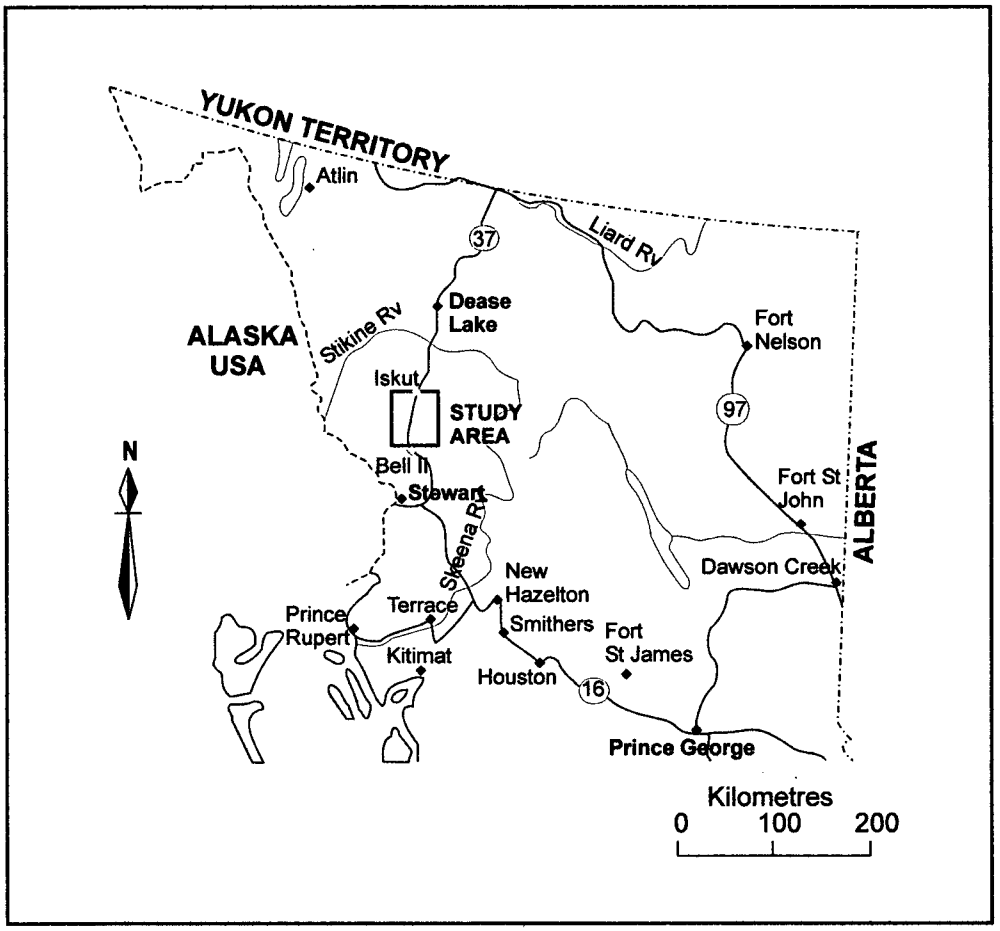

Figure 1.1 Map of northern British Columbia, showing the location of the region of study with respect to major rivers and highways [modified from *Natural Resources Canada,* 2000].

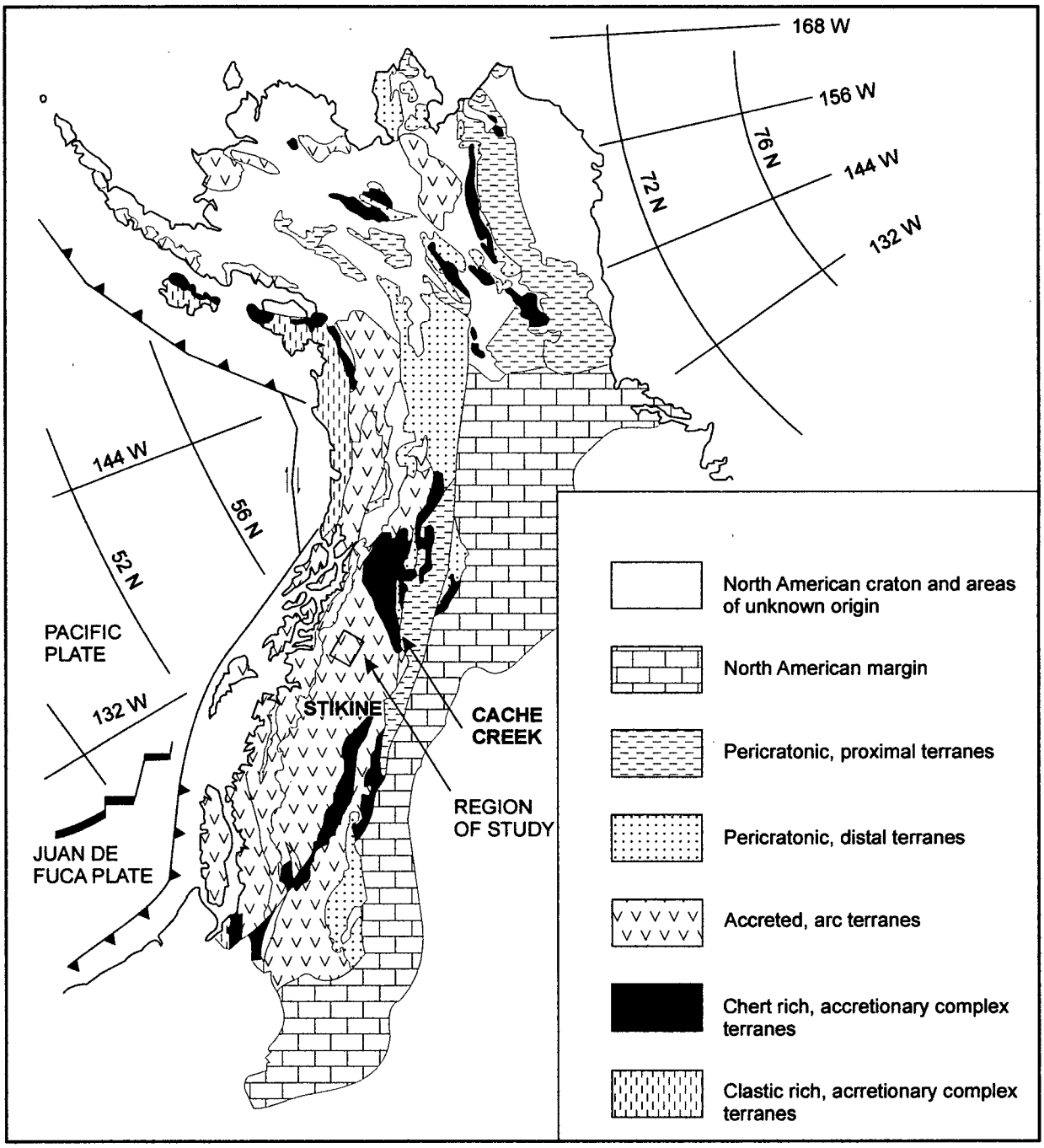

Figure 1.2 Map showing general terrane map for the Canadian Cordillera. The region of study is identified by the rectangle [*Monger and Nokleberg,* 1996].

1.2 STUDY AREA

The region of study comprises the northwest corner of the Bowser Basin and surrounding area. It is bounded by the town of Iskut in the north and the crossing of the Bell Irving River by Highway 37 (Bell II) in the south (Figure 1.3). This incorporates Stikine rocks of the Hazelton and Stuhini groups plus Bowser Lake Group sediments of the Bowser Basin. The Triassic Stuhini Group is located in fault-bounded slivers to the north of the basin in roadside outcrops and on ridges to the west. Overlying these are units of the Lower to mid Jurassic Hazelton Group locally including the Abou and Quock formations [*Evenchick*, 1991c] which define the beginning of Bowser Basin sedimentation. The contact of the Bowser Lake Group with Early Jurassic, Triassic and older rocks is crossed by the highway 22 km south of Iskut [*Evenchick et al.*, 2001]. Lithologies comprising the Bowser Lake Group are separated into a number of assemblages describing the progression of distal turbidite to nonmarine facies across the basin from the Middle Jurassic to mid Cretaceous [*Evenchick et al.*, 2001].

Two separate objectives were met, within the geological fieldwork for this study. A survey of all strata along the trace of the seismic transect within the area was carried out, incorporating rocks of Stikine Terrane and the Bowser Basin as described above. The second objective was to obtain detailed structural data from select areas within the basin to elucidate the kinematic relationship between the dominant northwest structural trend and the more elusive northeast trending structures. Data from the seismic line were combined with detailed structural mapping carried out along the highway for the same distance and in three locations east of the road. Study Area 1 (Figure 1.3), the most central of these locations, surrounds and extends to the northwest of Mount Pinhorn, 82 km north of Bell II. Study Area 2 at the northern end of the transect is located east of Kinaskan Lake Provincial Park, 30 km south of Iskut. Study Area 3 is located northeast of the Ningunsaw River, 25 km north of Bell II. Study areas 1 and 3 comprise strata of the Ritchie-Alger assemblage [*Evenchick*, 2001] of Middle to Upper Jurassic age. Study Area 2 comprises Late Jurassic to Early Cretaceous strata of the Skelhorne assemblage [*Evenchick*, 2001].

1.3 LITHOPROBE REFLECTION PROFILES

In the winter of 1999-2000, the final component of the SNORCLE (Slave-Northern Cordillera Lithospheric Evolution) Transect seismic experiment was undertaken. This was a

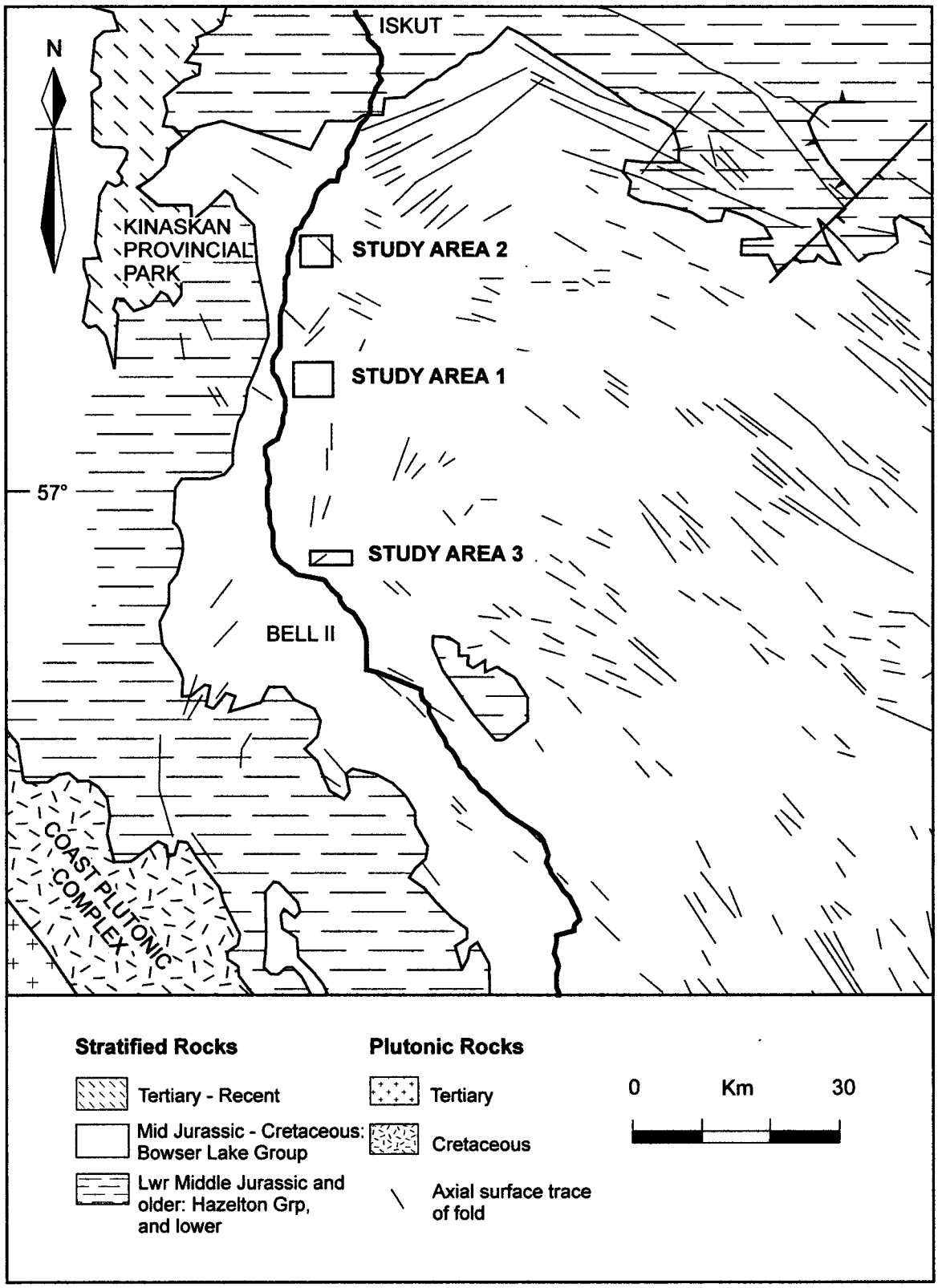

Figure 1.3 Regional geology and structural features of the northwest Bowser Basin, indicating location of study areas for detailed structural analysis [modified from *Evenchick*, 1991a and 2001].

contribution to the Canada-wide Lithoprobe project, which seeks an understanding of the structure and past evolution of the Canadian landmass through a collaborative, multidisciplinary research programme. The SNORCLE seismic experiments involved the collection of seismic refraction and reflection data along four profiles across the northern Cordillera extending into cratonic North America (Figure 1.4). Transect 1 is located in the Northwest Territories and extends for 600 km southwest of Yellowknife. Transect 2 is separated into two lines crossing at Watson Lake, Yukon Territory. Line 2A extends from Watson Lake to Stewart on the British Columbia-Alaska border, a distance of 675 km, while Line 2B extends from Watson Lake east to Fort Nelson, a distance of 570 km. Transect 3 extends for 600 km northeast-southwest across the Yukon. Refraction/wide angle reflection data sets were collected along all transects in 1997, including Line 2A (known as Line 22 in the refraction experiment). The final component of the experiment, the acquisition of seismic reflection data, was accomplished in the winter of 1999-2000.

1.4 GEOLOGICAL WORK

The first geological mapping of the region was completed in the 1930's [*Kerr*, 1930] by the Geological Survey of Canada. The extent of Bowser Basin strata was identified in mapping in 1956 [*Geological Survey of Canada*, 1957]. The Mesozoic stratigraphy of the southern basin was defined by *Tipper and Richards* [1976]. Work in the northern section of the basin was undertaken primarily by *Eisbacher* [1973; 1976; 1981], and *Gabrielse and Tipper* [1984].

More recent Geological Survey of Canada mapping, [*Evenchick* 1991b; *Evenchick et al.*, 2001], defined lithofacies assemblages applicable to the northern two thirds of the Bowser Basin and in the definition of the geometry and kinematics of the Skeena Fold Belt. In addition to the work of *Evenchick* throughout the mid to late 1980's and 1990's, comprehensive work on the stratigraphy of portions of the Bowser Basin near the study area has been undertaken by *Ricketts* [1990], *Green* [1991; 1992], *Greig* [1991], and *Ricketts and Parrish* [1992]. Structural style and stratigraphy of the Groundhog Coalfield in the east of the Bowser Basin has been discussed in a number of publications [*Moffat,* 1985; *Moffat and Bustin*, 1984; 1993], as is the geology of Oweegee Dome in the west central part of the basin [*Greig*, 1991; 1995].

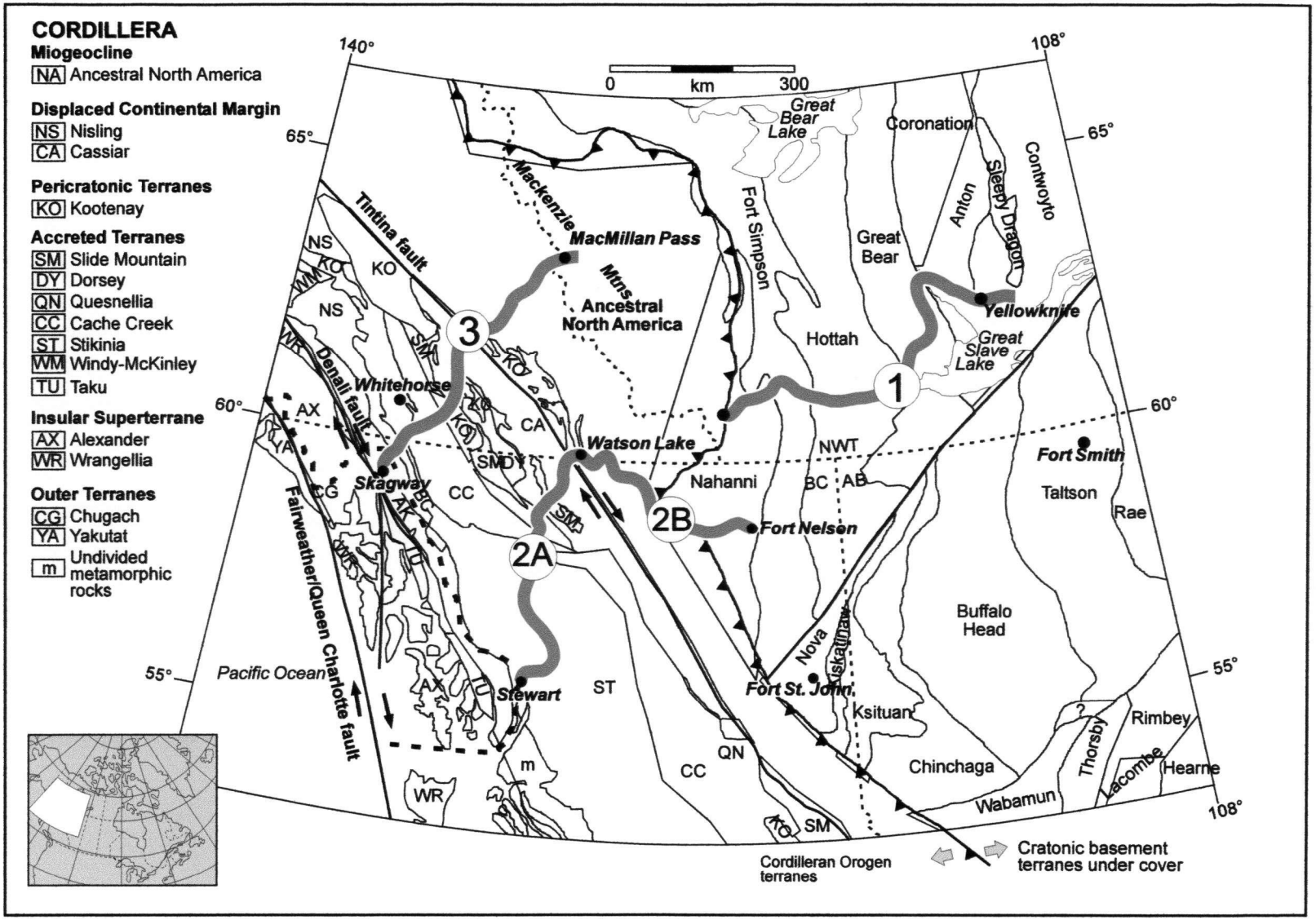

Figure 1.4 Regional extent of SNORCLE transects, 1, 2A, 2B and 3 northwestern Canada [*Hammer et al.,* 1998].

1.5 GEOPHYSICAL WORK

Prior to the acquisition of seismic reflection data along Highway 37 a number of projects have provided subsurface information for this area. Gravity data are available for the Bowser Basin [*Lowe et al.,* 1992]. The SNORCLE refraction and wide-angle reflection experiment was completed in 1997 [*Hammer et al.,* 2000]. Aeromagnetic data for Stikinia are also available and analysis of the data along the seismic transect has been reported by *Lowe et al.* [1998].

1.6 METHOD OF STUDY

Within this study detailed structural mapping was undertaken in the summer of 2000. This work mainly concentrated on areas known to have distinct structural trends [*Evenchick,* 2001] and allowed the analysis of both northwest- and northeast-trending folds. Structural data comprises mainly bedding and cleavage measurements, which were recorded with the lithology of the unit defined. Fractures, faults and veins are also common throughout the region; these were recorded together with information regarding sense of movement. Study Area 1 contains both northwest- and northeast-trending folds. Work in this area was undertaken to obtain evidence of the relationship between the two orientations of folding and their relative timing. Study Area 2 contains a large basinal feature interpreted to be a Type 1 interference structure [*Evenchick,* 2001]. Data from this area were collected to provide a detailed structural data set in an attempt to define the style of and relationship between the interacting folds. Study Area 3 is contained within an area of exclusively northeast-trending structures and was studied to obtain a detailed understanding of the style of northeast-trending folds and associated fabrics, including cleavage, fractures and faults.

2 REGIONAL GEOLOGY

The Bowser Basin (Figure 2.1) is described as a 'successor basin' [*Eisbacher*, 1976], a term applied to a number of western Canadian intermontane basins in which a rapidly subsiding trough developed on deformed and intruded basement [*Ricketts and Evenchick*, 1991]. The basin developed on top of Stikine Terrane rocks of Palaeozoic to Aalenian age [*Evenchick et al.*, 2001] and was filled with marine to nonmarine sediments shed from uplift to the north, east and south [*Gabrielse et al.*, 1992]. The Bowser Lake Group is identified throughout the Bowser Basin with successive units deposited, dependent on position within the basin. In the south, the Bowser Lake Group is succeeded by the Skeena Group in the Early Cretaceous [*Bassett and Kleinspehn*, 1997]. To the northeast the Sustut Basin is present; a late-stage basin of cannibalized Bowser Lake Group sediment [*Evenchick*, 1991a]. The Sustut Basin comprises the Sustut Group of Tango Creek and Brothers Peak formations. The western edge of the Bowser Basin is marked by intrusions of the Coast Plutonic Complex, which is predominantly mid Jurassic to Tertiary. This complex acted as a metamorphic hinterland for the evolution of the Skeena Fold Belt [*Evenchick*, 1992].

2.1 STIKINE TERRANE

Stikine Terrane is composed of late Palaeozoic to early Mesozoic rocks mainly comprising a series of volcanic-plutonic island arc sequences [*Gabrielse*, 1991]. The terrane has origins outboard of North America and records progressive arc activity culminating in collision with inboard terranes of North America in the early Middle Jurassic [*Ricketts et al.*, 1992]. The stratigraphy includes dominantly marine, oceanic arc and plateau volcanic rocks plus sedimentary strata and coeval plutons [*Greig and Gehrels*, 1995].

2.1.1 Stikine Assemblage

The oldest strata in the Stikine Terrane belong to the Stikine assemblage, as defined by *Monger* [1977]. These are Early Devonian to Late Permian rocks of varying origin. The majority of pre-Permian units display unconformable, commonly structural, boundaries and therefore any thickness estimates of these strata probably bear little correlation to the true stratigraphic thickness of the units [*Gunning*, 1990]. Devonian units comprise intermediate to mafic

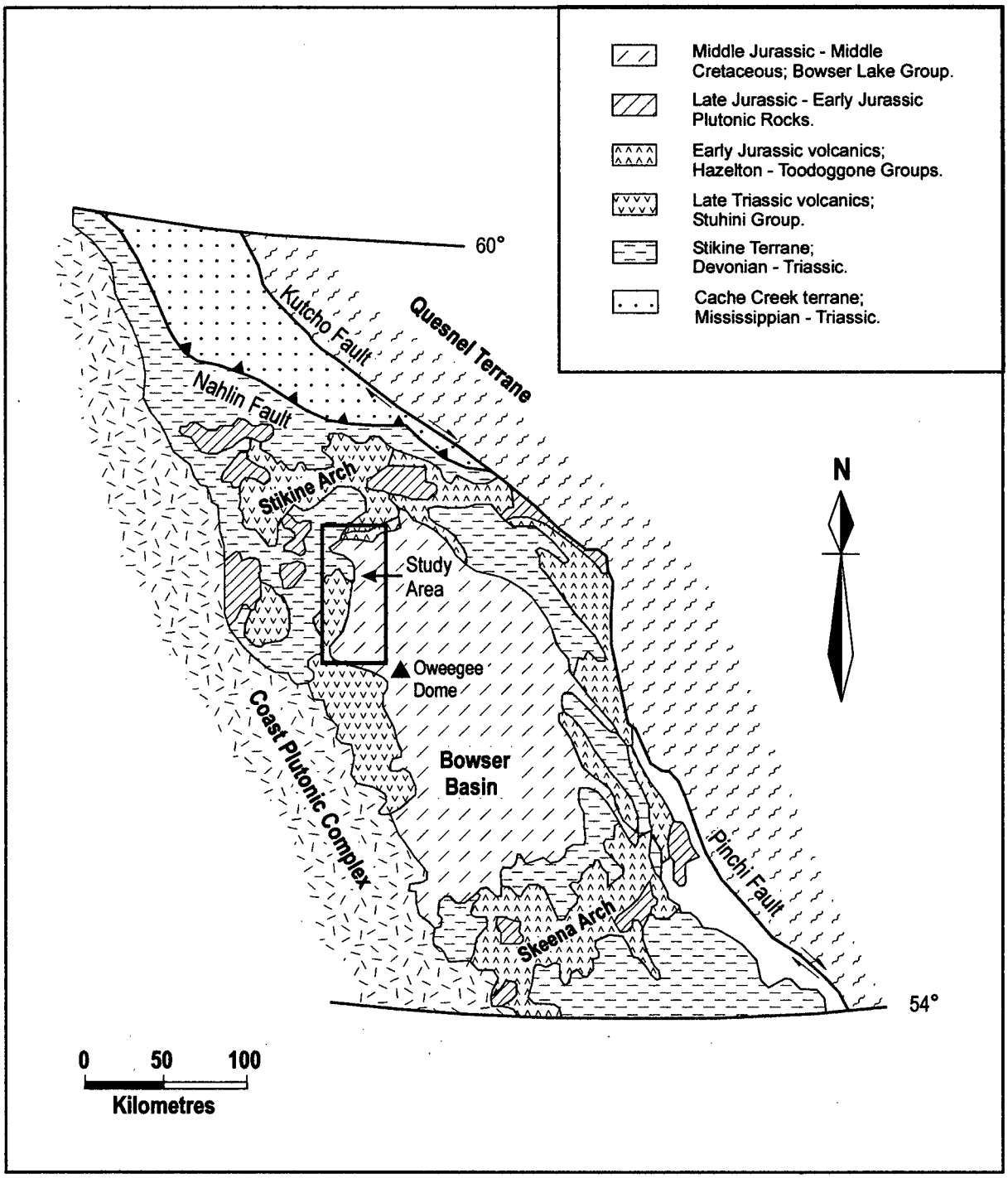

Figure 2.1 Geology of the Bowser Basin [modified from *Thomson et al.*, 1986].

volcaniclastics, limestone, argillites and epiclastics [*Logan and Koyanagi*, 1989; *Anderson*, 1989]. Devonian sequences are estimated to be approximately 750-1000 m in thickness [*Logan and Koyanagi*, 1989; *Brown and Gunning*, 1989]. These are overlain by less deformed thick coralline reef carbonates interbedded with chert, pillow basalts, hyaloclastites and epiclastic rocks of Mississippian age [*Anderson*, 1989], estimated to be approximately 1250 m thick [*Logan and Koyanagi*, 1989]. The most extensive units within the Stikine assemblage are a number of thick Permian limestone units; these are interbedded with mafic to felsic rocks similar to the Jurassic Hazelton Group [*Anderson*, 1989], plus argillites and epiclastics. Permian units tend to be conformable [*Gunning*, 1990] and are identified along >500 km of the eastern border of the Coast Plutonic Complex. Estimates of the thickness of Permian stratigraphy are between 1000 and 2000 m [*Logan and Koyanagi*, 1989; *Gunning*, 1990] and in some areas structural thickening has produced thicknesses greater than 2800 m [*Brown et al.*, 1992].

All strata within the Stikine assemblage have been weakly metamorphosed; Devonian rocks display metamorphism up to greenschist facies whereas younger sequences are subgreenschist [*Logan and Koyanagi*, 1989]. Volcanic rocks of Pennsylvanian age have been identified near Oweegee Dome (Figure 2.1) [*Greig and Gehrels*, 1995]. Volcanic rocks of this age are unusual but have been correlated with outcrops in the Telegraph Creek area near the northern boundary of the Bowser Basin [Anderson, 1989] and in the Terrace area where they give a U-Pb zircon age of 285 ±9 Ma [*Gareau et al.*, 1997].

2.1.2 Stuhini Group

Overlying the Palaeozoic Stikine assemblage is a sequence of Middle and Upper Triassic units. The Stuhini Group is a sequence of Upper Triassic volcanic and sedimentary rocks. An unconformable boundary exists between Permian limestones and Middle Triassic fine-grained clastic rocks, mainly chert, siliceous siltstones and ash tuffs [*Brown et al.*, 1992] with a stratigraphic thickness of 200-300 m [*Logan and Koyanagi*, 1989; *Logan et al.*, 1992]. These units conformably grade into thick bedded turbiditic tuffaceous sandstones, siliceous siltstones, thin limestone lenses, crystal lithic dacite, andesitic ash and lapilli tuff of the Stuhini Group [*Greig*, 1991]. The contacts between units within the Stuhini Group are typically conformable [*Brown et al.*, 1992] and the thickness of the unit is approximately 3000 m [*Logan and Koyanagi*, 1989; *Brown et al.*, 1992]. Within Oweegee Dome, a structural culmination of Stikine Terrane rocks surrounded by the Bowser Basin, the Stuhini Group displays an unusual faulted relationship with both the Permian limestone and the Hazelton Group [*Greig*, 1991].

The Stuhini Group is the result of volcanic arc activity in a low energy pelagic environment [*Brown et al.*, 1992]. To the northwest of the Bowser Basin there is a gradational east-west transition from chert to ash tuff signifying shallowing conditions [*Brown et al.*, 1992] with volcaniclastic rocks prograding from the east implying an eastern centre of arc activity. A period of variable deformation, weak in the south near Terrace [*Gareau et al.*, 1997] and stronger in the north, is thought to be coeval with, and continued after, deposition of the Stuhini Group [*Greig and Gehrels*, 1995].

2.1.3 Hazelton Group

The Hazelton Group is widespread across the Stikine Terrane and was described as including 'basaltic to rhyolitic rocks, sedimentary rocks, their tuffaceous equivalents and minor limestones, deposited in the Early to Mid Jurassic; Sinemurian to Early Callovian' [*Tipper and Richards*, 1976]. *Marsden and Thorkelson* [1992] defined a shorter timespan concluding in the Early Bajocian. Although widespread, units within the group cannot easily be correlated across distance due to later deformation, lateral facies changes and difficulty in dating sedimentary units [*Marsden and Thorkelson*, 1992].

The Hazelton Group unconformably overlies the Palaeozoic and Triassic successions within the region [*Greig and Gehrels*, 1995]. Lateral facies variations throughout the Hazelton Group imply contemporaneous subaerial and marine environments existing in an emergent island setting [*Brown and Greig*, 1990]. Separate units within the group may represent several volcanic episodes related to discrete island arcs [*Brown and Greig*, 1990]. The Hazelton Group marks the terminal stages of island arc migration and tectonism within the Stikine Terrane [*Marsden and Thorkelson*, 1992].

2.1.4 Spatsizi Assemblage

A group of intercalated sedimentary and volcanic units on the northern margin of the Bowser Basin known as the 'Spatsizi assemblage' represent the middle Jurassic component of the Hazelton Group (Figure 2.2) [*Marsden and Thorkelson,* 1992]. Volcanic units within the assemblage have been dated to 190 ±3 Ma [*Thorkelson et al.*, 1991].

The Spatsizi assemblage spans the gradational boundary between the end of Stikinian island arc activity and the beginning of Bowser Basin sedimentation. Work of *Evenchick* [1992] and *Marsden and Thorkelson* [1992] contains the Spatsizi assemblage within the later stages of the Hazelton Group, prior to these works it was thought of as a separate group conformably overlying the Hazelton Group [*Marsden and Thorkelson*, 1992].

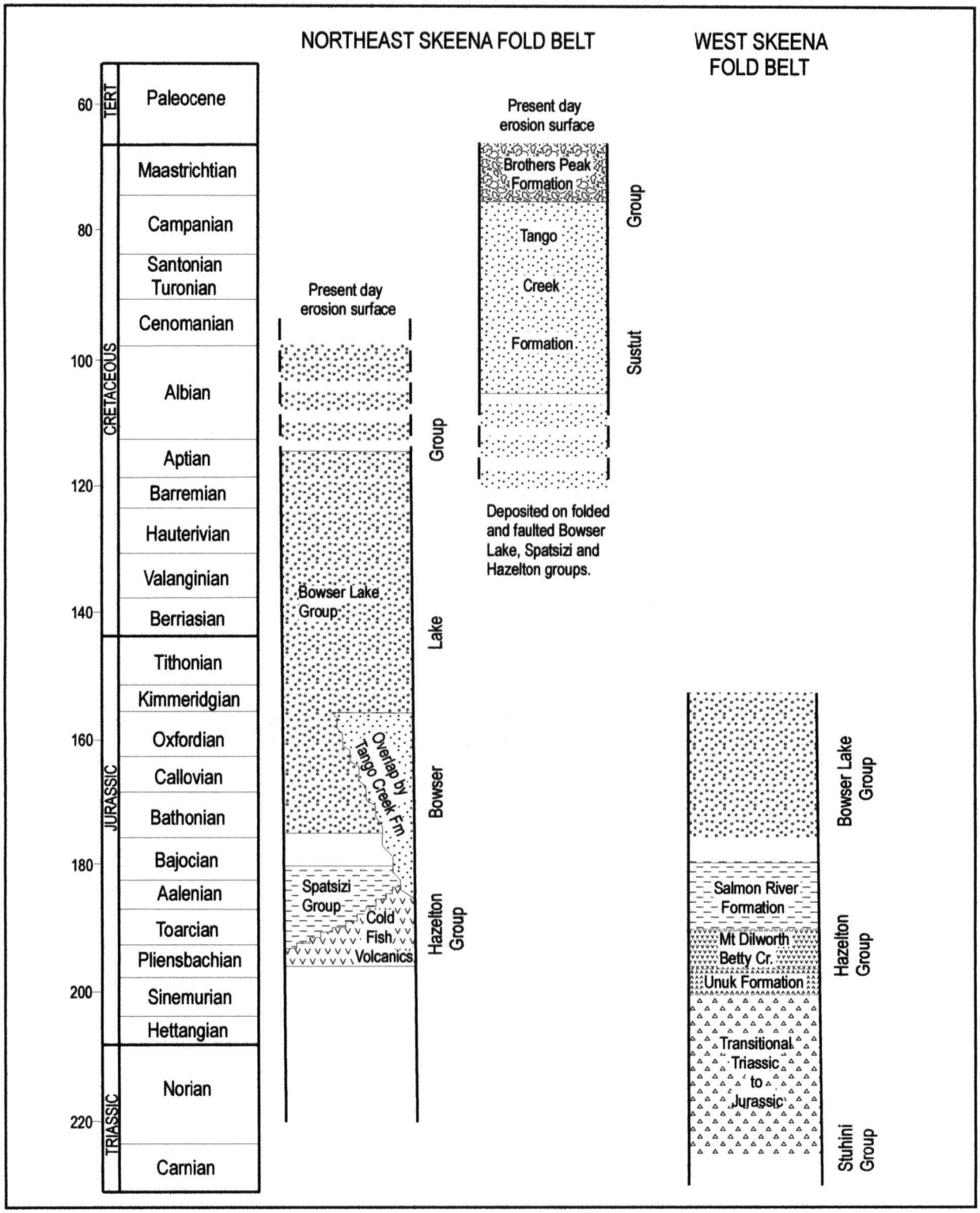

Figure 2.2 Stratigraphic units of the Skeena Fold Belt. The Bowser Lake Group contains the Ritchie-Alger, Todagin, Muskaboo Creek, Eaglenest, Skelhorne, Groundhog-Gunanoot and Jenkins Creek asemblages depending on location within the northern Bowser Basin [*Evenchick*, 1991b; *Evenchick et al.*, 2001].

The initial unit of the Bowser Basin is interpreted to be the Abou Formation, which is of Aalenian age and comprises organic siliceous shales that overlie lower Spatsizi units [*Ricketts et al.*, 1992]. This formation has the characteristics of a condensed stratigraphy accumulating in a starved basin environment [*Ricketts and Evenchick*, 1991]. This development is the result of Cache Creek Terrane beginning to overlie Stikinia, but within an initial period remaining below sea-level and therefore allowing only a small amount of sediment to the early Bowser Basin. The Abou Formation is overlain by thin, interbedded shales, fine grained sandstones and water-lain tuffs of the Bajocian Quock Formation [*Thomson et al.*, 1986]. The Quock Formation is distinctive and occurs extensively around the northwest edge of the basin [*Evenchick et al.*, 2001].

2.2 BOWSER BASIN

2.2.1 Bowser Lake Group

The Bowser Lake Group forms the bulk of Bowser Basin stratigraphy. The boundary between upper Hazelton units and the Bowser Lake Group is gradational. The Bowser Lake Group is at least 3500 m thick [Evenchick, 1992] and ranges in age from mid Jurassic to mid Cretaceous [*Evenchick et al.*, 2001]. Within the northwestern region of the basin the Bowser Lake Group has been separated into a number of lithofacies assemblages.

The lower units of the Bowser Lake Group, spanning the Middle to Upper Jurassic, are the Ritchie-Alger, Todagin, Muskaboo Creek, Eaglenest and Skelhorne assemblages [*Evenchick et al.*, 2001]. These assemblages reflect differing submarine environments across the northern span of the basin. They range from the submarine fan deposits of the Ritchie-Alger assemblage, dominated by interbedded siltstones and sandstones (>50 m thick) and rare conglomerates, through the Todagin assemblage to the Muskaboo Creek shelf assemblage, to the Eaglenest and Skelhorne deltaic assemblage, with increasing indication of proximity to terrestrial environments suggested by characteristic lithofacies assemblages [*Evenchick et al.*, 2001]. The Skelhorne assemblage of deltaic sediments is characterised by thinly interbedded sandstones and siltstones with thick units of conglomerate in cycles of tens of metres. *Ricketts* [1990] and *Green* [1991] suggest a marine environment of coarse sediment accumulating in fan deltas with some dispersal over narrow, interfan shelves, with a large proportion of coarse material bypassing the shelf environment by funnelling down submarine canyons mainly facing south, eroding into muddy prodelta-slope strata. This environment produces coarse-grained material in fan shaped zones a

large distance into the basin and is the result of a highly dynamic environment probably controlled tectonically by the interaction of Cache Creek and Stikinia and the rapid subsidence of the basin [*Green*, 1991].

Deposition continued through the Upper Jurassic and Lower Cretaceous with thick units of deltaic to nonmarine facies that define the Groundhog and Jenkins Creek assemblages [*Evenchick et al.*, 2001]. These define a marine margin which migrated southwest with time giving a succession of shallower marine and nonmarine deposits [*Evenchick*, 2000].

2.2.2 Sustut Group

To the northeast of the Bowser Basin the Sustut Basin formed on the foreland of the evolving Skeena Fold Belt. The Sustut Group comprises two units; the lower Tango Creek Formation and the upper Brothers Peak Formation, forming a total stratigraphic thickness of greater than 2000 m [*Eisbacher*, 1981]. The Sustut Group has an unconformable basal surface and overlies Hazelton, Spatsizi and Bowser Lake groups in different areas [*Eisbacher*, 1981]. The base of the group is thought to be Aptian or Early Albian in age and the uppermost units are of Early Maastrichtian age [*Evenchick et al.*, 2001].

2.3 BASIN EVOLUTION

The onset of clastic sedimentation in the mid Jurassic and the development of the Bowser Basin is interpreted to mark the amalgamation of Stikine and Cache Creek terranes and their accretion to the North American margin because the Bowser Lake Group forms an 'overlap assemblage' across both Stikine and Cache Creek terranes [*Gabrielse et al.*, 1992].

According to *Ricketts et al.* [1992] the stratigraphic history of the Bowser Basin appears to be analogous to that predicted by the theoretical starved-basin and flexural subsidence model of marine foredeep evolution suggested by *Stockmal et al.* [1986]. This model predicts low sedimentation rates during the early stage of flexural subsidence, characterized by fine grained condensed stratigraphic successions, represented in the Bowser Basin by the Spatsizi and Salmon River formations [*Ricketts et al.*, 1992; *Stockmal et al.*, 1986]. Only when the overthrust panel is subaerially exposed will a substantial amount of coarse grained sediment be supplied to the foredeep and, as further sediment is added to the basin, sediment loading will also add to subsidence rates [*Ricketts et al.*, 1992; *Stockmal et al.*, 1986]. Within the early history of the Bowser Basin, from Bathonian to Early Oxfordian, deposition was restricted to the north-

northeastern part of the basin [*Evenchick*, 2000]. On the western side of the basin a condensed marine section formed at this time [Evenchick, 2000]. Through the mid Oxfordian and Early Kimmeridgian a rapid south and southwest migration of the basin occurred [*Evenchick*, 2000]. The stratigraphy of the present day western Bowser Basin demonstrates marine conditions continued in this part of the basin throughout its evolution, while shelf, deltaic and fluvial environments migrated from northeast to southwest within the basin through the Cretaceous [*Evenchick*, 2000].

2.4 SKEENA FOLD BELT

The Skeena Fold Belt is a thin-skinned fold and thrust belt which extends across most of the northern Intermontane Belt (Figure 2.3) [*Evenchick*, 1991a]. Contractional structures within the Skeena Fold Belt are mainly represented by folds with two dominant orientations. Northwest-trending folds dominate the central and eastern parts of the fold belt and are found in large areas of the western fold belt. Northeast-trending folds are confined to specific areas within the western fold belt [*Evenchick*, 2001]. Northwest trending folds commonly verge northeast, have wavelengths of hundreds of metres to kilometres depending on whether folding involves purely Bowser Lake Group units or igneous Stikinian rocks which produce far larger wavelengths [*Evenchick*, 2001]. Northeast-trending folds are on the same scale as their northwestern counterparts and verge both northwest and southeast [*Evenchick*, 2001].

Shortening in the Skeena Fold Belt has been calculated from balanced cross sections. It is hypothesized that folding in the belt is detached and thrust faults within the basal units of the Bowser Basin act as detachment horizons above and below the fold trains, therefore producing a regional blind thrust system [*Evenchick*, 1991b]. Shortening calculations across the Skeena Belt vary from 32% to 60% with an average of 44% [*Evenchick*, 1991b]. These values imply the Skeena Fold Belt has been shortened by at least 160 km [*Evenchick*, 1991a]. These are minimum calculations and are considered to be very conservative [*Evenchick*, 1991a]. Arguments that volcanic Hazelton Group rocks record a very different amount of shortening have been made, but this variation can be explained by the competency contrast between volcanic strata and the sedimentary rocks of the overlying Bowser Lake Group [*Evenchick*, 1991a]. Within the Hazelton Group, deformation is expressed as broad folds and thrust faults rather than smaller scale tight folds characteristic of the basin sediments [*Evenchick*, 1991b].

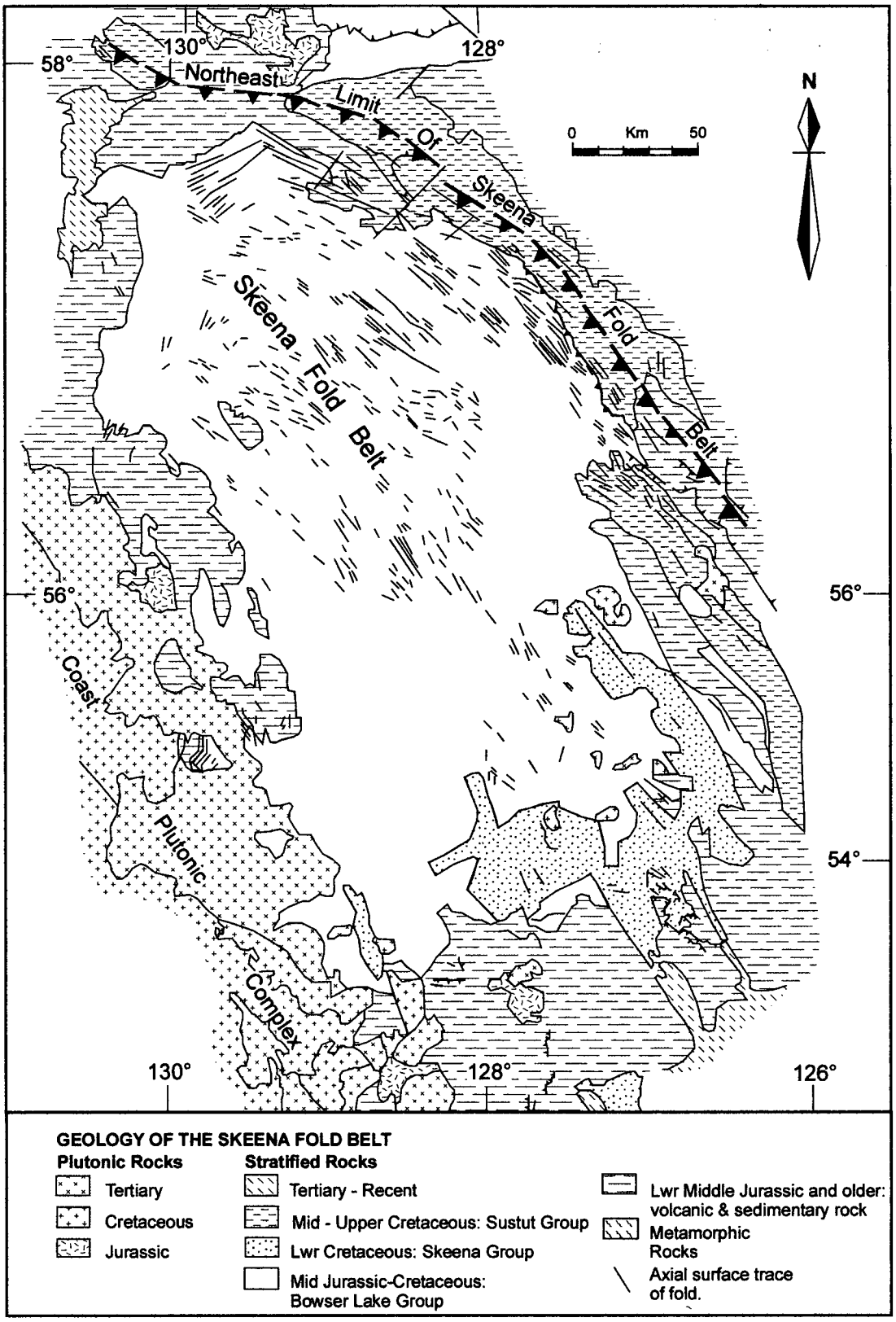

Figure 2.3 Geology and major structures of the Skeena Fold Belt [*Evenchick*, 1991a].

The age of deformation within the Skeena Fold Belt has been inferred mainly from fault crosscutting relationships and unconformity surfaces and is therefore a broad estimate. The lower formation in the Sustut Group, the Tango Creek Formation, has an unconformable relationship with the underlying Bowser Lake and Hazelton groups, implying deformation occurred prior to and during deposition of the Sustut Group [*Evenchick*, 1991b]. The age of the youngest strata before the Sustut Group is around the Jurassic-Cretaceous boundary [*Evenchick*, 2000]. This, combined with the evidence from the Sustut Basin, implies deformation initiated some time in the Early Cretaceous before the initial Albian strata of the Tango Creek Formation [*Evenchick*, 2000]. The youngest strata affected by the deformation are the Brothers Peak Formation of late Campanian to Early Maastrichtian age (Figure 2.2), indicating some deformation occurred in the latest Cretaceous and possibly into the Early Tertiary [*Evenchick*, 1991b].

The Intermontane and Coast belts interacted at least from the Cretaceous onwards [*Evenchick*, 1991a]. The Skeena Fold Belt involves shortening in the Bowser Basin and Stikinian rocks to the west. It roots into the Coast Plutonic Complex, implying the shortening seen in the Intermontane Belt has been taken up within the Coast Belt [*Evenchick*, 1991a]. If the age of initial Skeena deformation is Early Cretaceous, this is contemporaneous with intrusion and uplift of Early Cretaceous plutons on the west side of the Coast Plutonic Complex [*Evenchick*, 1991a]. Contractional deformation was coeval in both belts, and models that involve the Skeena Fold Belt rooting to the west suggest a kinematic link between the fold belt and the Coast Plutonic Complex, which acted as a metamorphic hinterland [*Evenchick*, 1991a]. The difference in deformation style between the two belts is suggested to be due to the Coast Belt showing deeper, more ductile deformation [*Evenchick*, 1991a]. The geometry of the Skeena Fold Belt supports hypotheses that the Coast and Intermontane belts have been interacting since the Cretaceous [*Evenchick*, 1991a], either due to the amalgamation of the Insular and Intermontane superterranes [*Evenchick*, 1991a; *Monger et al.*, 1982] or due to intra-terrane shortening and magmatism related to subduction beneath a single terrane [*Evenchick*, 1991a; *van der Heyden,* 1989]. Skeena Fold Belt shortening is coeval with shortening in the northern Coast Belt, Omenica Belt and the Rocky Mountain Fold and Thrust Belt, implying a large amount of shortening over the northern Cordillera in the Cretaceous [*Evenchick*, 1991a].

2.5 Western Skeena Fold Belt Evolution

2.5.1 Regional structural trends

Extensive regional work in the Skeena Fold Belt has been undertaken by *Evenchick* [1986; 1987; 1990; 1991a; 1991c; 1992a; 1996; 1998; 2001]. Northwest-trending folds encompass large areas within the western Skeena Fold Belt. These folds characteristically verge northeast, are upright to overturned, have interlimb angles between 140-30° and wavelengths of hundreds of metres. Cleavage is parallel with or fans through the axial surface of folds [*Evenchick,* 2001]. Northeast-trending folds are found in discrete areas of the western fold belt; these trend from northeast- to north-northeast, verge both southeast and northwest, and have a similar scale to northwest-trending folds. They have cleavage parallel to axial surfaces in most cases [*Evenchick,* 2001]. The eastern Skeena Fold Belt is dominated by northwest-trending folds with similar geometry and wavelength to those in the west of the fold belt [*Evenchick,* 1992; *Moffat and Bustin*, 1993].

Deformation across the Skeena Fold Belt is suggested to be progressive with a sequence of initial northeast-trending folds succeeded by a rotation through north-trending structures to the dominant northwest-trending folds produced by northeast directed shortening [*Evenchick,* 2001]. *Moffat* [1985], studying a region of the eastern fold belt surrounding the Groundhog Coalfield, suggests a differing sequence of deformation with initial northwest-trending folding overprinted by northeast-trending structures and subsequently further northwest-trending structures.

2.5.2 Importance of northeast-trending structures

Northeast- and north-northeast-trending structures are present along at least 900 km of the boundary between the Coast and Intermontane belts [*Evenchick*, 2001]. The northeast-trending structures within the western Skeena Fold Belt account for ~500 km of this distance. Northeast-trending folds accommodate southeast shortening and are highly oblique to the Coast Belt, a zone of crustal thickening interpreted to control the geometry and shortening direction within the fold belt [*Evenchick*, 2001]. A number of explanations for the origin of northeast-trending folds are discussed by *Evenchick* [2001] and are summarized below.

Lateral differences in the amount of shortening within the fold belt result in gradual changes in fold orientation [*Evenchick*, 2001]. Within the Skeena Fold Belt this is discounted as fold interaction produces complex folding and fold interference rather than a gradual change in fold orientation [*Evenchick*, 2001].

Rotation of previously formed folds about a vertical axis due to drag or accommodation of indentors could produce folds oblique to the plate margin. The 90° block rotation required to produce northeast-trending folds would be expected to be accompanied by strike-slip faulting and space accommodation structures [*Evenchick*, 2001]. Within the Skeena Fold Belt there are no examples of identified structures large enough to result in the domains of northeast-trending folds observed [*Evenchick*, 2001].

The influence of basement structures could cause large variations in fold orientation, if basement structures oblique to the structural grain were reactivated [*Evenchick*, 2001]. Reactivated northeast-trending basement structures could produce zones of southeast shortening during a rotation from northeast to southeast convergence. No evidence of northeast-trending basement structures are known in Stikinia west of the Bowser Basin [*Evenchick*, 2001]. The northeast-trending folds could reflect dextral or sinistral wrenching along easterly or northerly striking basement faults [*Evenchick*, 2001]. East striking dextral faults of significant magnitude to produce the domains of northeast-trending folds observed are unknown in the region [*Evenchick,* 2001], but to the west of the Bowser Basin a north trending sinistral fault, the South Unuk Shear Zone [*Lewis*, 1996] is present. This could be a controlling structure on the northeast-trending folds in the west-central Bowser Basin area, but there is no evidence for comparative structures near the area of this study. This control of northeast-trending folds by basement structures may be clarified by examination of the seismic reflection data, where relatively large-scale basement structures might be apparent.

The orientation of structures within obliquely convergent settings varies dependent on the amount of strain, the angle of convergence, the degree of partitioning into strike-slip and convergent zones and the percentage of strike-slip partitioning [*Evenchick*, 2001]. Models of oblique convergence [*Teyssier and Tikoff*, 1998] predict the initiation of folds at a maximum of 45° to the plate boundary for a situation of wrenching with no convergence. The angle of orientation is significantly lower in zones of transpression with increasingly oblique angles of convergence plus degrees of strike-slip partitioning. With continued boundary-parallel displacement combined with convergence, the orientation of folds would be expected to rotate to lower angles with the plate boundary [*Evenchick*, 2001]. This model can be applied to the western Skeena Fold Belt with a number of assumptions concerning the orientation of the plate margin relative to the emerging fold belt within the early history of deformation [*Evenchick*, 2001].

From these hypotheses of the mechanism of northeast-trending fold formation those pertaining to lateral differences in shortening and block rotation can be discounted as the results

of these processes would not produce the style or orientation of folds observed in the region. As discussed above the presence of north and east striking basement structures is plausible in the region and therefore could be the mechanism for northeast-trending fold formation. The most appropriate mechanism for northeast-trending fold formation in this region is variations in the environment of deformation caused by oblique convergence. This mechanism correlates well with knowledge of Mesozoic plate movement outboard of western North America [*Engebretson et al.*, 1985].

Recent work has concentrated on defining the controlling geometries of oblique convergence that have produced the style of folding observed within the western Skeena Fold Belt [*Evenchick*, 2001]. This research is intended to clarify aspects of fold relationships within the northwestern portion of the fold belt to assist in this investigation.

3 STRUCTURAL DATA DESCRIPTION

Three study areas were defined within this investigation. Structural data collection within these areas was undertaken with the intention of discerning the timing of northeast- and northwest-trending fold sets within the western Skeena Fold Belt. Study Area 1 contains both northeast- and northwest-trending folds and data from this area sheds light on the geometry of the fold sets and relationship between the two sets. Study Area 2 contains a macroscopic Type 1 interference structure produced by the interaction of northeast- and northwest-trending synclines. Study Area 3 is located within an area of predominantly northeast-trending folds and so provides the opportunity to study this fold set without the direct influence of the more dominant northwest-trending fold set.

3.1 DEFINITIONS AND METHODOLOGY

3.1.1 Cleavage

The cleavage style seen in the area can be named a 'fracture cleavage' but is more accurately referred to as a 'spaced, disjunctive cleavage' [*Powell*, 1979]. The name 'fracture cleavage' giving an incorrect inference of the processes of cleavage formation. Disjunctive cleavage is produced by a number of processes occurring at shallow crustal levels (<6 km) where rock-water interactions including pressure solution and diffusion plus advection are the dominant deformation process [*Engelder and Marshak*, 1985].

Spaced cleavage is defined as a foliation plane which cuts across pre-existing lithologic layering without reorienting this layering and can be identified in hand-specimen or outcrop scale [*Engelder and Marshak*, 1985; *Powell*, 1979]. *Alvarez et al.* [1978] classified spaced cleavage into four subdivisions of weak; >10-8 cm separation between planes; moderate; 8-1 cm separation, strong; 1-0.5 cm separation and very strong; <0.5 cm separation (Figure 3.1a). In the study region, the separation of cleavage planes is strongly controlled by lithology with cleavage within conglomerates being weakly spaced, while cleavage within sandstones and siltstones ranges from moderate to strongly developed. Cleavage planes generally have a planar pattern (Figure 3.1b).

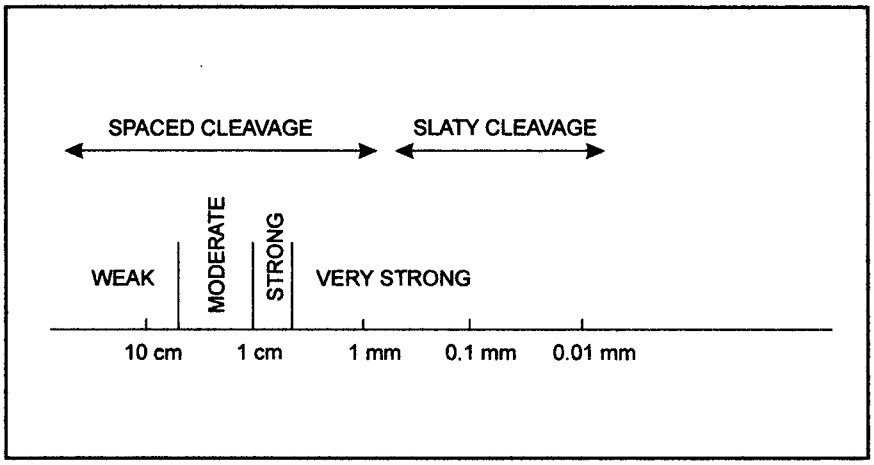

Figure 3.1a Classification of cleavage based on spacing between planes. Cleavage was subdivided into spaced and slaty by *Powell* [1979], while the subdivision of weakly to very strongly cleaved was defined by *Alvarez et al.* [1978]. *Engelder and Marshak* [1985].

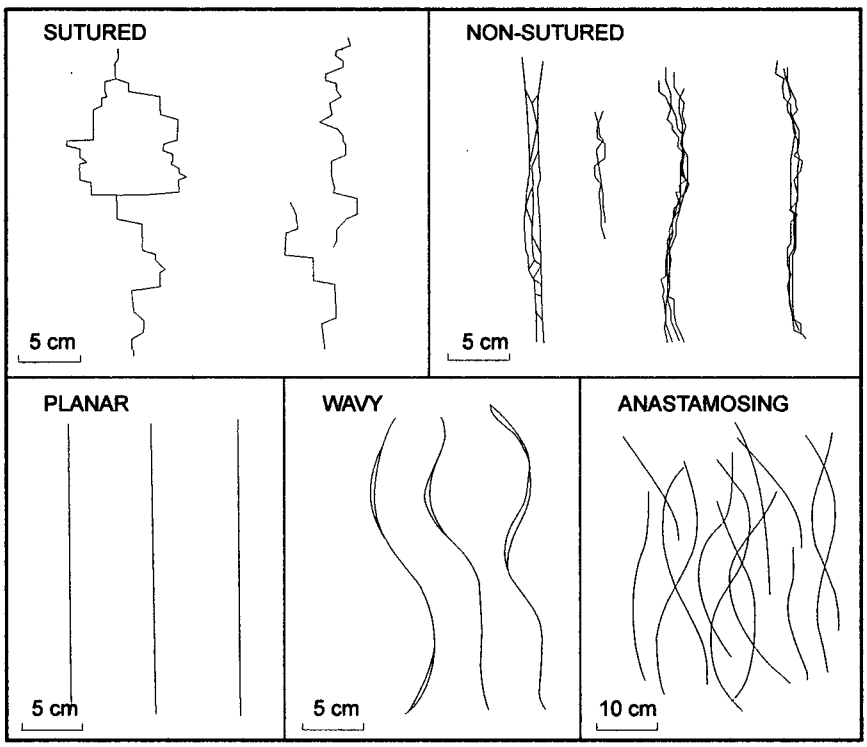

Figure 3.1b Patterns of varying types of disjunctive cleavage. From *Engelder and Marshak* [1985].

Cleavage characteristically refracts through siltstone units and more competent sandstone and conglomerate layers [*Twiss and Moores*, 1992]. Within the region of study this is expressed as a 10-15° difference towards the fold hinge between conglomerate and siltstone units.

3.1.2 Transected cleavage

A number of folds within the region display cleavage which is not axial planar but transects the fold at an angle. In these cases the angle of transection has been calculated using the definition of *Johnson* [1991]. The lack of axial surface data for most folds within the area requires that two of the three transection angles are measured with respect to the limb-bisecting plane instead of the axial surface (this is identified by the * following the angles t and d). Angle t* is defined by *Johnson* [1991] as the angle between the limb-bisector plane and the mean cleavage plane measured within the plane normal to the limb-bisector plane (Figure 3.2). The angle t* gives an estimate of the variation between the trend of the fold and the strike of the cleavage. d* is the angle between the limb-bisector plane and the mean cleavage plane within the profile plane (Figure 3.2). Angle d* gives an estimate of the variation between the dip of the cleavage and the dip of the assumed position of the axial plane. Without knowing the true strike and dip of the axial surface these two angles only provide an estimated value of transection. A third angle Δ is the angle between the trend of the fold axis and the strike of the mean cleavage plane measured within the plane normal to cleavage (Figure 3.2). The angle Δ gives the degree of transection, while the angle t* describes the direction of transection with respect to the trend of the fold axis. The direction of transection is defined by placing the fold axis on the north-south axis, of an equal angle stereonet (Figure 3.2b), if the angle t* is located in the northeast or southwest quadrants then transection is clockwise, conversely if t* is located in the northwest or southeast quadrants then transection is counter-clockwise.

3.1.3 Fractures

Systematic fracture sets are common throughout the study region. These differ from cleavage, having a less consistent separation between planes and a predominance of conjugate fractures.

Fractures have been interpreted within an orthogonal system of co-ordinates related to fold geometry and bedding orientation [*Price,* 1966]. Three axes are used to define the orientation of fractures relative to folding; a, perpendicular to the fold axis within the bedding plane, b, parallel to the fold axis and having the same orientation regardless of attitude of folded surface and c, perpendicular to bedding plane (Figure 3.3a). Throughout the study area

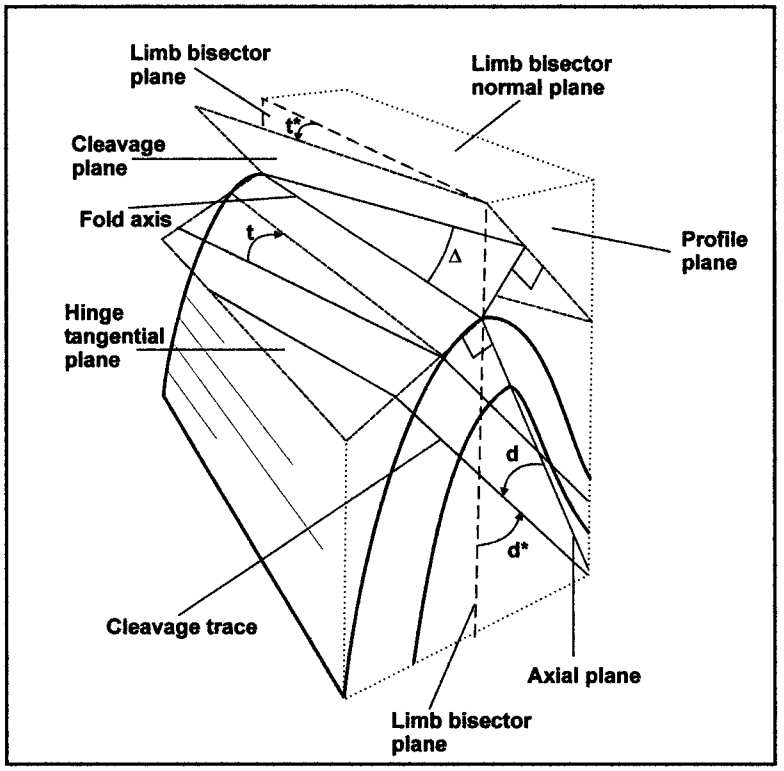

Figure 3.2a Theoretical asymmetric fold with non-coincident fold axial plane and limb-bisector plane. Transection angles relative to axial plane (d and t) and relative to limb-bisector plane (d* and t*). Angle Δ remains of constant magnitude regardless of which system is used. Modified from *Johnson* [1991].

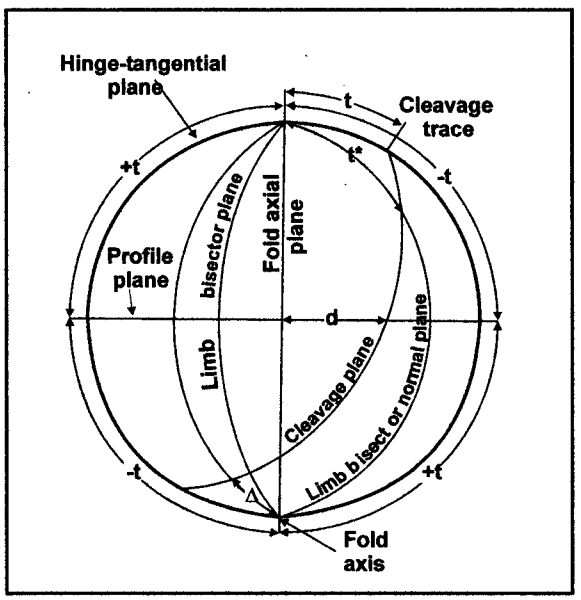

Figure 3.2b Lower-hemisphere equal-area projection showing main cleavage transected fold angles for a theoretical fold. +/- distinction defines sense of 'rotation'. + is counter-clockwise, - is clockwise. Modified from *Johnson* [1991].

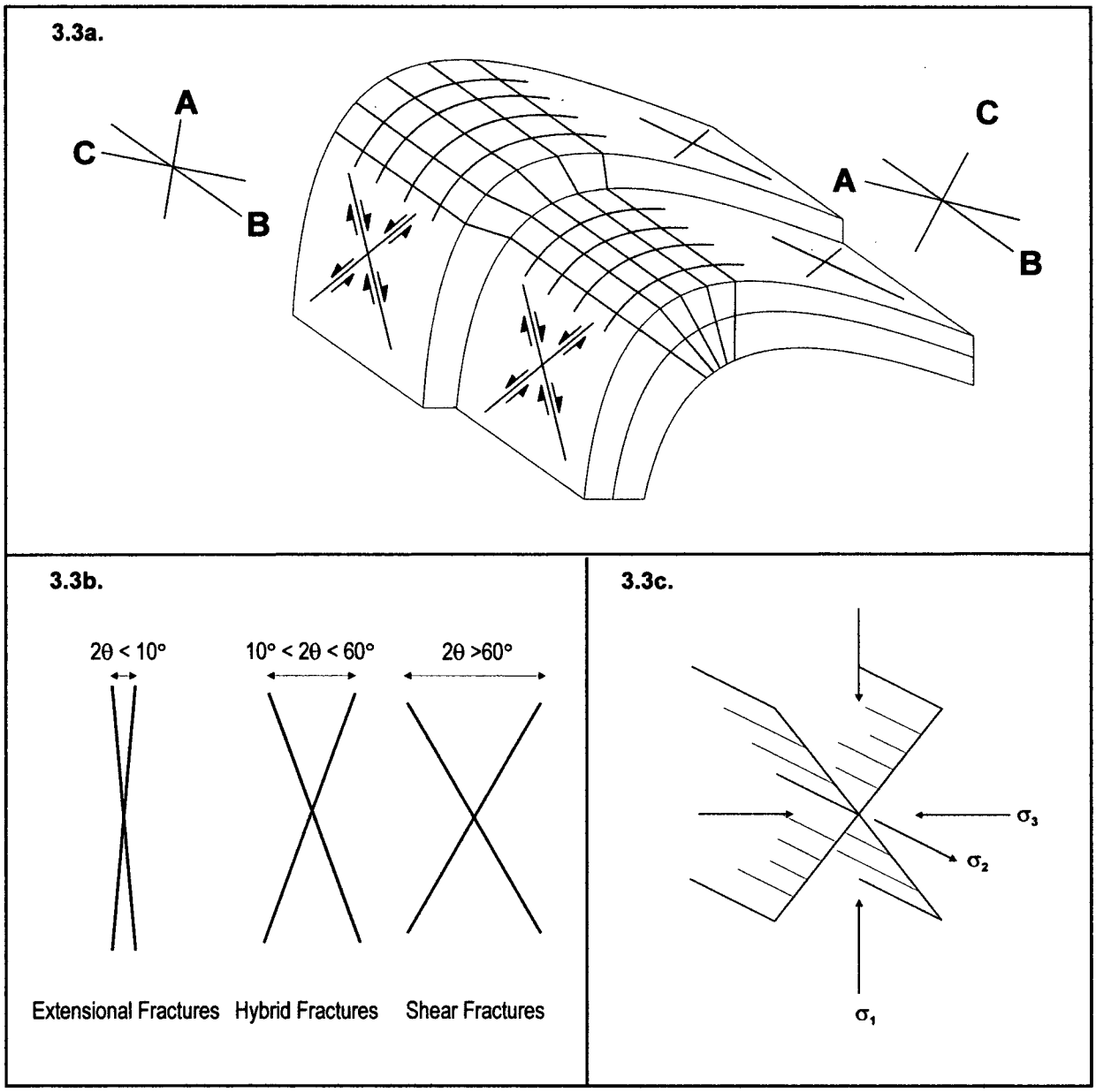

Figure 3.3 Fracture-fold relationships. a) Orthogonal system of co-ordinates relating fractures to fold geometry [*Price,* 1966]. Axis a; perpendicular to fold axis within bedding plane. Axis b; parallel to fold axis within bedding plane. Axis c; perpendicular to bedding surface. b) Definition of conjugate fractures using dihedral angle (2θ) [*Hancock,* 1986]. c) Principal stress axes for conjugate fractures.

extensional and shear fractures are frequent. These commonly separate into two main sets [*Salvini and Storti*, 2001] –

- Longitudinal fractures, within the b-c plane.
- Transverse fractures, within the a-c plane, including conjugate arrays.

Sets of fractures parallel and normal to the fold axis tend to be extensional in origin [*Price,* 1966].

Conjugate shear fractures have been defined using the classification of *Hancock,* [1985] where the dihedral angle (2θ) is used to define whether the fractures formed purely by shear movement or a combination of extension and shear movement (Figure 3.3b). Purely extensional fractures are assumed when the angle between a fracture pair is less than 10°. Hybrid fractures, a combination of extensional and shear movement generally have dihedral angles between 10 and 60°, while purely shear fracture pairs have dihedral angles >60°. The intersection lineation of the two conjugate planes indicates the direction of σ_2 (Figure 3.3c), and σ_1 the axis 90° from σ_2 within the plane bisecting the dihedral angle between the fractures.

3.1.4 Faults and veins

Faults and veins are common within the region. Faults range in length from centimetres to metres. Thin layers of quartz often overprint fault planes; in some cases these have strongly developed slickenlines. Veins are typically composed of quartz and can reach up to 5 cm wide.

3.1.5 Structural data analysis

To aid in the analysis of data, the study areas have been separated into a number of domains mainly on the basis of fold trend. Study Area 1 has been separated into six sections (Figure 3.4a) called 'domains' although these are not structural domains in the correct use of the term. They are generally separations of data into manageable groups based on location within the study area and general structural orientation. Structural domains in the correct sense are distinct areas of consistent structural orientation within a polydeformed terrane [*Mosher and Helper*, 1998]. Study Area 2 has five domains distinguishing differing sections of the basin (Figure 3.4b); these are domains using the accurate definition. Study Area 3 is not subdivided (Figure 3.4c).

Orientation data were collected for bedding, cleavage, and fractures, plus bedding-cleavage intersection and slickenside lineations, together with observations relevant to the kinematics and relative timing of structures. Structural data are presented within this thesis mainly on lower-hemisphere equal-area stereonets, plus tables listing general attributes for each structure. A comprehensive collection of structural data can be found in Appendix A.

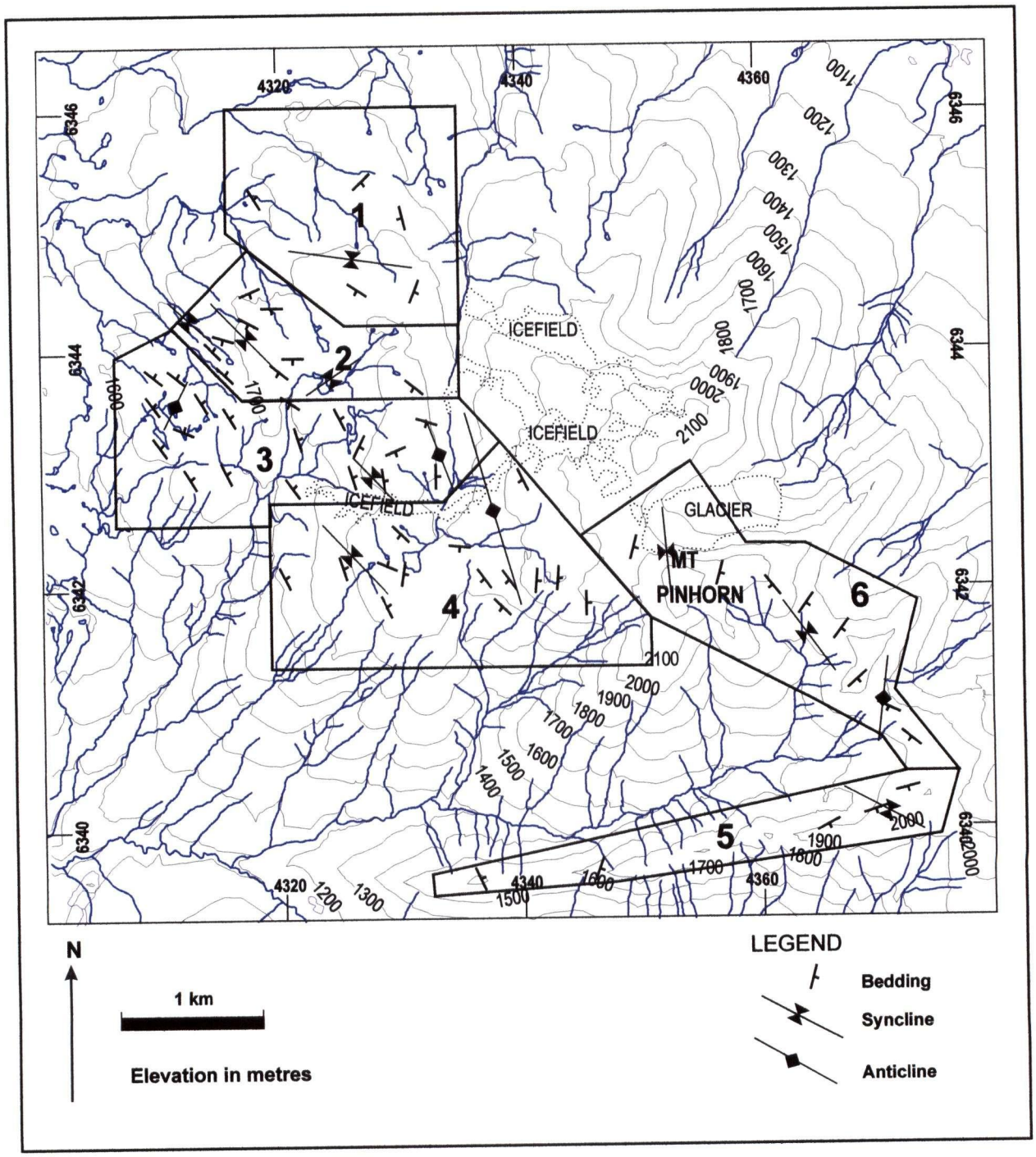

Figure 3.4a Map of Study Area 1. Black outlines indicate domains of structural data described within text. Bedding data plotted as oriented strike lines with dip direction shown.

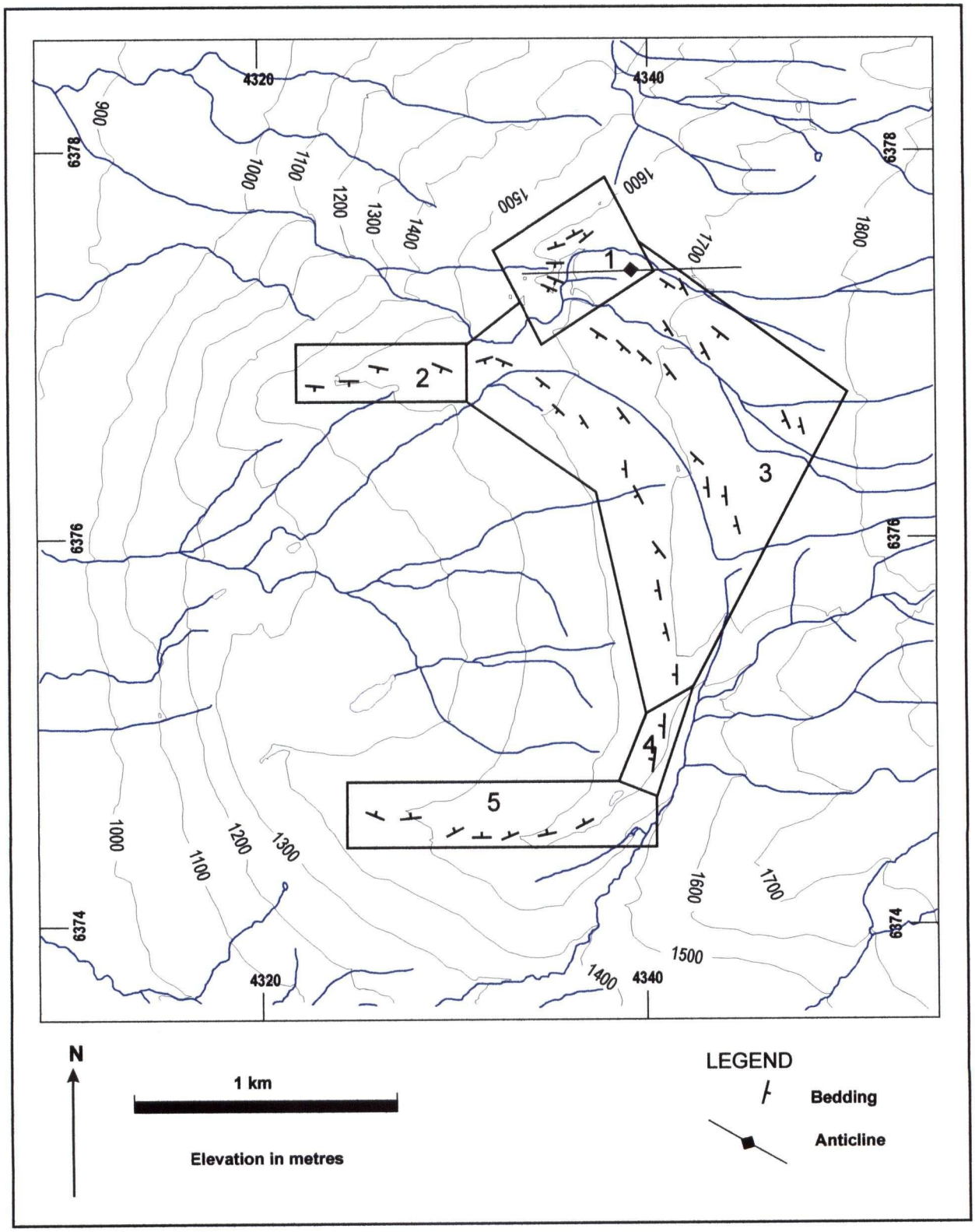

Figure 3.4b Map of Study Area 2. Black outlines identify five structural domains. Bedding data plotted as oriented strike lines with dip direction shown.

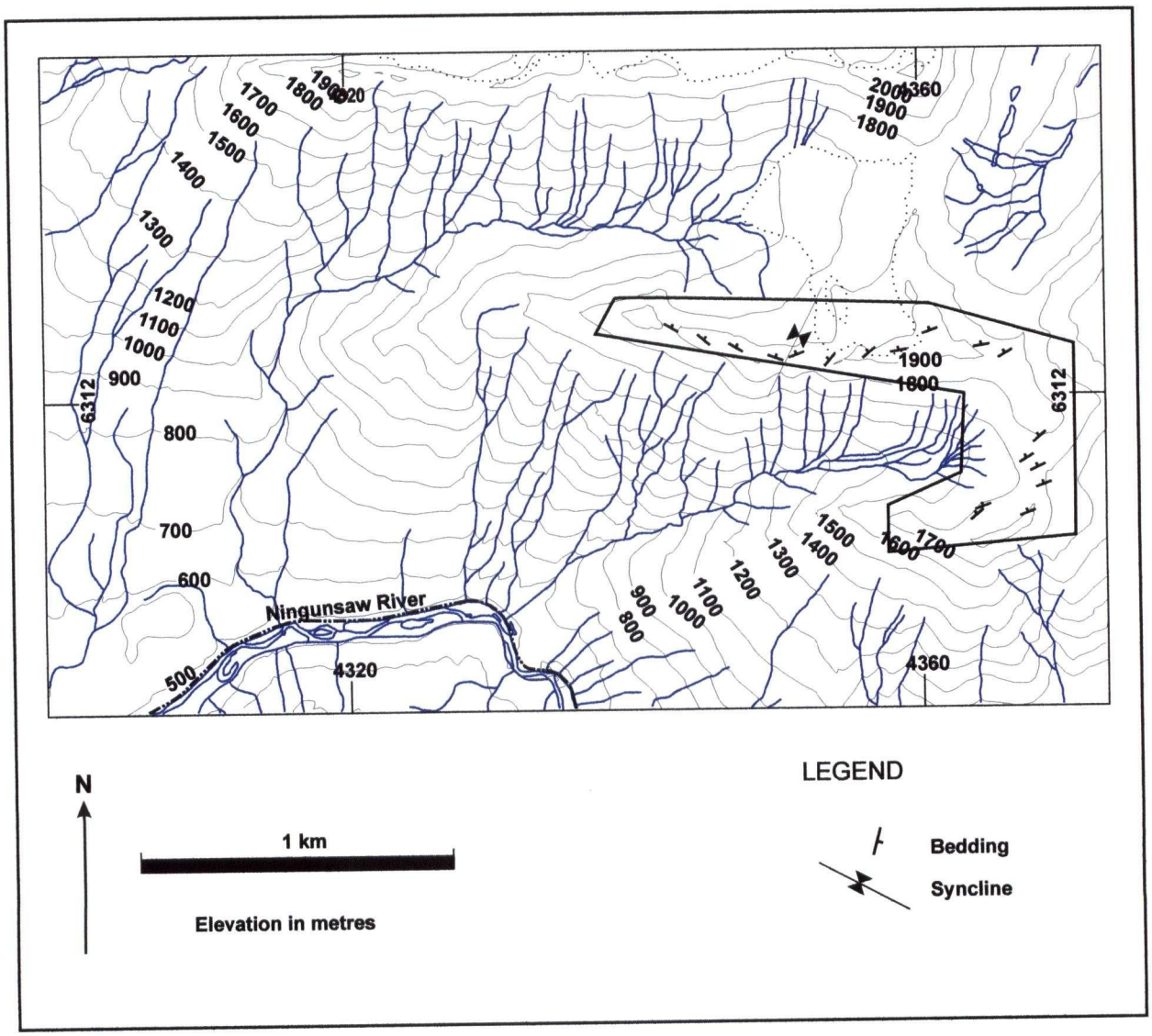

Figure 3.4c Map showing Study Area 3. Study area outlined in black, average bedding data plotted as oriented strike lines with dip direction shown.

3.2 STUDY AREA 1

Study Area 1, 40 km north of Bell II, contains distinct localities of northwest- and north-northeast-trending folds [*Evenchick,* 2001]. The purpose of structural analysis in this area is to identify in more detail these separate areas of folding and to document the structural fabrics associated with the two fold trends.

3.2.1 Lithology

The study area comprises strata of the Ritchie-Alger assemblage [*Evenchick et al.,* 2001], consisting predominantly of sandstone and siltstone units with locally abundant conglomerate. Sandstone makes up 60% of the area and is composed predominantly of chert clasts showing local iron staining within beds. The sandstones are medium to coarse-grained, with bed thickness ranging between 0.5-1.5 m. Massive, thick sandstone beds have a relatively low density of fractures and cleavage, whereas thinner beds (0.5 m thick) interbedded with siltstone units (Figure 3.5) have a relatively well-developed cleavage. Sandstone units occasionally display sedimentary structures such as channels (Figure 3.6) and undulatory bases, characteristic of marine shelf deposits. Pebbly sandstone consisting of a coarse-grained sandy matrix with rare rounded pebbles is also present. Within turbidite classification systems this type of unit is not recognised and are generally described as sandstone units [*Walker*, 1992]. Thus, for ease of analysis within this study, these units are classified as sandstones due to the very rare nature of the clasts.

Siltstone units range from a few centimetres to >0.5 m in thickness. The thicker units often show strong banding between pale yellow and dark grey layers and commonly display dramatic soft sediment deformation structures (Figure 3.7).

Conglomerate units have an average thickness of 0.5 m and are polymictic with pebble sized and smaller, predominantly chert clasts, which display a preferred orientation. Clasts of Stuhini or Hazelton Group volcanic rocks, from Stikine Terrane are also found in the conglomerate. The matrix is medium grained and is of a similar composition to the clasts. Conglomerate is interbedded with sandstones and is locally interbedded with siltstone. Conglomerate beds commonly display fining up sequences on a scale of centimetres and channel features, characteristic of turbidite deposits. Within the Ritchie-Alger assemblage, conglomerate units are present but do not produce the same large-scale units seen in the younger Skelhorne assemblage of Study Area 2.

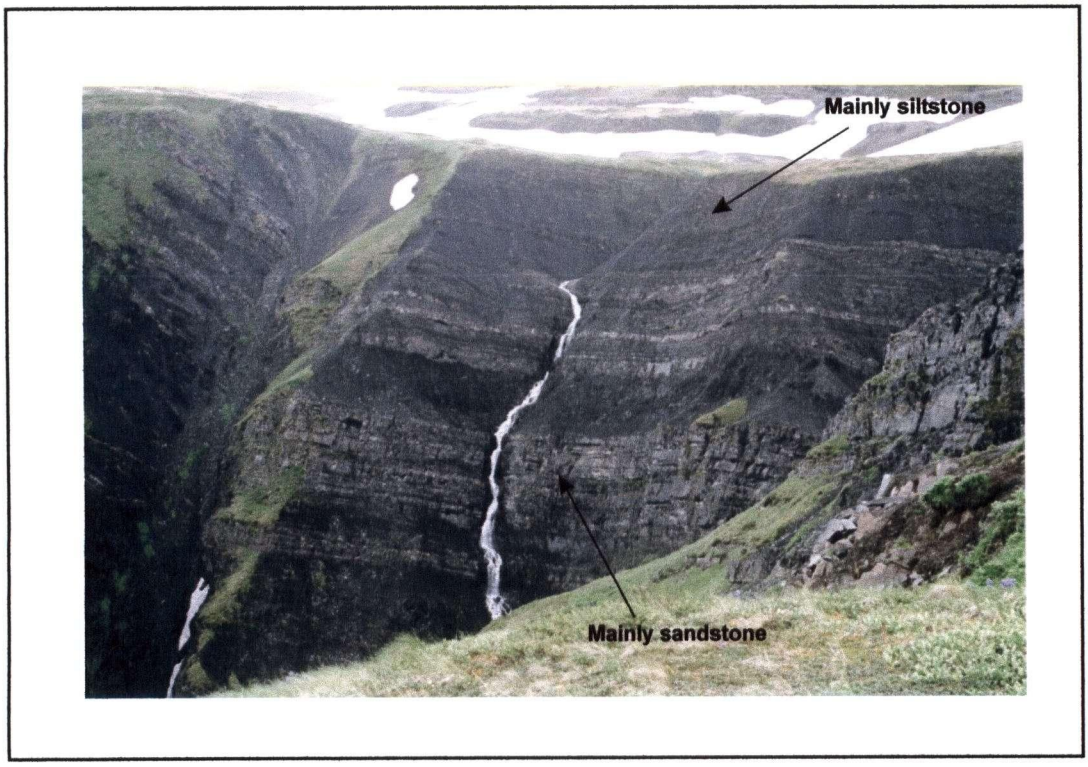

Figure 3.5 Interbedded sandstones and siltstones. Field of view = 50 m, looking southeast. Extreme northeast of study area. Domain 1, Study Area 1.

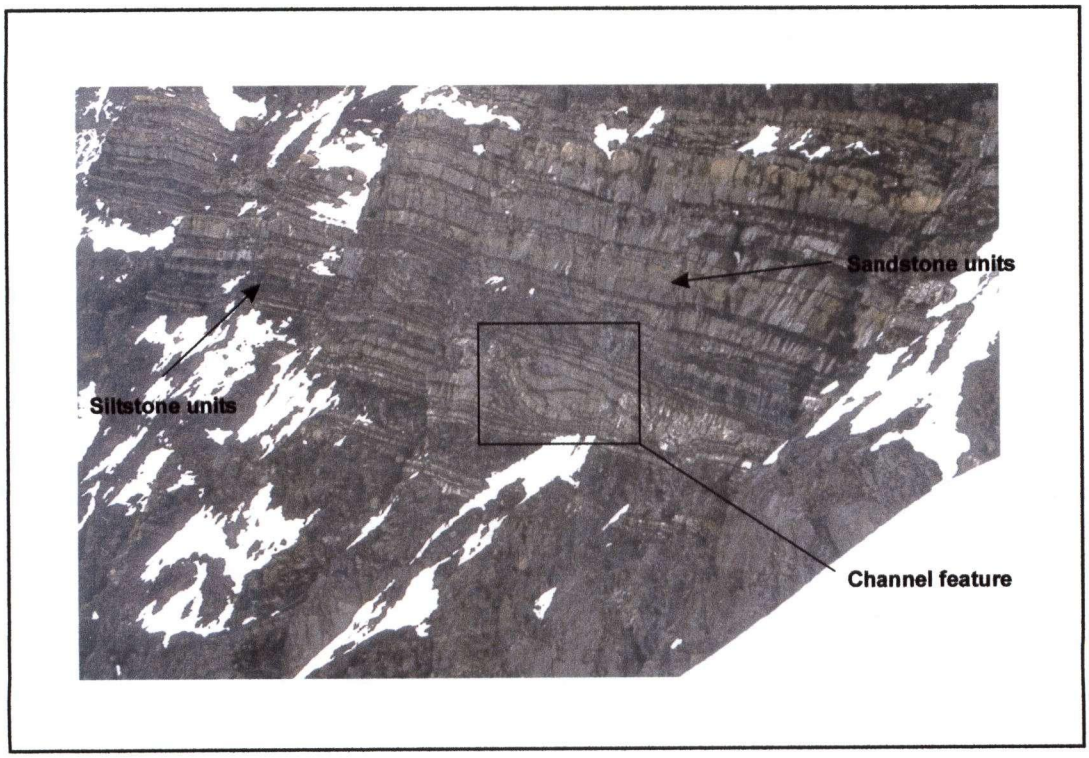

Figure 3.6 Channel feature within sandstones of the Ritchie-Alger asssemblage. Field of view = 30 m, view looking east. Box outlines sandstone channel transecting sequential bedding. Domain 6, Study Area 1.

Figure 3.7 Soft sediment deformation within siltstones. Displaying distinct banding of dark and light sediment. Domain 1, Study Area 1.

3.2.2 Structure

Within the region folds have wavelengths of ≤800 m. Northwest-trending folds are common and a number of northeast-trending folds are also present. Both fold trends have similar scale features and are easily identifiable in valley cross sections. The region also contains cleavage, fractures, faults and veins throughout.

Cleavage ranges in separation from >100 mm in conglomeratic units to <5 mm in siltstones (Figure 3.8). Cleavage cuts bedding planes and fluctuates in length from 10's mm within siltstone units to 10's cm in more competent units.

Fractures within the area vary in spacing from 1-<0.5 m and can extend up to 2 m. Fractures can be associated with veins and commonly show evidence for displacement parallel to fracture walls.

Two different vein systems have been identified within Study Area 1. Thick, vuggy veins with no consistent orientation are found in concentrated areas within the study area. Thinner veins with a more systematic morphology are found throughout the study area.

3.2.3 Domain 1

Domain 1 is located in the north-central area of the plateau northwest of Mount Pinhorn (Figure 3.4a). Massive sandstone units and interbedded siltstone and sandstone sequences dominate the area, these beds range in thickness from 0.1-<0.5 m. The domain contains an east trending fold, cleavage is well developed and fractures and veins are common (Figure 3.8a).

East-trending fold: Bedding data describe a syncline plunging 12° towards 098 (Figure 3.9a), verging to the south (Figure 3.10). The southern limb dips 28°N while the northern limb dips 19°S (Table 3.1). Cleavage strikes between 130 and 165 (Figure 3.9a). Cleavage transects the fold by 43° in a counter-clockwise direction. Fanning of cleavage due to lithology is present with cleavage dipping ~10° less in siltstone units than sandstone (Table 3.1).

Fractures: The main group of fractures is oblique to the fold axis by a mean value of 43° (Table 3.2) and is normal to the western limb of the fold (black diamonds, Figure 3.9b). One pair of conjugate shear fractures was recorded in the field, striking 007 and 082 (Figure 3.9c), this gives a northeast oriented σ_1 (Table 3.2).

3.8a.

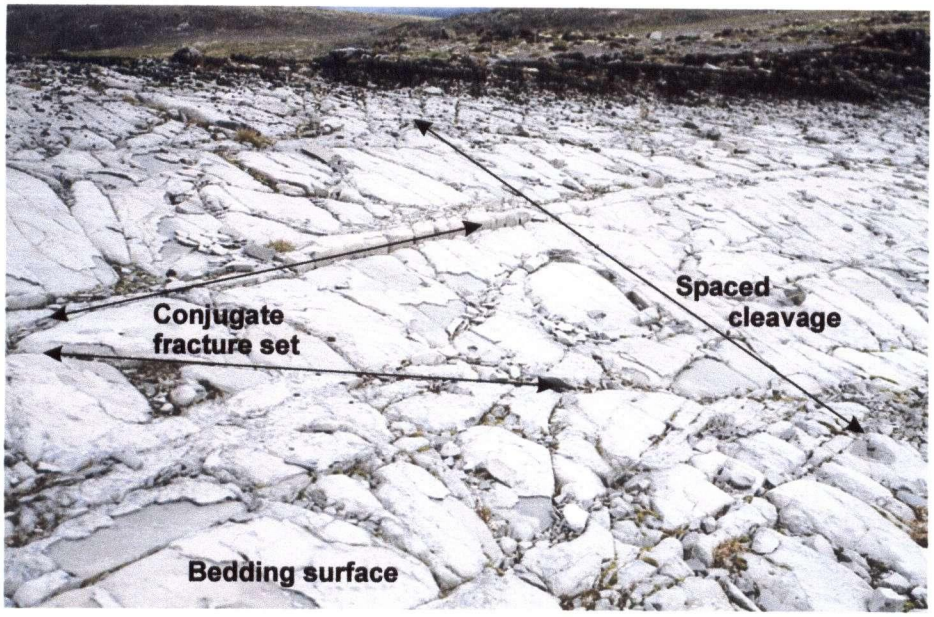

3.8b.

Figure 3.8 Fracture-cleavage relationships. a) Spaced cleavage and conjugate fracture sets in sandstone. Cleavage has systematic 200 mm separation. Domain 1, Study Area 1. b) Spaced cleavage and conjugate fracture set within siltstone. Cleavage has separation of ≤10 mm. Bedding is subhorizontal. Domain 2, Study Area 1.

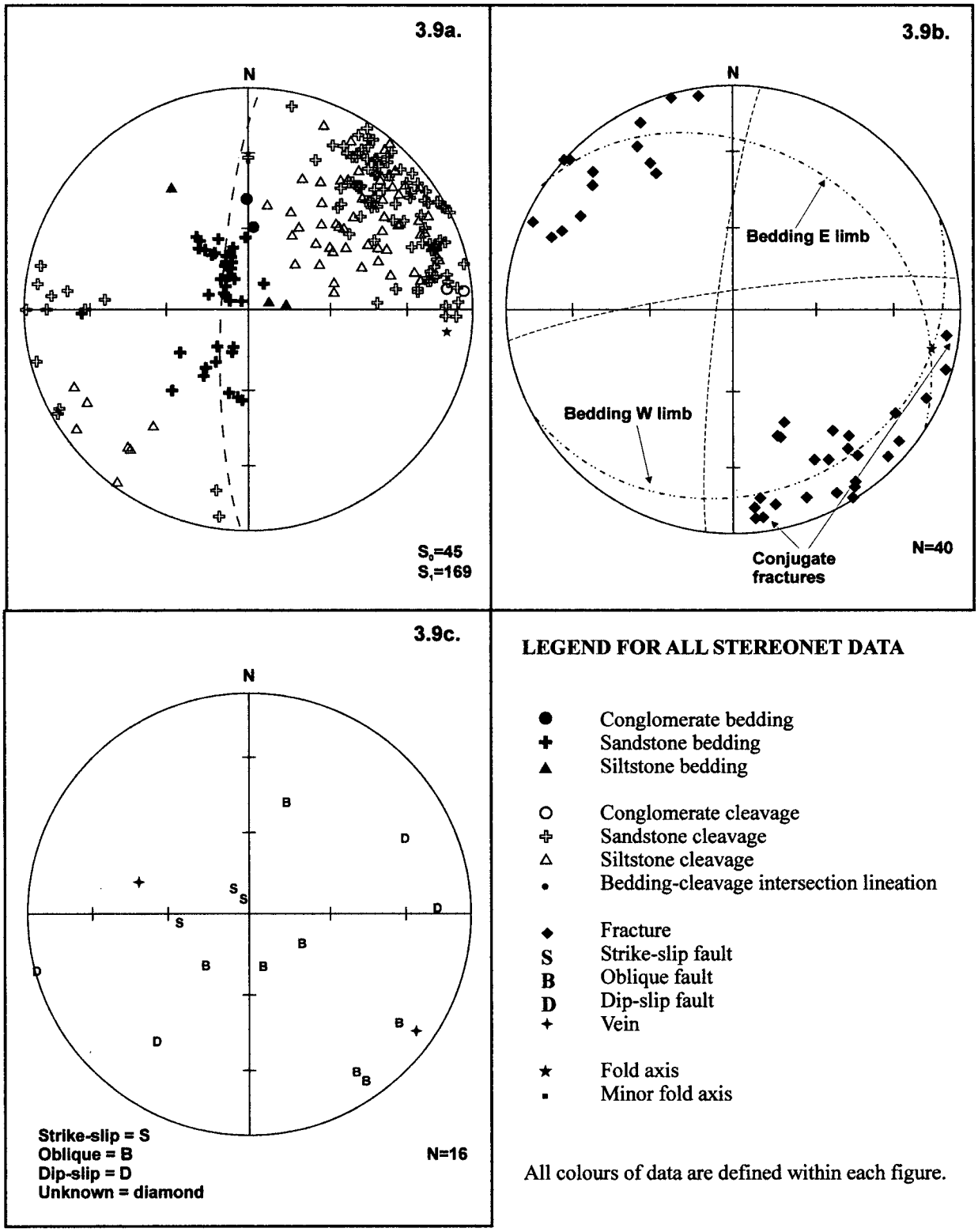

Figure 3.9 Study Area 1, Domain 1, east-trending syncline. a) Bedding and cleavage data. Fold axis trend and plunge 098/12°, b) fracture data, d) fault and vein data, defined by slickenside orientation on fault planes.

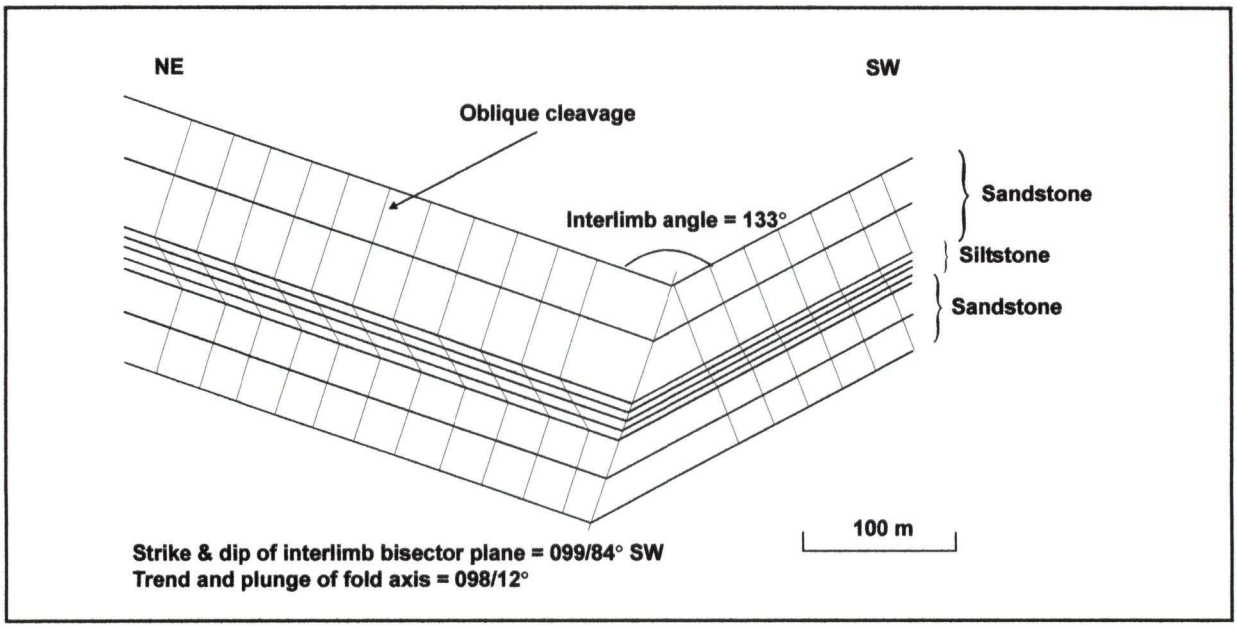

Figure 3.10 Down plunge view of east-trending syncline, identified from stereonet analysis. Drawing is constructed using mean values for bedding and cleavage within separate lithologies for each limb of fold. Construction method from *Marshak and Mitra* [1998]. Cleavage transects fold by 43° counter-clockwise. Profile plane = 008/78°NW. Domain 1, Study Area 1.

Figure 3.11 Folded veins within sandstone unit, southeastern corner of Domain 1, Study Area 1. Bedding oriented normal to vein. View looking west. Pencil for scale.

Faults and veins: The three main types of faults are observed in the domain (Figure 3.9c), crosscutting fractures and cleavage. Shallowly dipping veins (average dip 14°) with slickensides on surfaces are parallel to bedding, suggesting they are a product of bed parallel slip. A number of faults of varying strike and dip have slickensides that indicate oblique movement in varying directions (Table 3.3). A third group of steeply dipping faults (dip >60°) have slickensides plunging >60° indicating predominantly dip-slip movement. The extreme southeast of the domain contains a high density of quartz veins within massive sandstone. The majority of veins are oriented at a high angle to bedding with a small number of veins parallel to bedding. Veins oriented normal to bedding and parallel to the fold trend are typically tightly folded. An observed fold in a vein has a fold axis which trends 100 and plunges 10° SE (Figure 3.11). The vein has a slickensided surface and these lineations trend northeast. These folds are interpreted to be parasitic folds, implying that vein formation predates or is synchronous with folding.

Table 3.1 Bedding and cleavage data for Domain 1, Study Area 1. See Figure 3.9a.

LOCATION	LITHOLOGY	BEDDING	CLEAVAGE		
		Average strike/dip	Average strike/dip	Spread in orientation[1]	Spread in dip[1]
South limb	Sst 100%	124/28°NE	145/73°SW	69°	40°
North limb	Sst 76% Slst 24%	064/19°SE	Slst 141/62°SW Sst/Co 153/78°SW	58° 71°	99° 79°

[1] Calculated from opposing extremes of cluster.

Table 3.2 Fracture data for Domain 1, Study Area 1. See Figure 3.9b.

LOCATION	FRACTURES				
	Number	Average strike/dip	2θ angle	Style	Orientation of σ_1
	38 2	055/84°NW 007/84°NW & 082/83°NW	- 84°	Extensional - oblique Conjugate shear	- 0°/050

Table 3.3 Fault data for Domain 1, Study Area 1. See Figure 3.9c.

LOCATION	FAULTS & VEINS				
	Number	Orientation	Average plunge/trend	Style	Number of veins
	3	173/26°NE, 069/6°SE, 057/11°SE	6°/162, 0°/075, 2°/070	Bed-parallel	3
	7	029/22°NW, 075/20°NW, 130/25°NE, 055/81°NW, 109/44°SW, 036/72°NW, 056/75°NW	14°/244, 11°/044, 25°/048, 25°/051, 44°/187, 14°/220, 29°/047	Oblique	
	4	126/60°NE, 154/67°SW, 165/89°NE, 187/74°SW	59°/023, 69°/239, 89°/090, 75°/247	Dip-slip	

3.2.4 Domain 2

Domain 2 consists of massive sandstone units in the north (1 m thick). Towards the south and west, sandstone is increasingly interbedded with thin siltstone or conglomerate beds (~0.5 m thick). Domain 2 contains two northwest-trending folds and one northeast-trending fold. Quartz veins are prevalent throughout the area with a number of areas containing folded vein systems.

Northwest-trending folds: An asymmetric, open, syncline plunging 7° towards 132 with an interlimb angle of 83° is located in the northwest of the domain (Figure 3.12a). The southwest limb dips steeply at 70°NE and the northeast limb dips at 15°SW (Figure 3.13a; Table 3.4). Cleavage associated with this fold strikes 112 (SW limb) and 142 (NE limb) and is approximately axial planar. Bedding data 200 m to the northeast describe a syncline with an axis plunging 13° towards 142. Along-strike towards the southeast, a second data set describes a syncline plunging 26° towards 131. Field observations suggest this is the same syncline with an average plunge of 20° towards 136 and an interlimb angle of 103° (Figure 3.12a). The geometry of the two data sets is slightly different with the fold limbs in the north dipping at 50° while in the south one limb dips at 30° and the other near 60° (Figure 3.13b; Table 3.4). Cleavage located on this syncline strikes between 135 and 127 (SW limb) and 123 (NE limb) (Table 3.4) and is axial planar. Fanning of cleavage due to lithology is well defined within the syncline (Figure 3.13b), cleavage within siltstone units is ~15° shallower than within sandstone units. Bedding-cleavage intersection lineations for northwest-trending folds in Domain 2 trend predominantly southeast and have 50° of spread in trend in the southeastern quadrant (Figure 3.14a).

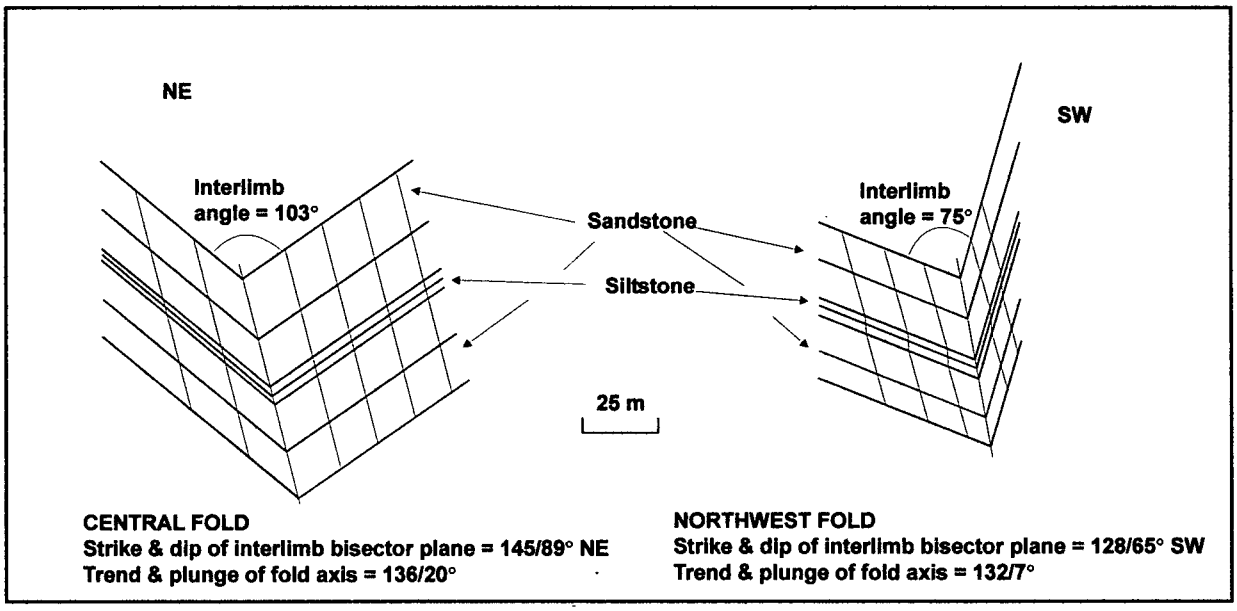

Figure 3.12a Down plunge view of bedding and cleavage relationships within the northwest trending folds, observed in the field. Central fold, profile plane = 045/70° NW. Northwest fold, profile plane = 042/83°NW. Domain 2, Study Area 1. Cleavage is axial planar.

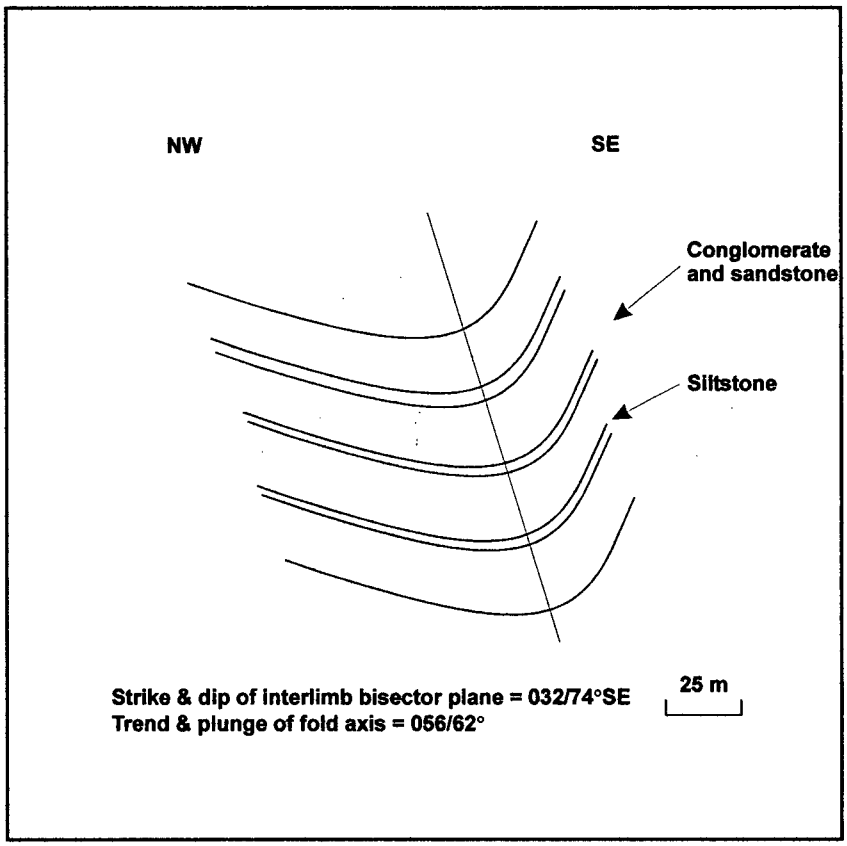

Figure 3.12b Down plunge view of northeast trending fold, observed in the field. Cleavage transects fold by 53° counter-clockwise. Profile plane = 146/38°SW. Domain 2, Study Area 1.

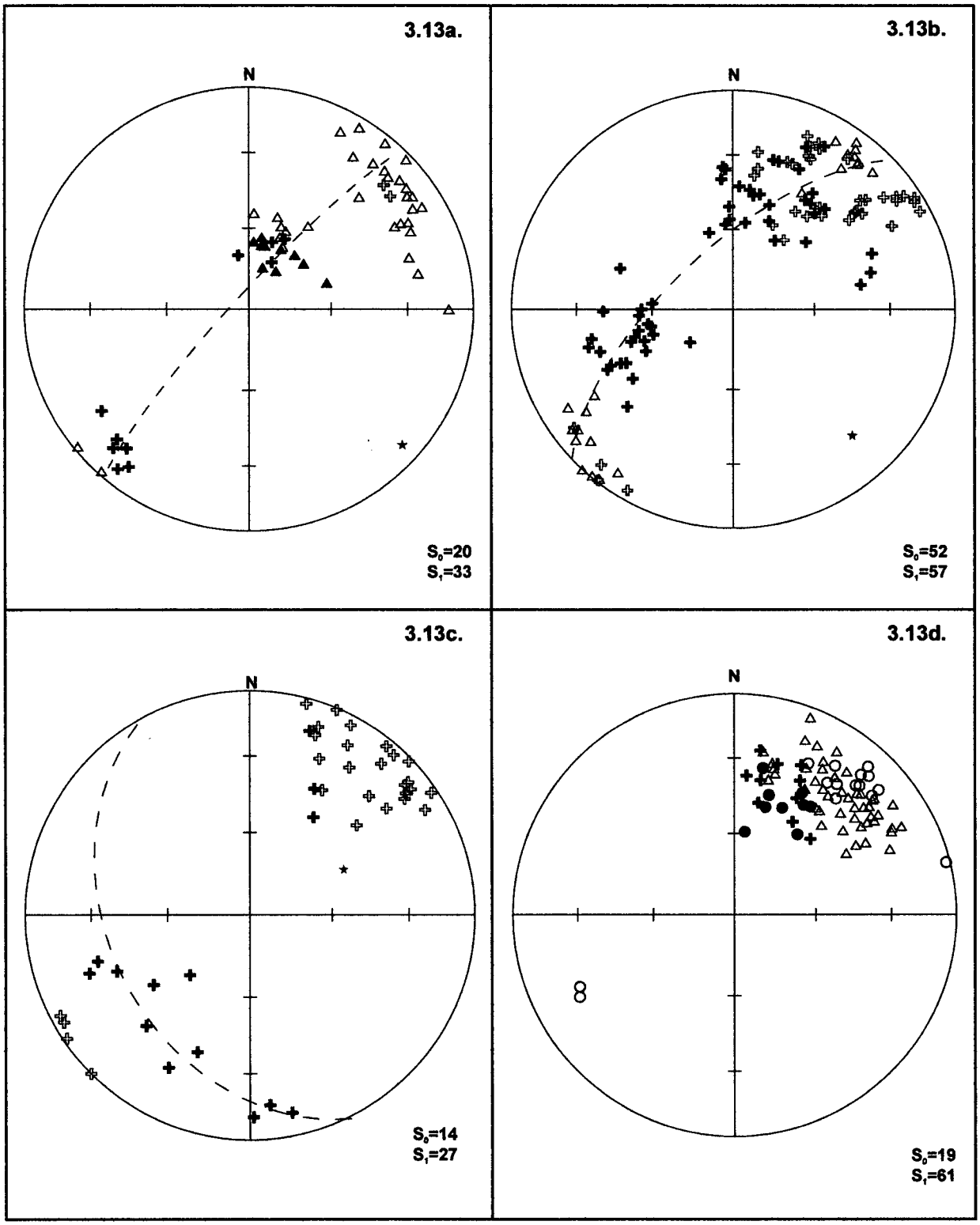

Figure 3.13 Study Area 1, Domain 2, bedding and cleavage data. a) Data from extreme northwest of domain, describing northwest trending syncline, fold axis trend and plunge: 132/7°. b) Data from centre of domain, describing northwest trending syncline, fold axis trend and plunge: 136/20°. c) Data from southern-centre of domain, northeast trending syncline, fold axis trend and plunge: 064/52°. d) Data from extreme east of domain.

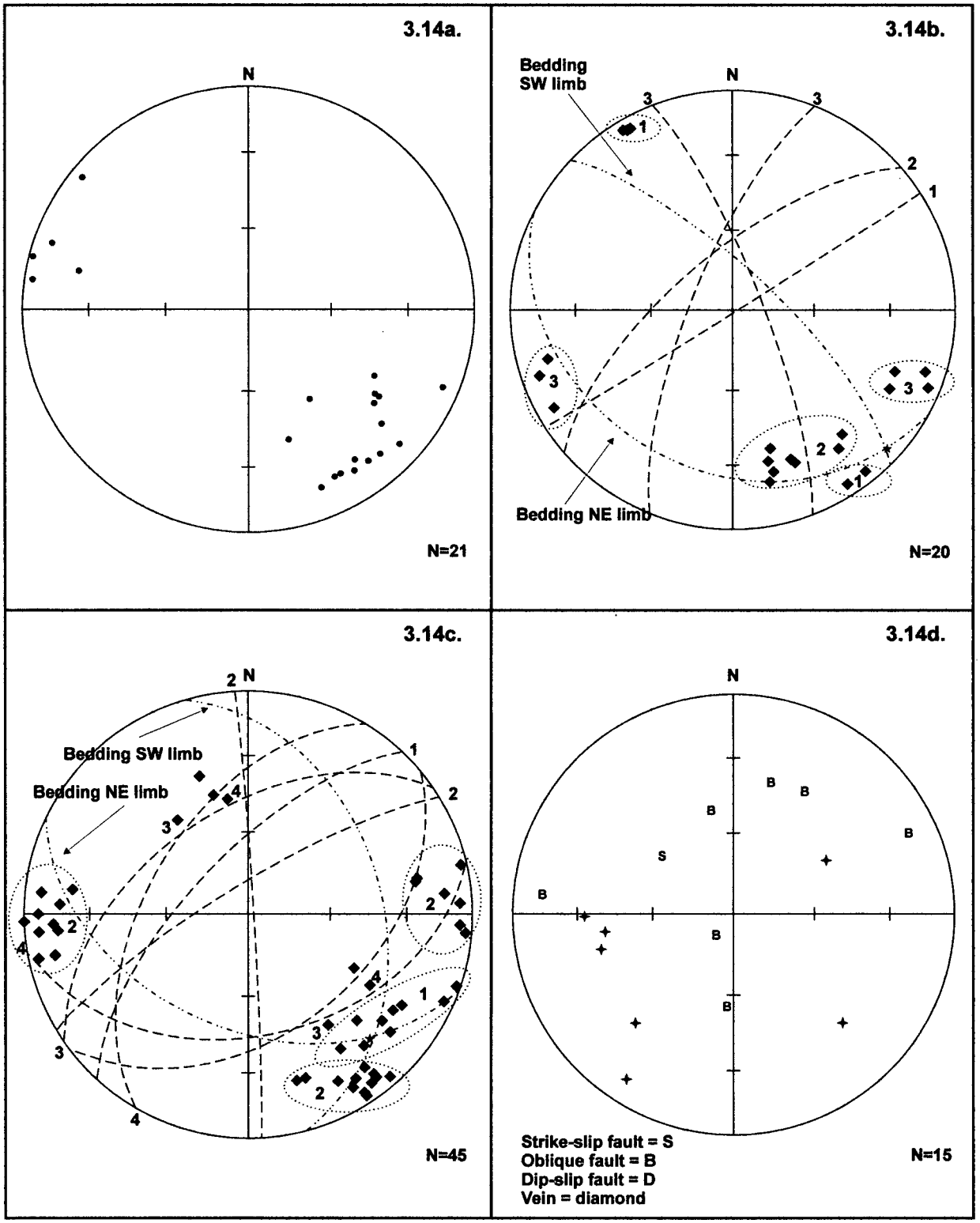

Figure 3.14 Study Area 1, Domain 2. a) Bedding-cleavage intersection lineations from northwest-trending folds. b) Fracture data from northwest-trending syncline in extreme northwest of domain, colours define geometric groups described in text. c) Fracture data from northwest-trending syncline, both northern and southern exposures, colours define geometric groups described in text, d) all fault and vein data, style of faults defined by orientation of slickensides on fault surfaces.

Northeast-trending fold: In the south of the domain, a northeast trending syncline plunges 52° towards 064 (Figure 3.13c), verging towards the northwest. The limbs of this fold are non-planar (Figure 3.12b) and the fold therefore looks very different to those present in the west of the domain. Cleavage across the fold is northwest striking (Figure 3.13c) and transects the fold by 53° in a counter-clockwise direction. The extreme east of the domain contains bedding dipping towards the southwest and appears to be unrelated to other structures within the domain.

Fractures: The most westerly northwest-trending fold in the domain contains a small number of fractures (Table 3.5). Extensional fractures in the a-c plane (Figure 3.3a) (1, Figure 3.14b) are present. A number of hybrid fractures are oriented 74° from the fold axis and normal to bedding (2, Figure 3.14b). A second set have a 2θ angle of 43° (3, Figure 3.14b), these have a σ_2 axis plunging 57° towards 357 and suggest a north-south σ_1 axis. Fractures spatially associated with the central northwest-trending syncline (Table 3.5) include extensional fractures in the a-c plane (1, Figure 3.14c). A second group of fractures (2, Figure 3.14c) are oriented 62° from each other, these have a σ_1 axis oriented northeast-southwest. Conjugate fracture pairs with a 2θ angle of 84° (3, Figure 3.14c) are normal to bedding on the northeastern limb and have a vertical σ_1 axis. This indicates a vertical compression direction and is likely to be a product of post deformation exhumation. A hybrid fracture pair were observed in the field (4, Figure 3.14c), these fractures are normal to bedding on the southwestern limb and have a σ_1 direction plunging 48° towards 178 (Table 3.5). A small number of fractures were recorded in the southern area of the domain near the northeast trending fold, no patterns can be identified due to the small number (Table 3.5). Fractures from the extreme east of the domain have a similar distribution to those associated with the two synclines to the west.

Faults and veins: Faults have no pattern throughout the domain (Figure 3.14d). Slickensides record oblique movement on the fault planes (Table 3.6). No faults were observed in the northwest of the domain but a high density of quartz veins are present throughout the domain, these are particularly well developed in the northwest. En-echelon vein sets varying in length from 1-10 cm are common, examples record sinistral movement in a northeast-southwest orientation and dextral movement in a northwest-southeast orientation, suggesting north-south contraction across the area. The majority of veins within these large systems have a geometry of thin (~ 5 mm) veins arranged in parallel, striking ~060, with very thin veins oriented obliquely to the main system (strike, ~020). The eastern area of the domain contains concentrated areas of

thick (10-15 cm) vuggy veins (Figure 3.15). These commonly show evidence of deformation including a folded vein with a fold axis plunging 20° towards 143, parallel to the large syncline present in the northwestern and central areas of the domain.

Table 3.4 Bedding and cleavage data for Domain 2, Study Area 1. See Figure 3.13.

LOCATION	LITHOLOGY	BEDDING	CLEAVAGE		
		Average Strike/Dip	Average Strike/Dip	Spread in orientation[1]	Spread in dip[1]
Western fold	Sst 50% Slst 50%	133/75°NE	112/32°SW	31°	12°
		115/23°SW	142/75°SW	63°	27°
Central fold (N)	Sst 100%	163/42°NE	Sst 133/64°SW	38°	55°
		127/43°SW	Slst 133/89°SW	25°	57°
Central fold (S)	Sst 100%	165/34°NE	127/70°SW	50°	49°
		104/48°SW			
Southern fold	Sst 100%	125/56°NE	132/79°SW	44°	43°
		115/57°SW			
East of domain	Cg 47% Sst 53%	112/49°SW	133/65°SW	58°	28°

[1] Calculated from opposing extremes of cluster.

Table 3.5 Fracture data for Domain 2, Study Area 1. See Figure 3.14b and c.

LOCATION	FRACTURES				
	Number	Average strike/dip	2θ angle	Style	Orientation of σ_1
Western fold	8	068/63°NW	-	Extensional	-
	5	058/89°SE	-	Hybrid Shear	-
	7	159/79°NE, 022/75°NW	43°	Hybrid Shear	33°/181
Central fold	8	044/64°NW	-	Extensional	-
	17	177/88°NE, 059/80°NW	62°	Conjugate Shear	12°/228
	2	051/44°SE, 056/52°NW	84°	Conjugate Shear	87°/243
	2	078/43°SE, 032/53°NW	46°	Hybrid Shear	48°/178
Southern fold	2	060/34°NW, 061/65°NW	81°	Conjugate Shear	vertical
East of domain	12	009/85°NW	-	?	-
	4	057/81°NW	-	?	-
	9	058/55°NW	-	Extensional	-

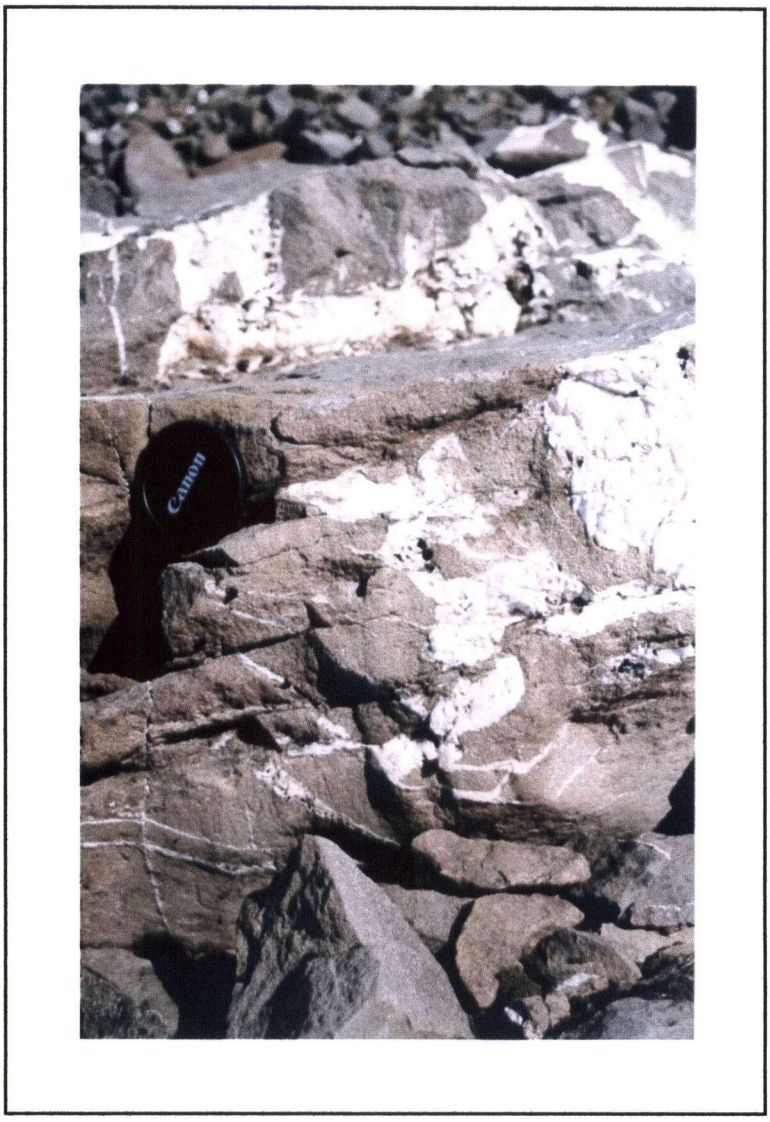

Figure 3.15 Vuggy veins in sandstone units. Veins can reach up to 5 cm width, with singular crystals >1 cm in length, view looking east. Domain 2, Study Area 1.

Table 3.6 Fault data for Domain 2, Study Area 1. See Figure 3.14d.

LOCATION	FAULTS & VEINS				
	Number	Orientation	Average plunge/trend	Style	Number of veins
	1	039/34°SE	2°/215	Strike-slip	
	4	078/40°SE, 094/34°SE, 120/54°SW, 106/52°SW,	35°/136, 12°/91, 53/235, 36°/141	Oblique	
	2	006/76°SE, 55/76°SW	38°/017, 45°/166	Oblique	
	1	130/10°NE	10°/030	Oblique	
	7	179/57°NE, 150/40°SW, 045/59°NW, 123/78°NE, 165/52°NE, 172/49°NE, 132/56°NE			7

3.2.5 Domain 3

This domain incorporates a large area in the centre of the plateau (Figure 3.4a). It is lithologically very similar to Domain 2. The amount of conglomerate decreases southward. Two northwest-trending folds are located in the eastern half of the domain, while a northeast-trending fold is located in the west.

Northwest-trending folds: In the eastern centre of the domain a syncline plunges 24° towards 136 (Figure 3.16a). The syncline has non-planar limbs and symmetric geometry (Figure 3.17a). The extreme east of the domain contains an anticline plunging 16° towards 159 (Figure 3.16b) with a southwest limb dipping 32° and a northeast limb dipping 44° (Figure 3.17a). Throughout the eastern half of the domain cleavage strikes between 139 and 171 (Table 3.7) and is axial planar to the northwest-trending folds. These folds display fanning of cleavage due to variation of lithology from sandstone into siltstone units, this varies but is normally around 10° (Figure 3.16). Bedding and cleavage intersection lineations for the northwest-trending folds dominantly trend northwest (Figure 3.17c) and show relatively diffuse distribution (~60° variation in trend).

Northeast-trending folds: A minor northeast-trending fold was identified within the eastern centre of the domain, with a wavelength of 2 m and a fold axis of 23° towards 028 (Figure 3.16b). Bedding describes a northeast-trending anticline in the west-central part of the domain (Figure 3.17b). This plunges 27° towards 044 (Figure 3.16c). The anticline verges towards the northwest and has non-planar limbs (Figure 3.17b). It resembles the northeast trending fold identified in Domain 2. In the western half of the domain, cleavage strikes between 128 and 139 and dips

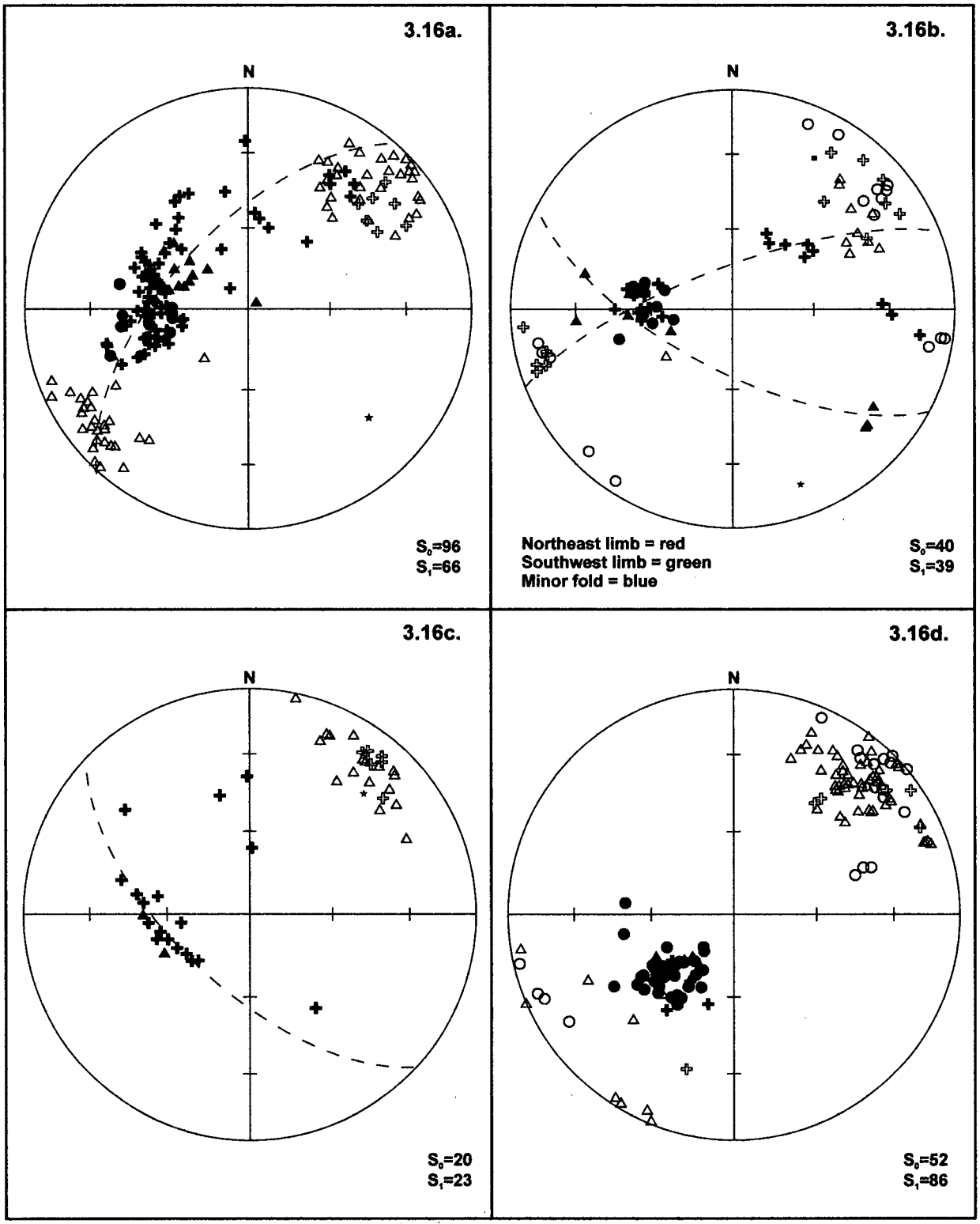

Figure 3.16 Study Area 1, Domain 3, bedding and cleavage data. a) Northwest-trending syncline from the east central part of the domain, fold axis trend and plunge: 136/24°. b) Northwest-trending anticline from the extreme eastern part of the domain, fold axis trend and plunge: 159/16°, trend and plunge of minor fold axis: 028/23°. c) Northeast-trending syncline from the west central part of the domain, fold axis trend and plunge: 044/27°. d) Data from the extreme west of the domain.

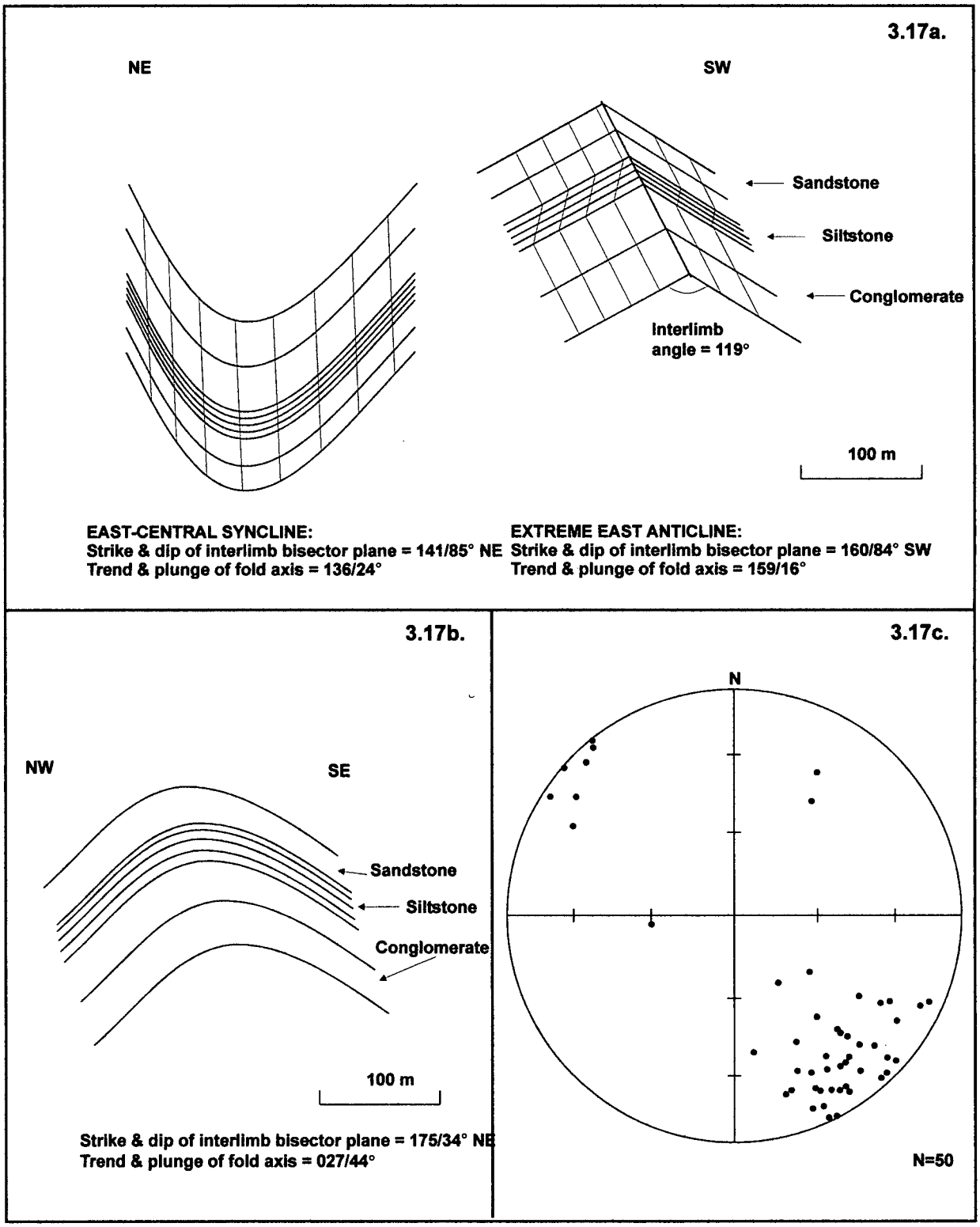

Figure 3.17 Study Area 1, Domain 3. a) Down plunge view of northwest-trending folds, observed in the field. Profile plane of syncline = 046/66°NW, profile plane of anticline = 069/74°NW, cleavage is axial planar. b) Down plunge projection of northeast trending anticline, from stereonet analysis, profile plane = 117/46°SW. c) Bedding-cleavage intersection lineations for northwest-trending folds.

~70° towards the southwest (Table 3.7). This transects the fold in a counter-clockwise direction by 82°.

Fractures: Within Domain 3 fractures are commonly steeply dipping towards the northwest (Table 3.8). All fractures are oriented in the a-c plane approximately perpendicular to the two northwest-trending fold axes and normal to bedding (Figure 3.18a-c). The average strike of fractures varies from 028 to 063 with the greatest variation seen in the western half of the domain.

Faults and veins: The orientation of faults within the domain is very variable (Figure 3.18d). Two strike-slip faults have been identified in the area both striking northeast (Table 3.9). Other faults within the area record oblique movement with varying plunge directions (Table 3.9). Faults cross cut all other features in the area. The extreme east and west quarters of the domain contain a higher concentration of veins than the centre. Vein sets tend to contain thick (>1 cm) relatively straight veins from which thin (~5 mm) veins extend at ~90° (Figure 3.19a), similar to those seen in the central area of Domain 2. There are also a number of en-echelon vein systems within the area, which extend for 0.5 m and contain veins of 5-10 mm thickness. These veins indicate dextral movement (Figure 3.19b).

Table 3.7 Bedding and cleavage data for Domain 3, Study Area 1. See Figure 3.16.

LOCATION	LITHOLOGY	BEDDING	CLEAVAGE		
		Average Strike/Dip	Average Strike/Dip	Spread in orientation[1]	Spread in dip[1]
West	Cg 73% Sst 14% Slst 13%	138/32°NE	Slst 134/74°SW	46°	75°
			Sst/Cg 141/79°SW	47°	56°
West-centre	Sst 90% Slst 10%	171/32°NE	128/73°SW	53°	21°
		068/43°SE			
East-centre	Cg 13% Sst 75% Slst 12%	017/31°SE	Slst 145/58°SW	28°	17°
			Sst/Cg 151/84°SW	79°	52°
East	Cg 20% Sst 62% Slst 18%	132/32°SW	139/86°SW	40°	79°
		005/33°SE			
		001/44°SE			
		039/68°NW			
		003/64°SE			

[1] Calculated from opposing extremes of cluster.

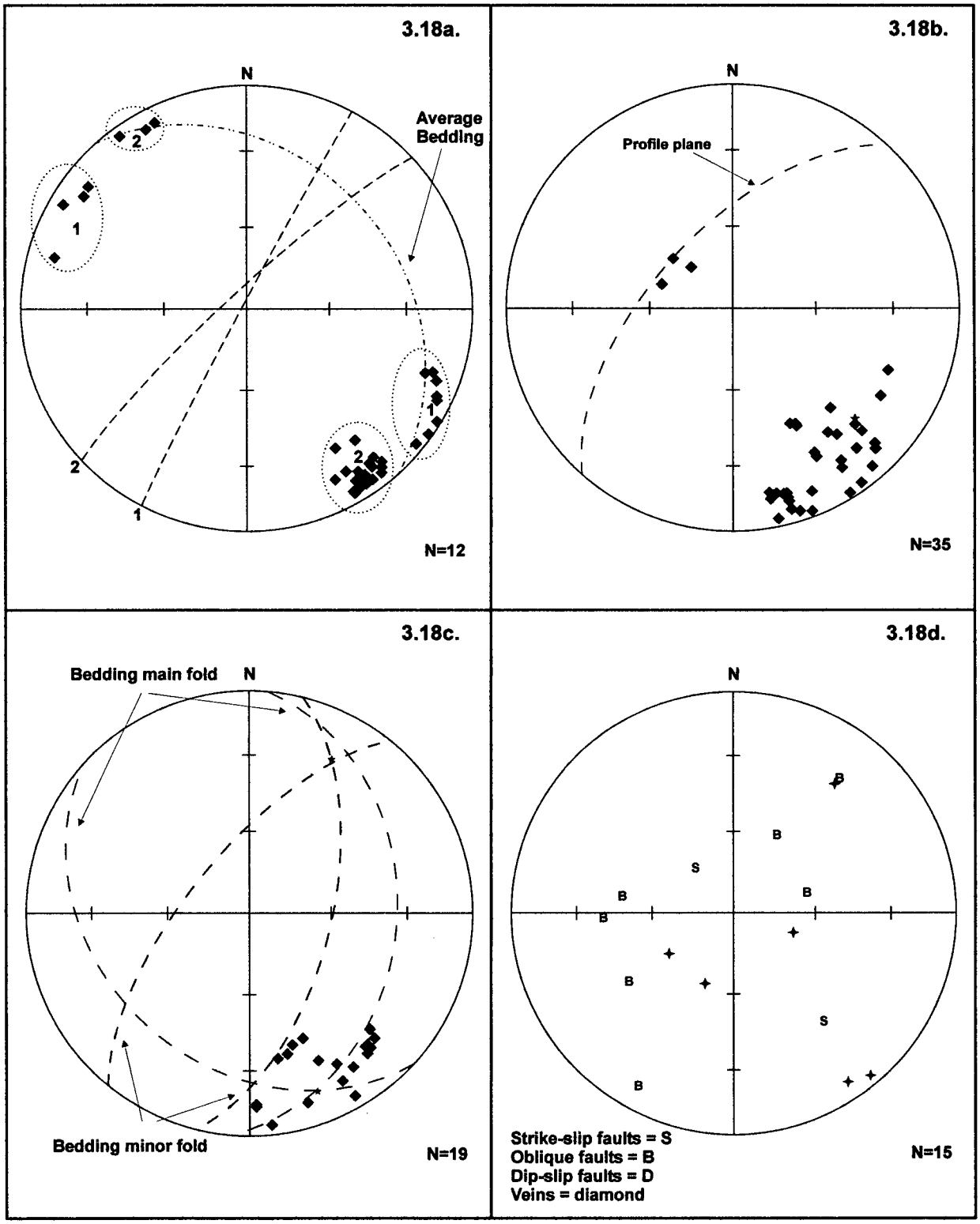

Figure 3.18 Study Area 1, Domain 3. a) Fracture data from extreme west of domain, colours define geometric groups defined in text. b) Fracture data east-central area of domain, profile plane and fold axis shown of northwest-trending fold seen in this area. c) Fracture data from extreme east of domain, fold axis and bedding data for major and minor folds in area shown. d) Fault and vein data for domain, style of faults defined by orientation of slikensides on fault plane.

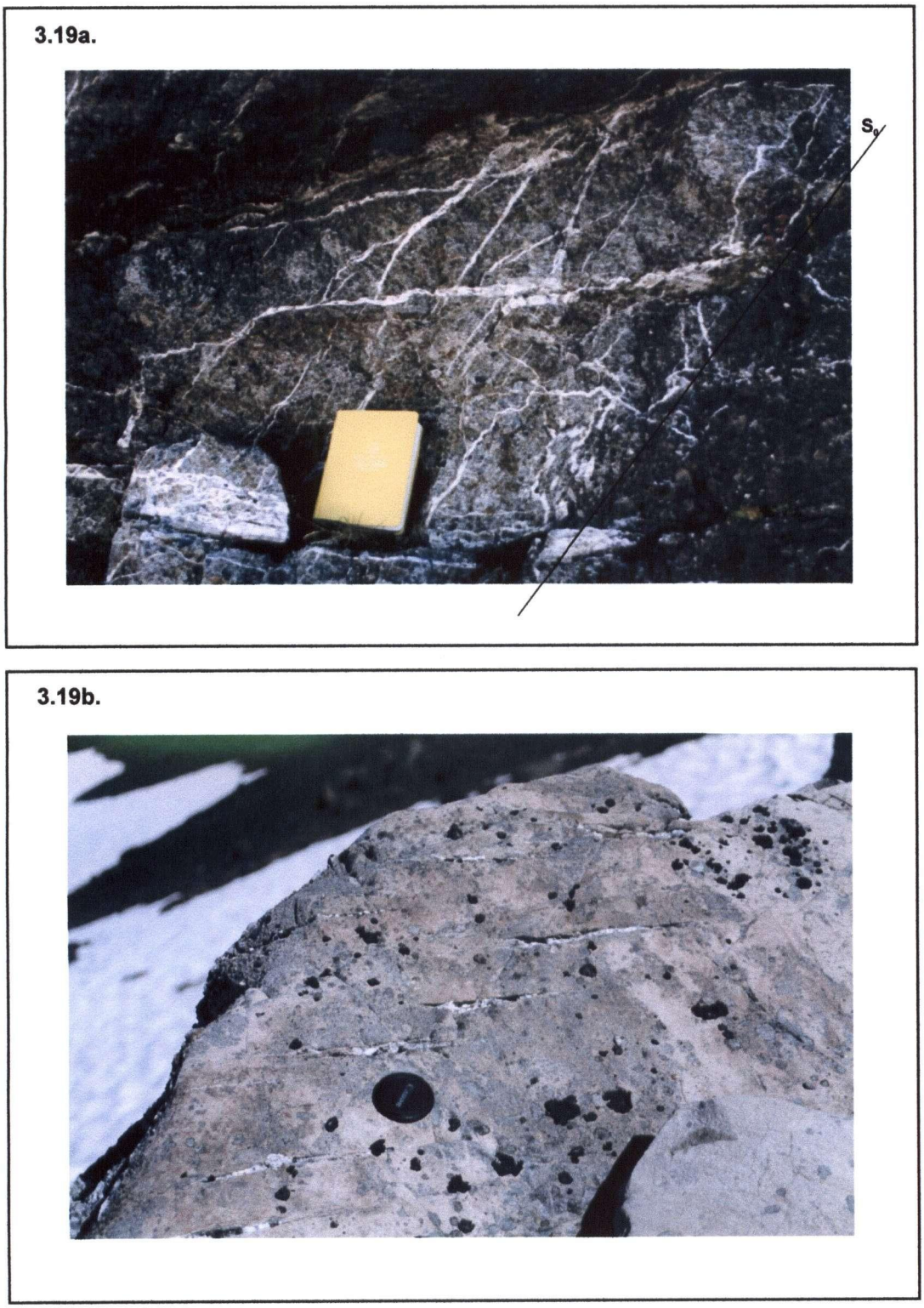

Figure 3.19 Sub-parallel vein systems averaging >1 cm width, associated with oblique interlinking veins, indicating sinistral movement. Viewed towards 076. Domain 3, Study Area 1. b) En-echelon vein set indicating dextral movement. View looking northwest, bedding is subhorizontal. Domain 3, Study Area 1.

Table 3.8 Fracture data for Domain 3, Study Area 1. See Figure 3.18a to c.

LOCATION	FRACTURES				
	Number	Average strike/dip	Maximum 2θ angle	Style	Orientation of σ_1
West	12	028/88°NW	-	Extensional	-
	25	056/81°NW	-	Extensional	-
East-centre	32	060/71°NW	-	Extensional	-
East	19	063/68°NW	-	Extensional	-

Table 3.9 Faulting for Domain 3, Study Area 1. See Figure 3.18d.

LOCATION	FAULTS & VEINS				
	Number	Orientation	Average plunge/trend	Style	Number of veins
	2	050/22°SE, 050/53°NW	4°/221, 0°/230	Strike-slip	
	7	178/49°NE, 009/42°SE, 147/47°NE, 164/28°SW, 119/78°NE, 119/33°SW, 128/66°SW	34°/142, 36°/133, 46°/072, 27°/231, 19°/303, 33°/222, 18°/300	Oblique	
	6				6

3.2.6 Domain 4

Domain 4 is located on the southern border of the plateau (Figure 3.4a) and contains a northwest-trending fold and a north-northwest-trending fold. The stratigraphy is primarily siltstone. Areas of siltstone and minor interbedded sandstone average 200 m in thickness. Individual siltstone beds average ~10 cm thickness. Conglomerate is present in the area but beds are thinner (20-30 cm) than to the north, most grade into sandstone units and are commonly interbedded with sandstones.

Northwest-trending fold: A syncline plunging 9° towards 137 (Figure 3.20a) with an interlimb angle of 102° (Figure 3.21a) is inferred in the western half of the domain from stereonet data. Both limbs have a similar dip of ~40° (Table 3.10). Near the center of the syncline on the southwest limb poorly developed slickensides are present on bedding surfaces trending northeast. Cleavage associated with the syncline strikes ~130 and dip varies between 60° and 80° (Figure 3.20a). Due to the scatter contained within the data a confident estimate of the relationship of cleavage to the syncline cannot be made. There is a strong lithologic control on the dip of cleavage, siltstone units have convergent planes while sandstone and conglomerate units contain cleavage diverging away from the centre of the fold (Table 3.10).

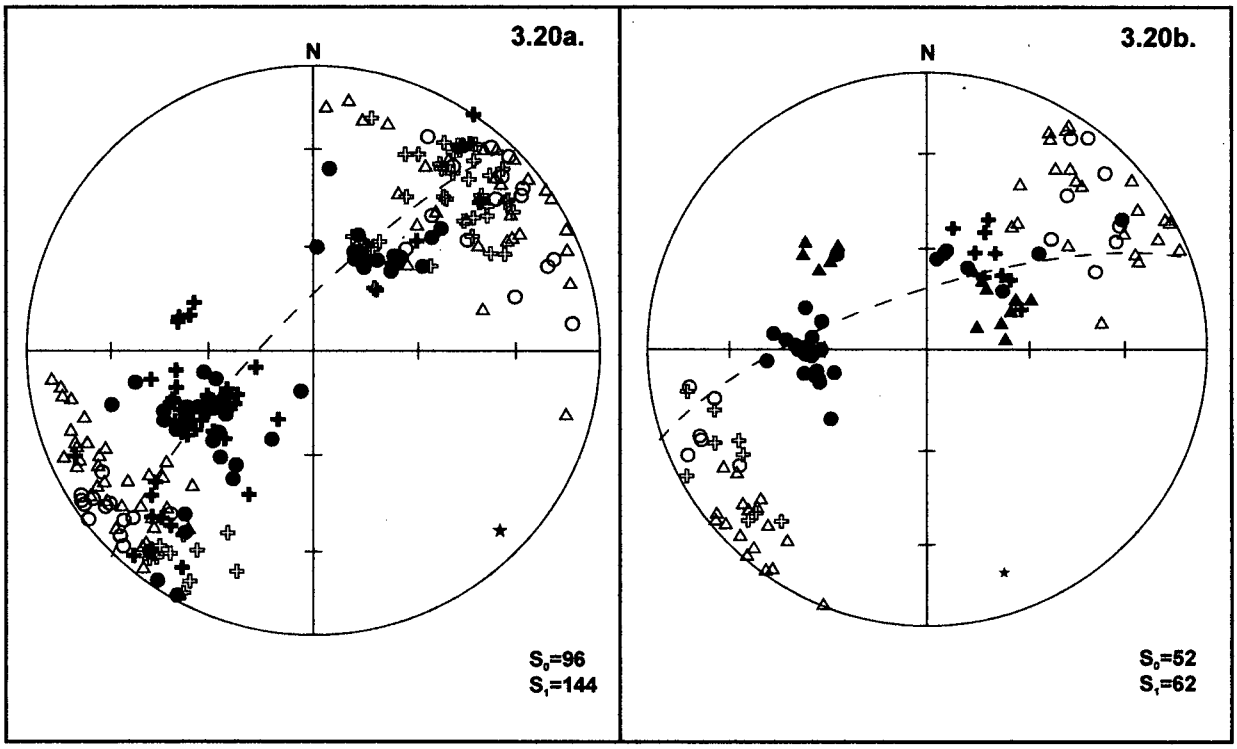

Figure 3.20 Study Area 1, Domain 4, bedding and cleavage data. a) Data from western half of domain, containing northwest-trending syncline, trend and plunge of fold axis: 137/09°. b) Data from eastern half of domain, containing north-trending anticline, trend and plunge of fold axis: 164/16°.

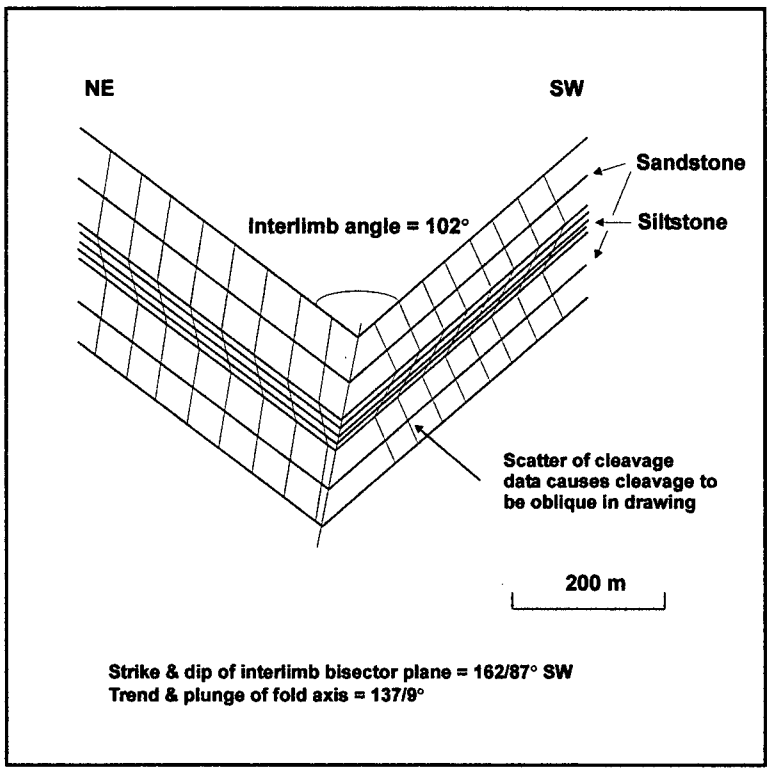

Figure 3.21a Down plunge view of northwest-trending syncline, from stereonet analysis. Relationship of cleavage cannot be defined due to scatter of data. Profile plane = 047/81° NW. Domain 4, Study Area 1.

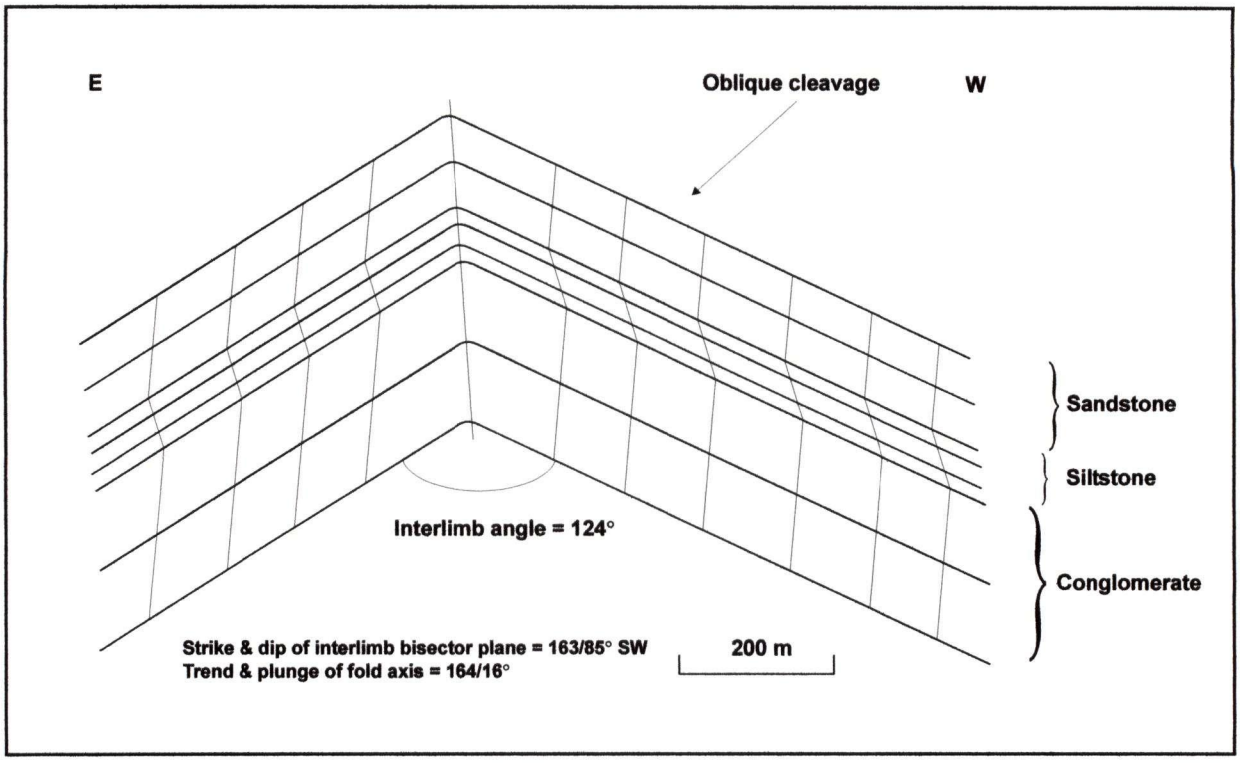

Figure 3.21b Down plunge view of eastern anticline. Cleavage transects fold by 20° in clockwise direction. Profile plane = 074/74° NW. Fold appears to have different geometry than photo in Figure 3.21b this is due to the different orientation of the view; line drawing looking towards 164, while photo was taken looking north-northwest. Domain 4, Study Area 1.

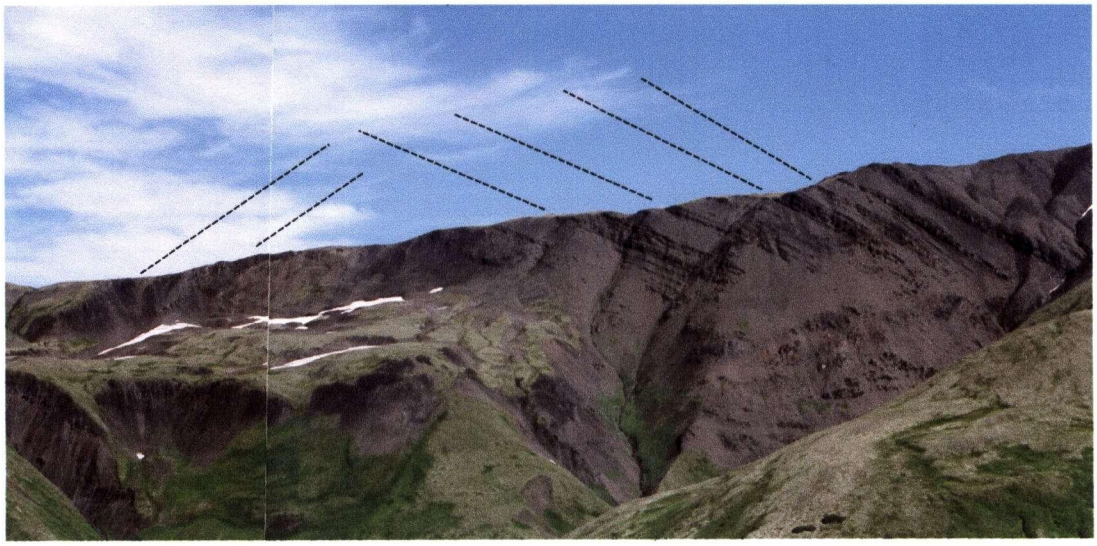

Figure 3.21c View of anticline plunging north-trending anticline. Photograph taken from Domain 5. Scale of photograph is 1 km. View looking north-northwest. Domain 4, Study Area 1.

North-northwest-trending fold: An anticline plunging 16° towards 164 (Figure 3.20b), verging towards the northeast, is located in the eastern half of the domain. The fold has planar limbs with an interlimb angle of 124° (Figure 3.21b) and was observed in the field (Figure 3.21c). Cleavage strikes between 143 and 133 (Table 3.10), dipping almost vertically (Figure 3.20b). Cleavage transects the fold by 20° in a clockwise direction.

Fractures: The western syncline contains fractures within the a-c plane (Figure 3.22a). Only a small number of fractures were observed on the eastern anticline (Table 3.11; Figure 3.22b).

Faults and veins: Faults are poorly developed throughout the domain (Figure 3.22c). Veins are localised in the hinge of the western syncline and may be an artifact of faulting. Veins are thick (<2 cm) and contain large well-developed vuggy quartz crystals.

Table 3.10 Bedding and cleavage for Domain 4, Study Area 1. See Figure 3.20.

LOCATION	LITHOLOGY	BEDDING	CLEAVAGE		
		Average Strike/Dip	Average Strike/Dip	Spread in Orientation[1]	Spread in dip[1]
West fold SW limb	Cg 85% Sst 15%	125/36°SW	131/63°NE (slst)	49°	44°
			135/65°SW (sst, cg)	40°	33°
West fold NE limb	Cg 38% Sst 62%	147/42°NE	150/76°SW (slst)	74°	41°
			134/80°NE (sst, cg)	69°	55°
East fold W limb	Cg 12% Sst 50% Slst 38%	132/30°SW	143/87° SW	48°	74°
East fold E limb	Cg 81% Sst 19%	009/35°SE	133/86°NE	15°	26°

[1] Calculated from opposing extremes of cluster.

Table 3.11 Fracture data for Domain 4, Study Area 1. See Figure 3.22a and b.

LOCATION	FRACTURES				
	Number	Average strike/dip	Maximum 2θ angle	Style	Orientation of σ_1
West fold	24	031/58°NW	-	Oblique	-
	42	053/78°NW	-	Extensional	-
East fold	9	077/85°NW	-	Extensional	-
	8	047/87°NW	-	Oblique	-

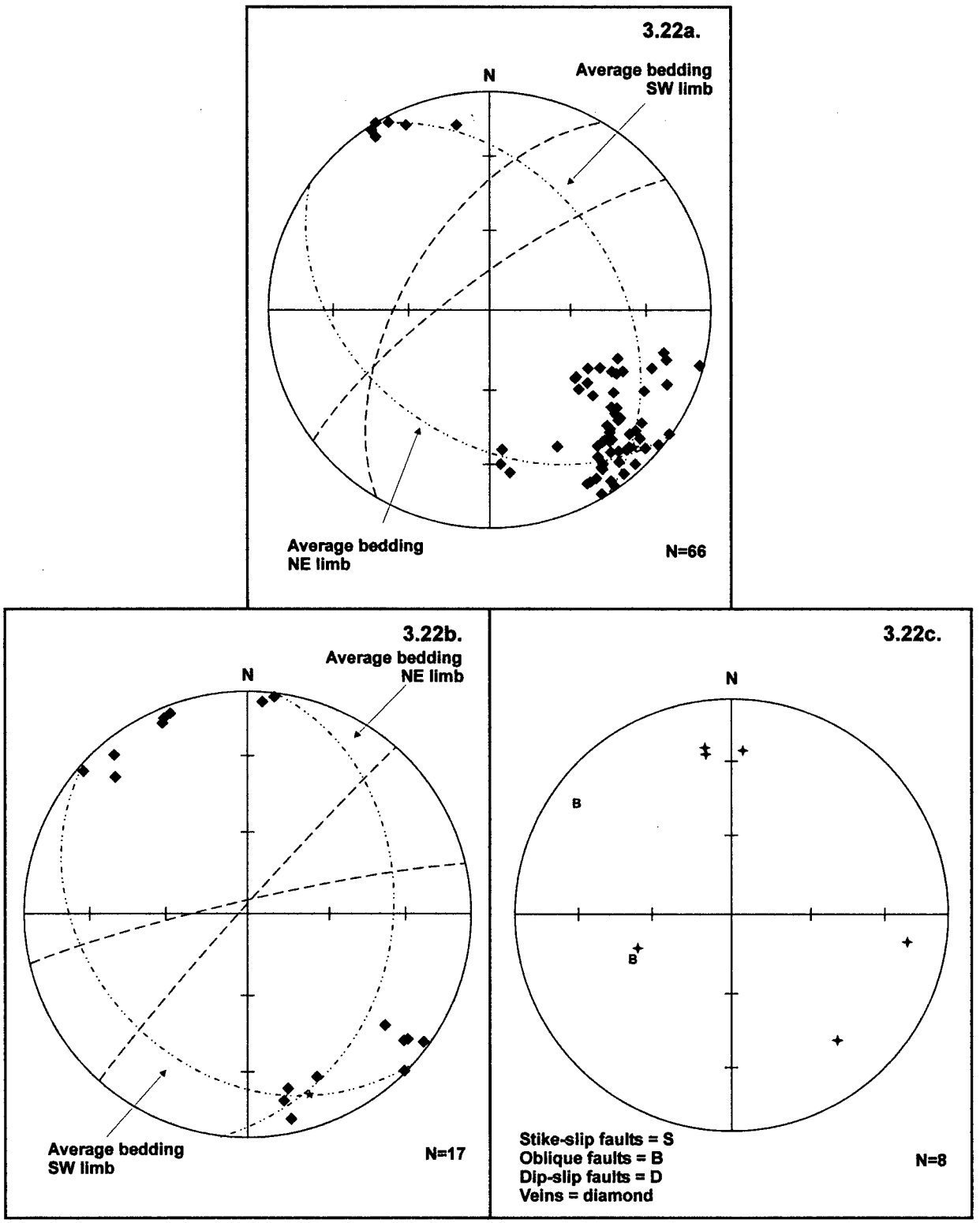

Figure 3.22 Study Area 1, Domain 4. a) Fracture data associated with northwest-trending syncline. b) Fracture data associated with north-trending anticline. c) Fault and vein data, faults defined by orientation of slikensides on fault planes.

Table 3.12 Fault data for Domain 4, Study Area 1. See Figure 3.22c.

LOCATION	FAULTS & VEINS				
	Number	Orientation	Average plunge/trend	Style	Number of veins
West fold	2 6	156/41°NE, 036/77°NW	35°/032, 64°/088	Oblique	6

3.2.7 Domain 5

Domain 5 is situated on the ridge south of Mount Pinhorn, extending westward across the width of the study area (Figure 3.4a). The domain contains a thick sequence (>200 m) of interbedded conglomerate, sandstone and siltstone. These tend to vary from sections of interbedded conglomerate and sandstone with minor siltstone around 50 m thick to siltstone with minor interbedded sandstones ranging from 50-70 m thick (Figure 3.23). Bedding within this area shows characteristics of turbidite deposition with prominent lenses of conglomerate within sandstone units.

Northwest-trending fold: A syncline plunging 24° towards 118, verging towards the southwest, is present in the eastern half of the area. The syncline has an interlimb angle of 133° (Figure 3.24) with the northeast limb dipping 42°S and the southwest limb 27°SE (Table 3.13). The strike of bedding varies from 090 in the east near the fold hinge to 002 in the west (Figure 3.25a). Cleavage strikes between 102 and 165 and dips ~70° to the southwest and northeast (Table 3.13), with the greatest variation in orientation seen in planes dipping southwest (Figure 3.25a). The relationship of cleavage to the syncline cannot be defined due to the spread in orientation of cleavage.

Fractures: Almost all fractures within the domain dip steeply westward (Table 3.14) and form one group (Figure 3.25b) striking around 012. Fractures are oblique to the syncline trend with orientation varying by 54°. Dip varies by ~40°.

Faults and veins: Few faults and veins were recorded in this area (Figure 3.25c). Movement on one fault plane implies dip-slip movement towards the southeast (Table 3.15). A number of en-echelon vein sets were identified oriented north-south and these give a dextral sense of movement.

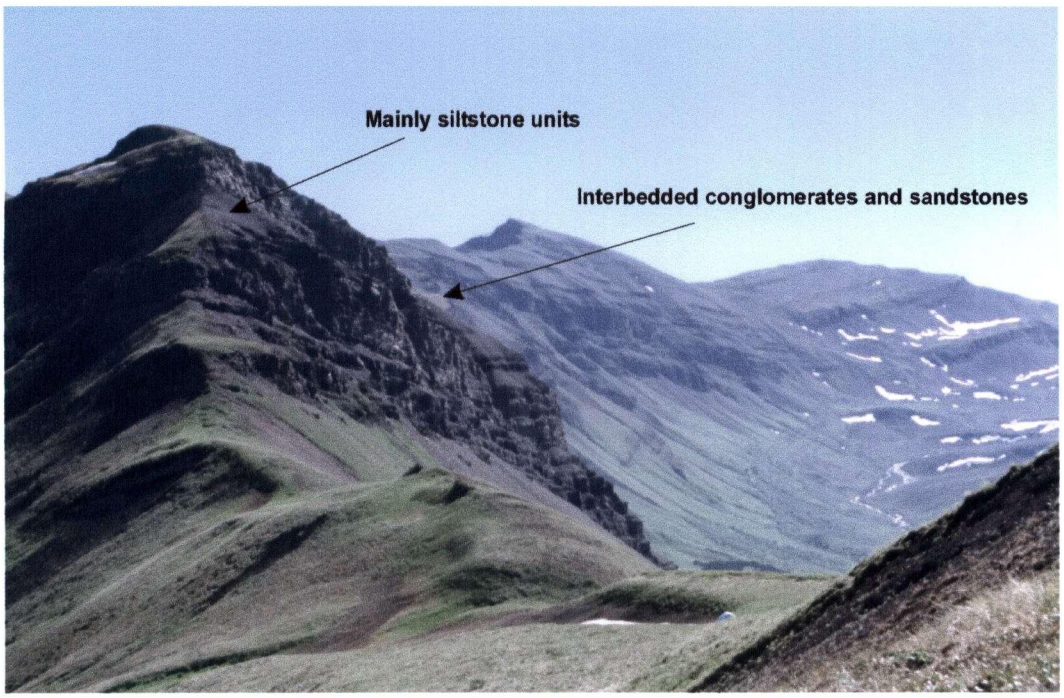

Figure 3.23 Interbedded conglomerates and sandstones forming cliffs, and mainly siltstone units forming steep unconsolidated slopes. Scale of cliff face ~100 m high. View looking east. Domain 5, Study Area 1.

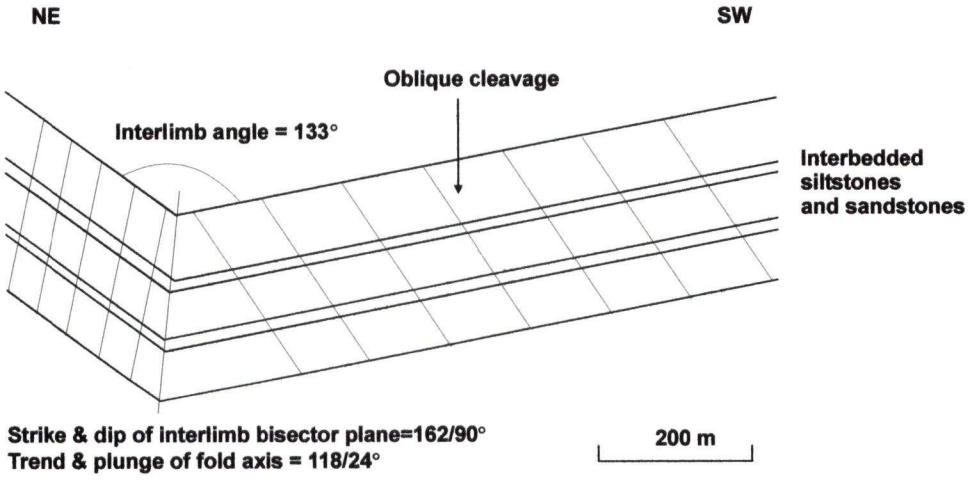

Figure 3.24 Down plunge view of northwest-trending syncline, observed in field. Cleavage transects fold by 18° in counter-clockwise direction. Profile plane =028/66°NW. Domain 5, Study Area 1.

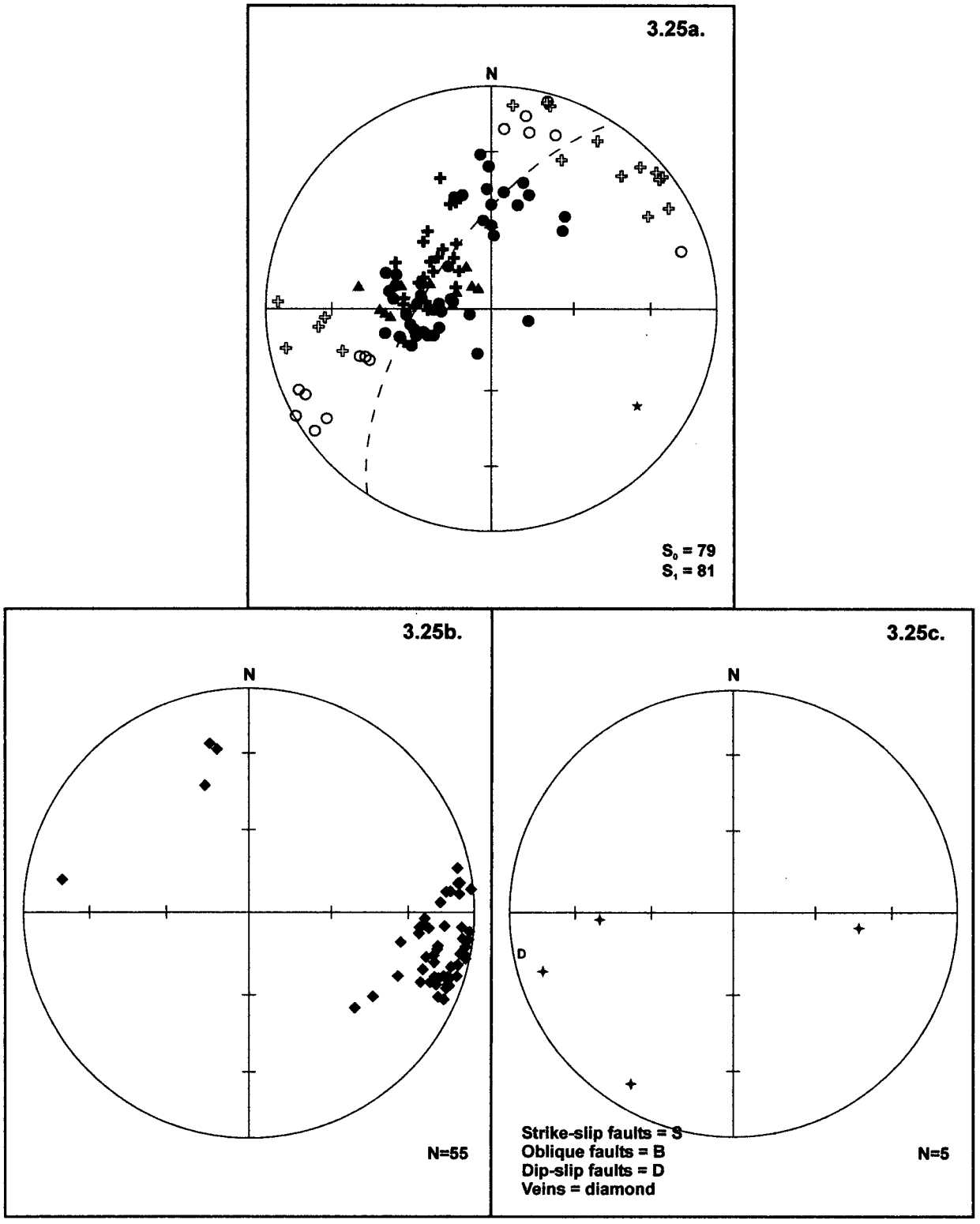

Figure 3.25 Study Area 1, Domain 5. a) Bedding and cleavage data, trend and plunge of fold axis: 118/24°. b) Fracture data. c) Fault and vein data, faults define by orientation of slikensides on fault planes.

Table 3.13 Bedding and cleavage for Domain 5, Study Area 1. See Figure 3.25a.

LOCATION	LITHOLOGY	BEDDING	CLEAVAGE		
		Average Strike/Dip	Average Strike/Dip	Spread in Orientation[1]	Spread in dip[1]
West	Cg 58% Sst 19% Slst 23%	002/26°SE	165/77°NE	17°	15°
			102/78°SW	17°	26°
Centre	Sst 65% Slst 35%	047/28°SE	136/75°SW	35°	22°
East	Cg 88% Sst 12%	090/42°S	154/74°NE	12°	53°

[1] Calculated from opposing extremes of cluster.

Table 3.14 Fracture data for Domain 5, Study Area 1. See Figure 3.25b.

LOCATION	FRACTURES				
	Number	Average strike/dip	Maximum 2θ angle	Style	Orientation of σ_1
	55	012/78°NW	-	Oblique	-

Table 3.15 Fault data for Domain 5, Study Area 1. See Figure 3.25c.

LOCATION	FAULTS & VEINS				
	Number	Orientation	Average plunge/trend	Style	Number of veins
	1	169/86°NE	85°/120	Dip-slip	
	4				4

3.2.8 Domain 6

Domain 6 is a large area on and southeast of Mount Pinhorn (Figure 3.4a). Bedding in this area contains a large amount of sandstone and interbedded siltstones. This difference in stratigraphy from the rest of the study area is reflected in the far darker colour of the rocks (Figure 3.26). Sandstone units display sedimentary features strongly characteristic of turbidite sequences such as the channel features described at the beginning of Section 3.1 (Figure 3.6). One northwest-trending and two north-trending folds were observed within the domain.

Northwest-trending fold: Bedding data from the centre of the domain describes a syncline plunging 32° towards 144 (Figure 3.27a), with an interlimb angle of 141° (Figure 3.28b) and verging towards the northeast. Cleavage transects the syncline by 32° in a counter-clockwise direction (Figure 3.27a).

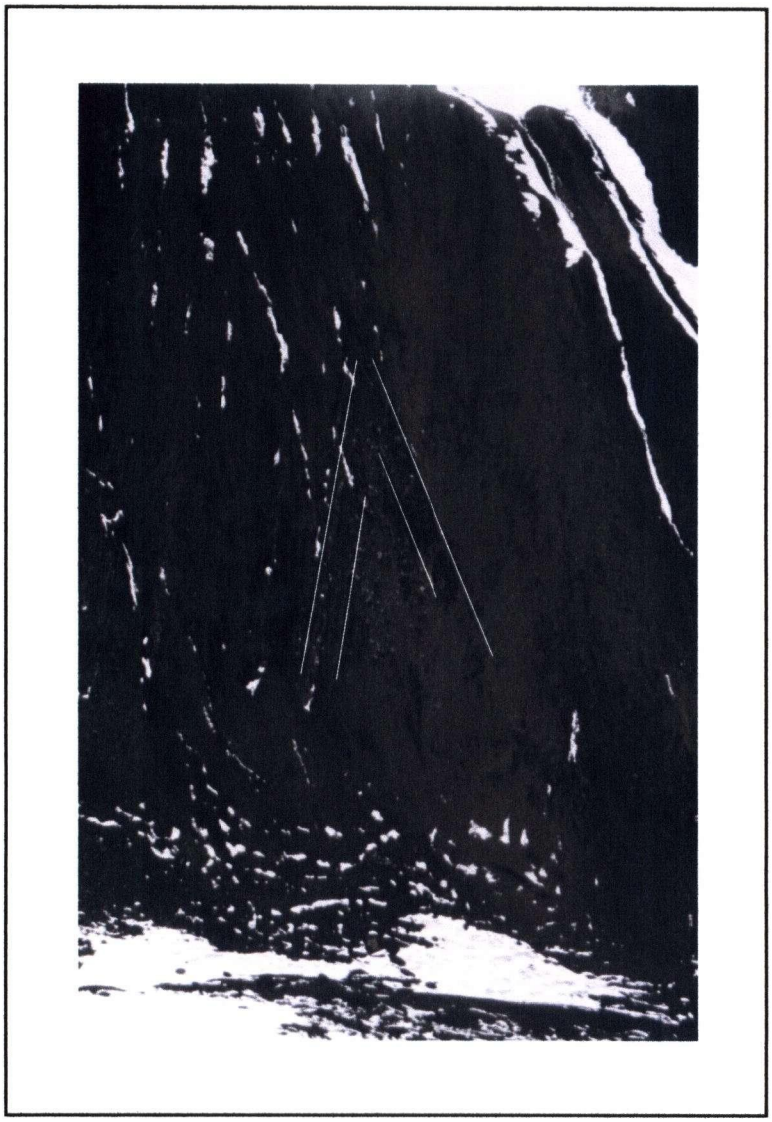

Figure 3.26 Small anticline within siltstone units. Fold trends northwest. View looking northwest, field of view = 20 m. Domain 6, Study Area 1.

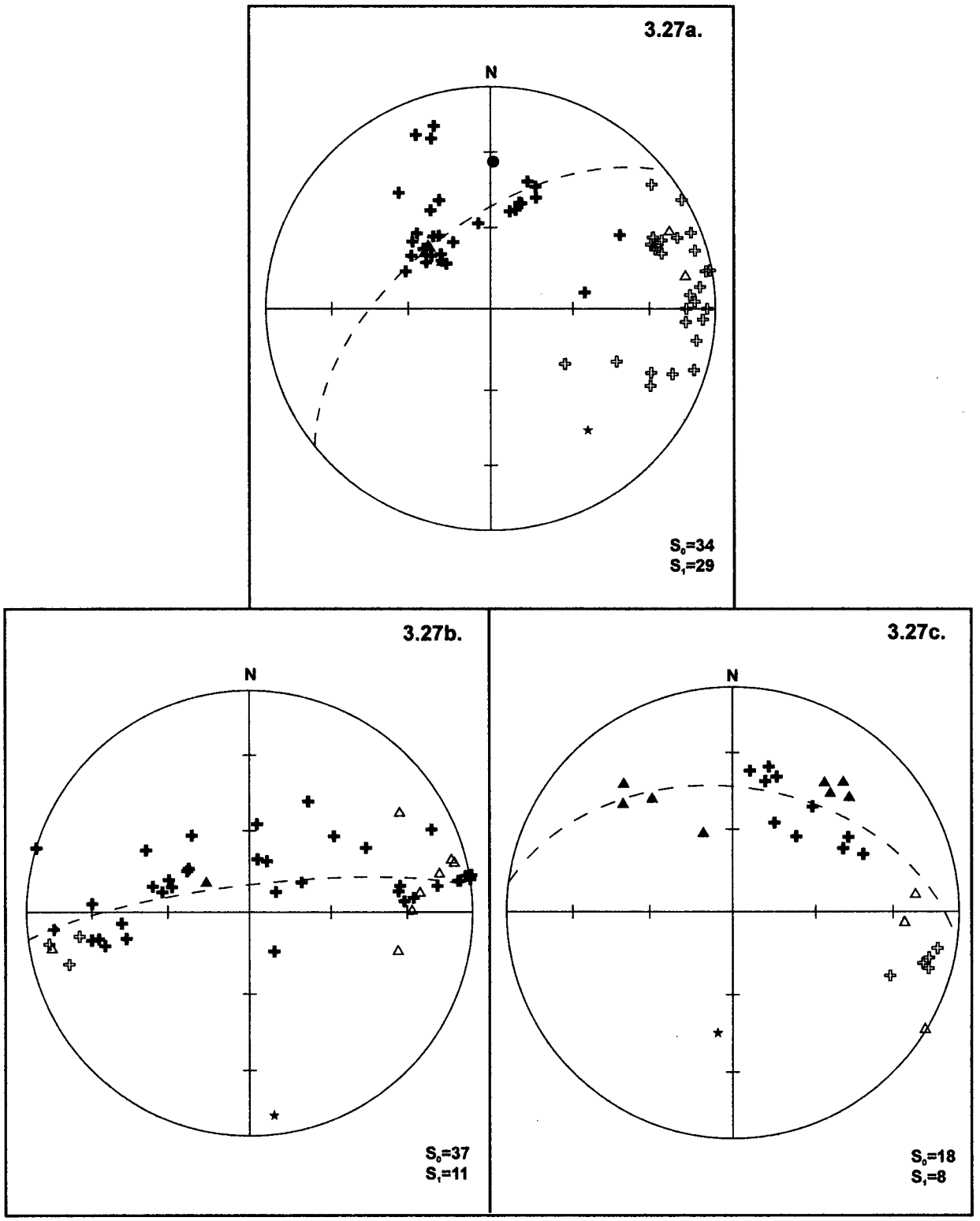

Figure 3.27 Study Area 1, Domain 6, bedding and cleavage data. a) Northwest-trending syncline in centre of domain, trend and plunge of fold axis: 144/32°. b) Northwest-trending syncline in northern third of domain, trend and plunge of fold axis: 175/8°. c) Northeast-trending anticline in southern third of domain, trend and plunge of fold axis: 187/45°.

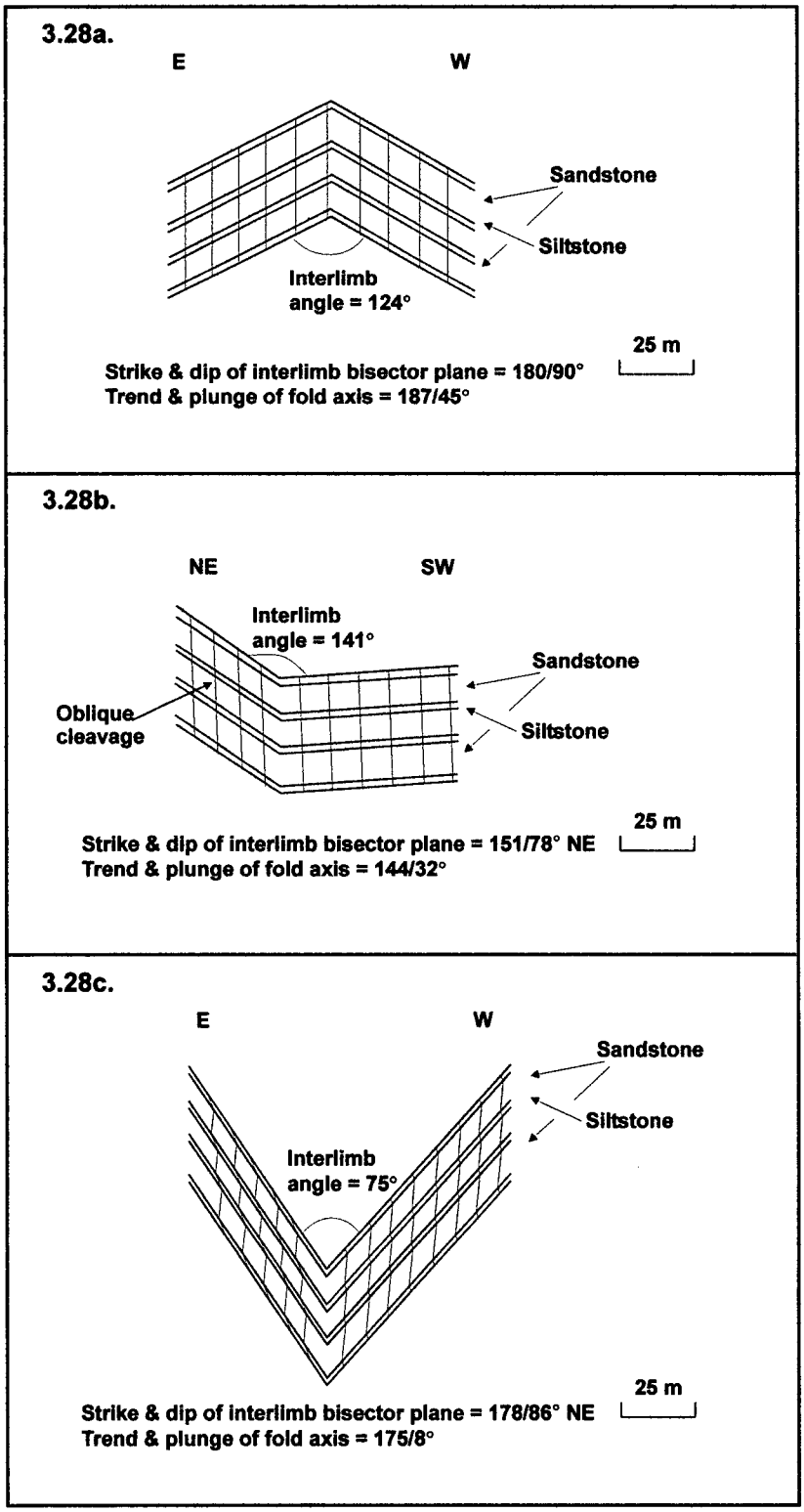

Figure 3.28 Down plunge view of bedding and cleavage relationships from stereonet analysis. a) Northeast-trending fold in southeast third of domain, relationship of cleavage cannot be determined. Profile Plane = 097/45°NE. b) Northwest-trending fold, centre of domain, cleavage transects fold by 32° in counter-clockwise direction. Profile Plane = 058/58° NW. c) Northwest-trending fold in northern third of domain, cleavage is axial planar. Profile Plane = 085/82°NW. Study Area 1, Domain 6.

North-trending folds: The north of the domain contains a number of folds seen in cross section from a distance (Figure 3.26) and one contained within collected data; a syncline plunging 8° towards 175 (Figure 3.27b), with an interlimb angle of 75° (Figure 3.28c). This is similar to the close geometry of the anticline observed from a distance. Cleavage is axial planar to this fold (Figure 3.27b). The southeastern third of the domain contains an anticline plunging 45° towards 187, with an interlimb angle of 124° (Figure 3.28a) and verging towards the northeast. The limbs have very similar dips (Figure 3.27c) but strike southeast and southwest (Table 3.16). Bedding contains evidence of bed-parallel slip in the form of fibrous quartz and slickensides on bedding planes. Mean cleavage strikes 013 (Figure 3.27c), the relationship of cleavage to the northeast-trending fold cannot be determined due to lack of data.

Fractures: Only a small number of fractures were recorded in the southeast and northwest of the domain (Table 3.17) and therefore no patterns can be deduced. Within the centre of the area spatially associated with the northwest-trending fold, two main groups of conjugate fractures identified in the field are present (Figure 3.29a). Both groups are oblique to the northwest fold trend in this area and have intersection lineations with trend and plunges of 022/68° and 020/27° (Figure 3.29a). This indicates a south-trending σ_1 for (1) and southeast-trending σ_1 for (2) (Table 3.17).

Faults and veins: Two strike-slip faults were identified within the domain. One fault strikes southeast with slickensides plunging towards 142, and a second strikes northeast with slickensides plunging towards 054 (Table 3.18). Faults with slickensides indicating oblique movements were recorded these strike northeast (Figure 3.29b). All veins recorded in the domain strike between 124 and 130, and dip towards the southwest (Figure 3.29b).

Table 3.16 Bedding and cleavage for Domain 6, Study Area 1. See Figure 3.27.

LOCATION	LITHOLOGY	BEDDING	CLEAVAGE		
		Average Strike/Dip	Average Strike/Dip	Spread in Orientation[1]	Spread in dip[1]
Southeast	Sst 55% Slst 45%	053/51°SE 126/51°SW	013/75°NW	38°	27°
Centre	Cg 3% Sst 85% Slst 12%	048/32°SE 104/44°SW	173/75°SW	65°	56°
Northwest	Sst 97% Slst 3%	002/48°SE 169/55°SW	169/74°NE 170/71°SW	48° 9°	25° 13°

[1] Calculated from opposing extremes of cluster.

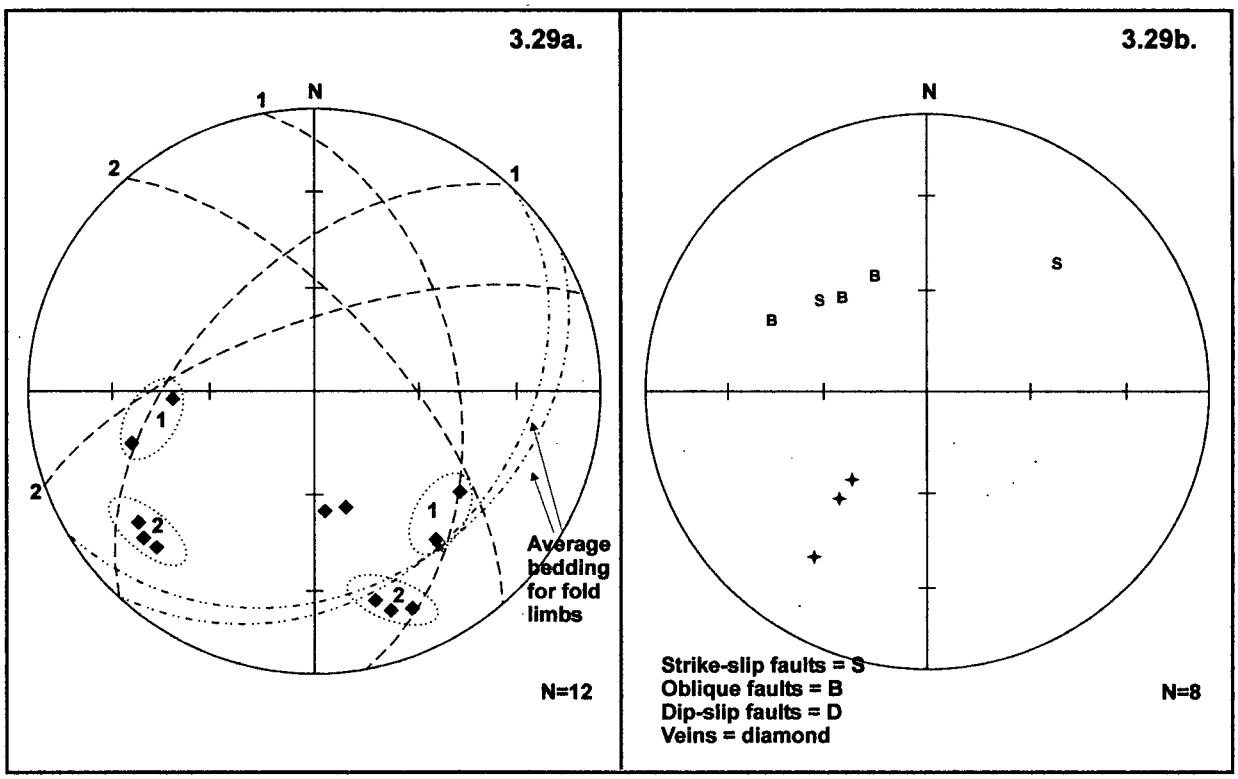

Figure 3.29 Study Area 1, Domain 6. a) Fracture data from centre of domain, colours used to define geometric groups of fractures. b) Fault and vein data, faults defined by orientation of slikensides on fault planes.

Table 3.17 Fracture data for Domain 6, Study Area 1. See Figure 3.29a.

LOCATION	FRACTURES				
	Number	Average strike/dip	Maximum 2θ angle	Style	Orientation of σ_1
Southeast	2	004/74°SE	-		-
Centre	4	043/54°NW, 170/48°NE	53°	Conjugate shear	62°/197
	6	070/70°NW, 139/67°NE	69°	Conjugate shear	0°/110
	2	080/35°NW	-	Extensional	-
Northwest	3	152/65°SW	-		-

Table 3.18 Fault data for Domain 6, Study Area 1. See Figure 3.29b.

LOCATION	FAULTS & VEINS				
	Number	Orientation	Average plunge/trend	Style	Number of veins
	2	135/55°SW, 041/42°SE	9°/142, 11°/054	Strike-slip	
	3	066/38°SE, 049/38°SE, 025/51°SE	37°/140, 36°/164, 24°/184	Oblique	
	3				3

3.3 SUMMARY OF DATA, STUDY AREA 1

The majority of folds in Study Area 1 trend northwest, with a small number of northeast-, east- and north-trending folds (Table 3.19; Figure 3.30).

3.3.1 East-trending fold

An east-trending syncline is located in the northern most domain of Study Area 1, with a trend and plunge of 098/12°. The fold is asymmetric and is ~500 m wide. Cleavage transects the syncline by 43° in a counter-clockwise direction.

3.3.2 North-trending folds

North-trending folds are located within the eastern half of Domain 4 and the northern two thirds of Domain 6. The anticline in Domain 4 was the only fold within the study area to be directly observed in cross-section while in the field. North-trending folds vary in scale from wavelengths of 800 m in Domain 4 to 100 m in Domain 6. The orientation of north-trending folds varies from 164 to 187, the degree of plunge is highly variable from 8° associated with a fold trending 175 and 45° trending 187.

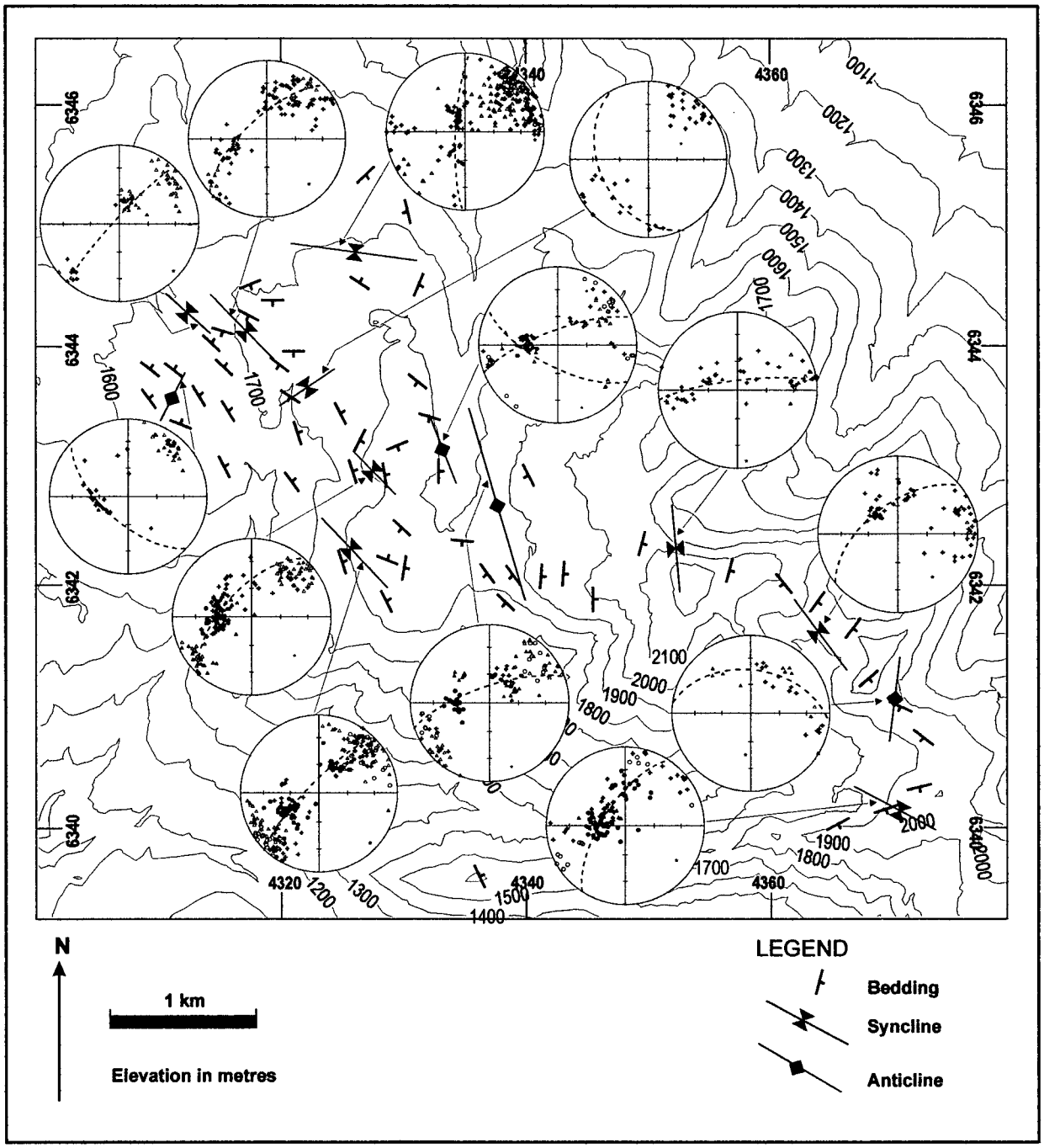

Figure 3.30 Map of Study Area 1, highlighting northwest and northeast trending folds identified within area. Stereonets contain bedding and cleavage measurements for each fold. Structures are listed in Table 3.19.

3.3.3 Northwest-trending folds

Northwest-trending folds plunge towards the southeast and verge both northeast and southwest. Wavelength ranges from 100 m to >500 m. Fold style commonly comprises two main types a) symmetric fold limbs with similar dip and length (Domain 2, 3, 4, and 6), and b) asymmetric fold limbs, one limb being long and shallow the other shorter and steeper (Domain 2, and 5). Fold trend varies between 118 and 159, all folds have sub-horizontal (7°) to shallow (32°) plunges.

3.3.4 Northeast-trending folds

Northeast-trending folds plunge towards the northeast and verge northwest. Wavelengths range between 100 and 200 m. Northeast-trending folds differ in style from northwest-trending folds, the former having non-planar limbs and a generally symmetric shape. Northeast-trending folds vary in orientation between 027 and 056. They have plunges of 44° and 62°, far steeper than folds trending northwest (Table 3.19).

Table 3.19 Summary of fold information for Study Area 1 (Figure 3.30).

	FOLD TYPE	FOLD AXIS	CLEAVAGE RELATIONSHIP				INTERLIMB ANGLE	VERGENCE
		Plunge/Trend	t*	d*	Δ	Transection sense		
Domain 1	Syncline	12°/098	45°	10°	43°	counter-clockwise	133°	SW
Domain 2	Syncline	7°/132	axial planar			-	83°	NE
	Syncline	20°/131	axial planar			-	103°	NE
	Syncline	52°/064	87°	44°	53°	counter-clockwise	-	NW
Domain 3	Anticline	27°/044	79°	25°	82°	counter-clockwise	-	NW
	Syncline	24°/136	axial planar			-	-	-
	Anticline	16°/159	axial planar			-	119°	NE
Domain 4	Syncline	09°/137	unknown			-	102°	SW
	Anticline	16°/164	22°	4°	20°	clockwise	124°	NE
Domain 5	Syncline	24°/118	13°	7°	18°	counter-clockwise	133°	SW
Change from	northwest- to	north striking cleavage						
Domain 6	Anticline	45°/187	unknown			-	124°	NE
	Syncline	32°/144	24°	11°	32°	counter-clockwise	141°	NE
	Syncline	8°/175	axial planar			-	75°	NE

3.3.5 Spaced cleavage

Throughout the study area a disjunctive spaced cleavage is present; this varies in density primarily due to lithologic controls. Within conglomerate sequences cleavage plane spacing is on the scale of 10's cm. This is reduced to 1-5 cm's in sandstone units and <1 cm in siltstone units.

Within Study Area 1 there is a large-scale change in orientation of cleavage from the western two thirds of the study area (Domains 1-5) and the eastern third (Domain 6). In the west cleavage is primarily striking northwest while in the east cleavage strikes north (Figure 3.30). This change in orientation may be associated with a change in the orientation of the dominant fold set to the southeast of Study Area 1. The western two thirds of Study Area 1 is contained within an area of dominantly northwest-trending folds, which extends further to the north and east. While to the south and southeast of the study area northeast-trending folds are the dominant structures [*Evenchick et al.*, 2001].

The east-trending fold (Domain 1) is spatially associated with northwest striking cleavage, this transects the fold by 43° in a counter-clockwise direction. Northeast-trending folds in the western two thirds of the study area (Domains 2 and 3) are accompanied by northwest striking cleavage, which transects the folds by 53° and 82°. The north-trending anticline within the northern third of Domain 6 contains axial planar cleavage while the lack of cleavage data for the north-trending syncline in the northern third of Domain 6 does not allow the relationship of the cleavage and this syncline to be defined. Northwest-trending folds in the western two thirds of the study area have axial planar cleavage. The northwest-trending fold from the centre of Domain 6 is spatially associated with north striking cleavage, which transects the syncline by 32° in a counter-clockwise direction.

3.3.6 Fractures

The majority of fractures within Study Area 1 are spatially associated with northwest-trending folds and indicate northeast-southwest compression.

Extensional fractures lying in the a-c and b-c planes are associated with all northwest-trending folds in Study Area 1. Fracture sets located on fold limbs and parallel to the fold axis, in Study Area 1, appear to display the same features as those of *Engelder and Peacock* [2001], including cross-cutting of bedding and a non-orthogonal relationship to bedding, plus they are inclined towards the axial plane of the fold. *Engelder and Peacock* [2001] suggest these types of fractures are associated with folding occurring by flexural slip.

Conjugate fractures associated with the east-trending fold in Domain 1 give an oblique, northeast oriented shortening axis. The majority of conjugate shear fractures within Study Area 1 occur on the limbs of northwest-trending folds these generally indicate southwest shortening. Conjugate fractures spatially associated with the central northwest-trending fold have a vertical shortening direction and are possibly the product of sedimentary burial/exhumation forces.

Hybrid fractures on northwest-trending folds indicate an oblique shortening direction oriented south.

3.3.7 Faults

The largest faults in Study Area 1 record predominantly strike-slip movement on steeply dipping faults often in excess of 2 m in length. These faults commonly display well-developed slickensides on several millimetres thick quartz vein surfaces within the fault plane. The majority of strike-slip faults recorded in the area strike northeast (Figure 3.31). The vast majority of the faults recorded in the area have slickensides indicating oblique movement histories. Faults with oblique movement have no preferred orientation pattern with strike values through 360°, but the majority do have dip values of ~60° (Figure 3.32). The small number of dip-slip faults identified in the area are all steeply dipping and appear to separate into two groups, dipping northeast and southwest. Faults are observed commonly crosscutting all other structures in the area. The distribution of faults across Study Area 1 has no indication of concentration in certain areas.

3.3.8 Veins

Throughout the study area description of vein systems has identified a number of characteristics. En-echelon veins were identified in a number of localities (Figure 3.20b), these strike either northeast with sinistral movement or northwest with dextral movement, indicating an north-south compression orientation. Other veins combine to form blocky systems of thin straight veins interlinked by oblique veins (Figure 3.19a). The major vein sets in these systems strike northeast, while the minor interlinking veins suggest sinistral movement. Across Study Area 1 discrete areas, normally less that 10 m^2, contain concentrated amounts of thick, vuggy veins with a great variation in orientation. Within these systems there is some degree of parallelism to northwest-trending folds and they appear to correlate to some degree with northwest-trending fold hinges.

3.4 STUDY AREA 1 FOLD ORIGIN

3.4.1 Folding mechanism

Fold geometry and slickensides on bedding surfaces of both fold sets, oriented perpendicular to fold axes, indicate that folds formed by a flexural-slip mechanism. This is supported by the geometry of fractures parallel to the fold axes as discussed above. Flexural-slip

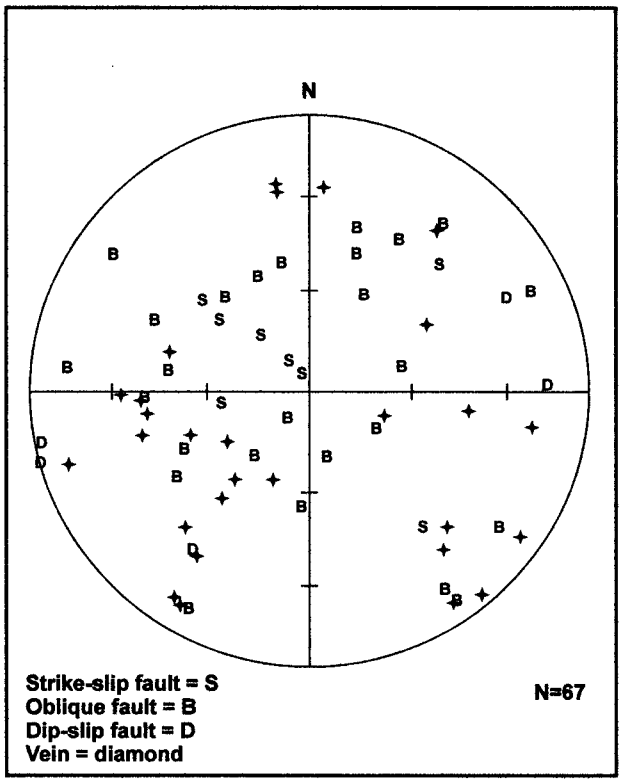

Figure 3.31 Fault and vein data for all of Study Area 1.

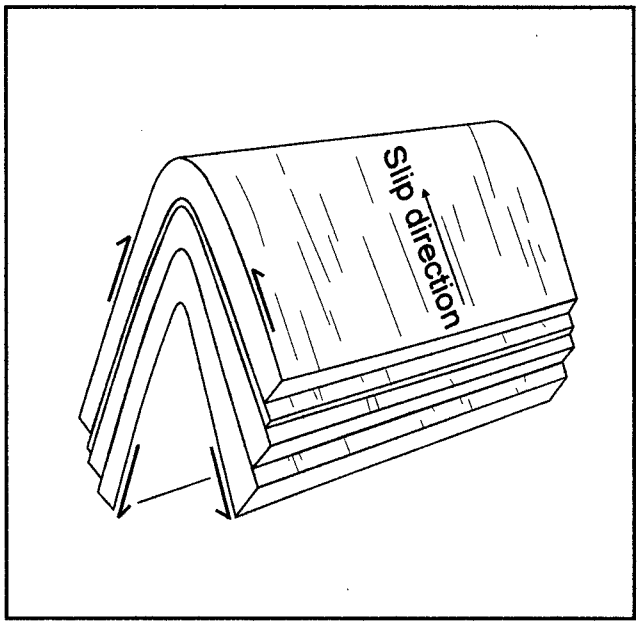

Figure 3.32 Flexural-shear mechanism of formation of folds [*Tanner*, 1985].

involves the movement of upper horizons over lower horizons towards the fold axis during the folding of regularly bedded rock sequences [*Tanner*, 1989]. Flexural-slip occurs on distinct 'movement' horizons that are distributed on a decimetre to metre spacing through the bedding sequence (Figure 3.32). The separation distance between movement horizons decreases with the tightness of the fold. Evidence for flexural-slip is predominantly obtained from thin vein sheets and slip indicators on bedding surfaces. Within Study Area 1 bed-parallel vein sheets are common and bedding occurs on 10's of centimetre to metre cycles, therefore being at an optimum separation for bedding surfaces to become movement horizons within flexural-slip folding.

3.4.2 Relative timing of fold sets

The use of transection terminology and the inference that these fold-cleavage relationships were produced by progressive deformation as opposed to polydeformation from multiple events is based on regional evidence of a progressive rotation of shortening directions through the development of the Skeena Fold Belt [Section 2.5, this volume].

Northeast-trending folds do not display axial planar cleavage. Northeast-trending folds are transected by northwest striking cleavage in the western two thirds of Study Area 1. Northwest-trending folds in the west of Study Area 1 have axial planar cleavage and are contained within a large area of dominantly northwest-trending folds that extends to the north and east of the study area. The presence of axial planar cleavage associated with northwest-trending folds suggests these folds have not undergone further deformation whereas the association of northwest striking cleavage with northeast-trending folds would suggest these folds formed before the northwest striking cleavage. The northwest striking cleavage is thought to be genetically associated with the northwest-trending folds and therefore indicates that northeast-trending folds predate those trending northwest.

The relationship of north-trending folds to cleavage is variable, mainly due to lack of cleavage data for these folds. In the western part of the study area a north-trending fold is spatially associated with northwest striking cleavage. This fold has an opposing direction of transection to all other transected fold-cleavage relationships in Study Area 1. In the southeastern third of Study Area 1, one north-trending fold has axial planar cleavage while the relationship of a second fold cannot be determined due to lack of data. A northwest-trending fold in this part of Study Area 1 is transected by north-trending cleavage. Cleavage in the southern third of the area strikes north and is axial planar to at least one north-trending fold. The presence of a northwest-trending fold with north striking cleavage suggests that north-trending cleavage developed after

the northwest-trending fold. This is contradicted by a north-northwest-trending fold transected by northwest striking cleavage to the southwest of Mount Pinhorn (Domain 4).

Fold-cleavage relationships within Study Area 1 indicate that northeast-trending folds predate northwest-trending folds. The large-scale change in cleavage orientation from west to east across Study Area 1 suggests two periods of cleavage development, the east associated with north-trending folding and the west associated with northwest-trending folding. Evidence of the relationship between north- and northwest-trending folds is inconclusive and contradictory in this area.

3.5 STUDY AREA 2

Study Area 2 is situated to the east of the Stewart-Cassiar Highway at the southern end of Kinaskan Lake, 50 km south of Iskut. The area contains both northeast and northwest trending folds and was studied to define the relationship between these two orientations of folding.

3.5.1 Lithology

The area comprises thick interbedded units of conglomerate and sandstone of the Skelhorne assemblage [*Evenchick*, et al., 2001], resulting in conglomerate dominated sequences with thickness of >100 m. Conglomerate units in the area are thickly bedded (>0.5 m) and polymictic, with a large proportion of predominantly pebble sized chert clasts, plus clasts from variable volcanic sources mainly from the Stuhini or Hazelton Groups in the surrounding area. The matrix is medium-grained and has a similar mineralogy to the clasts. The provenance of chert clasts is mainly from the oceanic Cache Creek assemblage to the east of the Bowser Basin [*Gabrielse et al.,* 1992].

Sandstone is consistently medium-grained and predominantly composed of quartz with few sedimentary structures. Bedding thickness ranges from 0.2-0.5 m. The lack of sedimentary structures is not characteristic for this type of unit within the Bowser Lake Group. Deformation associated with fold interference is interpreted to have destroyed much of the sedimentological structure by overprinting.

3.5.2 Structure

A large structural basin, open to the west, with a diameter of 2.4 km dominates the study area (Figure 3.33). This structure is interpreted as a Type 1 fold interference pattern produced by

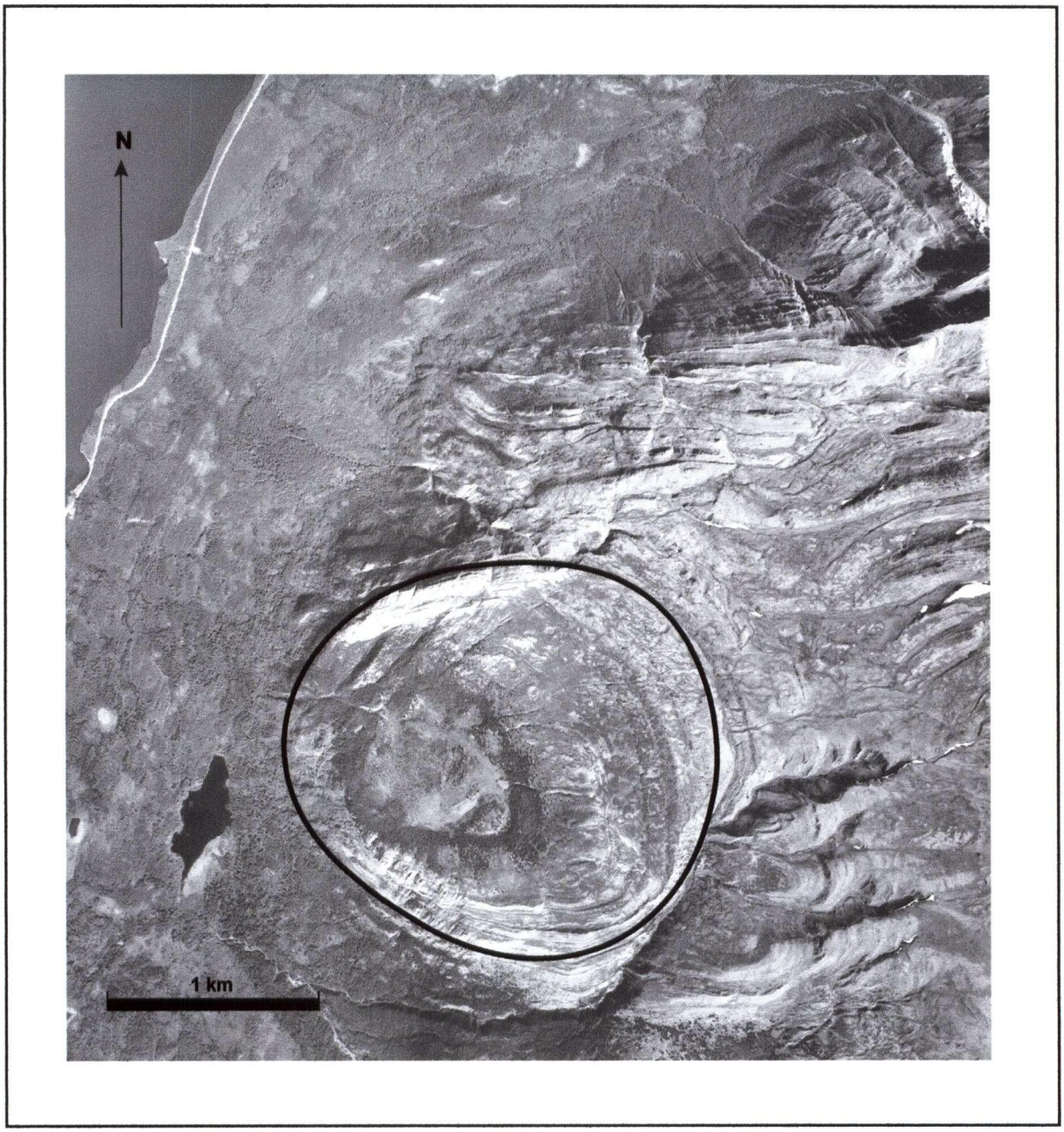

Figure 3.33 Air photo of Study Area 2, showing interference structure.

the interaction of two synclines [*Evenchick*, 2001], one trending northeast the other northwest. The northwest-trending syncline can be traced for a number of kilometres to the southeast of the basin [*Evenchick et al.*, 2001]. A second fold, plunging west-southwest is present to the north of the basin.

A pervasive spaced cleavage is present in the area. The cleavage is planar and has a systematic <50 mm separation in sandstone units; this is classified as a 'moderately spaced cleavage' by *Alvarez et al.* [1978]. In conglomerate units a 100-150 mm separation, a 'weakly spaced cleavage' under the same classification system, is seen.

Faults within the area are relatively small scale, most extending for a few 10's of cm. The majority have strike-slip movement and often exhibit slickensides and fibered vein growth. Mineralisation is mainly quartz and ranges in width from a few millimetres to centimetres. Faults crosscut cleavage and fracture planes. Veins are most commonly found within sandstone dominated areas, possibly indicating that fluid carrying dissolved material has a predominantly local provenance. At a number of sites strong iron staining is present. This is typically found within conglomerate units and is also likely to be an effect of fluid migration through the area.

3.5.3 Domain 1

Domain 1 is situated to the north of the basin (Figure 3.4b). Lithologically, interbedded sequences of predominantly conglomerate or sandstone dominate the area and average 10 m in thickness. Conglomerate beds are occasionally interbedded with thin sandstone units (~10 cm). Sandstone units often display strong iron staining, which can continue into conglomerate beds.

East-northeast-trending fold: Bedding describes an anticline plunging 10° towards 261. The anticline is open to gentle in shape with an interlimb angle of 113° (Figure 3.34) and planar limb geometry (Figure 3.35a). Both limbs dip ~30° (Table 3.20). On the southern limb there is a ~110° distribution of cleavage strike around 097 and a second group of cleavage measurement striking about 177 (Table 3.20). Cleavage is less variable on the northern limb where strike values are distributed around 025 (Figure 3.35a). Cleavage transects the fold by 68° in a clockwise direction.

Fractures: Fractures on the southwest limb of the anticline can be separated into two sets (1, Figure 3.35b). The first set strike 095 (Table 3.21) and are extensional fractures within the b-c plane of the southwest limb, parallel to the fold trend and normal to bedding. The second set of

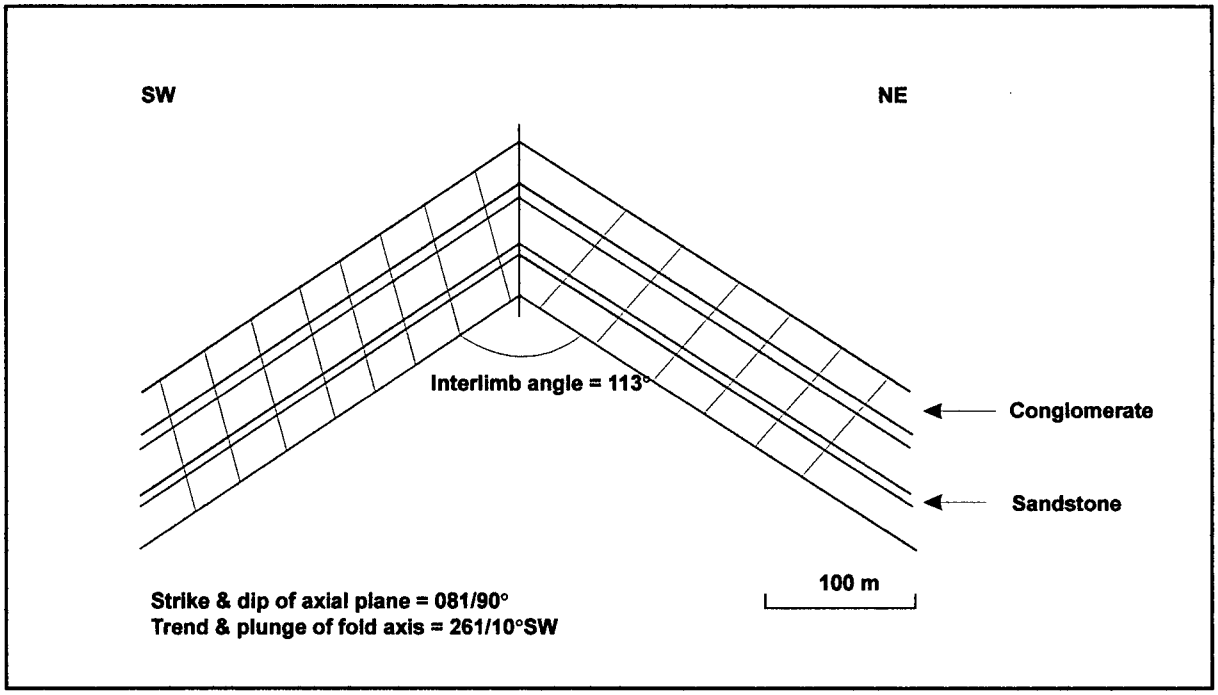

Figure 3.34 Down plunge, line drawing of east-northeast-trending anticline showing bedding and cleavage data calculated from field data. Cleavage transects the fold by 68° in a clockwise direction. Down plunge section oriented along profile plane of fold striking 341/80°NE. Domain 1, Study Area 2.

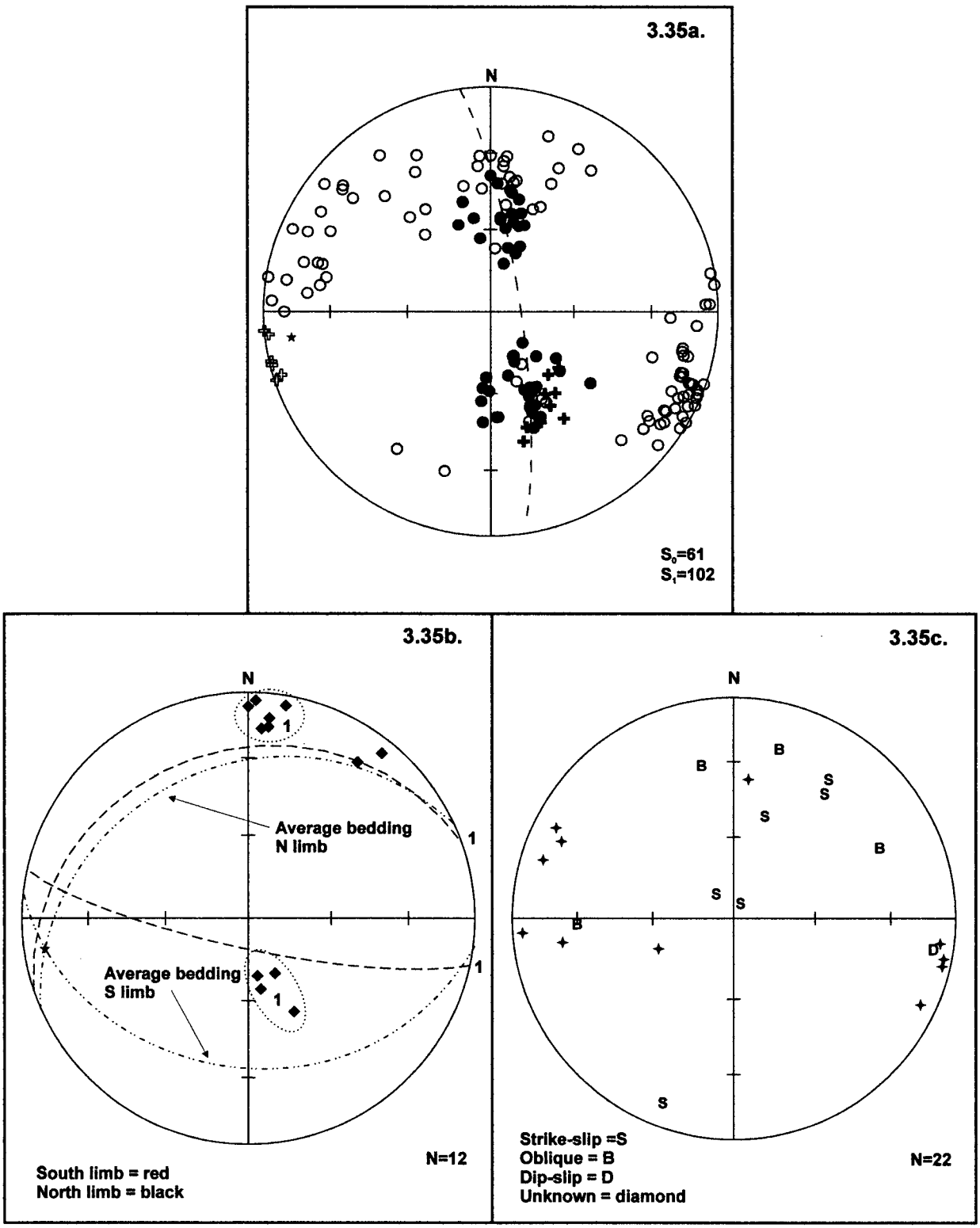

Figure 3.35 Study Area 2, Domain 1, a) all bedding and cleavage data, b) fracture data for both fold limbs, c) all fault and vein data.

fractures is oblique to the fold trend, striking 071 (Table 3.21) and lies in a plane bisecting the tectonic axes a-b-c.

Faults and veins: Strike-slip faults have consistent strike orientation of 113 across the anticline (Figure 3.35c). Quartz slickensides have an average plunge of 14° on these planes, the orientation of the slickensides varies with the majority plunging towards the east while a small number plunge towards the west (Table 3.22). Fault surfaces with oblique movement sense from slickenside trends have no consistent strike across the anticline. Veins across the fold strike 011 with dips near 85°, this correlates with a dip-slip fault striking 009/80°NW (Table 3.22).

Table 3.20 Bedding and cleavage data for Domain 1, Study Area 2. See Figure 3.35a.

LOCATION	LITHOLOGY	BEDDING	CLEAVAGE		
		Average Strike/Dip	Average Strike/Dip	Spread in orientation[1]	Spread in dip[1]
SW limb	Cg 100%	097/34°SW	025/89°NW	95°	70°
NE limb	Cg 65% Sst 35%	066/33°NW	097/50°SW	74°	50°
			177/90°	58°	33°

[1] Calculated from opposing extremes of cluster.

Table 3.21 Fracture data for Domain 1, Study Area 2. See Figure 3.35b.

LOCATION	FRACTURES			
	Number	Average strike/dip	Maximum 2θ angle	Style
SW limb	6	095/80°SW	-	Extensional
	4	071/26°NW	-	Extensional-oblique
NE limb	2	127/78°SW	-	

Table 3.22 Fault and vein data for Domain 1, Study Area 2. See Figure 3.35c.

LOCATION	FAULTS & VEINS				
	Number	Orientation	Average plunge/trend	Style	Number of veins
SW limb	7	Variable	-	-	6
	4	107/40°SW, 124/65°SW	5°/114, 8°/128	Strike-slip	
		126/59°SW, 118/78°NE	9°/132, 10°/293		
	2	154/62°SW, 078/60°SE	21°/322, 26°/094	Oblique	2
	1	009/80°NW	59°/352	Dip-slip	
NE limb	3	Variable	-	-	3
	2	055/11°SE, 114/6°SW	7°/091, 6°/151	Oblique	
	2	178/60°NE, 105/68°SW	34°/155, 40°/113	Oblique	

3.5.4 Domain 2

Domain 2 is situated on the northern limb of the basin (Figure 3.4b). Stratigraphy in this domain and surrounding locations is over 90% conglomerate with the remaining 10% comprising sandstones. The conglomerate within the domain forms very dominant ridges. Sandstone units tend to be thinly bedded and intercalated with thicker conglomerate units.

Bedding: Bedding strikes 090 (Figure 3.36a), with an average dip of 47° towards the south (Table 3.23).

Cleavage: Cleavage strikes 006 with an average dip of 90° (Table 3.23). Cleavage shows a smaller distribution variation than most domains in this study area (Figure 3.36a).

Fractures: In the western third of Domain 2 (Figure 3.36b) a group of fractures strike around 061 (Table 3.24) 30° anticlockwise from the strike of bedding in this area. These fractures dip towards the northwest (1, Figure 3.36b). Pairs of hybrid and conjugate fractures were also recorded in this area (Table 3.24). Hybrid fractures strike 003 and 130 (2, Figure 3.36b) with a 2θ angle of 53°, they have a northwest-southeast compression direction (σ_1=157). Conjugate fractures strike 014 and 084 (3, Figure 3.36b), with a 2θ angle of 70°, they have a northeast-southwest shortening direction (Table 3.24). The eastern two thirds of the domain shows a similar pattern of fractures. A diffuse group of fractures (1, Figure 3.36c) strike between 033 and 060 (Table 3.24), with dip values clustering near 50° and 70°. Those fractures striking near 060 are normal to bedding and lie within tectonic plane c (Figure 3.3a). Hybrid fractures are also present in the area (2, Figure 3.36c) these strike 007 and 162 and have a 2θ angle of 25°. These fractures have a steeply dipping south trending shortening direction. A second hybrid shear pair (3, Figure 3.36c) strike 005 and 151 (Table 3.24) and have north-northwest trending shortening. Conjugate shear fractures (4, Figure 3.36c) strike 012 and 137 (Table 3.24) with a 2θ angle of 55° and north-northwest oriented shortening.

Faults and veins: Faults within the area strike east-west (Table 3.25) and have an oblique movement sense (Figure 3.36d). The faults vary in dip between 35 and 89° (Table 3.25). Veins strike north-south, the same orientation as seen across Domain 1 (Figure 3.36d).

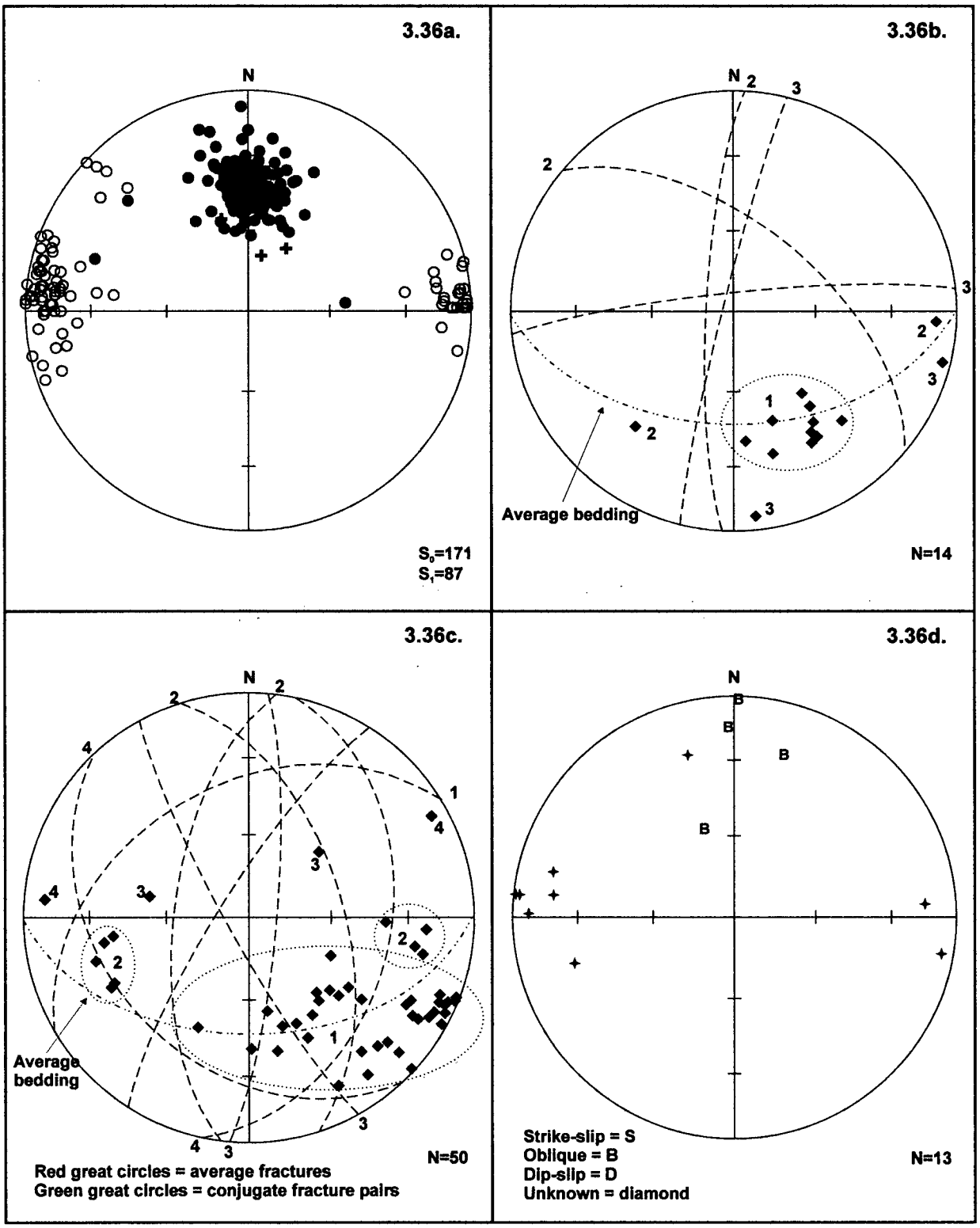

Figure 3.36 Study Area 2, Domain 2, a) all bedding and cleavage data, b) fracture data for western third of domain, conjugate relationships shown in red and green great circles, c) fracture data for eastern two thirds of domain, conjugate relationships shown in red and green, d) all fault and vein data.

Table 3.23 Bedding and cleavage data for Domain 2, Study Area 2. See Figure 3.36a.

LOCATION	LITHOLOGY	BEDDING	CLEAVAGE		
		Average Strike/Dip	Average Strike/Dip	Spread in orientation[1]	Spread in dip[1]
	Cg 96% Sst 4%	090/47°S	006/90°	63°	70°

[1] Calculated from opposing extremes of cluster.

Table 3.24 Fracture data for Domain 2, Study Area 2. See Figures 3.36b and c.

LOCATION	FRACTURES				
	Number	Average strike/dip	Maximum 2θ angle	Style	Orientation of σ_1
West	10	061/51°NW	-	Extensional	
	2	003/80°NW & 130/58°NE	52°	Conjugate shear	44°/157
	2	014/88°NW & 084/83°NW	70°	Conjugate shear	3°/229
East	22	033/79°NW	-	Extensional	
	15	060/41°NW	-	Extensional	
	9	007/63°NW & 162/56°NE	25°	Hybrid shear	71°/175
	2	012/37°SE & 137/35°SW	55°	Conjugate shear	72°/344
	2	005/80°SE & 151/82°SW	34°	Hybrid shear	29°/348

Table 3.25 Fault and vein data for Domain 2, Study Area 2. See Figure 3.36d.

LOCATION	FAULTS & VEINS				
	Number	Orientation	Average plunge/trend	Style	Number of veins
	8	004/83°SE	-		8
	4	091/89°SW, 107/66°SW 071/35°SE, 088/75°SE	21°/271, 13°/280 16°/095, 23°/094	Oblique	

3.5.5 Domain 3

Domain 3 covers a large area on the eastern side of the basin (Figure 3.4b). Conglomerate is dominant throughout the domain with sandstone only present in the northeast. Sandstone units are centimetres thick and show a concentration of vein activity.

Bedding: Bedding generally dips southwest (Figure 3.37). Data from the extreme east of the domain describes bedding dipping 20° more steeply than observed in the rest of the area (Table 3.26). In the north of the domain slickensides on bedding planes plunging southwest, provide evidence of bed-parallel movement.

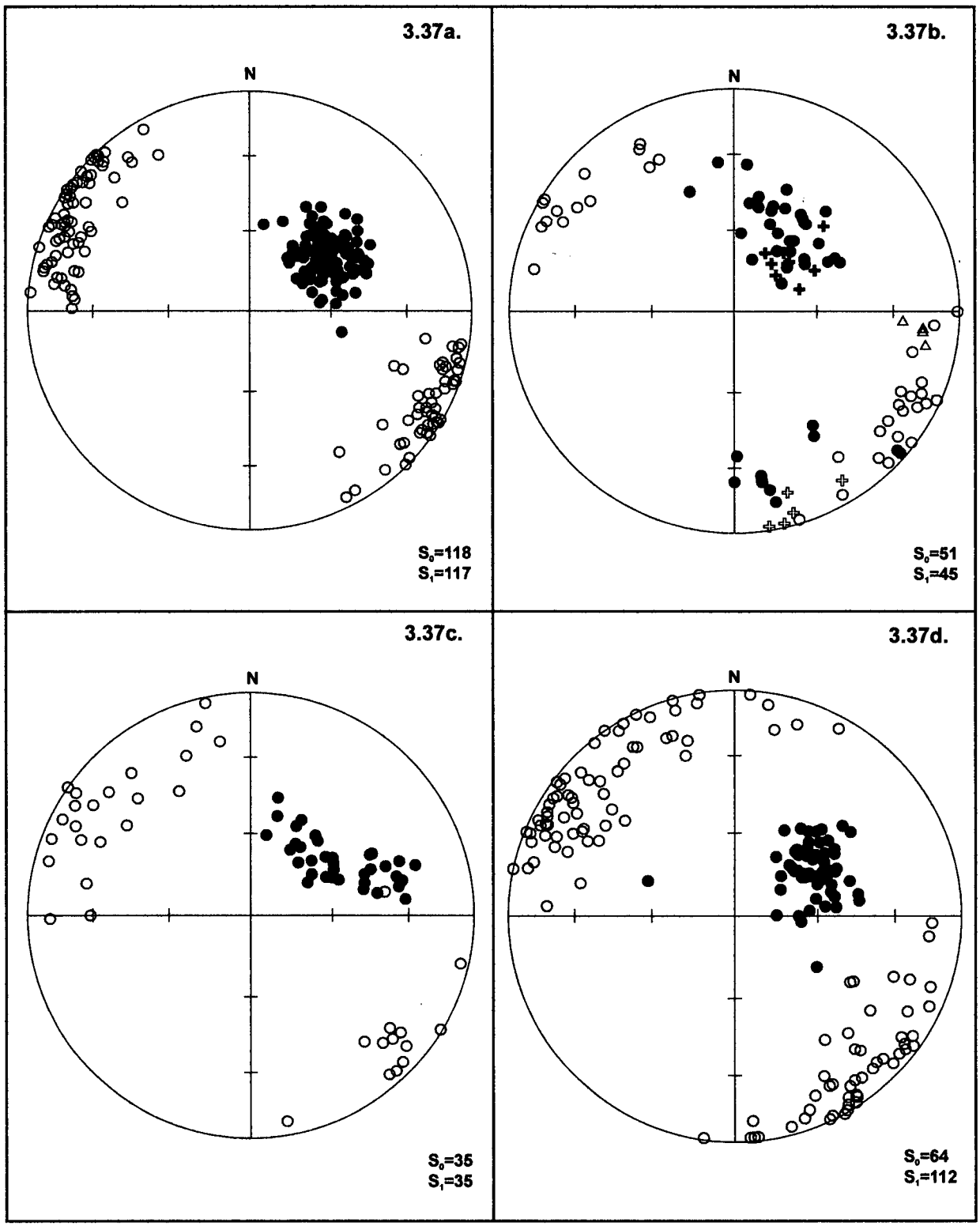

Figure 3.37 Study Area 2, Domain 3, bedding and cleavage data, a) from the northwest of the domain, b) from the north-central part of the domain, c) from the northeast of the domain, d) from the south of the domain.

Cleavage: Similar to bedding, cleavage strike ranges from 028 in the northwest to 046 in the southeast (Table 3.26). The dip of cleavage is almost vertical throughout the domain (Figure 3.37).

Fractures: Fractures show a different pattern in the north and south halves of the domain (Figure 3.38). The northwest of the domain contains a number of fractures with strike and dip normal to the average bedding surface (1, Figure 3.38a). Four sets of conjugate pairs have varying strikes (Table 3.27). 2θ angles for three of the pairs indicate conjugate shear fractures (87°; 2, 89°; 3, 81°; 4, Figure 3.38a), while one pair indicates a hybrid origin combining extensional and shear movement (2θ = 42°; 5, Figure 3.38a). These conjugate sets have northwest-southeast shortening directions. In the north-central area of the domain fractures describe two separate systems. The largest number of fractures record two conjugate sets. The first strike 136 and 150 and dip ~45° to the southwest and northeast (1, Figure 3.38b), with a 2θ angle of 83° and a σ_1 direction of 325 (Table 3.27). The second group are hybrid fractures, which strike 132 and 160 (2, Figure 3.38b), with a 2θ angle of 28° (Table 3.27). These two groups indicate a northwest-southeast shortening direction. A further set of fractures present in the north-central area of the domain are represented by a far smaller number of fractures, which record conjugate pairs. One pair strikes 081 and 035 (light blue diamonds, Figure 3.38b), they have a 2θ angle of 46° indicating hybrid shear fractures (Table 3.27). The second pair are also hybrid fractures, having strikes of 067 and 061 and dipping ~75° to the northwest and southeast (dark blue diamonds, Figure 3.38b). These fractures indicate a northeast-southwest oriented σ_1 direction. Within the southern and eastern areas of the domain fractures dip west and are contained in two main groups striking 006 and 136 (Table 3.27), normal to the average bedding surface (Figure 3.38c). These fractures are probably hybrid fractures with a 2θ angle of 46° (Table 3.27).

Faults and veins: Faults are very common in the northern half of the domain and produce a widely scattered distribution on an equal-area stereonet (Figure 3.38d). The small numbers of veins identified in the area also appear to describe no consistent pattern and are not consistent with any of the vein orientation patterns described in Domains 1 and 2.

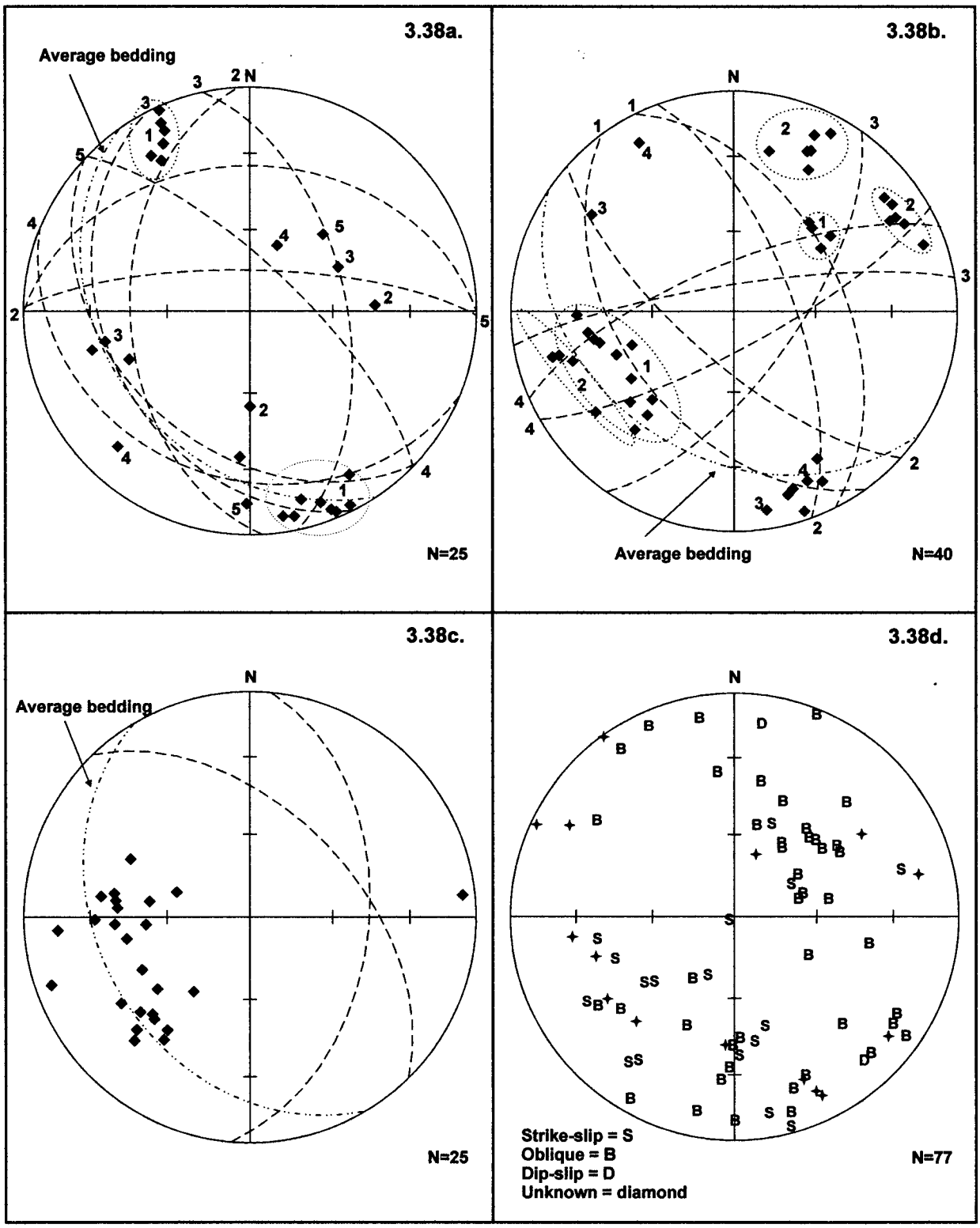

Figure 3.38 Study Area 2, Domain 3, a) fracture data from the northwest of the domain, b) fracture data from the north-central part of the domain, c) fracture data from the south and east of the domain, d) all fault and vein data from the domain.

Table 3.26 Bedding and cleavage data for Domain 3, Study Area 2. See Figure 3.37.

LOCATION	LITHOLOGY	BEDDING	CLEAVAGE		
		Average Strike/Dip	Average Strike/Dip	Spread in orientation[1]	Spread in dip[1]
Northwest	Cg 100%	144/35°SW	028/88°SE	59°	52°
North-central	Cg 80% Sst 20%	124/34°SW	035/86°NW	81°	52°
Northeast	Cg 100%	163/53°SW 133/32°SW	038/84°SE	81°	54°
South-central	Cg 100%	150/33°SW	046/88°SE	116°	68°

[1] Calculated from opposing extremes of cluster.

Table 3.27 Fracture data for Domain 3, Study Area 2. See Figure 3.38a-c.

LOCATION	FRACTURES				
	Number	Average strike/dip	Maximum 2θ angle	Style	Orientation of σ_1
Northwest	14	067/89°SE	-	Extensional	-
	2	090/35°N & 177/46°SW	87°	Conjugate shear	60°/132
	2	153/36°SW & 168/55°NE	89°	Conjugate shear	86°/173
	2	133/39°SW & 091/75°NE	42°	Hybrid shear	64°/111
	2	112/26°SW & 134/73°NE	81°	Conjugate shear	82°/303
North-central	15	136/43°SW & 154/50°NE	83°	Conjugate shear	82°/325
	16	132/71°SW & 160/68°NE	28°	Hybrid shear	59°/325
	2	081/80°NW & 035/67°NE	46°	Hybrid shear	37°/238
	2	067/72°NW & 061/77°SE	31°	Hybrid shear	78°/244
	5	068/74°NW	-	Unknown	-
South & East	22	004/51°SE, 138/53°NE	46°	Hybrid shear	25°162

Table 3.28 Fault data for Domain 3, Study Area 2. See Figure 3.38d.

LOCATION	FAULTS & VEINS				
	Number	Orientation	Average plunge/trend	Style	Number of veins
North-central	32	071/64°	- -	5 Strike-slip, 8 Dip-slip, 12 Oblique	6
	34	141/46°	- -	9 Strike-slip, 7 Dip-slip, 12 Oblique	6
Northwest	3	025/79°	-		3
South-central	4	063/68°	-	Oblique	
	5	137/41°	-	3 Dip-slip, 2 Oblique	

3.5.6 Domain 4

Domain 4 is located in the southeast corner of the basin (Figure 3.4b). This domain contains the greatest proportion of sandstone in the study area, approximately 40%. The other

60% of outcrop is conglomerate. Sandstone in this area is fractured to a far greater degree than in the north of the basin (Figure 3.39).

Bedding: Bedding strikes 005 and has an average dip of 31°NW within this domain (Table 3.29). The distribution of bedding continues in the small circle pattern created as a result of deformation throughout the basin (Figure 3.40a).

Cleavage: Cleavage strikes 072 with near vertical dip angles (Table 3.29). Cleavage orientation has a distribution of ~60° a relatively small variation for this Study Area (Figure 3.40a).

Fractures: Fractures form one group, with an average strike of 166 (Table 3.30). Fractures dip east and are normal to bedding (Figure 3.40b).

Faults and veins: No fault measurements were recorded within Domain 4.

Table 3.29 Bedding and cleavage data for Domain 4, Study Area 2. See Figure 3.40a.

LOCATION	LITHOLOGY	BEDDING	CLEAVAGE		
		Average Strike/Dip	Average Strike/Dip	Spread in orientation[1]	Spread in dip[1]
	Cg 62% Sst 38%	005/31°NW	072/87°SE	65°	81°

[1] Calculated from opposing extremes of cluster.

Table 3.30 Fracture data for Domain 4, Study Area 2. See Figure 3.40b.

LOCATION	FRACTURES				
	Number	Average strike/dip	Maximum 2θ angle	Style	Orientation of σ_1
	40	166/60°NE			

3.5.7 Domain 5

Domain 5 is situated along the southern boundary of the basin (Figure 3.4b). The domain contains a large proportion of sandstone (~40%), which is confined to the western end of the ridge. Further east the ridge is comprised almost entirely of conglomerate. As in Domain 4 the sandstone has a large number of fractures.

Bedding: Along the southern ridge of the basin, bedding strike changes by 20° (Figure 3.41a) from 080 in the east of the domain to 103 in the west (Table 3.31).

Figure 3.39 Sandstone unit from southeast corner of basin, showing the confused nature of planar features within these units. Width of picture 1 m. View looking northwest. Domain 4, Study Area 2.

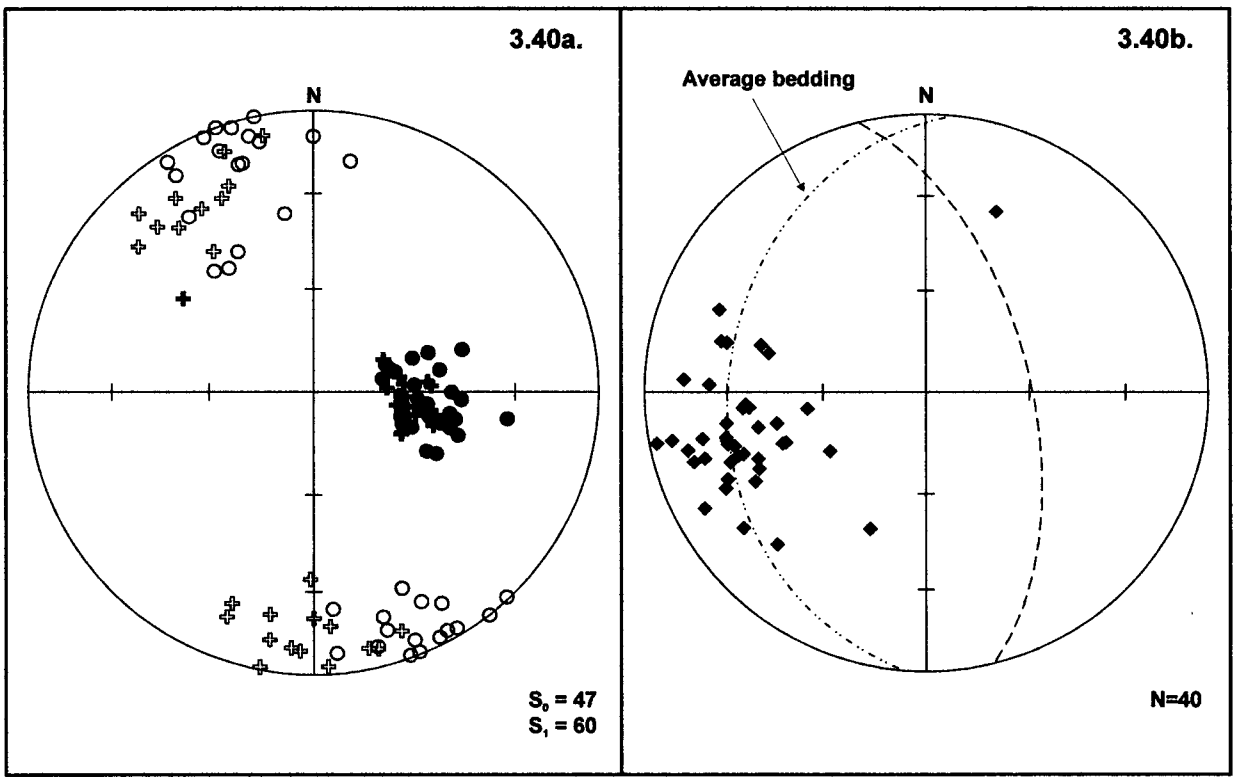

Figure 3.40 Study Area 2, Domain 4, a) all bedding and cleavage data, b) all fracture data.

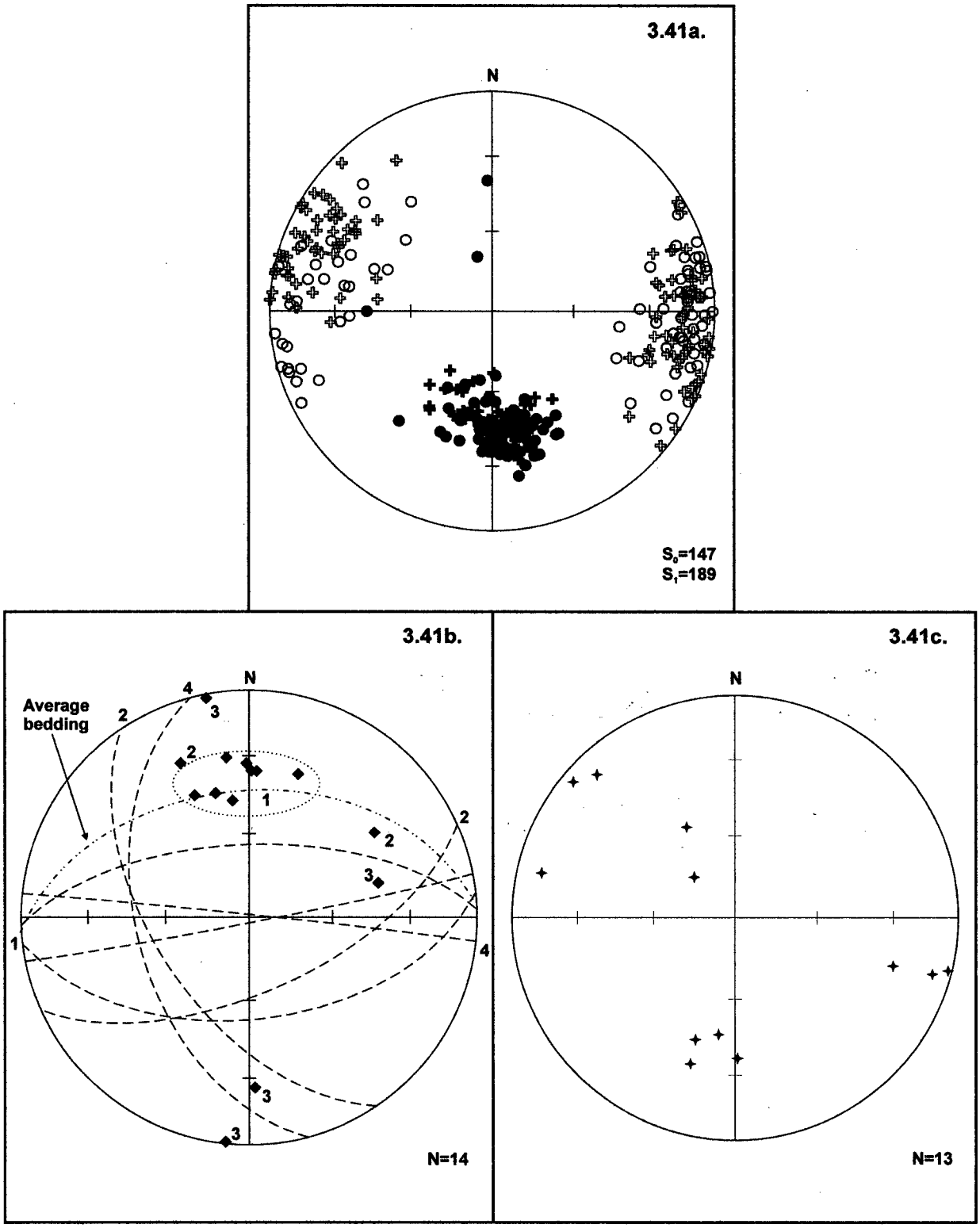

Figure 3.41 Study Area 2, Domain 5, a) all bedding and cleavage data, b) all fracture data, c) all fault and vein data.

Cleavage: Cleavage data also shows a change in orientation from 358 in the east of the domain (Table 3.31) to 016 in the west. The direction of dip also varies from east to west with cleavage planes predominantly dipping southwest at the eastern end of the ridge (Figure 3.41a) and southeast in the west.

Fractures: A dominant group of fractures are present in the domain normal to bedding (Table 3.32). Three sets of conjugate pairs are also present describing variable orientations (Figure 3.41b). The first of these pairs strike 066 and 146 (2, Figure 3.41b) with a 2θ angle of 80° (Table 3.32), a second pair strike 096 and 165 (3, Figure 3.41b). These conjugate pairs have a southeast oriented σ_1. A third pair strike 079 and 088 (4, Figure 3.41b), having a west-southwest shortening direction. The two conjugate pairs with southeast trending σ_1 have an oblique relationship with bedding suggesting they may have been deformed subsequent to their formation.

Faults and veins: Veins are predominant through the domain with no faults being recorded. The veins can be separated into three main groups (Figure 3.41c). The first group has a strike and dip of 101/50°NE, the second 056/19°SE and a third 024/89°NW (Table 3.33). These groups indicate variable vein orientation and do not correspond to other vein orientations within the study area.

Table 3.31 Bedding and cleavage data for Domain 5, Study Area 2. See Figure 3.41a.

LOCATION	LITHOLOGY	BEDDING	CLEAVAGE		
		Average Strike/Dip	Average Strike/Dip	Spread in orientation[1]	Spread in dip[1]
West	Cg 58% Sst 42%	103/39°NE	017/88°SE	59°	90°
East	Cg 71% Sst 29%	080/47°NW	358/86°SW	68°	71°

[1] Calculated from opposing extremes of cluster.

Table 3.32 Fracture data for Domain 5, Study Area 2. See Figure 3.41b.

LOCATION	FRACTURES				
	Number	Average strike/dip	Maximum 2θ angle	Style	Orientation of σ_1
	2	066/63°SE & 146/56°SW	80°	Conjugate shear	7°/105
	2	165/49°SW & 096/89°NE	70°	Conjugate shear	38°/119
	2	079/88°SE & 088/64°NW	Unknown	Hybrid shear	78°/263
	8	086/52°SE	-	Extensional	

Table 3.33 Fault data for Domain 5, Study Area 2. See Figure 3.41c.

LOCATION	FAULTS & VEINS				
	Number	Orientation	Average plunge/trend	Style	Number of veins
	4	101/50°NE	-		4
	3	056/19°SE	-		3
	6	024/89°NW	-		6

3.6 DISCUSSION OF STRUCTURAL STYLE, STUDY AREA 2

The basin dominating Study Area 2 is almost totally circular on its northern, eastern and southern sides. On the western side where the basin is open, extrapolation shows an elliptical extension to the basin shape (Figure 3.42). The open geometry of the basin on the western side is interpreted to have resulted from erosion. Bedding data were collected from a fairly constant elevation (within ~100 m), giving a horizontal slice through the basin at an elevation of 1600 m. When studied as a whole, bedding defines two best-fit small-circle distributions (Figure 3.43) indicating the basin changes shape.

3.6.1 Type 1 fold interference

The basin is the result of fold interference of a northeast-trending syncline and a northwest-trending syncline [*Evenchick*, 2001]. Superposed folding can occur by either simple shear or layer parallel flexural slip leading to the buckling of strata [*Ramsay*, 1967]. Evidence from Study Area 1 and the common presence of bed-parallel veins within Study Area 2 suggest folding in this case occurred by flexural slip. The style of interference structure produced is dependent on the style and morphology of the original structures. *Ramsay's* [1967] methods of classifying superposed folds (Figure 3.44) are based on the behaviour of layers undergoing simple shear, but produce patterns that are thought to sufficiently represent the range of patterns

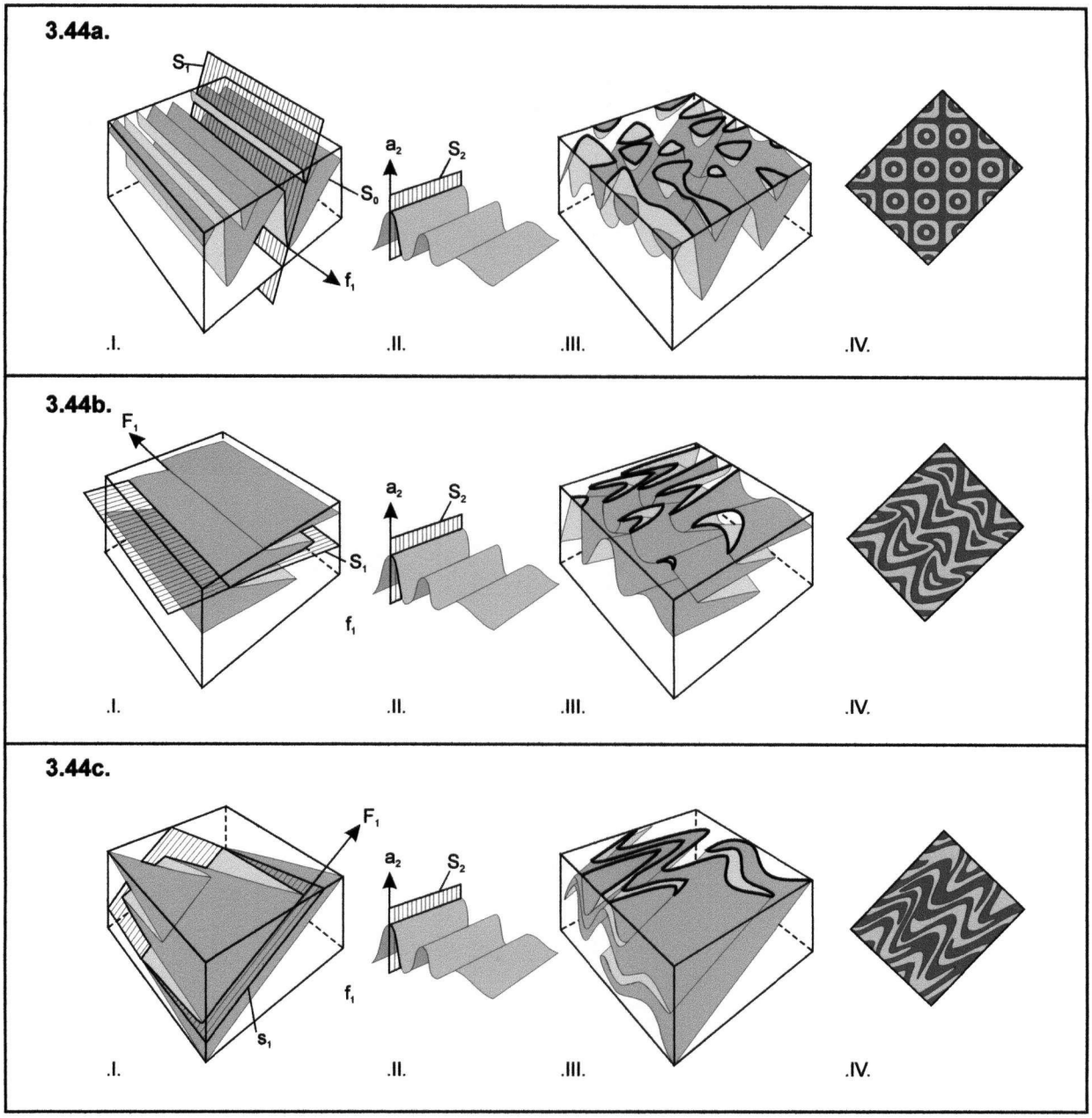

Figure 3.44 Classification of end member interference structures [modified from *Ramsay*, 1967; *Twiss and Moores*, 1992], a) Type 1 interference pattern b) Type 2 interference pattern, c) Type 3 interference pattern. i) initial fold, ii) superposed fold, iii) interference structure, iv) map view of interference pattern.

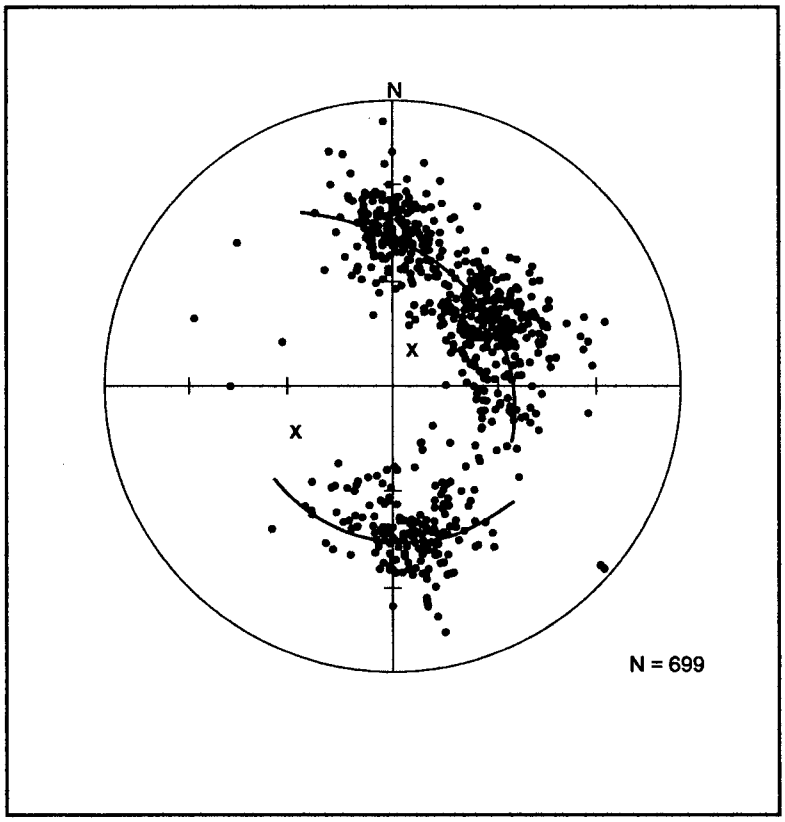

Figure 3.43 Small circle distribution of all bedding data from Study Area 2. Data from the south and east define a small circle with a cone axis plunging 62° towards 241, while data from the north of the basin define a small circle around an axis plunging 78° towards 019. The spread in data can be attributed to the rounded nature of the original fold hinges which causes the basin to be modelled by a large number of slightly varying cone geometries.

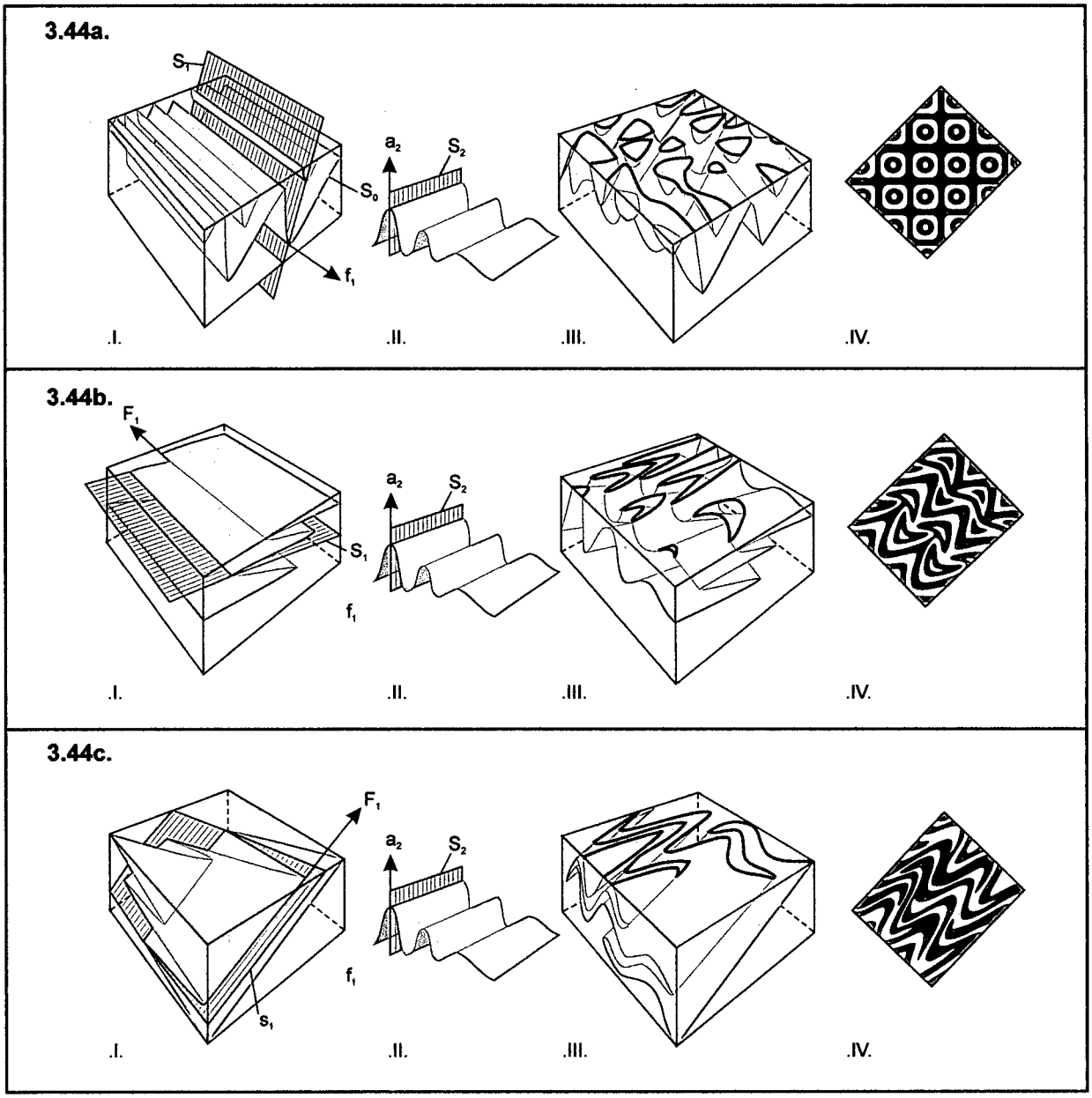

Figure 3.44 Classification of end member interference structures [modified from *Ramsay*, 1967; *Twiss and Moores*, 1992], a) Type 1 interference pattern b) Type 2 interference pattern, c) Type 3 interference pattern. i) initial fold, ii) superposed fold, iii) interference structure, iv) map view of interference pattern.

encountered in nature even though natural superposed folding must rarely occur by such simple deformation methods [*Thiessen and Means*, 1980].

The effects of superposed folding depend on the orientations of the axes describing the first generation of folding; d_1, the normal to the fold axis within the axial plane, f_1, the direction of the fold axis and c_1, the pole to the axial plane, relative to those of the second generation; a_2, the shear direction within the axial plane, b_2, the direction perpendicular to a_2 within the axial plane and c_2, the pole to the axial plane (Figure 3.45) [*Thiessen and Means*, 1980]. The relationship of these axes produces a number of interaxial angles α, between f_1 and b_2, β, between c_1 and a_2 [*Ramsay*, 1967], δ, between c_1 and c_2 and lastly γ, between f_1 and c_2 [*Thiessen and Means*, 1980]. These interaxial angles have been used to define a classification system for interference structures containing four end member models (Figure 3.44) [*Ramsay*, 1967] the distribution of these end members within the $\beta - \gamma$ plane is shown in Figure 3.46.

Type 1 interference occurs where the compressional force of the second fold generation is oriented close to the axial surface of the first folds, $\gamma + \alpha = 90°$. Where two antiforms are superimposed a culmination occurs, producing a dome. Two synforms produce mutual depressions; as a result, structures form a series of alternating domes and basins. The geometry of this type of interference structure produces a conical fold with a small circle distribution and a cone axis on a stereographic projection (Figure 3.43).

The structure in Study Area 2 forms a classic basin shape from above and in cross-section (Figure 3.47). The basin resulted from interaction between a northeast-trending syncline and a northwest-trending syncline [*Evenchick*, 2001]. According to *Ramsay* [1967] a Type 1 interference structure should be surrounded by four structures of the opposite polarity due to the effects of fold interaction. This is not seen in the area studied in this investigation due to the scale of the structures and the type of alpine terrain characterising most of the region, which causes interference structures to be difficult to observe unless in areas of relatively flat topography, as found in Study Area 2 [*Evenchick*, 2001].

3.6.2 Basin geometry

The geometry of the conical folds produced by Type 1 interference is controlled by three main factors [*Nicol*, 1992]; a) hinge zone curvature, b) interlimb angle and, c) the dip of the fold limbs. Hinge zone curvature defines the curvature of the dome or basin. Upright folds typically show a reduction in dip towards their hinge zone, therefore the interference of two folds at a high angle to each other results in a reduction in dip of the fold surface towards the centre of the

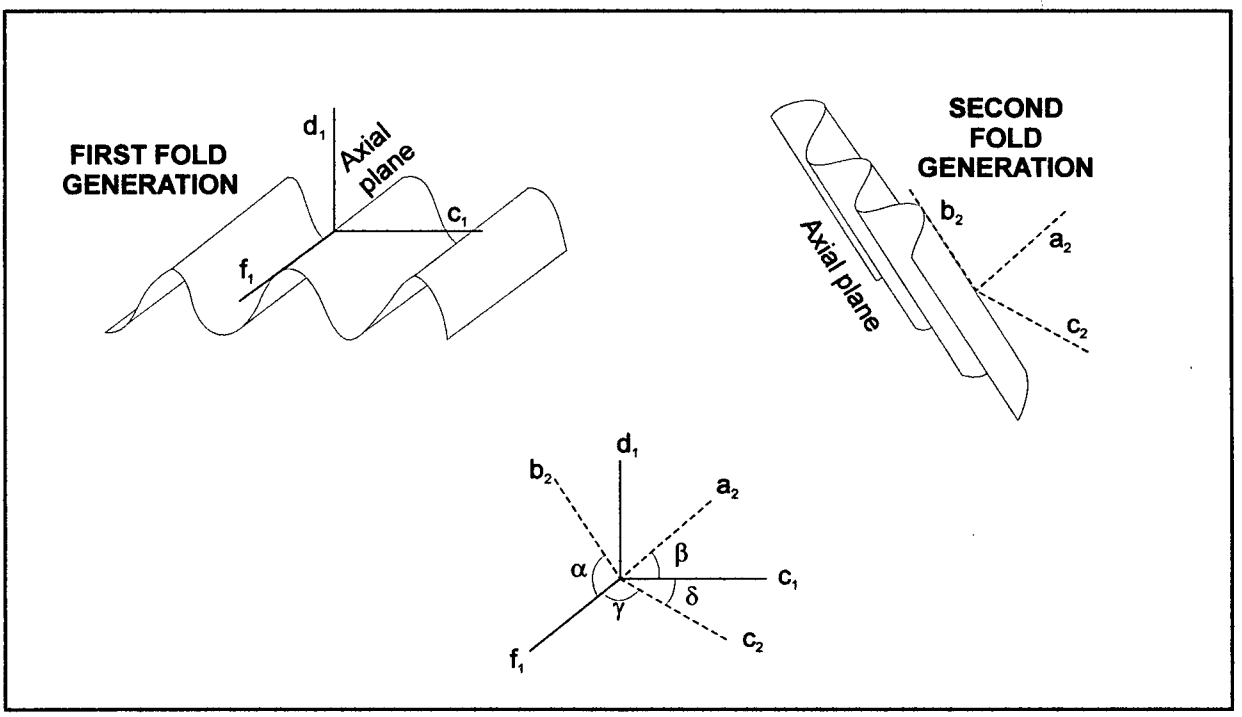

Figure 3.45 Orientation of axes describing the relative orientations of the two generations of folding. The relationships between these axes describe a number of angles which can be used to describe fold interference [*Thiessen and Means*, 1980].

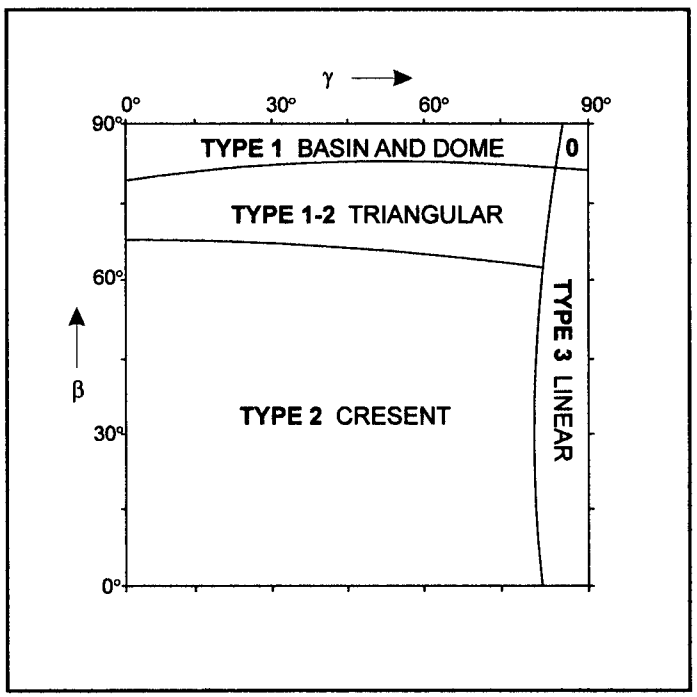

Figure 3.46 β-γ projection showing regions of the various fold interference styles. Boundaries are gradational [*Theissen and Means*, 1980].

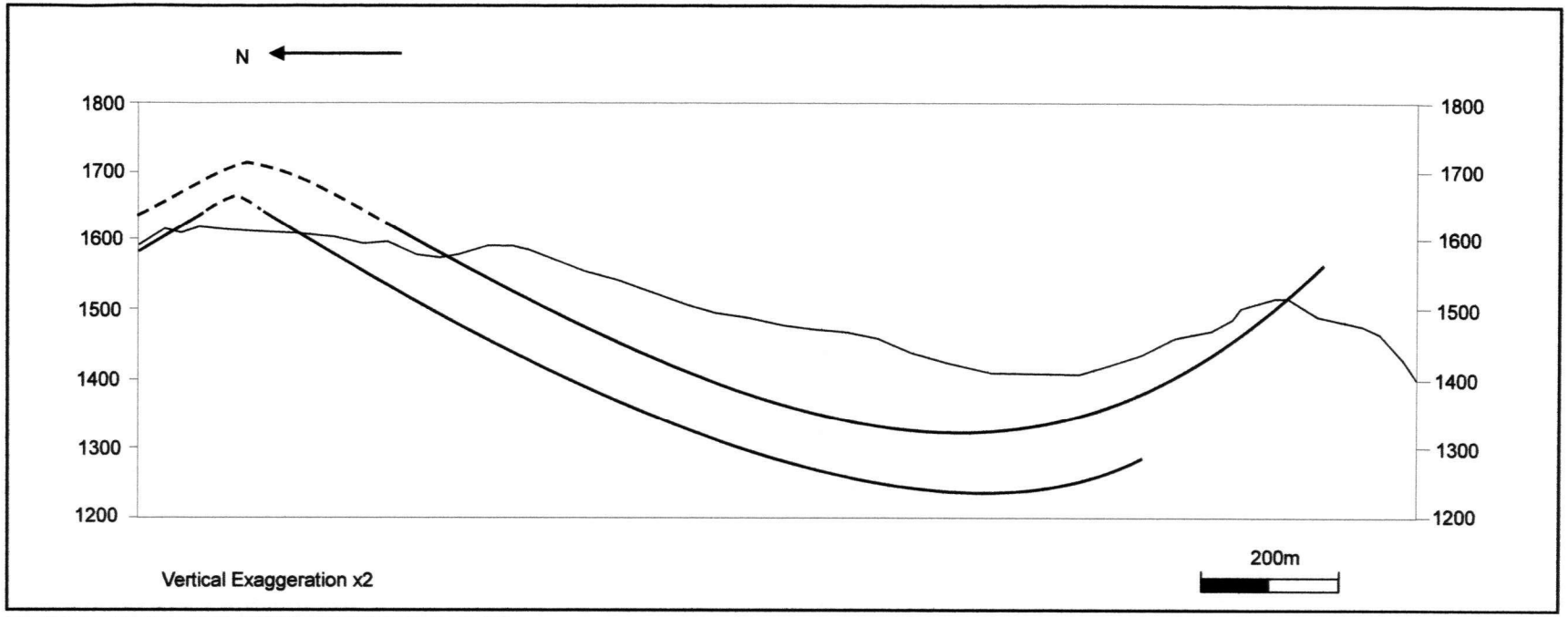

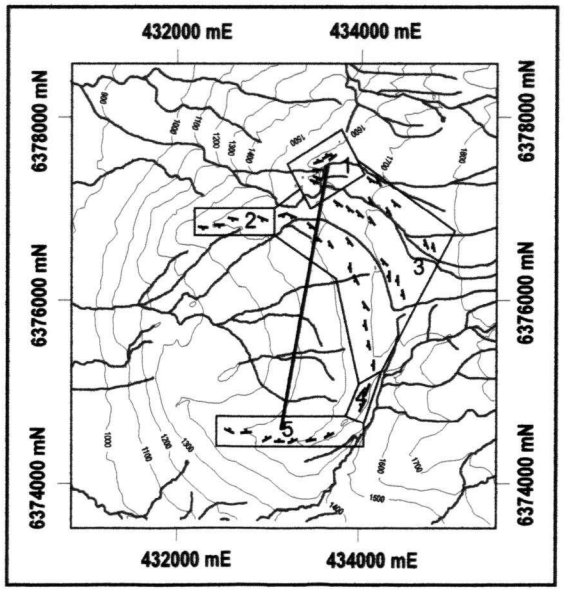

Figure 3.47 Cross-section through Study Area 2, showing curvature of basin in subsurface. Position of cross section can be seen in inset map.

interference structure (Figure 3.48). This is seen in the interference structure in Study Area 2. The interlimb angle of the fold sets controls the shape of the basin produced.

The combination of the two fold generations can be classified as a change in cone geometry where the superposition of similar interlimb angles will produce cones with a circular cross section whereas the combination of differing angles produces an elliptical cross section (Figure 3.49). From the general variations in basin geometry seen in Figure 3.49 it can be hypothesised that the two synclines forming the basin were either both open (8), or possibly one open and one gentle (9), producing a strongly circular basin with a relatively shallow base. This is supported by evidence from the cross section through the basin (Figure 3.47), fold geometries observed in Study Area 1 and regional structures where northeast- and northwest-trending folds are seen to be of comparable scales [*Evenchick*, 2001].

The dip of the fold limbs produces an increasingly complex basin geometry when one or both of the fold sets are asymmetric. Asymmetric limbs will produce differing cone geometries within the structure producing a dome or basin that has to be described by composite cone geometries. The geometry of the basin and the consistent dip values of bedding throughout suggest it was not produced by strongly asymmetric folds. The two folds are likely to be of a similar style to the en-echelon, symmetric northeast-trending syncline observed to the northeast of the study area and to the fold style of northwest-trending folds in Study Area 1.

3.6.3 Relative timing of folding

Type 1 interference does not allow conclusions to be drawn as to the relative timing of the interacting folds [*Ramsay*, 1967]. Cleavage across the basin varies from north striking on the western side to northeast striking on the eastern side. The west-trending anticline observed to the north of the basin has a variable orientation of cleavage ranging from northwest to northeast striking and an estimate of the fold-cleavage relationship from the mean cleavage value gives a transection angle of 63° in a clockwise direction. Cleavage across the basin is in general terms northeast-striking and no acceptable explanation for the variation in cleavage values within this area has been forthcoming. It is possible cleavage is associated with early folding and has subsequently been folded by the second event but the spread in data observed is not correlative with predicted changes to cleavage during Type 1 interference [*Ramsay*, 1967].

Bedding-cleavage intersection lineations could be used to indicate which structure has been refolded by subsequent deformation. It would be expected that lineations produced by the initial folding event would be refolded. Therefore, the cluster of D_1 intersection lineations would be spread across a lower-hemisphere stereonet projection, while the intersection lineations

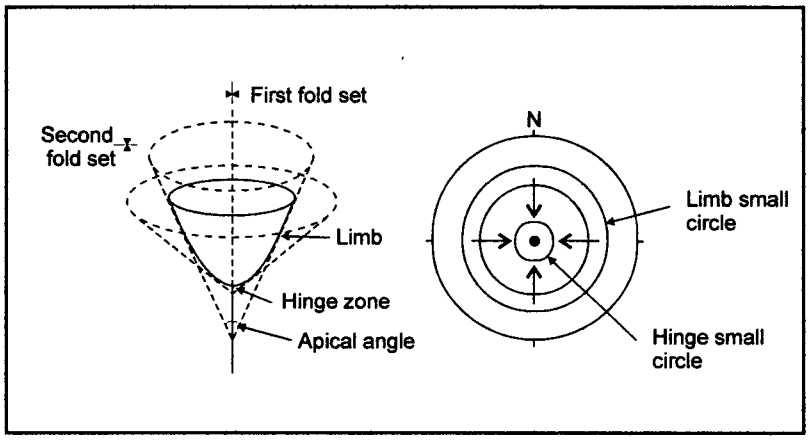

Figure 3.48 Schematic diagram and equal-area plot showing the expected changes in cone geometry with non-similar fold interaction. The arrows on the equal-area net indicate the reduction in small circle size representing the changes in fold limb geometry [*Nicol*, 1992].

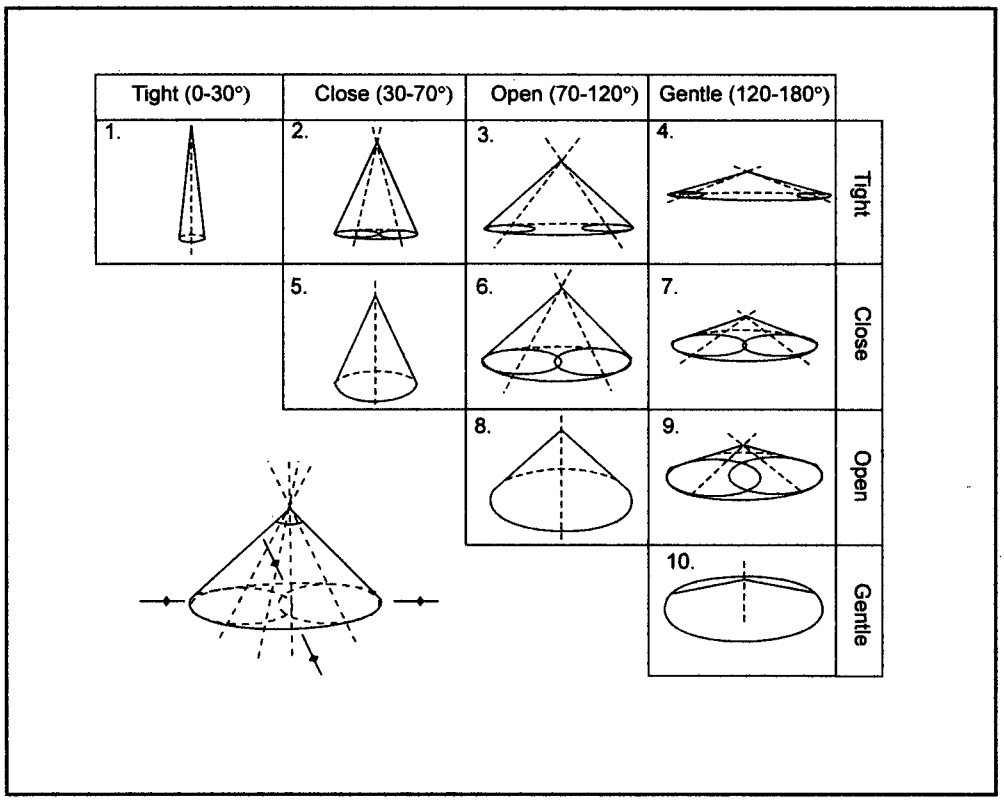

Figure 3.49 Predicted changes in the geometry of conical folds produced by changes in the tightness of the interfering fold sets. The fold sets are assumed to be upright and symmetrical; hinge zone curvature effects are neglected [*Nicol*, 1992].

produced by secondary folding would produce tight clusters in two quadrants. Bedding-cleavage intersection lineations, however, are unhelpful in this situation due to the transected nature of all northeast-trending folds observed within this study and the variable fold-cleavage relationships for northwest-trending folds.

The presence of a Type 1 interference structure in the region suggests that some folds in the western Skeena Fold Belt occurred as locally discrete events with one fold being produced independent of formation of the earlier structure [*Evenchick*, 2001].

3.7 STUDY AREA 3

Study Area 3 is located 25 km northwest of Bell II, 2 km northeast of the Ningunsaw River (Figure 3.4c). The area is situated northeast of the Stewart-Cassiar Highway and is the only study area located within a domain comprised solely of northeast-trending folds [*Evenchick*, 2001].

3.7.1 Lithology

The stratigraphy of the area is mapped as the Ritchie-Alger assemblage [*Evenchick et al.*, 2001]. The lithology in the study area is dominated by siltstone (~70%) with interbedded sandstone and minor conglomerate. The lithologic proportion values within Table 3.34 do not reflect this amount as they are calculated from recorded bedding measurements and these have a sampling bias of sandstone units. Sandstones occur as massive units ranging in thickness from 0.5-1.0 m (Figure 3.50a), or less commonly, as thin beds (<0.5 m thick) with well-developed cleavage and fracture planes (Figure 3.50b). Sandstone is medium grained throughout the area. Siltstone units occur as thin beds in sequences <0.5 m thick and are interbedded with sandstone units on a metre scale (Figure 3.51a). Beds show a range of sedimentary structures including cross-bedding in sandstones and concretions of greater than 50 mm within siltstone units.

3.7.2 Structure

The area is within a distinct zone of northeast trending folds [*Evenchick, et al.*, 2001]. Cleavage throughout the area is similar to the spaced cleavage observed in the other areas of this study. A normal separation of <5 mm in siltstones (Figure 3.51b) and ≥ 150 mm in sandstones (Figure 3.50b) is seen. The separation of cleavage planes in sandstone varies greatly depending on the type of sandstone.

3.50a.

3.50b.

Figure 3.50 a) Massive sandstone units, Study Area 3. Photograph is 1.5 m wide, looking northeast. Vein system observed is similar to blocky type seen in Study Area 1. b) Less massive sandstone units, well developed spaced cleavage and a number of conjugate fractures. Photograph is 0.8 m wide, up is left of page, looking northeast.

3.51a.

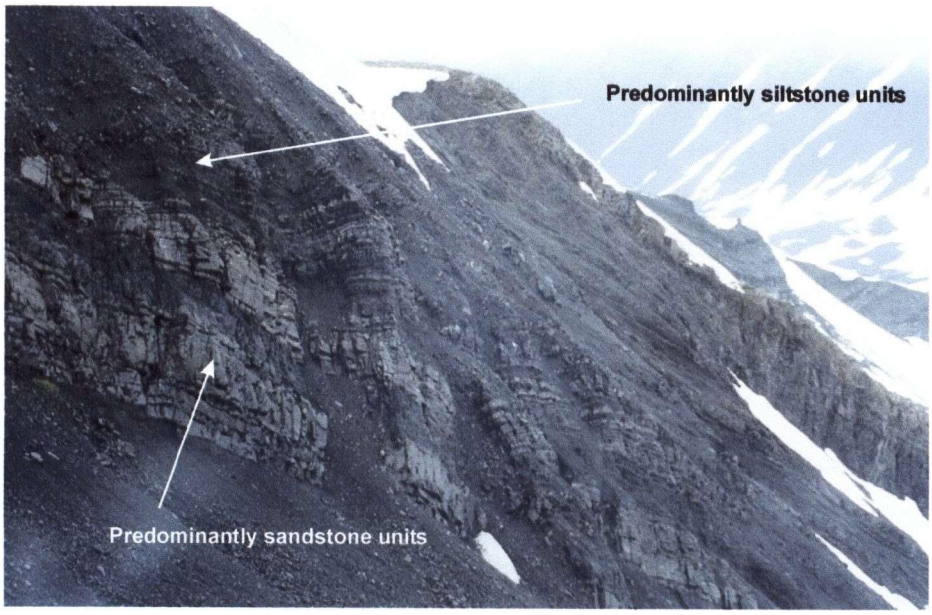

3.51b.

Figure 3.51 a) Interbedded sandstones and siltstones, sequences of predominantly sandstone or siltstone extend on metre scale. Field of view = 20 m, looking northeast. b) Spaced cleavage within siltstone unit, 0.5-1 cm between planes. Up is left of page, view looking northwest. Study Area 3.

Fracture planes are well developed throughout the area especially within siltstone units and conjugate shear fractures are common (Figure 3.52a). Faulting through the area is distinctly absent in comparison to the study areas further north. Within confined areas quartz veins are well developed, with areas of thick vuggy veins (Figure 3.52b) mainly within siltstone units, and areas of more systematic vein spacing (Figure 3.50a) mainly seen within sandstone sections.

3.7.3 Mesoscopic and Macroscopic Structures

North-northeast-trending fold: Study Area 3 contains an asymmetric syncline plunging 31° towards 013 (Figure 3.53c). Bedding strikes between 062 and 112 (Table 3.34) and dips ~35° towards the north and northeast (Figure 3.53a). The fold has non-planar limbs, indicated by the continuous distribution of bedding data along the profile plane, it has an average interlimb angle of 155° (Figure 3.53c). Cleavage strikes between 017 and 032 (Table 3.34) and is almost vertical throughout the fold. Cleavage transects the syncline by 13° in a clockwise direction.

Fractures: In the southeast of the study area fractures describe two main groups (Figure 3.54a). The largest of these groups (1, Figure 3.54a) strikes southeast (Table 3.35) 44° oblique to the fold axis. The second group of fractures (2, Figure 3.54a) describe conjugate pairs of fractures, those fractures with an average strike of 110 are parallel to the profile plane of the fold, perpendicular to bedding and fold trend. When combined with the opposing conjugate pair, this fracture system indicates a σ_1 direction of 079. In the northeast of the study area two main groups of fractures are also present (Figure 3.54b). Both fracture sets are oblique to the fold trend; the largest of these groups (1, Figure 3.54b) strike 026 (Table 3.35), 13° from the fold axis. The second group of fractures (2, Figure 3.54b) strikes 174 (Table 3.35), 19° from the fold axis. Other fractures recorded in this area are represented in too small a number to distinguish any pattern. In the northwest of the study area the same two groups of extensional fractures seen in the northeast are present striking 016 and 159 (Table 3.35). A number of conjugate shear fractures are also present in this area; a larger group (2, Figure 3.54c) have planes striking 055 and 114 (Table 3.35), implying a σ_1 direction of 085. A second group of conjugate fractures (3, Figure 3.54c) strike 004 and 168 (Table 3.35) and have a 2θ angle of 90°; these an almost vertical σ_1 suggesting these fractures were produced by burial compression/exhumation.

3.52a.

3.52b.

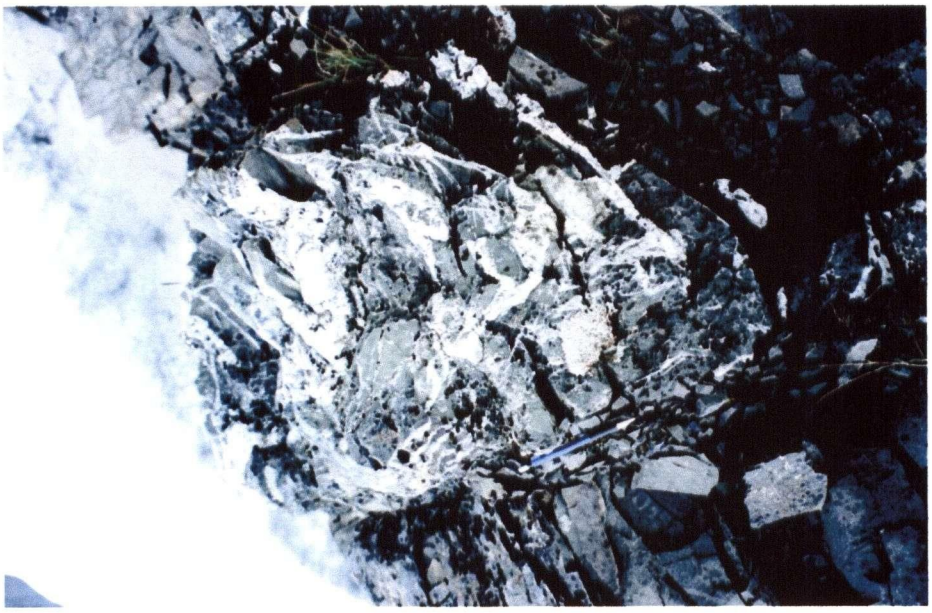

Figure 3.52 a) Conjugate fracture sets oriented east-northeast. Separation of fractures is 10's cm within sandstone units. View looking southeast. b) Well developed vuggy vein system within siltstone unit. Area of intense veins 0.5 m wide. Up is left of page, looking northwest. Study Area 3.

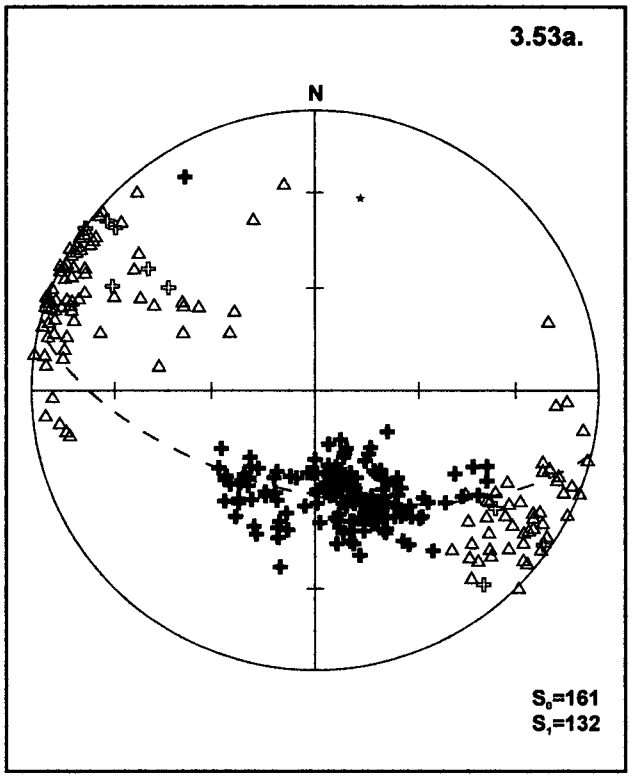

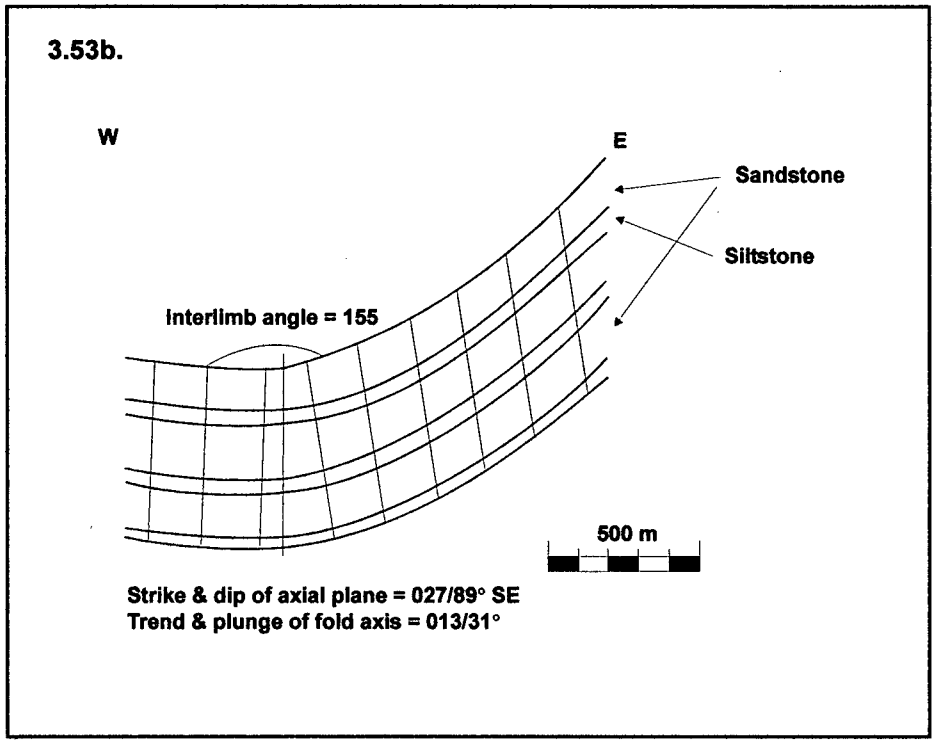

Figure 3.53 Study Area 3, a) all bedding and cleavage data showing northeast trending fold, b) down plunge view of northeast trending syncline, observed in the field. Cleavage transects by 53° in counter-clockwise direction. Profile Plane = 102/59°SW.

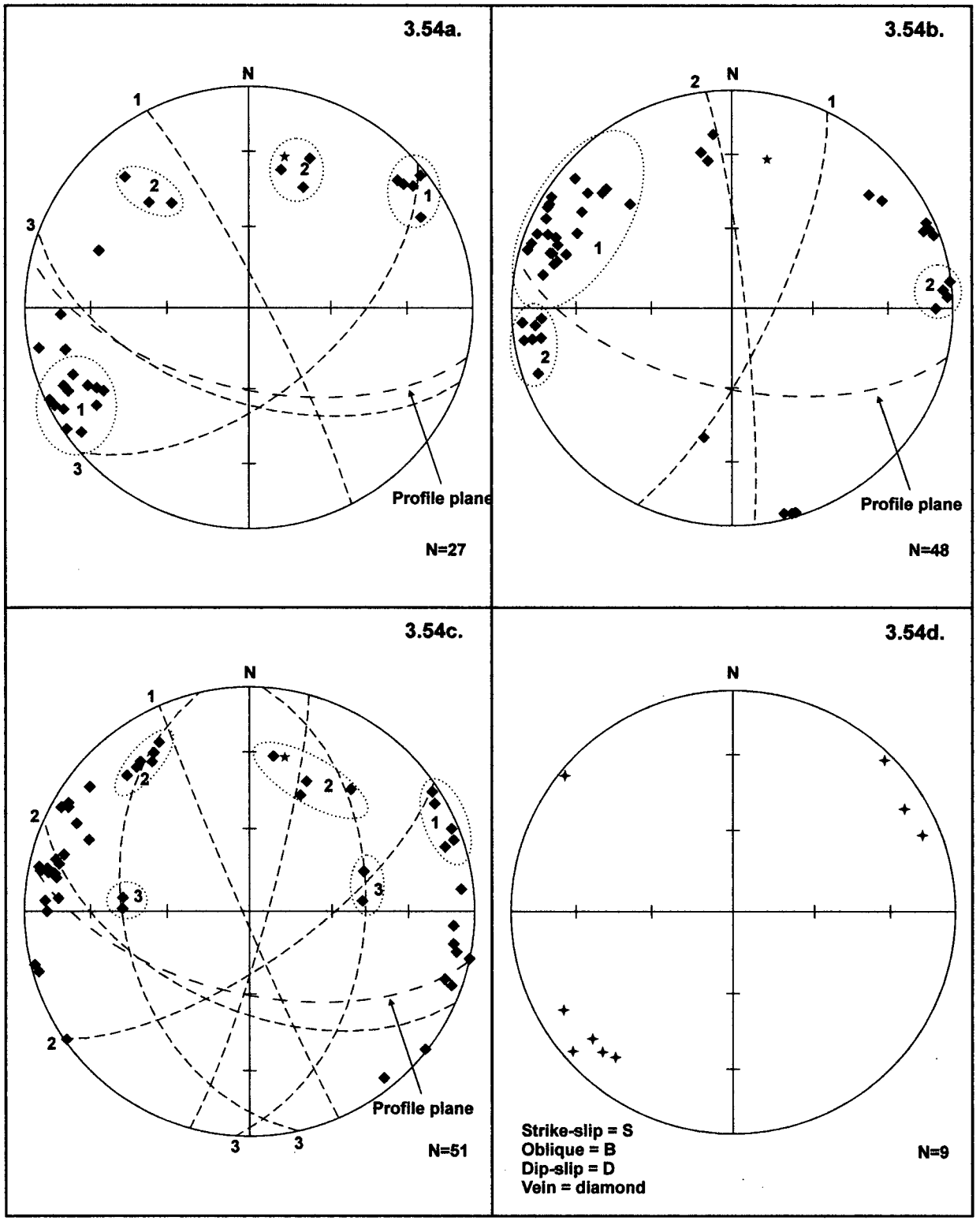

Figure 3.54. Study Area 3, a) fracture data from the southeast of the area, colours describe geometric patterns, described in text, b) fracture data from the northeast of the area, colours describe geometric patterns, c) fracutre data from the northwest of the area, colours describe geometric patterns, d) all fault data for area.

Faults and veins: Veins are concentrated in small areas with thick vuggy quartz veins with very complex systems (Figure 3.54d). Veins strike northwest but are poorly represented throughout the study area.

Table 3.34 Bedding and cleavage data for Study Area 3. See Figure 3.53a.

LOCATION	LITHOLOGY	BEDDING	CLEAVAGE		
		Average Strike/Dip	Average Strike/Dip	Spread in orientation[1]	Spread in dip[1]
Southeast	Sst 98% Slst 2%	067/38°NW	032/77°SE	29°	96°
Northeast	Sst 100%	071/27°NW	017/83°SE	64°	34°
	Sst 100%	062/37°NW	023/89°NW	36°	42°
Northwest	Sst 100%	112/34°NE	027/88°SE	42°	58°

[1] Calculated from opposing extremes of cluster.

Table 3.35 Fracture data for Study Area 3. See Figure 3.54a-c.

LOCATION	FRACTURES				
	Number	Average strike/dip	Maximum 2θ angle	Style	Orientation of σ_1
Southeast	17	149/84°NE	-	Oblique	-
	6	049/58°SE, 110/55°SW	61°	Conjugate shear	3°/078
	4	178/73°NE	-		-
Northeast	23	026/76°SE	-	Extensional	-
	12	174/84°NE	-	Extensional	-
	3	081/63°SE	-		-
	2	142/71°SW	-		-
	4	158/85°SW	-		-
	3	074/88°NW	-		-
Northwest	26	016/83°SE	-	Extensional	-
	9	159/87°SW	-	Extensional	-
	10	055/71°SE, 114/54°SW	59°	Conjugate shear	20°/084
	4	004/47°SE, 168/43°SW	90°	Conjugate shear	84°/357

Table 3.36 Fault data for Study Area 3. See Figure 3.54d.

LOCATION	FAULTS & VEINS				
	Number	Orientation	Average plunge/trend	Style	Number of veins
	2	158/81°SW, 149/79°SW			2
	1	039/87°SE			1
	6				6

Study Area 3 contains a large north-northeast-trending, asymmetric syncline with non-planar limbs. Cleavage is generally northeast striking and transects this fold by 13° in a

clockwise direction. Fractures across the fold are consistently oblique to the fold trend and suggest an approximate east-west compression direction.

3.8 DISCUSSION OF ALL STRUCTURAL DATA

3.8.1 Temporal progression of structure orientation in the study region

Northeast-trending folds consistently display transected fold-cleavage relationships. In Study Area 1, northeast-trending folds are transected in a counter-clockwise direction by northwest-striking cleavage. In Study Area 3, a north-northeast-trending fold is transected in a clockwise direction by northeast-striking cleavage. Within Study Area 2, no conclusion can be made as to whether northeast- or northwest-trending folding was first due to the nature of the fold interference. The relationship between northeast- and northwest-trending folds and cleavage in Study Area 1 suggests northeast-trending folds predate northwest-trending folds. Fold-cleavage relationships in Study Area 3 suggest a rotation of deformation from more northerly to northeast-trending structures.

North-trending folds within Study Area 1 are spatially associated with north or northwest-striking cleavage. These folds are predominantly located within an area of north-trending folds and cleavage in the eastern third of the domain, suggesting a partitioning of structural style. This area of north-trending structures contains a northwest-trending fold, transected by north striking cleavage. This would indicate that in this area northwest-trending folds predate north-striking cleavage. A north-northwest-trending fold, transected by northwest-striking cleavage is also present within Study Area 1, which would suggest the converse relationship between north- and northwest-trending structures.

A northeast-north-northwest temporal sequence of fold development is compatible with a model of development of deformation where fold orientations rotate through north as deformation orthogonal to the fold belt becomes increasingly dominant. An explanation of fold-cleavage spatial relationships may be the degree of compartmentalism of deformation within the fold belt. As the fold belt evolved and northwest-trending structures became increasingly dominant, areas of variation may still be present in the region and zones of structural overprinting in some areas may not follow the general large-scale trend of the fold belt. The style and orientation of controlling structures within the fold belt, such as a detachment horizon and large-scale faults, would also have a strong influence on fold orientation and may be an explanation for differences in fold orientations.

3.8.2 Mechanism of northeast-trending fold development

Northeast-trending structures are interpreted to be evidence of sinistral plate convergence in the early stages of the evolution of the Skeena Fold Belt [*Evenchick*, 2001]. Northeast-trending structures are suggested to have formed close to the plate margin in response to oblique convergence (Section 2.5). *Evenchick* [2001] suggested a number of possible explanations for the mechanics of fold belt development that account for the presence of northeast-trending folds (Figure 3.55) -

(i) Lateral change in the azimuth of the plate boundary.

(ii) Zones of high angle structures at the termination of wrenching.

(iii) Transtension [Sanderson and Marchini, 1984].

(iv) Partitioning of plate margin movement into en-echelon transpression zones.

(v) Plate margin had a more northerly orientation than thought.

(vi) Pure shear occurred in zones oblique to plate convergence.

As the evolution of the fold belt progressed, deformation in the fold belt was increasingly controlled by a thickening orogenic wedge encompassing the developing Coast Belt and fold belt, thereby producing the dominant northwest-trending structures of the Skeena Fold Belt in an easterly expanding zone [Evenchick, 2001].

According to the hypothesis of *Evenchick* [2001] the Skeena Fold Belt is the product of oblique plate convergence. This movement produced wrench faults parallel to the margin of the evolving Coast Belt. At the step-overs and tips of these faults southeast-trending shortening resulted in northeast-trending folds, option (ii) above (Figure 3.55b). As deformation continued the Coast Belt became a dominant control on the geometry of the developing fold belt and the orientation of plate convergence rotated to produce dextral convergence. This caused the shortening direction within the fold belt to rotate, becoming orthogonal to the plate margin, and northwest-trending folds to form in the easterly expanding fold belt.

3.8.3 Spatial progression of structure orientation in the study region

The model of Skeena Fold Belt evolution suggested by *Evenchick* [2001] gives a spatial as well as temporal progression with deformation extending eastwards through the development of the fold belt (Figure 3.56). Within the area of this investigation an eastward progression of older to younger structures is not seen; instead, a spatial pattern of partitioned deformation is observed. Study Area 2 in the north contains both northeast- and northwest-trending structures. Study Area 1 in the centre of the region contains a western zone of northeast-trending folds spatially associated with predominant northwest-trending folds. However, in the east of this

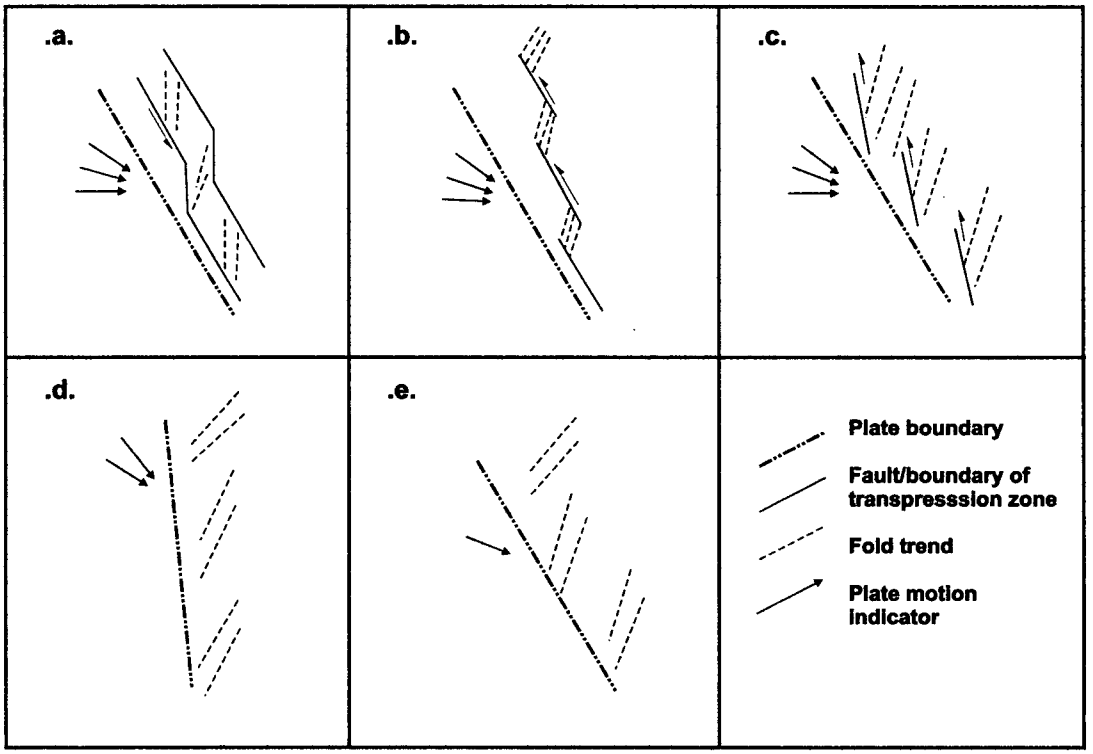

Figure 3.55 Possible environments of deformation producing northeast-trending folds within the Skeena Fold Belt. a) Lateral changes in the azimuth of the boundary. b) zones of high angle structures at the termination of wrenching. c) Partitioning of plate margin movement producing en-echelon transpression zones. d) Plate boundary had more northerly orientation than thought. e) Pure shear in zone oblique to convergence direction. Modified from *Evenchick* [2001].

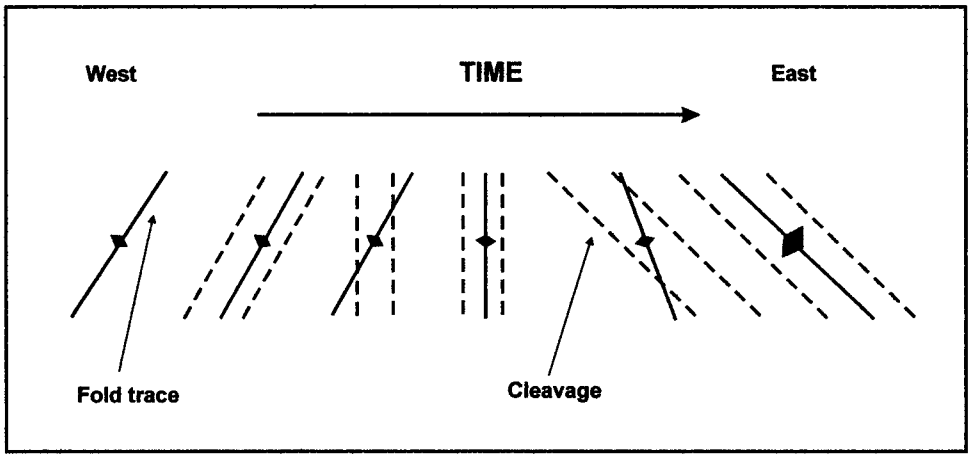

Figure 3.56 Spatial progression of changing fold and cleavage relationships across the Skeena Fold Belt [*Evenchick*, 2001].

study area northwest-trending folds are observed to be overprinted by north-trending folds. In Study Area 3 north-northeast-trending folds are transected by northeast striking cleavage.

The distribution of these patterns does not suggest a progression from west to east of northeast-north-northwest structures as observed by *Evenchick* [2001] in the southwestern Bowser Basin. This region in the northwest of the Bowser Basin suggests that deformation was occurring in different areas at different times, dependent on constraints other than an eastward expanding fold belt. A theory of deformation controlled by movement along relatively large-scale structures parallel to the Coast Belt can explain the spatial variation in progression of fold orientation by causing discrete areas of variable compression direction across jogs and crossovers within these structures.

3.8.4 Progressive versus poly-deformation

Changes in the orientation of structures within areas of the Skeena Fold Belt are interpreted to be the result of progressive deformation [*Evenchick*, 2001]. This is due to the development of deformation from northeast-trending through north to northwest-trending observed in the southwestern Bowser Basin [*Evenchick,* 2001]. Deformation in some areas of the Skeena Fold Belt has a spatial as well as temporal progression and suggests the orientation of shortening in this area changed as the fold belt developed, implying progressive deformation. In other areas of the Skeena Fold Belt structures are observed which do not follow a simple temporal and spatial progression [*Evenchick*, 2001], therefore it is hypothesized deformation is occurring by different sequences in different areas of the fold belt [*Evenchick*, 2001]. The fold belt is interpreted to be the result of plate convergence to the west of the Coast Belt. Investigations of plate motion from the Early Cretaceous to Early Tertiary [*Engebretson et al.*, 1985] show that plate margin convergence was continuous through the development of the fold belt, irrespective of changes in the orientation. Therefore the fold belt is interpreted to have been undergoing continuous if oblique compression throughout its evolution and deformation is interpreted on a large scale to be progressive.

Within the northwestern Skeena Fold Belt, structural evidence shows extreme variations in the orientation of shortening directions. The presence of a Type 1 interference structure within Study Area 2 suggests deformation in this area occurred as two separate events which interacted with each other to form the structural basin seen, therefore polydeformation. The presence of northeast-trending folds within Study Area 1 spatially associated with cleavage that has a strike of 90° away from their fold trend suggests overprinting of different fold events rather than transection through progressive deformation. The northwestern Skeena Fold Belt can be

interpreted as containing domains on scales of 10's km where observed deformation has occurred as relatively defined deformation events, however, the time lapse between these domains is unknown. All work in the area has concentrated on relative ages of structures as there is no definitive way to deduce the absolute temporal relationships of these structures. This also means we do not know the timing of similar structural styles in different areas of the fold belt and so cannot prove that one phase of deformation was occurring throughout at one time. In fact it is very likely from the mechanisms of deformation discussed above that deformation was not temporally consistent across regional scale areas.

The regional evidence indicates an overall progressive deformation sequence through the evolving Skeena Fold Belt [*Evenchick*, 2001]. Therefore the data within this investigation has been interpreted within the framework of progressive deformation. This allows the fold-cleavage relationships observed throughout the area to be defined as 'transected cleavage' rather than overprinted cleavage. Evidence from the current investigation suggests that within the Skeena Fold Belt regions on a scale of 10's of km show periods of deformation involving non-coaxial strain. This strain occurred during discrete events and therefore is interpreted on a small scale as polydeformation. This difference between the behaviour of the fold belt as a whole and areas within the belt is compatible with theories of the development of deformation. Deformation, although being continuous overall, is commonly partitioned within regions, with some regions showing a concentration while other areas have subtle or absent degrees of deformation [*Passchier and Trouw*, 1998]. This supports the observations and hypothesis of Skeena Fold Belt deformation developed by *Evenchick* [2001].

3.8.5 Fold development

The Skeena Fold Belt is a thin skinned fold and thrust belt. The dominant features of the belt are folds produced by thrust fault movement [*Evenchick*, 1998]. Thrust-related folds are described by three end-member geometries that depend on the relationship between thrust faults and overlying anticlines [*Storti and Poblet*, 1997]:

a) folds that develop at the tip line of thrust ramps,

b) folds that develop above layer-parallel thrusts,

c) folds that develop above non-planar thrusts.

These end-member geometries have been described by three kinematic models developed to quantitatively describe thrust-related folding. The models reflect the relative dominance of buckling versus faulting [*Jamison*, 1992]. Fault-propagation folding describes type (a) folding,

detachment folding describes type (b) folding, and fault-bend folding describes type (c) folding (Figure 3.57).

The presence of a number of strongly asymmetric anticline-syncline pairs within Study Area 1, the asymmetric geometry of a number of folds, the spatial association of vein and fault concentrations with hinge zones and the lack of large-scale break thrusts through fold hinges suggest the majority of folds in the region were produced by fault-propagation folding.

Within fault-propagation folding, faulting and buckling are synchronous [*Jamison*, 1992]. This occurs by fault displacement reducing to zero at the fault tip and all movement being transferred into the folding of overlying stratigraphy [*Mosar and Suppe*, 1992]. The key feature of fault-propagation folds is the fact that fault shape constrains fold geometry [*Thorbjornsen and Dunne*, 1997], and the steeper the fault ramp the tighter the folding above.

3.8.6 Fixed versus migrating hinge folding

Fault-related folding mechanisms can generally be divided into two separate categories: folding produced by limb rotation about fixed axial surfaces, 'fixed-hinge folding'; and folding involving the lateral migration of active axial surfaces, 'active-hinge folding' (Figure 3.58) [*Salvini and Storti*, 2001]. Classic models of fault-related folding tend to rely on fixed-hinge folding where anticlinal crests are the preferred site for concentrated deformation, whereas a number of recent models investigate the impact of active-hinge folding where deformation is concentrated in the limbs of the folds leaving the fold crests relatively undeformed [*Salvini and Storti*, 2001]. The main characterisics of these mechanisms can be seen in Table 3.37 below.

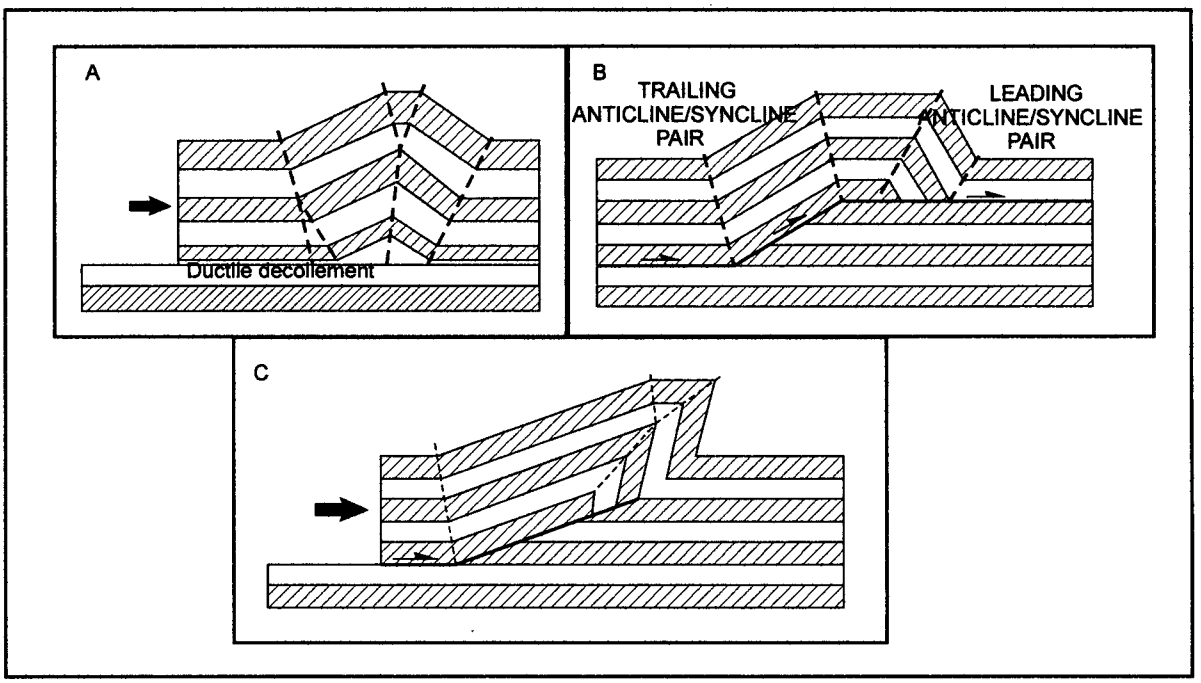

Figure 3.57 Models of thrust-related faulting a) detachment folding, b) fault-bend folding, c) fault-propagation folding [*McClay,* 1992].

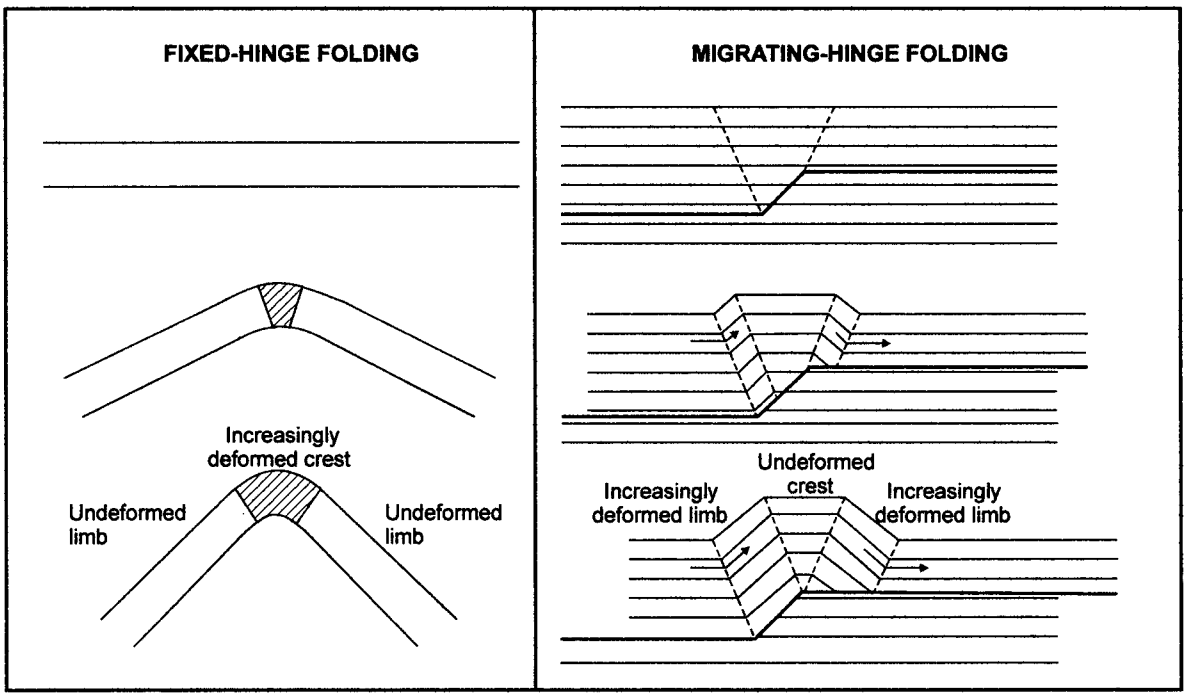

Figure 3.58 Fixed-hinge folding versus migrating-hinge folding [*Salvini* and *Storti*, 2001].

Table 3.37 Fixed-hinge folding versus active-hinge folding [*Salvini and Storti*, 2001].

FIXED-HINGE FOLDING	ACTIVE-HINGE FOLDING
- Deformation is concentrated in the axial surface area and as the fold develops the dimensions of the deformed zone do not significantly increase. - Deformation intensity is concentrated in the hinge zone and decreases towards the limbs. - A correspondence between layer curvature and deformation intensity is expected, with the maximum intensity at the fold hinges.	- Deformation develops in hanging wall rocks as they pass through an active axial surface. - Deformation is concentrated in fold limbs, leaving the crest of the fold unaffected. - Continued folding and fault slip produces an increase in the dimensions of deformed rock panels. - Deformation intensity may be assumed to depend on the angle, number and sense of rotation of deformation panels.

Within the region of study, the intensity of fractures and faults does appear to increase as a fold hinge is approached. The intensity of veins belonging to the thick, vuggy vein set also appear to cluster around fold hinge locations. This would suggest folds in this region were produced by fixed-hinge fold development.

3.8.7 Physical conditions of deformation

The predominance of a spaced cleavage, the abundance of extensional and shear fractures and small-scale faults are consistent with deformation having occurred at shallow depths of <6 km. This is supported by the lack of metamorphic minerals identified within the region. Regional work in the Bowser Basin indicates that the sediments have undergone sub-greenschist metamorphism [*Evenchick*, 1991a]. Work in the eastern region of the Bowser Basin, from clay analysis and coalification analysis, concluded that any metamorphism within the basin sediments was a product of burial metamorphism and temperatures were in the range of 150-200° [*Moffat*, 1985].

The high density of quartz veins in the area indicates that fluids were present during deformation. In particular bed-parallel veins with slickensides perpendicular to fold axes indicate that fluids were influential during fold development by flexural slip. Thick, vuggy veins with euhedral crystal development suggest high fluid pressure during formation. Quartz veins appear to occur in higher concentrations within sandstone units (Study Area 1, Domains 1 and 3), suggesting a likely local source of silica from within these units.

The presence of wet rocks being buried and deformed relatively quickly after burial will promote high fluid pressures. Fluids would be channelled along zones of weakness, most easily

fault planes [*Sibson*, 1996]. Along Highway 37 two areas of intense faulting were observed, 25 km and 40 km north of Bell 11. These areas contain thick (>10 cm) veins comprising multiple sequences of thin veins separated by laminae of country rock and containing up to three orientations of slickensides. These fault planes are shallowly dipping and indicate episodic fault movement associated with elevated fluid pressures [*Sibson*, 2001]. Thus, fluids are interpreted to have facilitated both thrust faulting and flexural slip folding during deformation.

4 REFLECTION DATA

Prior to the acquisition of seismic reflection data along Highway 37 a number of projects have provided subsurface information for this area. Gravity data are available for the Bowser Basin, but the normal use of these data to identify gravity anomalies and relate these to surficial rock types and structures lacks usefulness within a sedimentary basin where the majority of rock types have similar density values. However, the approach is useful for estimating the thickness of sediments because of the strong density contrast between sedimentary and crystalline rocks, but such work requires detailed modelling, which has not been undertaken thus far. The SNORCLE refraction and wide-angle reflection experiment produced an estimate of 4 km for the depth of the boundary between Bowser Basin sediments and rocks of Stikine Terrane [*Hammer et al.*, 2000]. This estimate is based on a rapid increase in velocities from 3.4-5.6 km/s within the first 1-6 km to 5.7-6.2 km/s below this depth [*Hammer et al.*, 2000]. Magnetic data for Stikinia are also available. Spectral analysis of the magnetic field in the area of the SNORCLE transect yields an estimate for the maximum depth to the magnetic basement of 3.5 km [*Lowe et al.*, 1998].

SNORCLE reflection data were acquired using equipment and parameters specified by Lithoprobe to enable imaging at depths into the upper mantle (Table 4.1). The data were recorded to 32s with a 20 s sweep length. However this study is interested primarily in images of the upper crust. Thus, only the upper 8 s (~24 km) of data have been used. Processing for Line 2A was carried out by personnel at the Lithoprobe Seismic Processing Facility (LSPF), at the University of Calgary. Table 4.2 indicates the data processing flow from uncorrelated shot gathers to the final stacked seismic section.

Table 4.1 Data acquisition parameters [*Cook et al.*, 2001].

PARAMETER	VALUE
Number of vibrators	4 or 5
Number of sweeps	5 or 4
Sweep frequencies	10-80 Hz (linear)
Sample rate	4 ms
Sweep length	20 s
Record length	32 s (uncorrelated)
Number of channels/record	576
Receiver station spacing	50 m
Number of geophones	9 per station
Vibrator point spacing	75 m
Geophone frequency	10 Hz
Nominal fold	192
Instrument	I/O 2000, 24 bit telemetered

Table 4.2 Data processing parameters [*Cook et al.*, 2001].

PARAMETER	VALUE
Diversity-type stack of uncorrelated records	
Extended cross-correlation	32 s record length
Crooked line geometry	25 m x 2000 m bins
Notch filter, where necessary	
Trace edits, first break picks	
Refraction statics computation	Two layer
Velocity analysis	Local constant velocity stacks
Application of first break mutes	
Automatic gain control	800 ms window
Gapped deconvolution	32 ms gap, 100 ms operator
Statics application	
Normal moveout correction on common midpoint gathers	
Residual statics computation	4.0-8.0 s window
Cross-dip correction	
Trim statics	4.0-12.0 s window +/- 12 ms
Stack	Nominally 192 fold

SNORCLE Line 2A extends for 690 km, from Stewart, British Columbia to north of Watson Lake, Yukon along available highways. A 100 km segment of the line, approximately from Bell II to Iskut, was selected to relate to the geological study of this thesis (Figure 1.3). This segment crosses the northwest part of the Bowser Basin and extends into rocks of Stikinia for ~20 km north of the basin. Two components of the data set are utilized in this study.

During the LSPF processing, first-arrival travel time picks are made for individual shot gathers in order to apply 'refraction statics' corrections; see Table 4.2. In this study, these first-arrival data are used to derive a near-surface (<3 km depth) velocity structure that could relate to the geologically observed features. Velocity analysis of the first-break data for a 50 km data segment nearest the three geological study areas is carried out using 3-D generalized linear inversion procedures (GLI-3D) and 2-D ray-trace modelling (RAYINVR) to produce models of velocity variations within the upper 3 km of the crust. These models take into account variations in surface features such as the presence of bog and glacial debris in comparison to areas of surficial weathered bedrock.

The stacked structural sections from the LSPF for the 100 km segment are used for a preliminary interpretation. However, to provide a more geometrically 'correct' presentation of the data and to be more useful for interpretive purposes, the stacked data need to be migrated. Migration requires the specification of velocity structure. For this study, the near-surface velocity structure derived from the first-arrival analyses are merged with velocities to depths of 25 km determined from the earlier SNORCLE refraction/wide-angle reflection experiment carried out

along the same highway [*Hammer et al.*, 2000]. This laterally varying upper crustal velocity model was then used to migrate the portion of Line 2A within this investigation for the upper 8 seconds of data.

4.1 ANALYSIS OF FIRST-BREAK ARRIVALS

4.1.1 GLI-3D analysis

First-break travel time picks from the selected 50 km segment of reflection data are used to calculate a 2-D velocity versus depth model with the commercial software package, GLI-3D. This package generates the velocity model and 2-D and 3-D refraction statics using a 'generalised linear inversion' (GLI) algorithm [*Hampson and Russell*, 1984]. Application of the refraction statics is one stage in the processing stream (Table 4.2), but within this research the analyses were used for velocity information only. The 3-D capabilities of the algorithm are employed to take into account the non-linear nature of the recording line. This procedure allows modification of the data set such that it can be represented by a straight line for computational purposes. An initial subsurface model, comprising a series of layers whose thickness and velocity may vary both laterally and vertically, is defined. In this case, the initial model is defined by identifying breaks in slope on time versus distance plots of first-break travel time picks. Three main layers are identified (Figure 4.1). This preliminary model is used as the starting model for a 2-D tomographic inversion procedure undertaken within the GLI-3D package.

Tomographic inversion involves calculation of travel time data from a specified (initial) velocity model and comparison of these data to the observed travel times. The comparison uses a least squares calculation from which the error between the observed and modeled travel times is calculated. The velocity model is revised by the algorithm, which uses an algebraic reconstruction inversion technique in an attempt to reduce the error. Then a new set of travel time data is calculated for comparison with the observed travel times. This process is repeated until the model generates a best fit between the calculated and observed travel times, taking into account the timing errors assigned to the observed data. For the selected 50 km segment of Line 2A, the inversion was undertaken within a grid of 50 m squares to a total depth of 1 km. Three iterations from the starting model were necessary to meet the stopping criterion.

The derived velocity model shows complex velocity variations within the upper 300 m that range from 2.0 to 4.1 kms^{-1} (Figure 4.2). Such variations may reflect differences within the uppermost layer associated with weathering and glacial deposits. These slower near-surface velocities increase in depth toward the northern end of the line. A gradual increase in velocity in

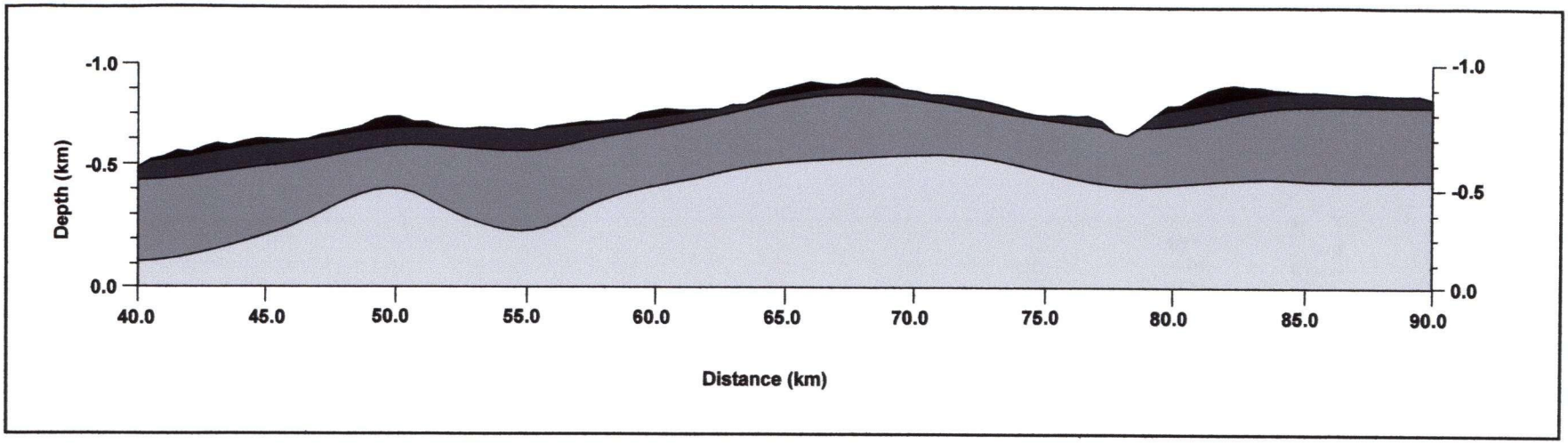

Figure 4.1 Depth versus distance model of velocity layers defined within GLI-3D. Layers defined by assessing changes of slope in time versus distance plots of first break arrival picks. Distance is defined from Bell II.

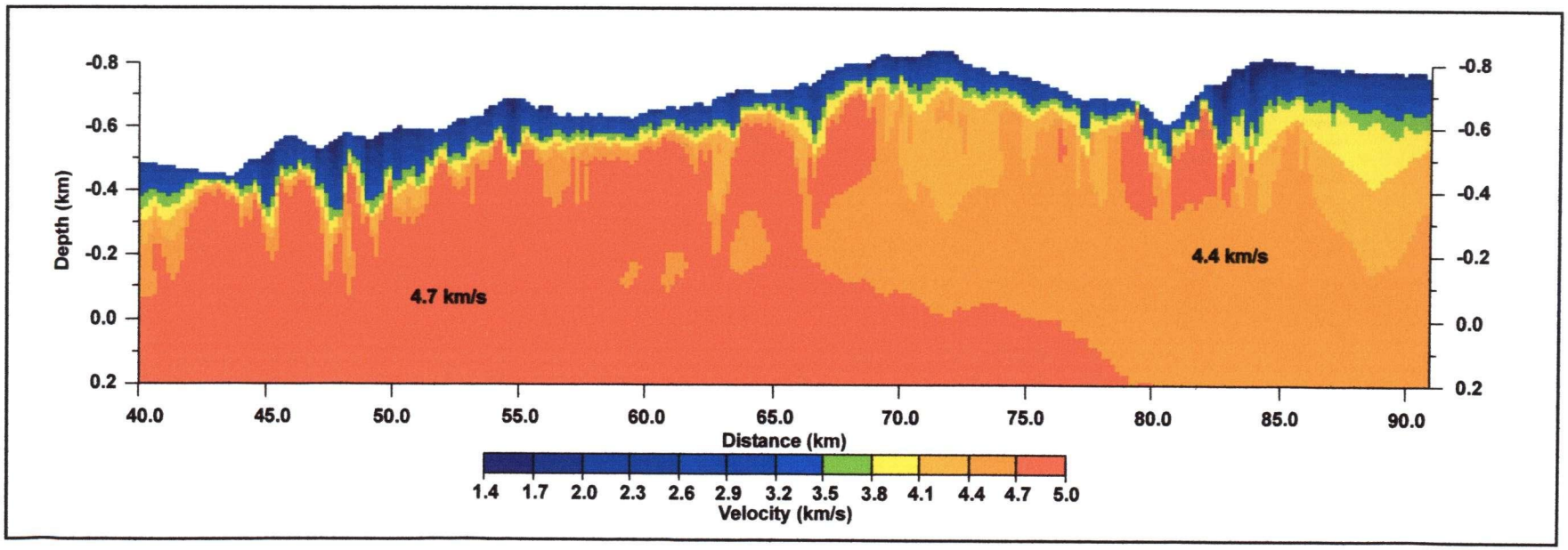

Figure 4.2 Tomographic inversion of initial model within GLI-3D. Inversion uses an algebraic reconstruction technique within a grid of 50 m squares. Distance is defined from Bell II.

the lower 700 m of the model from 4.1-4.7 kms^{-1} to 4.7-5.0 kms^{-1} occurs from kilometre 80 to kilometre 40 at the southern end of the line segment.

4.1.2 2-D ray tracing

The basic principle of ray tracing for forward modelling to generate a velocity model is to repeatedly compare the theoretical response of a laterally heterogeneous medium with observed data until a velocity model is constructed that provides a suitable match between the calculated and observed response [*Zelt and Smith*, 1992]. Ray tracing for this investigation also uses the first-break travel times derived from the LSPF processing. Analysis is undertaken using the TRACE algorithm of the RAYINVR programme [*Zelt and Smith*, 1992].

Within RAYINVR, an input velocity model is constructed as a layered, variable-block-size representation of a 2-D isotropic velocity structure. Laterally and vertically varying layers are constructed across the model with the only specification being that they must not cross another boundary (Figure 4.3). Within each layer, an arbitrary number and spacing of upper and lower layer velocity points specify the P-wave velocity. This enables a laterally and vertically heterogeneous velocity field to be defined within each layer. This parameterization allows the velocity model to be treated during ray tracing as a lateral sequence of trapezoidal blocks separated by vertical boundaries wherever a change in layer boundaries or velocity is specified (Figure 4.3). The advantages of this structure within the input velocity model include allowing variations in velocity to be represented in an efficient and predictable manner, and producing a model which is easily adjusted while remaining consistent and well defined [*Zelt and Smith*, 1992]. Rays are traced through the velocity model using zero-order asymptotic ray theory by solving the ray tracing equations numerically [*Cervený et al.*, 1977] using the Runge-Kutta method [*Sheriff and Geldart*, 1995]. Snell's Law is applied at the intersection of a ray with a layer boundary.

For this investigation, the preliminary model produced by GLI-3D is used as the starting velocity model for the forward modelling 2-D ray tracing procedure. Rays are traced from every twentieth shot point, or at 1.5 km intervals. The model results are then compared to the results from the observed first-break picks at each of these shot points (Figure 4.4). This process is repeated with an adjusted velocity model until the chi-squared values, an indication of the quality of fit between the calculated and observed models, are as near to or less than unity as is possible [*Zelt and Smith*, 1992].

The road along which the studied section lies runs along the bearing 305° for its southern 10 km in comparison with an approximate north-south trace for its northern 40 km (Figure 4.5). To accommodate the 2-D ray tracing procedure, this change in orientation is accommodated by

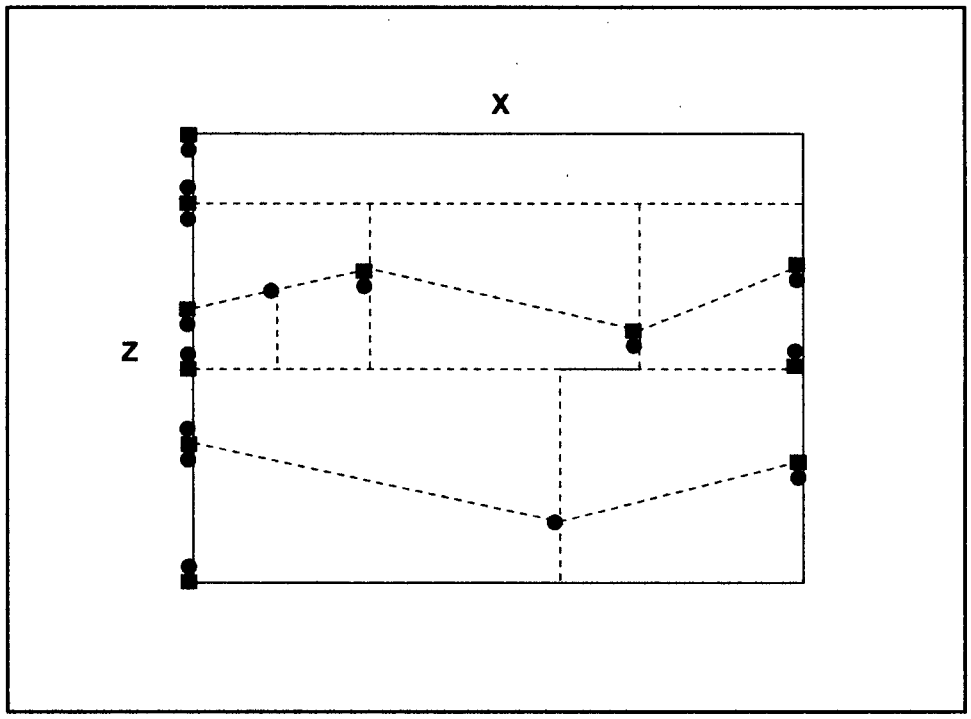

Figure 4.3 Schematic diagram of RAYINVR parameterization. Boundary nodes (squares) define layers and velocity points (circles) define velocity changes within layers causing model to be separated into trapezoidal blocks for ray tracing [*Zelt and Smith*, 1992].

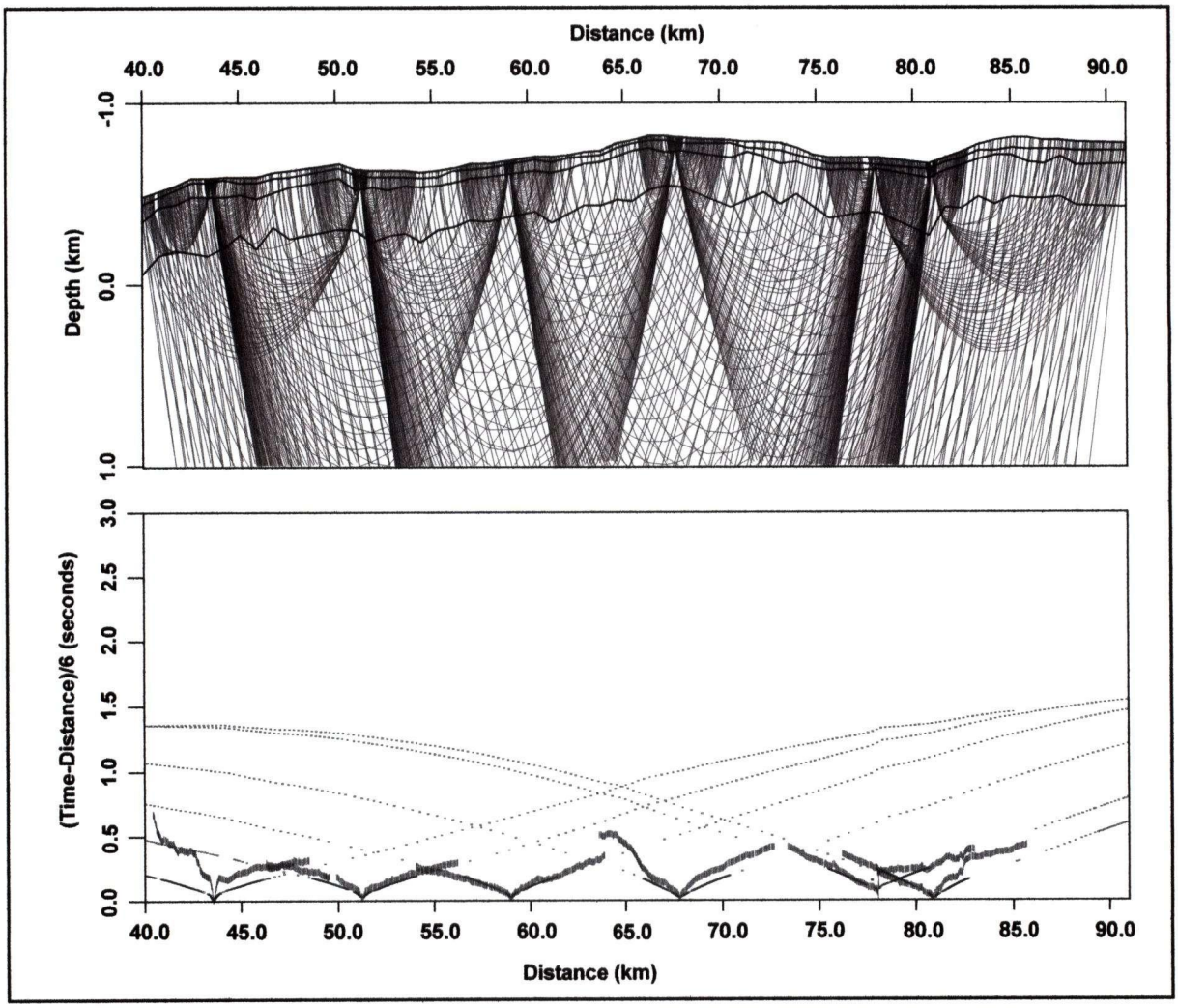

Figure 4.4 a) Distance-depth representation of model ray paths. b) Distance-time representation of observed picks and model picks. Distance is defined from Bell I. Every third shot-point used in the ray-trace modelling is displayed on this diagram.

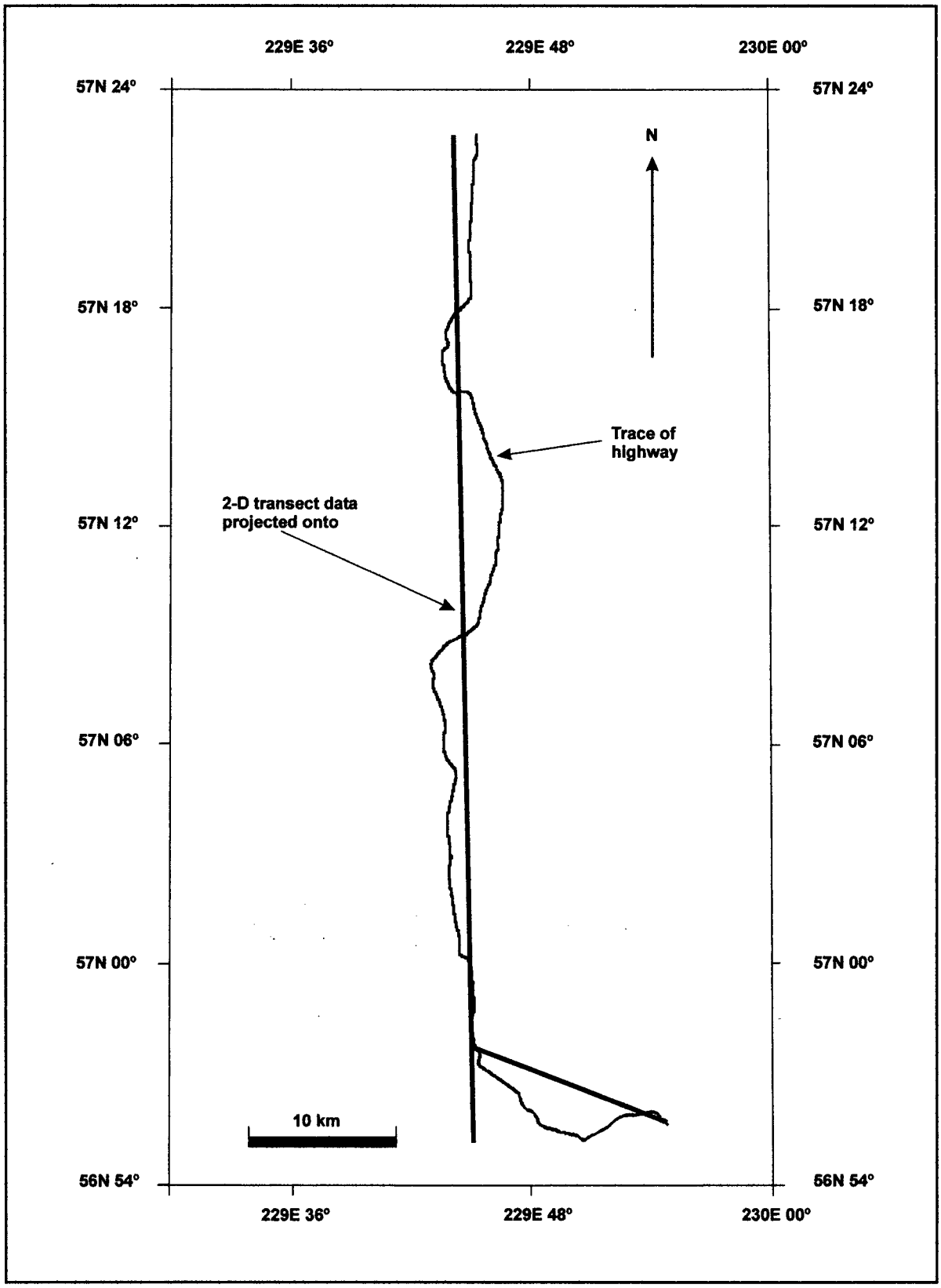

Figure 4.5 Map displaying orientation of the two straight line transects used for 2-D ray tracing with respect to the route of the highway. Area within first break arrivals analysis extends from 40 km to 90 km north of Bell II.

undertaking two ray tracing sequences, one dealing with the southern 10 km and another dealing with the main northern section. Other bends in the road are located at 25 and 42 km from the southern end of the section (Figure 4.5). These positions produced chi-squared values between 10 and 15 that were impossible to reduce using the ray-tracing technique. The errors associated with the bends in the line of section occur due to a variation in distance from source to receiver that is not predicted by the input model, due to its straight-line nature. This effect caused low velocity spikes extending to 0.7-1 km depth (Figure 4.6). Therefore, following completion of the analyses, these spikes are removed due to their artificial nature (Figure 4.6).

The velocity model obtained from 2-D ray tracing extends to a depth of 1.5 km (Figure 4.6). It is best constrained in the upper 500 m where most of ray paths are located (Figure 4.4). The uppermost 100 m of the velocity section is characterised by a band of low velocities ranging from 2.5-3.0 kms^{-1}. Below this, a zone of velocities around 4.0-4.5 kms^{-1} varies in thickness from ~100 m in the southern region to 300 m in the north. In the lower 1.0-1.5 km, the velocity increases from 4.5 to 5.0 kms^{-1} from north to south.

4.1.3 Comparison of tomographic and ray tracing velocity models and geological structure

The tomographic inversion and forward modelling techniques produce similar velocity sections (Figure 4.7). In both models, a band of slow velocities is observed within the upper 300 m. This band has greater complexity within the GLI-3D inversion technique than that produced by forward modelling. The analysis sequence within the tomographic inversion takes into account the 3-D structure of the subsurface whereas the forward modeling undertaken by RAYINVR does not. In addition, the tomographic procedure used all the first-break travel time picks, whereas the forward modeling was limited to every twentieth source point (1.5 km) due to its time-consuming nature. These characteristics account for the greater complexity within the GLI-3D model. Both velocity models show a gradual increase in velocity from 4.5-5.0 kms^{-1} at depths below ~500 m from north to south. This increase in velocity appears to be a larger feature than shown by this investigation as it correlates with a similar increase in velocity from the SNORCLE refraction/wide angle reflection results [*Hammer et al.*, 2000].

As noted previously, the goal in carrying out the velocity modelling was two-fold: (1) to determine if the near-surface velocity model could add to geological information in the area (for example, through definition of faults or layering); and (2) to provide velocities for improved migration, the topic of the next section. The primary characteristic of the velocity models (Figure 4.7) is the north to south increase in velocities below 200 m depth. This characteristic may relate to an increase in the siltstone/shale portion of Bowser Lake Group sediments within the southern half of the region.

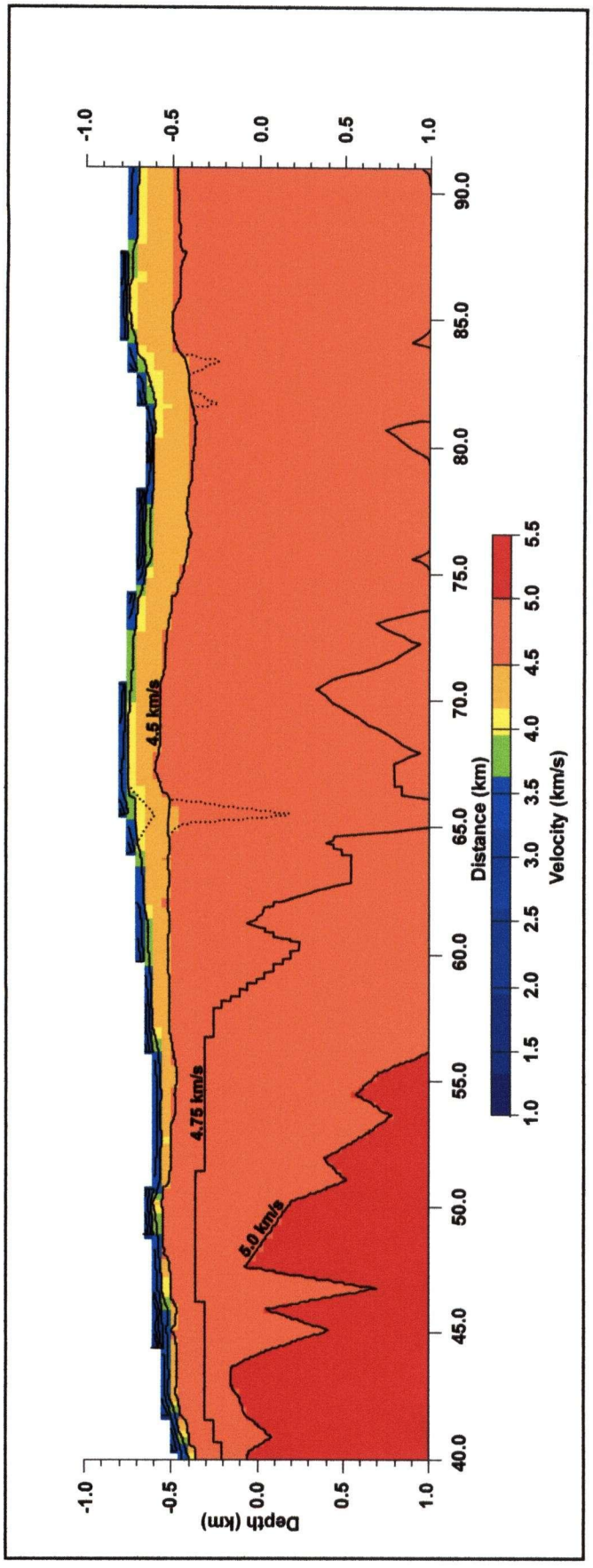

Figure 4.6 Velocity model for upper 2 km of section, obtained from forward modeling within RAYINVR. Distance is defined from Bell II.

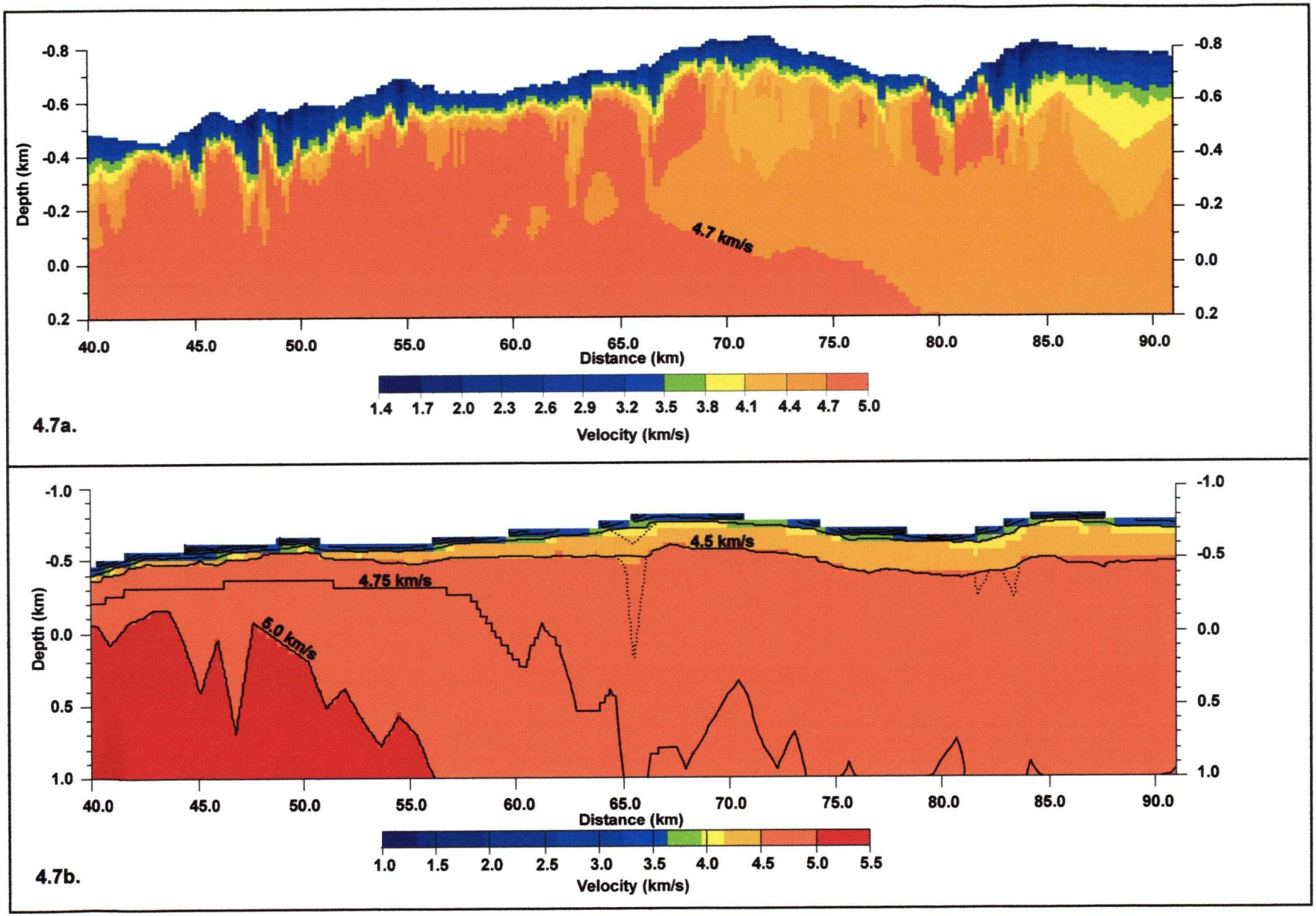

Figure 4.7 Near surface velocities from refraction statics analysis. a) Velocity model for upper 1 km of section, obtained from tomographic inversion sequence within GLI-3D. b) Velocity model for upper 2 km of section, obtained from forward modeling within RAYINVR. Distance is defined from Bell II.

4.2 POST-STACK MIGRATION

Standard processing of seismic reflection data to the stage of a structural stack (e.g. Table 4.2) employs assumptions that place dipping reflectors at incorrect locations in the subsurface and generate diffraction energy from localised (relative to a wavelength) scatterers. The process of migration repositions dipping reflectors to their true sub-surface location and tends to collapse diffractions to their location of scattering. However, correct migration requires good velocity information. Within the LSPF processing of Line 2A pre-stack migration was undertaken and within this study only post-stack migration procedures are varied from the LSPF processing.

Processing of all of Line 2A by staff at the LSPF included migration using a laterally homogeneous velocity model (Figure 4.8a). This was adequate for a first look at the data on a regional basis. However, for consideration of features in the upper crust on a more localised scale, this was not considered suitable. Thus, as part of this thesis, post-stack migration is applied using a laterally varying velocity model (Figure 4.8b). Within this model, the near-surface velocities to depths of ~1.5 km (~0.7 s) are obtained from the RAYINVR refraction static model described above. Below these depths, this model was merged with a deeper velocity structure, to 8 s, derived from interpretation of the seismic refraction data acquired along the same roadway [*Hammer et al.*, 2000].

For this study, migration used a finite difference process and was primarily undertaken to elucidate near-surface structure within the area of the northwest Bowser Basin. Finite difference migration uses the differential solution of the scalar wave equation in a downward continuation procedure to collapse reflected energy to the reflector from which the reflection derived and diffracted energy to its source [*Yilmaz*, 1987]. The advantages of using finite difference migration as opposed to other methods, such as Kirchhoff migration, include its ability to better handle lateral velocity variations [*Yilmaz*, 1987]. To account for extreme dip values that may not be migrated correctly due to limitations of the algorithim or that may not be real, a mild dip filter is applied across the section. Data presented in the following section are migrated in this manner.

4.3 INTERPRETATION OF REFLECTION DATA

4.3.1 Large-scale structures

The Bowser Basin primarily comprises sequences of interbedded conglomerate, sandstone and siltstone. This is in stark contrast to the sequences of Stikine rocks surrounding the basin in the northwest region. Stikine Terrane rocks adjacent to the northwestern border of the

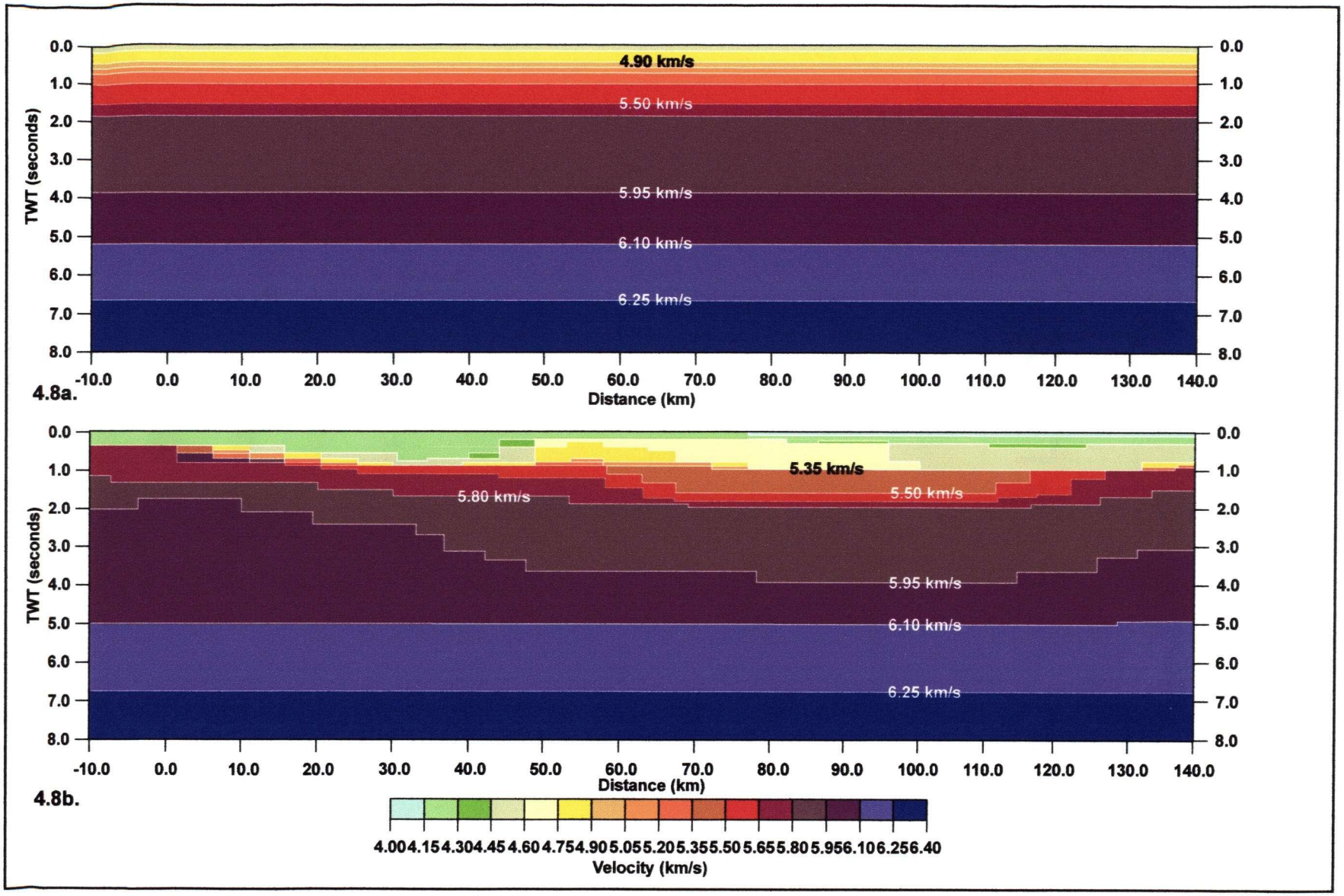

Figure 4.8 Input velocity models for finite difference migration. a) Original laterally continuous model using velocity data from the LSPF. b) Laterally variable model using near surface velocities from first break arrival analysis and deeper velocities from SNORE refraction data [*Hammer et al.*, 2000]. Distance 0.00 is Bell II.

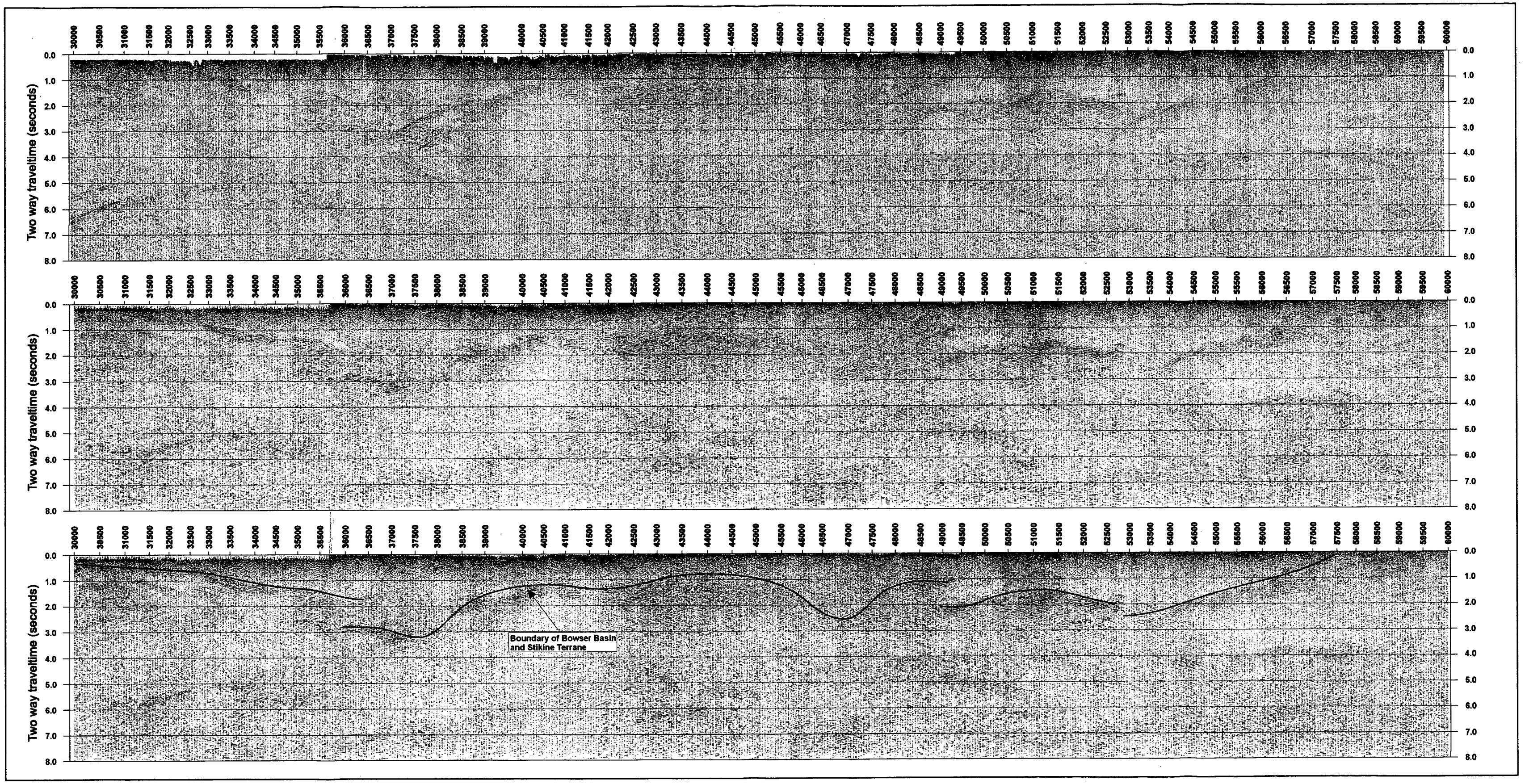

Figure 4.9 Reflection data for section of SNORCLE Line 2A from Bell II in south (32000 CDP's) to near 10 km south of Iskut (60000 CDP's) in the north. a) Stacked data. b) Post-stack migrated section using finite difference migration with laterally variable velocities. c) Post stack migrated section showing interpreted boundary between Bowser Basin and Stikine Terrane.

Bowser Basin are predominantly Triassic Stuhini and Jurassic Hazelton volcanic arc sequences. The volcanic components primarily within the Hazelton Group would be expected to produce highly reflective horizons within reflection data. In contrast less linear sequences of plutonic rocks if located in the area would be expected to produce very poor reflection data and therefore may appear within reflection sections as areas of reduced reflectivity.

From the surface geology through this area, the northern boundary of the Bowser Lake Group and the Hazelton Group is known to be located 22 km south of Iskut. Within the reflection data a strong change in reflectivity observed varying from 0.0 to 3.2 seconds (Figure 4.9) is interpreted to be the boundary between the Bowser Basin and Stikine Terrane rocks. Below this horizon a number of areas show a greater degree of reflectivity; this may be a result of bands of volcanic units within the underlying Triassic and Jurassic rocks of Stikine Terrane.

The boundary as observed within the reflection data gives an average depth of 6 km (~2 seconds) for the Bowser Basin in this area. This correlates well with data from the refraction experiment [*Hammer et al.*, 2000] where a sharp change in velocity from 5.6 to 6.0 kms^{-1} is observed at 1.9 seconds, approximately 5.75 km depth (Figure 4.10). This sharp increase was interpreted to be the change caused by moving from Bowser Lake Group sediments into the more variable and significantly volcanic Stikine rocks. Within the SNORCLE refraction/wide angle reflection data, a shallower change in velocities was observed at 0.9 seconds (~2.75 km); this corresponds to the shallower level of the boundary within the reflection data.

Based on the reflection data, the Bowser Basin is interpreted to taper at the northern end of the section. This taper reaches the surface 135 km north of Bell II at CDP 57400 (Figure 4.11), which correlates well with the boundary between the Bowser Basin and Hazelton Rocks defined by surface geology [*Evenchick*, 2001]. Within the studied segment, the southern part of the basin also appears to taper (Figure 4.9). The boundary of the basin rises from an average of 1.3 seconds (~4 km) to 0.5 seconds (~1.5 km) below Bell II. This thinning of the basin around Bell II is also observed within the refraction data (Figure 4.10) and is predicted by known geology in the area [*Evenchick*, pers. comm. 2002].

The variable nature of the observed boundary between the rocks of the Bowser Basin and Stikine Terrane is highlighted by the two thick sections of Bowser Lake Group observed between CDP's 32800 to 40000 and 51600 to 56200 (10 to 50 km and 105 to 130 km north of Bell II). In the southern area the boundary extends to around 9 km depth (Figure 4.12). This region appears to suggest a more complex nature to the boundary than observed through the rest of the section. A zone consisting of a series of reflections can be identified between 1.5 s and 2.5 s at CDP 35200 (25 km). This package is interpreted as a section of Stikine rocks, which may be thrust over or imbricated with Bowser Lake Group sedimentary rocks. A possible second package of

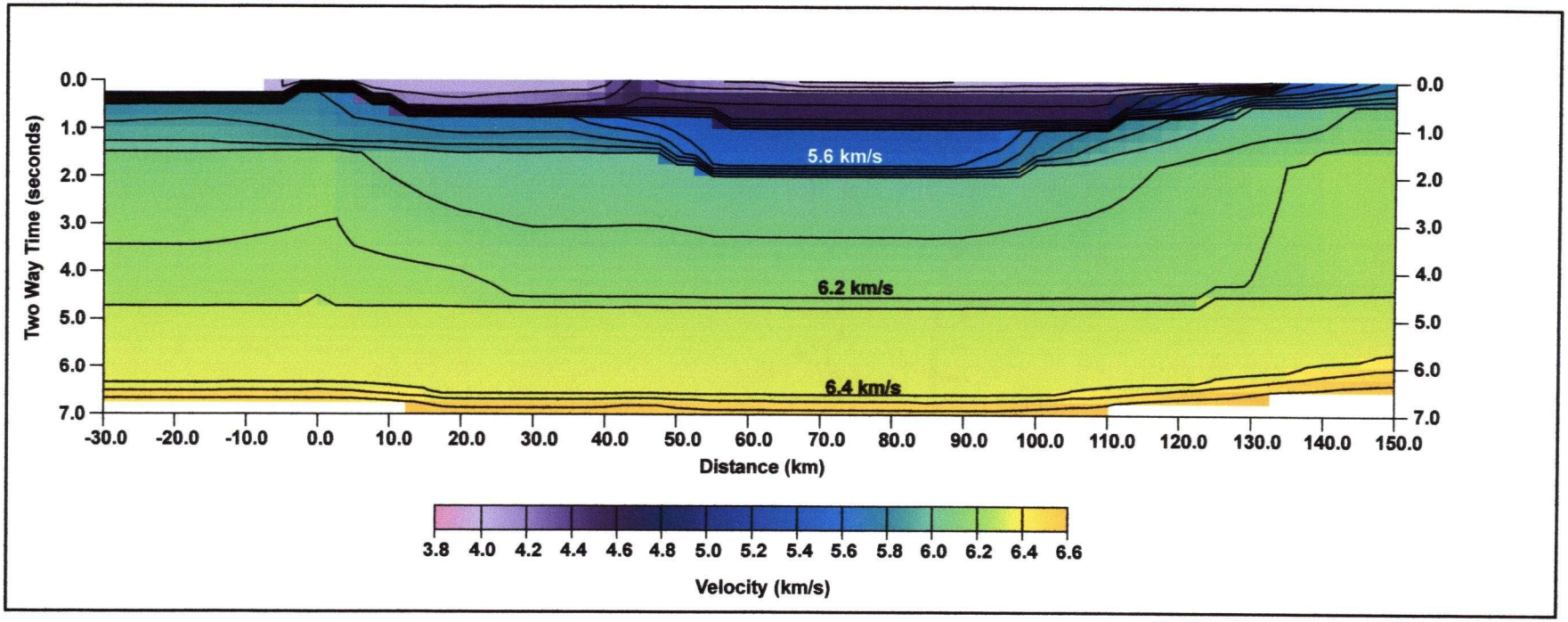

Figure 4.10 Velocity section for area 30 km south of Bell II in south to Iskut in north. Velocities from Lithoprobe SNORE refraction experiment [*Hammer et al.*, 2000].

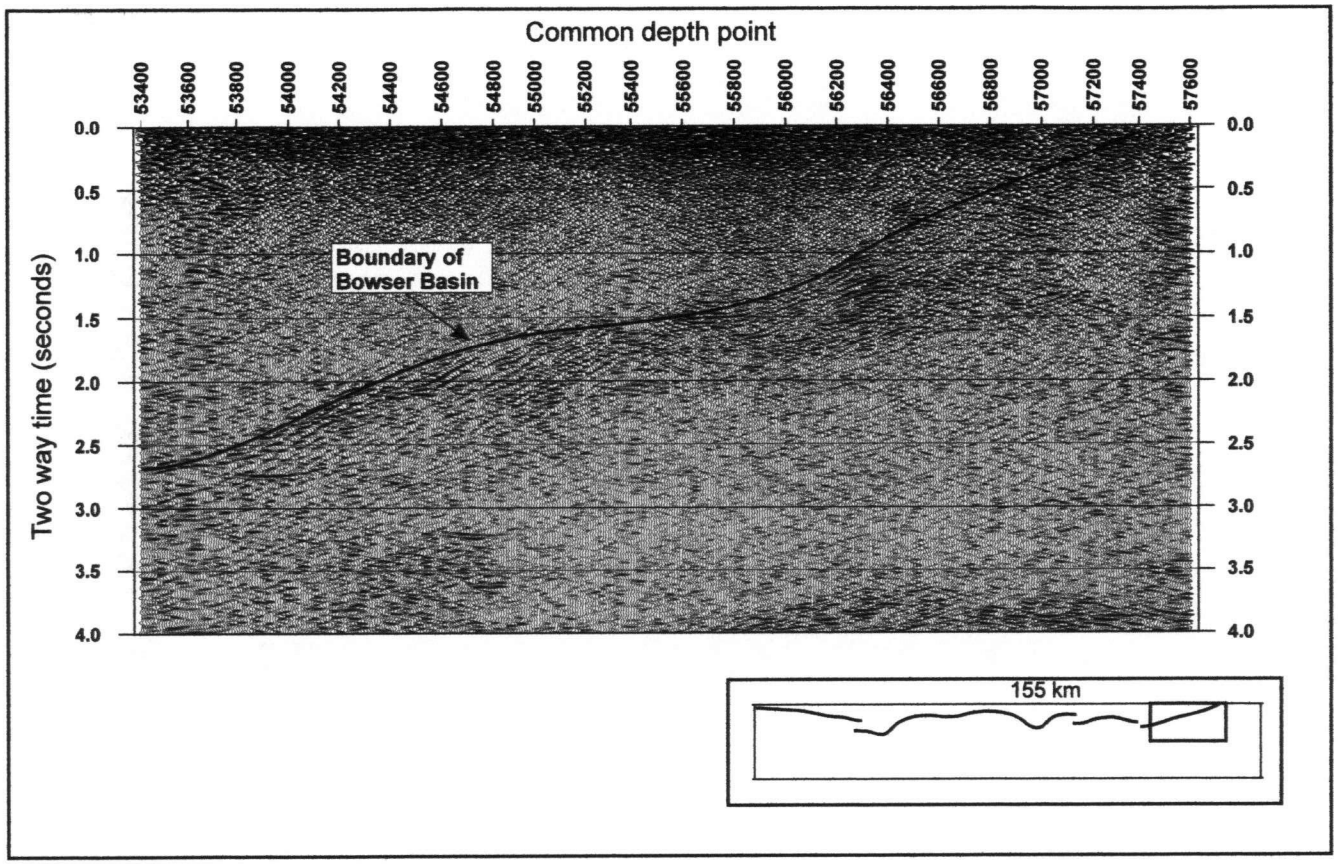

Figure 4.11 Reflection data showing northern taper of Bowser Basin reaching the surface at 57400 (~20 km south of Iskut). Inset: Location of Figure 4.11 in relation to complete section, red line indicates the boundary of the Bowser Basin.

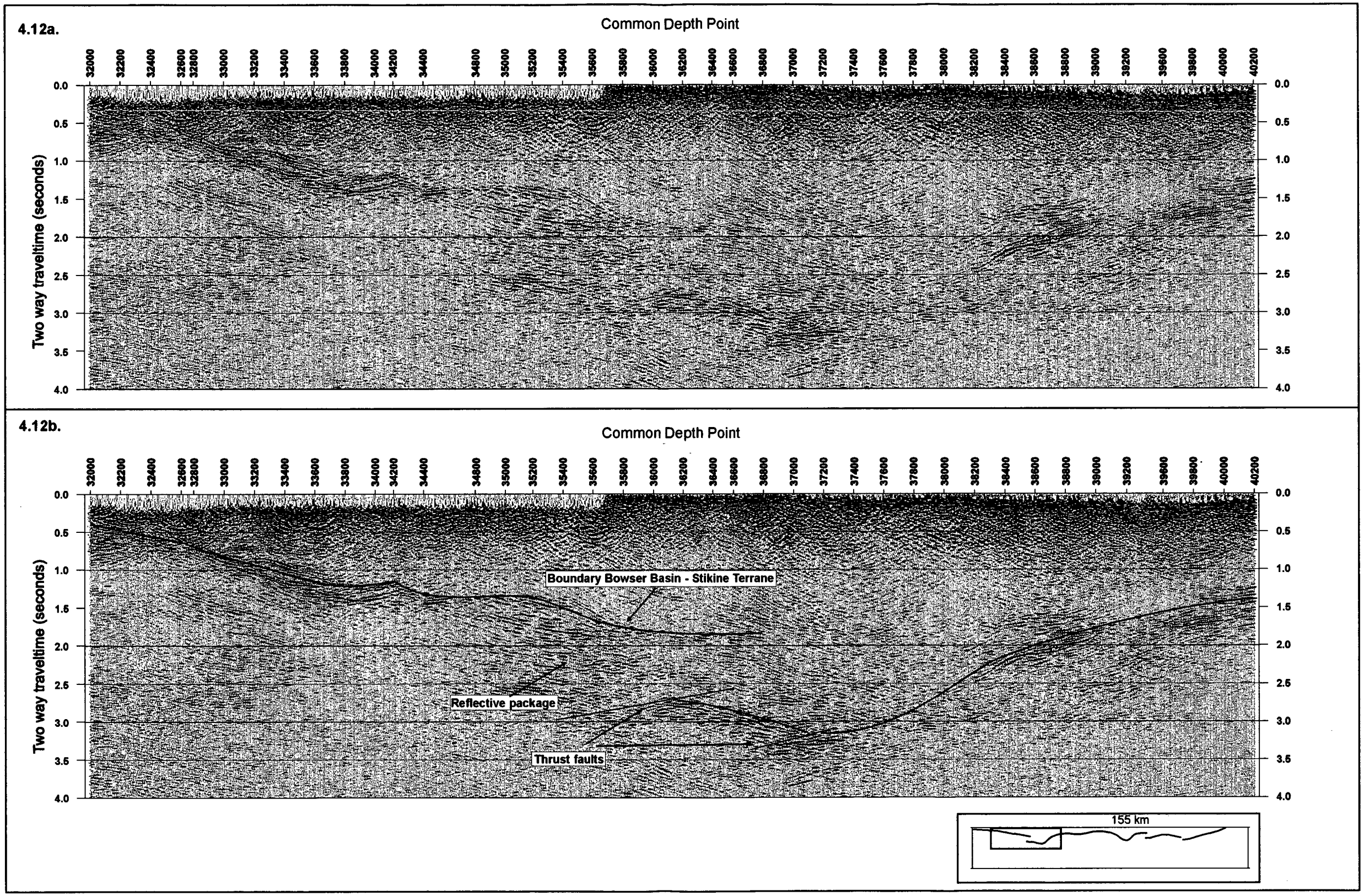

Figure 4.12 Migrated reflection data from CDP 32000 to 40200. a) uninterpreted, b) interpreted. Interpretation places Bowser Basin - Stikine Terrane boundary increasing in depth from 0.5 seconds (~1.5 km) at 32000 to 3.2 seconds (~9 km) at 37000. Thickening of the basin is interpreted to be due to structural stacking of Stikine Terrane units by thrust faulting. Inset indicates location of Figure 4.12 in relation to full section; the red line is the boundary of the Bowser Basin.

Stikine rocks and thrust faulting may be present at CDP 37000 (35 km) between 3.0 and 3.5 seconds.

The relationship between Stikine and Bowser Basin rocks strongly suggests interaction of Stikine Terrane within Skeena Fold Belt deformation. Evidence of structural interaction of Stikine Terrane and the Bowser Lake Group is known from a number of areas within the Skeena Fold Belt. In the northeast of the basin, the Joan Lake Anticline is cored by Hazelton units while flanked by Bowser Lake Group sediments [*Evenchick*, 1991b]. On the western side of the basin, Oweegee Dome, a structural culmination of Stikine rocks ranging in age from Devonian to Jurassic [*Greig*, 1991], is surrounded by Bowser Basin sediments (Figure 2.3). This is interpreted to be the result of Skeena Fold Belt deformation [*Greig*, 1992; *Evenchick*, 1991b] and confirms Stikine Terrane involvement in Skeena Fold Belt deformation within the western portion of the fold belt, as noted in many areas [*Evenchick*, 1991b].

Within the centre of the seismic section, the Bowser Basin appears to shallow to 1.0 second (~3 km) (Figure 4.13). In this area a thick package (~2 s) of highly reflective material is present just below the boundary. This may be a sequence of predominantly volcanic rocks within Stikine Terrane. To the south of this area, reflections have extremely low amplitudes and very little structure can be identified. This area correlates well with an Early Tertiary pluton identified just to the west of the basin boundary in this area [*Wheeler and McFeely*, 1991].

4.3.2 Near-surface structure

Within the reflection data, there is very little consistent and discernable structure within the upper zone of the section between ~0.5 and 1.0 s. Within this zone, where the lithology is entirely Bowser Lake Group, surface geology indicates that a large number of folds and inferred faults are present. Unfortunately, the nature of the lithologies present and the style of deformation preclude obtaining a great deal of useful information from the reflection data for this scale of interpretation.

The portion of data correlating with Study Area 1 (90 km north of Bell II) shows details in the near surface that have the best degree of observed continuity. Between CDP's 47000 and 48800 (85 and 95 km) at a depth of 0.5 to 0.75 s, a sequence of consistent subhorizontal horizons is observed (Figure 4.13). Large areas of consistently sub-horizontal units are rarely observed in the surface geology of this area. Observations of surface geology both on the road, where units dip from almost vertical to ~50° towards the southwest, and in Study Area 1, 5 km to the east, suggest a complex interaction of folds within this area. Thus, the horizons observed within the reflection data probably do not correlate with the surface data.

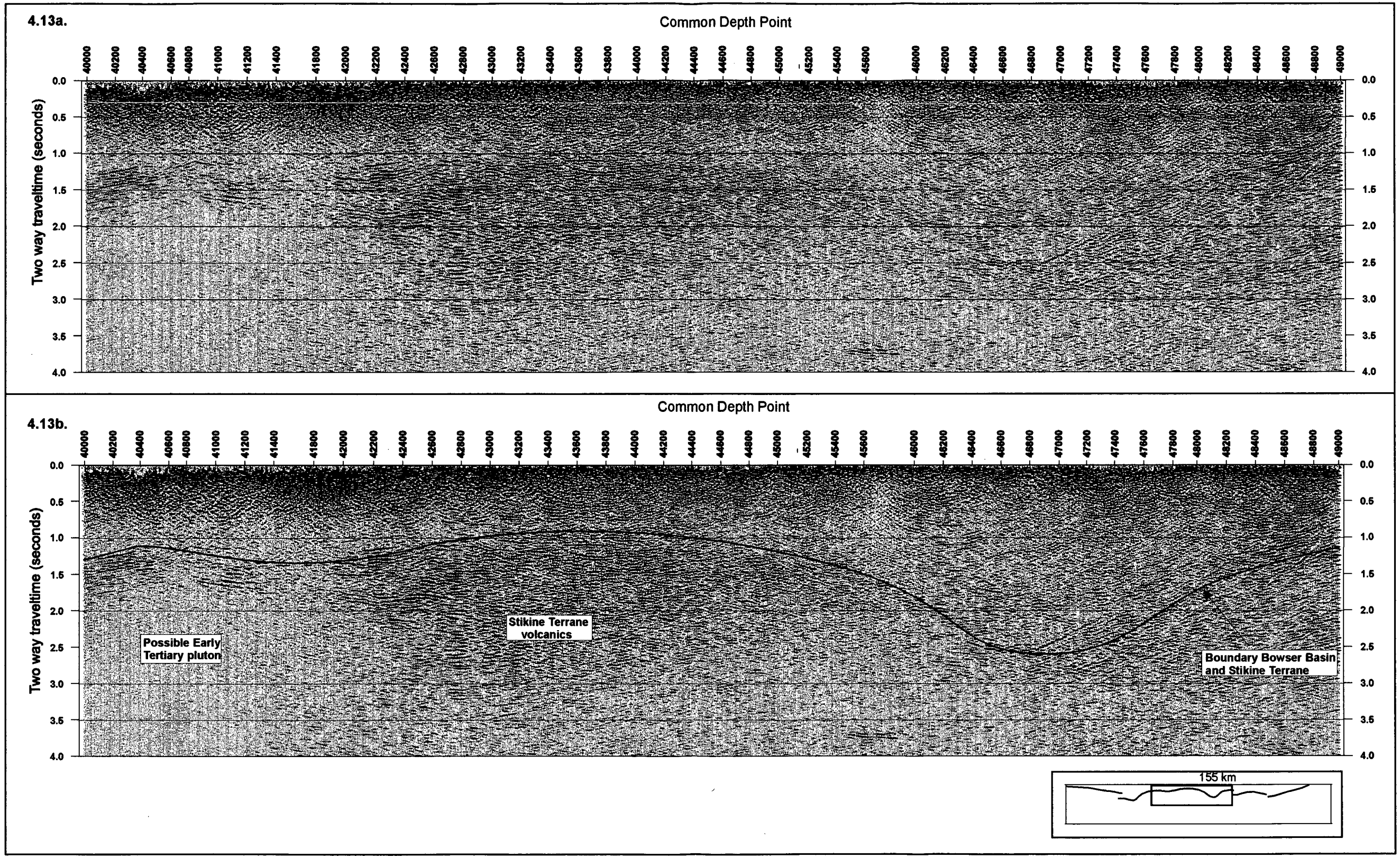

Figure 4.13 Reflection data from 40000 to 52000 CDP's (40 to 100 km north of Bell II). Section shows variable thickness of Bowser Basin sediments, within Stikine Terrane a package of highly reflective units can be seen through the centre of the section whilst to the south an area of poor reflectivity appears to correlate with an Early Tertiary pluton identified on the surface 5 km to the northwest. Inset: location of Figure 4.13 in relation to full section, red line indicates boundary of the Bowser Basin.

The difference in surface geology to the orientation of reflective horizons at depth could be due to a number of possibilities -

- The orientation of bedding sequences from the surface to an approximate depth of 2-3 km could change substantially; this possibility is extremely likely within this region, due to the presence of thrust fault systems controlling folding, these systems could change the structural fabric considerably.
- A shallowing of the dip of bedding sequences observed within the reflection data due to the orientation of the seismic transect with respect to the strike of bedding.
- Folding may be partitioned in relatively thin sequences of strata above detachments; this would allow different deformation styles within relatively narrow thicknesses.

The surface geology of Study Area 3 was studied due to its location within an area of dominantly northeast-trending folds. This area is also a zone across which the seismic transect traverses perpendicular to fold trend, making this area conducive to identifying fold structures within the near surface. Surface geology along the road provides evidence for folds with wavelengths of a number of kilometres, a similar size to the fold observed in Study Area 3. Reflection data from the area exhibit a high degree of reflectivity to around 1.0 second (3 km) (Figure 4.14). Within this area, little near-surface structure can be determined. The middle portion of the section from 1.0 to 1.7 seconds contains the boundary of Bowser Basin sedimentary rocks and Stikine Terrane. This zone outlines a large-scale anticline. This structure correlates well with the size of folds observed on the surface and may indicate that the scale of folding does not change substantially with depth through the fold belt although in other areas the orientation of folds is expected to change.

Along Highway 37, two major fault zones were identified 36 km and 82 km north of Bell II. Both zones are on the scale of tens of metres wide and comprise sequences of fault surfaces with thick vein sequences and disarranged rock sequences. The southern most of these zones contains shallow to subhorizontal fault surfaces recording at least three different orientations of slickensides. The northern zone contains more steeply dipping fault surfaces towards the northeast. Neither of these zones appears to be large enough to be identified within the reflection data. Assuming that these fault zones are typical of fault deformation within the region, it can be suggested that identification of these zones within the reflection data is unlikely due to their size relative to the size of structures that are best imaged by the seismic technique.

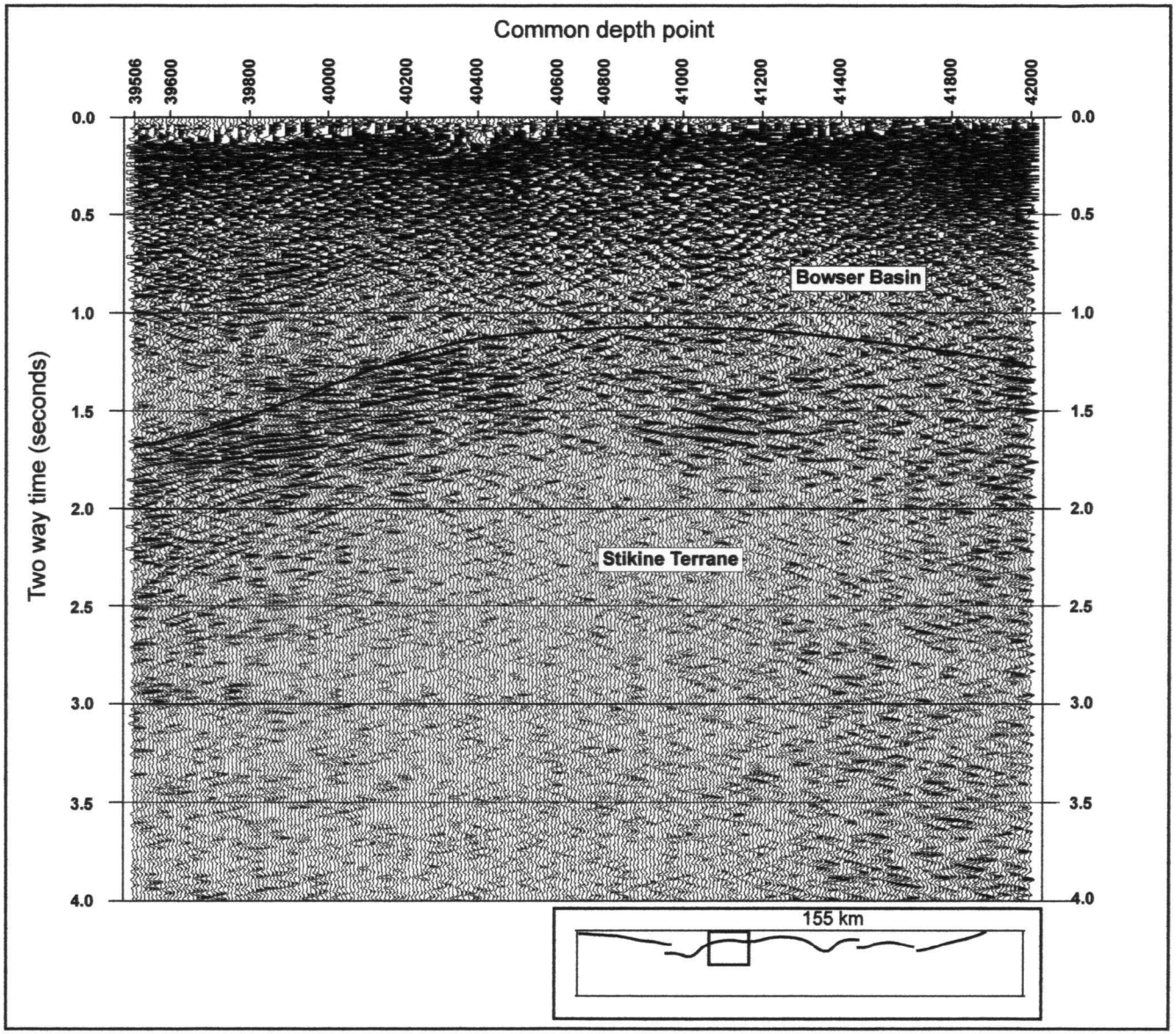

Figure 4.14 Reflection data parallel with Study Area 3. Boundary of Bowser Basin and Stikine Terrane forms anticline; this structure is of the same scale as folds observed along the highway and within Study Area 3 on the surface. Inset: location of Figure 4.14 in relation to full section, red line indicates the boundary of the Bowser Basin.

5 CONCLUSIONS

This work has used two foundations of geoscience research by combining detailed geological field mapping with the interpretation of near-surface seismic reflection data. This has led to a stronger understanding of the deformation history of the Skeena Fold Belt within the northwestern Bowser Basin.

5.1 STRUCTURAL DATA

The western Skeena Fold Belt comprises a number of different fold orientations and styles. These have been described within a history of progressive deformation across the belt. Structural data collection concentrated on three areas of specific structural style within the northwestern Bowser Basin, with the aim of determining the relative ages of folding.

The region contains three main fold groups: northeast-, north- and northwest-trending folds. Within Study Area 1, folds are consistently transected by cleavage within northeast-trending folds and less consistently within north- and northwest-trending folds. Fold transection by cleavage is consistent with a temporal progression of folding. In the western two thirds of the area, northeast-trending folds are consistently transected by northwest-striking cleavage, suggesting that these folds are the earliest structures. In the eastern third of the study area, cleavage is dominantly north-striking and the temporal relationship between north- and northwest-trending folds is inconclusive. Overall, this produces a temporal progression within Study Area 1 from northeast-trending through north-trending to northwest-trending folds.

The interaction of northeast- and northwest-trending synclines within Study Area 2 has produced a Type 1 interference structure. Due to the nature of the fold interaction, the relative timing of folding cannot be determined. Type 1 interference patterns generally indicate the overprinting of two separate folding events. It is therefore likely that deformation in this area occurred as separate events within a regional progression of deformation.

In the southernmost study area, the presence of northeast-striking cleavage transecting a north-northeast-trending fold, suggests cleavage orientation was oblique to fold orientation through the early stages of development within the fold belt.

Cleavage-fold relationships across the three study areas are interpreted to have formed as a result of the temporal progression of folds from northeast-trending through north- to northwest-

trending, during development of the Skeena Fold Belt. This supports the work of *Evenchick* [2001], who observes the same progression within an area to the southwest of this region.

Deformation within the northwestern Skeena Fold Belt is interpreted to have occurred in partitioned structural domains on scales of tens of kilometres. Within these domains, relative temporal relationships can be defined between fold orientations but these cannot be correlated with neighbouring domains. It appears plausible that deformation within the fold belt was highly localised, most likely due to the presence of thrust fault systems which control fold geometry on an individual scale and the style and orientation of folds within a domain.

5.2 SEISMIC REFLECTION DATA

The relationship of the Bowser Basin and underlying Stikine Terrane has been clarified through the interpretation of the reflection data. The boundary between the Bowser Basin and Stikine Terrane varies in depth from <3 km in the shallowest sections to >6 km in the deepest areas. The thickest areas of Bowser Basin sedimentary rocks are the result of structural thickening of basin strata by Skeena Fold Belt deformation. The geometry of the Bowser Basin – Stikine Terrane contact is commonly disrupted. Evidence of a faulted contact can be observed in a number of locations within the reflection data. The disrupted nature of the contact is interpreted to be a result of shortening within Stikine Terrane associated with Skeena Fold Belt development.

Within the near surface reflection data (0.0-0.5 s), a lack of structure is a result of lithology: conglomerate and sandstone sequences of the northern two-thirds of the region do not display significant changes in velocity. The increasing siltstone component of the southern third of the region is displayed as a subtle increase in reflectivity and clarity of reflections. Locally, the surface geology and reflection data can be correlated. Evidence of Skeena Fold Belt structures can be observed in the section of line parallel to Study Area 3 where a culmination in the boundary of the Bowser Basin is on the same scale as folds observed at the surface.

5.3 COMBINING RESULTS

This research has led to a greater understanding of fold style within the northwestern portion of the Skeena Fold Belt. The work corroborates the hypothesis of *Evenchick* [2001] of a temporal progression of changing orientations of folds within the northern Skeena Fold Belt. The

boundary of the Bowser Basin and Stikine Terrane within the reflection data has been identified. I suggest that this boundary has been strongly affected by Skeena Fold Belt deformation. Evidence from reflection data supports the hypothesis, developed from the geological work, of deformation occurring consistently over regions of tens of kilometres but being variable on larger scales than this.

5.4 FUTURE WORK

Future work to expand the work of this thesis would concentrate on a number of aspects.

1. A total reprocessing of reflection data for this section using the near-surface velocities obtained through first break arrivals analysis examined in this research and interpretations of coincident refraction data. Use of a laterally varying velocity model and the lower near surface velocities known to be present in the Bowser Lake Group may enable a better record of near surface structure to be produced.

2. The selection of specific fold structures upon which to undertake detailed structural analysis with the intention of defining the geometric relationship of thrusting and folding within the fold belt.

REFERENCES:

Alvarez, W., Engelder, T., Geiser, P. 1978. Classification of solution cleavage in pelagic limestones. Geology **6**: 263-266.

Anderson, R.G. 1989. A stratigraphic, plutonic, and structural framework for the Iskut River map area, northwestern British Columbia. *In* Cordillera and Pacific margin. Geological Survey of Canada. Paper 89-1E, 145-154.

Bassett, K.N., Kleinspehn, K.L. 1997. Early to Middle Cretaceous paleogeography of north-central British Columbia; stratigraphy and basin analysis of the Skeena Group. Canadian Journal of Earth Sciences, **34**: 1644-1669.

Brown, D.A., Gunning, M.H. 1989. Geology of the Skud River area, northwestern British Columbia (104G/5,6). *In* Geological fieldwork 1988; a summary of field activities and current research. British Columbia Ministry of Energy, Mines and Petroleum Resources. Paper 1989-1, 251-267.

Brown, D.A., Greig, C.J. 1990. Geology of the Stikine River-Yehiniko Lake area, northwestern British Columbia (104G/11W and 12E). *In* Geological fieldwork 1989; a summary of field activities and current research. British Columbia Ministry of Energy, Mines and Petroleum Resources. Paper 1990-1, 141-151.

Brown, D.A., Harvey-Kelly, F.E.L., Neill, I. and Timmerman J. 1992. Geology of the Chutine River-Tahltan Lake area, northwestern British Columbia (104G/12W and 13). Geological Fieldwork 1991; a summary of field activities and current research. *Edited by* Grant, B. and Newell, J.M. British Columbia Ministry of Energy, Mines and Petroleum Resources. Paper 1992-1, 179-195.

Cervený, V., Molotkov I.A. and Pšenvcik, I. 1977. Ray method in seismology. University of Karlova, Prague, Czechoslovakia.

Cook, F.A., Clowes, R.M., Snyder, D.B., van der Velden, A.J., Hall, K.W., Erdmer, P. and Evenchick, C.A. 2000. LITHOPROBE seismic reflection profiling of the northern Canadian Cordillera: first results of SNORCLE Profiles 2 and 3. *In* Slave-Northern Cordillera Lithospheric Evolution (SNORCLE) Transect and Cordilleran Tectonic Workshop Meeting. *Edited by* Cook, F.A. and Erdmer, P. Lithoprobe report **79**, 36-49.

Eisbacher, G.H. 1973. Tectonic framework of Sustut and Sifton basins, British Columbia. *In* Report of activities, Part A. Geological Survey of Canada. Paper 73-1A, 24-26.

Eisbacher, G.H. 1976. Successor basins of the western Cordillera. *In* Report of activities, Part A. Geological Survey of Canada. Paper 76-1A, 113-116.

Eisbacher, G.H. 1981. Late Mesozoic-Paleogene Bowser Basin molasse and cordilleran tectonics, western Canada. *In* Sedimentation and tectonics in alluvial basins. *Edited by* Miall A.D. Special Paper – Geological Association of Canada, **23**; 125-151.

Engebretson, D.C., Cox, A. and Gordon, R.G. 1985. Relative motions between oceanic and continental plates in the Pacific Basin. Geological Society of America Special Paper 206.

Engelder, T., Marshak, S. 1985. Disjunctive cleavage formed at shallow depths in sedimentary rocks. *In* Multiple deformation inductile and brittle rocks. *Edited by* Hancock, P.L. and Powell, C, McA. Journal of Structural geology, **7**; 327-343.

Engelder, T., Peacock, D.C.P. 2001. Joint development normal to regional compression during flexural-flow folding; the Lolstock buttress anticline, Somerset, England. *In* Paul Hancock memorial issue. *Edited by* Dunne, W.M., Stewart, I.S. and Turner, J.P. Journal of Structural Geology, **23**; 259-277.

Evenchick, C.A. 1987. Stratigraphy and structure of the northeast margin of the Bowser Basin, Spatsizi map area, north-central British Columbia. *In* Current research, Part A, Cordillera and Pacific margin. Geological Survey of Canada. Paper 87-1A, 719-726.

Evenchick, C.A. 1988. Structural style and stratigraphy in Northeast Bowser and Sustut basins, north-central British Columbia. *In* Current research, Part E, Cordillera and Pacific margin. Geological Survey of Canada. Paper 88-1E, 91-95.

Evenchick, C.A. 1989. Stratigraphy and structure in East Spatsizi map area, north-central British Columbia. *In* Current research, Part E, Cordillera and Pacific margin. Geological Survey of Canada. Paper 89-1E, 133-138.

Evenchick, C.A. 1990. Structural geometry and history of the northern Bowser and Sustut basins, north-central British Columbia. *In* Program with Abstracts - Geological Association of Canada; Mineralogical Association of Canada; Canadian Geophysical Union, Joint Annual Meeting, **15**; 38.

Evenchick, C.A. 1991a. Geometry, evolution and tectonic framework of the Skeena Fold Belt, north central British Columbia. Tectonics, **10**, 527-546,

Evenchick, C.A. 1991b. Structural relationships of the Skeena Fold Belt west of the Bowser Basin, northwest British Columbia. Canadian Journal of Earth Science, **28**, 973-983.

Evenchick, C.A. 1991c. Jurassic stratigraphy of East Telegraph Creek and West Spatsizi map areas, British Columbia. *In* Current research, Part A, Cordillera and Pacific margin. Geological Survey of Canada. Paper 91-1A, 155-162.

Evenchick, C.A. 1992. Bowser Basin facies and map units in Southwest Toodoggone map area, British Columbia. *In* Current research, Part A, Cordillera and Pacific margin. Geological Survey of Canada. Paper 92-1A, 77-84.

Evenchick, C.A. 1996. Style and significance of northeast and northwest trending structures in Nass River Area. *In* Slave-Northern Cordillera Lithospheric Evolution (SNORCLE) Transect and Cordilleran Tectonic Workshop Meeting. *Edited by* Cook, F.A. and Erdmer, P. Lithoprobe report 50, 190.

Evenchick, C.A. 1998. Contractional structures in the western Skeena Fold Belt: an indication of Cretaceous sinistral convergence within the Coast Belt. *In* Slave-Northern Cordillera Lithospheric Evolution (SNORCLE) and Cordilleran tectonics workshop. *Edited by* Cook, F.A. and Erdmer, P. Lithoprobe Report 64, 181.

Evenchick, C.A. 2000. Evolution of the Bowser Basin/Skeena Fold Belt: implications for tectonic models Models of the Rocky Mountain Fold and Thrust Belt and Omineca Belt. *In* Program with Abstracts - Geological Association of Canada; Mineralogical Association of Canada; Canadian Geophysical Union, Joint Annual Meeting,.

Evenchick, C.A. 2001. Northeast-trending folds in the western Skeena fold belt, northern Canadian Cordillera; a record of Early Cretaceous sinistral plate convergence. *In* Evolution of structures in deforming rocks; in honour of Paul F. Williams. *Edited by* Bleeker, W., Elliott, C., Lin, S. and van Staal, C. Journal of Structural Geology, **23**, 1123-1140.

Evenchick, C.A., Poulton, T.P., Tipper, H.W. and Braidek, I.G. 2001. Fossils and facies of the northern two-thirds of the Bowser Basin, British Columbia. Open File 3956; Geological Survey of Canada. Scale 1:250 000.

Gabrielse, H. 1991. Late Paleozoic and mesozoic terrane interactions in north-central British Columbia. *In* Contributions to the geology and geophysics of northwestern British Columbia and southeastern Alaska. *Edited by* Anderson, R.G. Canadian Journal of Earth Science, **28**, 947-957.

Gabrielse, H., Tipper H.W., 1984. Bedrock geology of Spatsizi map area (104H), British Columbia. Open File 1005; Geological Survey of Canada. Scale 1:125 000.

Gabrielse, H., Souther, G.J., Woodsworth, G.J., Tipper, H.W. and Monger, J.W.H. 1992. The intermontane belt. *In* Chapter 9, Geology of the Cordilleran Orogen in Canada. *Edited by* Gabrielse, H. and Yorath, C.J. Geological Survey of Canada, **4**, 345-352.

Gareau, S.A., Woodsworth, G.J. and Rickli, M. 1997. Regional geology of the northeastern quadrant of Terrace map area, west-central British Columbia. *In* Current research, Part A/B, Cordillera and Pacific margin, Interior plains and Arctic Canada. Geological Survey of Canada. Paper 1997-A/B, 47-55.

Geological Survey of Canada. 1957. Stikine River area, Cassiar District, British Columbia. 1:253 440 map.

Green, G.M. 1991. Detailed sedimentology of the Bowser Lake Group, northern Bowser Basin, British Columbia. *In* Current Research, Part A, Cordillera and Pacific margin. Geological Survey of Canada. Paper 91-A, 187-195.

Greig, C.J. 1991. Stratigraphic and structural relations along the west-central margin of the Bowser Basin, Oweegee and Kinskuch areas, northwestern British Columbia. *In* Current Research, Part A, Cordillera and Pacific margin. Geological Survey of Canada. Paper 91-A, 197-205.

Greig, C.J. 1995. Ramp anticline-blind thrust model for Oweegee Dome and other Mid-Cretaceous culminations of Lower Jurassic and older Stikinia, western Skeena fold belt (SFB)/ Bowser Basin (BB), NW B.C. *In* Program with Abstracts - Geological Association of Canada; Mineralogical Association of Canada; Canadian Geophysical Union, Joint Annual Meeting, **20**, 39.

Greig, C.J. and Gehrels, G.E. 1995. U-Pb zircon geochronology of Lower Jurassic and paleozoic Stikinian strata and Tertiary intrusions, northwestern British Columbia. Canadian Journal of Earth Sciences, **32**, 1155-1171.

Gunning, M.H. 1990. Stratigraphy of the Stikine Assemblage, Scud River area, northwestern British Columbia (104G/5,6). *In* Geological Fieldwork 1989; a summary of field activities and current research. British Columbia Ministry of Energy, Mines and Petroleum Resources. Paper 1990-1, 153-161.

Hammer, P.T.C., Clowes, R.M. and Ellis R.M. 1998. ACCRETE crustal velocity structure across the Coast plutonic complex/Stikinia transition. *In* Slave-Northern Cordillera Lithospheric Evolution (SNORCLE) and Cordilleran tectonics workshop. *Edited by* Cook, F.A. and Erdmer, P. Lithoprobe Report 64, 258-259.

Hammer, P.T.C., Clowes, R.M. and Ellis, R.M. 2000. Crustal structure of NW British Columbia and SE Alaska from seismic wide-angle studies; coast plutonic complex to Stikinia. Journal of Geophysical Research, B; Solid Earth and Planets, **105**, 7961-7981.

Hampson, D., Russell, B. 1984. First-break interpretation using generalized linear inversion. Journal of the Canadian Society of Exploration Geophysicists, **20**, 40-54.

Hancock, P. 1985. Brittle microtectonics; principles and practice. *In* Multiple deformation in ductile and brittle rocks. *Edited by* Hancock, P. and Powell, C. Journal of Structural Geology, 7, 437-457.

Jamison, W.R. 1992. Stress controls on fold thrust style. *In* Thrust tectonics. *Edited by* McClay, K.R. Chapman and Hall, London. 155-164.

Johnson, T.E. 1991. Nomenclature and geometric classification of cleavage-transected folds. Journal of Structural Geology, **13**, 261-274.

Kerr, F.A. 1930. Preliminary report on Iskut River area, British Columbia. Summary Report of the Geological Survey of Canada, 30-61.

Lewis, P.D. 1996. Metallogenesis of the Iskut River Area, Northwestern B.C. Mineral Deposit Research Unit, University of British Columbia. Map scale 1:50 000.

Logan, J.M., Koyanagi, V.M. 1989. Geology and mineral deposits of the Galore Creek area, northwestern British Columbia (104G/ 3, 4). *In* Geological fieldwork 1988; a summary of field activities and current research, Ministry of Energy, Mines and Petroleum Resources. Paper 1989-1, 269-284.

Logan, J.M., Drobe, J.R. and Elsby, D.C. 1992. Geology of the More Creek area, northwestern British Columbia (104G/2). *In* Geological fieldwork 1991; a summary of field activities and current research. *Edited by* Grant, B. and Newell, J.M. Ministry of Energy, Mines and Petroleum. Paper 1992-1, 161-178.

Lowe, C., Seemann, D. and Evenchick, C.A. 1992. A preliminary investigation of potential field data from north-central British Columbia. *In* Current Research, Part A, Geological Survey of Canada. Paper 92-1A, 85-93.

Lowe, C., Baker, J. and Evenchick, C.A. 1998. Estimates of sediment thickness in the Bowser Basin, Canada from spectral analysis of magnetic data. *In* Fall meeting supplement, EOS Transactions, American Geophysical Union, **79**(45), F809.

Marsden, H., Thorkelson, D.J., 1992. Geology of the Hazelton volcanic belt in British Columbia; implications for the Early to Middle Jurassic evolution of Stikinia. Tectonics, **11**, 1266-1287.

McClay, K.R. 1992. Glossary of thrust tectonic terms. *In* Thrust Tectonics. *Edited by* McClay, K.R. 1992, 419-432.

Mihalynuk, M.G., Ghent, E.D. 1986. Stratigraphy, deformation and low grade metamorphism of the Telkwa Formation near Terrace, British Columbia. *In* Current research, Cordillera and Pacific margin, Geological Survey of Canada. Paper 86-1B, 721-726.

Mihalynuk, M.G., Nelson, J. and Diakow, L.J. 1994. Cache Creek terrane entrapment: oroclinal paradox within the Canadian Cordillera. Tectonics, **13**, 575-595.

Moffat, I.W. 1985. The nature and timing of deformational events and organic and inorganic metamorphism in the northern Groundhog Coalfield; implications for the tectonic history of the Bowser Basin. Doctoral thesis, University of British Columbia.

Moffat, I.W., Bustin, R.M. 1984. Superposed folding in the northern Groundhog Coalfield; evidence for polyphase deformation in the northeastern corner of the Bowser Basin. *In* Current research, Part B, Cordillera and Pacific margin. Geological Survey of Canada. Paper 84-1B, 255-261.

Moffat, I.W., Bustin, R.M. 1993. Deformation history of the Groundhog Coalfield, Northeastern Bowser Basin, British Columbia; styles, superposition and tectonic implications. Bulletin of Canadian Petroleum Geology, **41**, 1-16.

Monger, J.W.H. 1977. Upper Paleozoic rocks of northwestern British Columbia. *In* Report of Activities, Part A. Geological Survey of Canada. Paper 77-1A, 255-262.

Monger, J.W.H., Nokleberg, W.J. 1996. Evolution of the northern North American Cordillera: generation, fragmentation, displacement and accretion of successive North American plate-margin arcs. *In* Geology and ore deposits if the American Cordillera: Geological Society of Nevada Symposium Proceedings. *Edited by* Coyner, A.R. and Fahey, P.L. 1133-1152.

Monger, J.W.H., Price, R.A. and Tempelman-Kluit, D.J. 1982 Tectonic accretion and the origin of the two major metamorphic and plutonic welts in the Canadian Cordillera. Geology (Boulder), **10**, 70-75.

Mosar, J. , Suppe, J. 1992. Role of shear in fault-propagation folds. *In* Thrust Tectonics. *Edited by* McClay, K.R. Chapman and Hall, 123-132.

Mosher, S., Helper, M. 1998. Interpretation of poly-deformed terranes. *In* Basic Methods of Structural Geology. *Edited by* Marshak, S. and Mitra, G. Prentice-Hall, New Jersey, 361-384.

Natural Resources Canada, 2000. Map of British Columbia. http://www.atlas.gc.ca/

Nicol, A. 1993. Conical folds produced by dome and basin fold interference and their application to determining strain; examples from North Canterbury, New Zealand. Journal of Structural Geology, **15,** 785-792.

Powell, C.McA. 1979. A morphological classification of rock cleavage. Tectonophysics, **58**, 21-34.

Price, N.J. 1966. Fault and Joint development in brittle and semi-brittle rocks. Oxford, Pergamon, 176pp.

Ramsay, J.G. 1967. Folding and fracturing of rocks. New York, McGraw-Hill, 567pp.

Ricketts, B.D. 1990. A preliminary account of sedimentation in the lower Bowser Lake Group, northern British Columbia. *In* Current Research, Part F, Frontier Geoscience Program, Cordilleran and offshore basins, British Columbia. Geological Survey of Canada. Paper 90-1F, 145-150.

Ricketts, B.D., Evenchick C.A. 1991. Analysis of the Middle to Upper Jurassic Bowser Basin, northern British Columbia. *In* Current Research, Part A, Cordillera and Pacific margin. Geological Survey of Canada. Paper 91-1A, 65-73.

Ricketts, B.D., Parrish R.R. 1992. Age and provenance of felsic clasts in Bowser Basin, northern British Columbia. *In* Radiogenic age and isotopic studies. Geological Survey of Canada. Paper 92-02, 141-144.

Ricketts, B.D., Evenchick, C.A., Anderson, R.G. and Murphy, D.C. 1992. Bowser Basin, northern British Columbia; constraints on the timing of initial subsidence and Stikinia-North America terrane interactions. Geology (Boulder), **20**, 1119-1122.

Salvini F., Storti F. 2001. The distribution of deformation in parallel fault-related folds with migrating axial surfaces; comparison between fault-propagation and fault-bend folding. Journal of Structural Geology, **23**, 25-32.

Sibson, R.H. 1996. Structural permeability of fluid-driven fault-fracture meshes. Journal of Structural Geology, **18**, 1031-1042.

Sibson, R.H. 2001. Seismogenic framework for hydrothermal transport and ore deposition. Society of Economic Geologist, Reviews, **14**, 25-50.

Sheriff, E.G., Geldart, L.P. 1995. Exploration Seismology. Cambridge University Press, 592pp.

Stockmal, G.S., Beaumont, C. and Boutilier, R. 1986. Geodynamic models of convergent margin tectonics; transition from rifted margin to overthrust belt and consequences for foreland-basin development. AAPG Bulletin, **70**, 181-190.

Storti, F., Poblet J. 1997. Growth stratal architectures associated to decollement folds and fault-propagation folds; inferences on fold kinematics. *In* Structural controls on sedimentary basin formation. *Edited* by Cloetingh, S., Fernandez, M., Munoz, J.A., Sassi, W. and Horvath F. Tectonophysics, **282**, 353-373.

Tanner, P.W.G. 1989. The flexural slip mechanism. Journal of Structural Geology, **11**, 652-655.

Teyssier, C., Tikoff, B. 1998. Strike-slip partitioned transpression of the San Andreas fault system: a lithospheric-scale approach. *In* Continental Transpressional and Transtensional Tectonics. *Edited by* Holdsworth, R.E., Strachan, R.A., Dewey, J.F. Geological Society of London Special Publication, **135**, 143-158.

Thiessen, R.L., Means, W.D. 1980. Classification of fold interference patterns; a reexamination. Journal of Structural Geology, **2,** 311-316.

Thorbjornsen, K.L, Dunne, W.M. 1997. Origin of a thrust-related fold; geometric vs kinematic tests. Journal of Structural Geology, **19**, 303-319.

Thomson, R.C., Smith, P.L. and Tipper, H.W. 1986. Lower to Middle Jurassic (Pliensbachian to Bajocian) stratigraphy of the northern Spatsizi area, north central British Columbia. Canadian Journal of Earth Science, **23**, 1963-1973.

Thorkelson, D.J., Marsden, H. and Mortensen, J.K. 1991. Early Jurassic volcanism north of the Bowser Basin and its role in paired subduction beneath Stikinia. *In* Geological Society of America, 1991 annual meeting. Abstracts with Programs, 191.

Tipper, H.W., Richards, T.A. 1976. Jurassic stratigraphy and history of north-central British Columbia. Bulletin of the Geological Survey of Canada, **270**, 73.

Twiss, R.J., Moores, E.M. 1992. Structural Geology. Freeman and Company, 532pp.

van der Heyden, P. 1989. U-Pb and K-Ar geochronometry of the Coast Plutonic Complex, 53 °N to 54 °N, British Columbia, and implications for the Insular-Intermontane superterrane boundary. PhD thesis, University of British Columbia.

Walker, R.G. 1992. Turbidites and submarine fans. *In* Facies Models: response to sea-level change. *Edited by* Walker, R.G. and James, N.P. Geological Association of Canada, 239-265.

Wheeler, J.O., McFeely, P. 1991. Tectonic assemblage map of the Canadian Cordillera and adjacent parts of the United States of America. Geological Survey of Canada, Map 1712A, 1:2 000 000.

Yilmaz, O. 1987. Seismic data processing. Society of exploration geophysicists, 526pp.

Zelt, C.A., Smith, R.B. 1992. Seismic traveltime inversion for 2-D crustal velocity structure. Geophysical Journal International, **108**, 16-34.

APPENDIX A:

Complete stereonet data for Study Areas 1, 2 and 3. Subdivided by domains.

TABLE OF CONTENTS: APPENDIX A

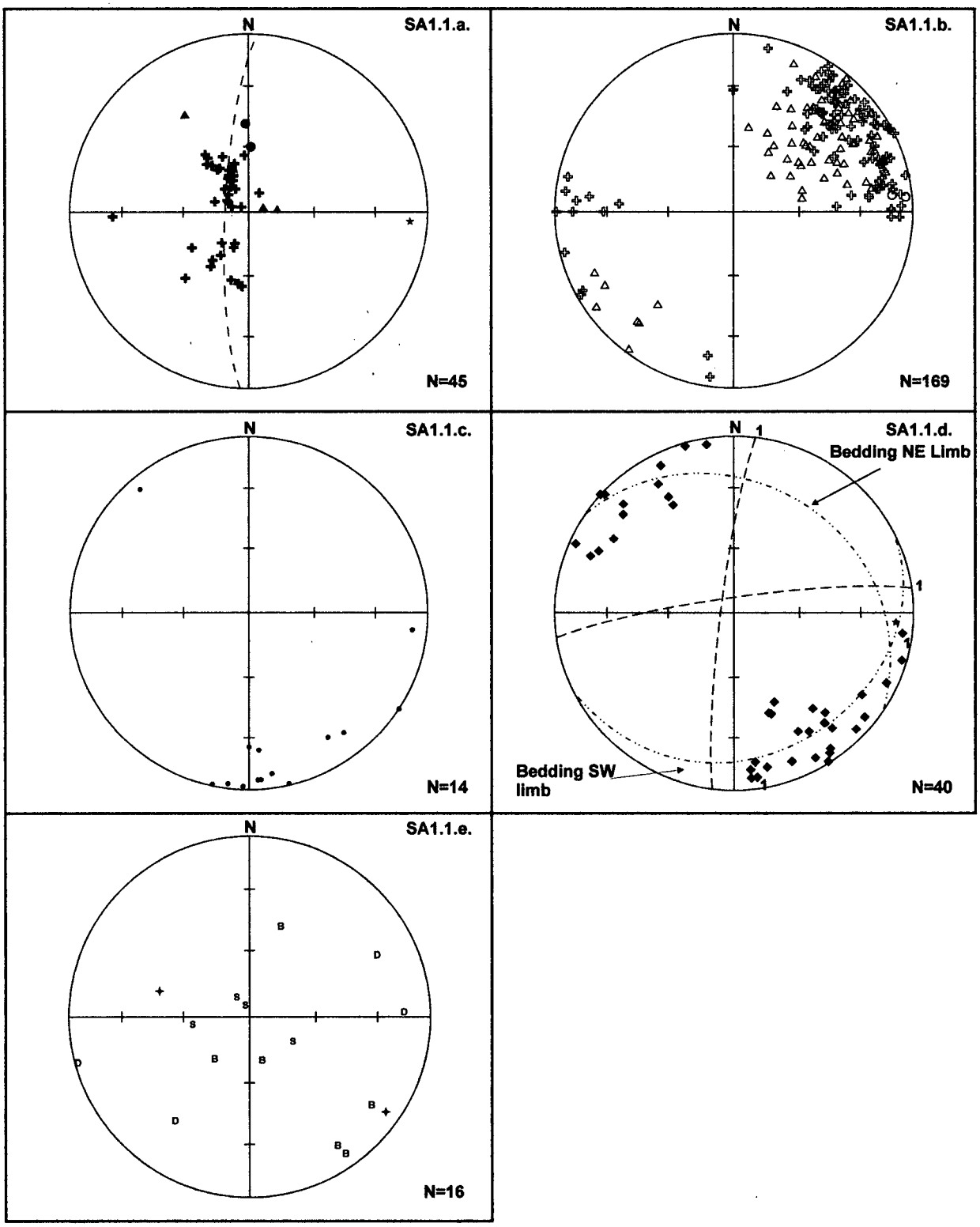

Study Area 1, Domain 1. a) Bedding, b) cleavage, c) bedding-cleavage intersection lineations, d) fracture, e) faults and veins.

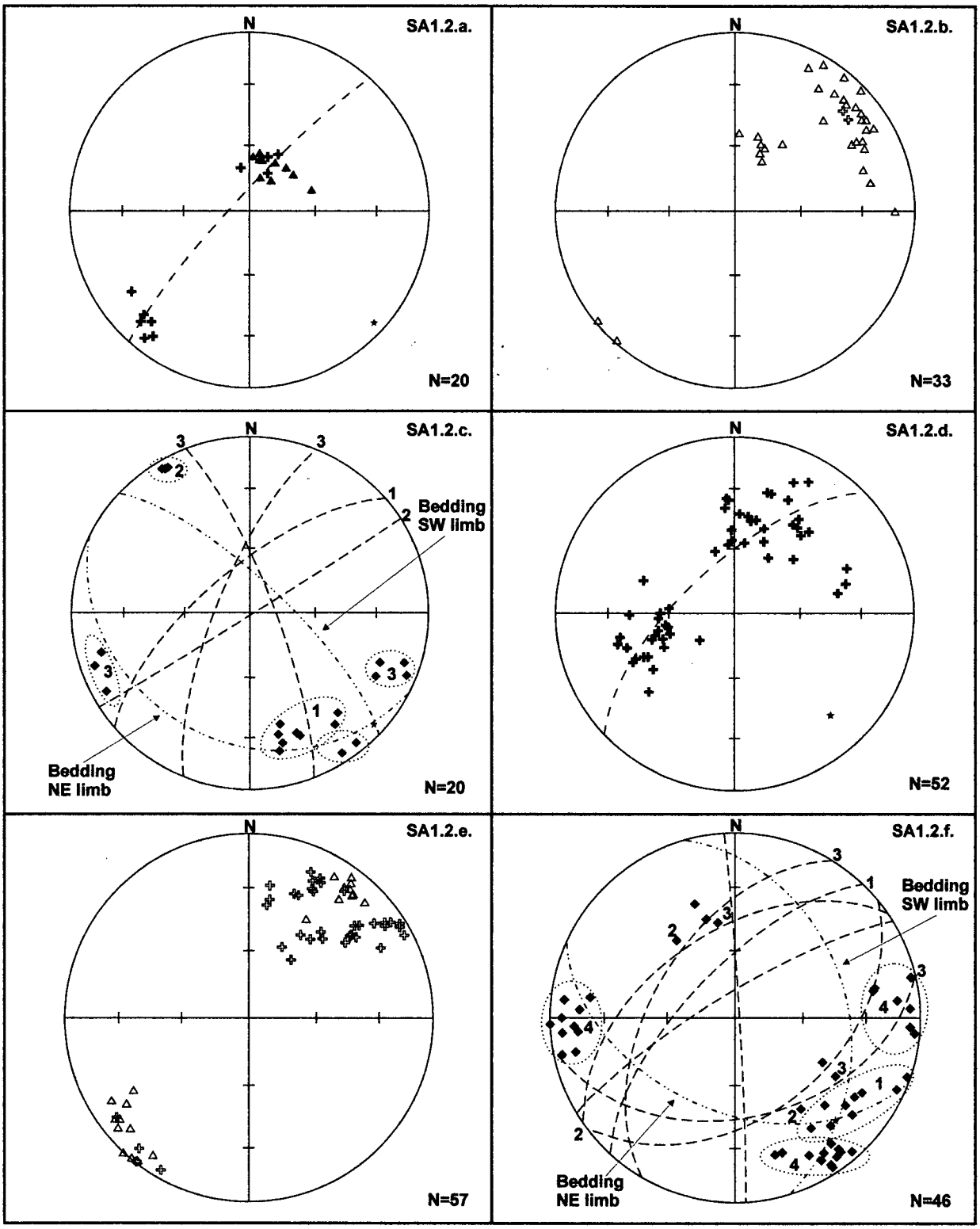

Study Area 1, Domain 2. a-c) Data for northwest-trending syncline in northwest of domain, a) bedding, b) cleavage, c) fractures. d-e) Data for northwest-trending syncline in centre of domain, d) bedding, e) cleavage, f) fractures.

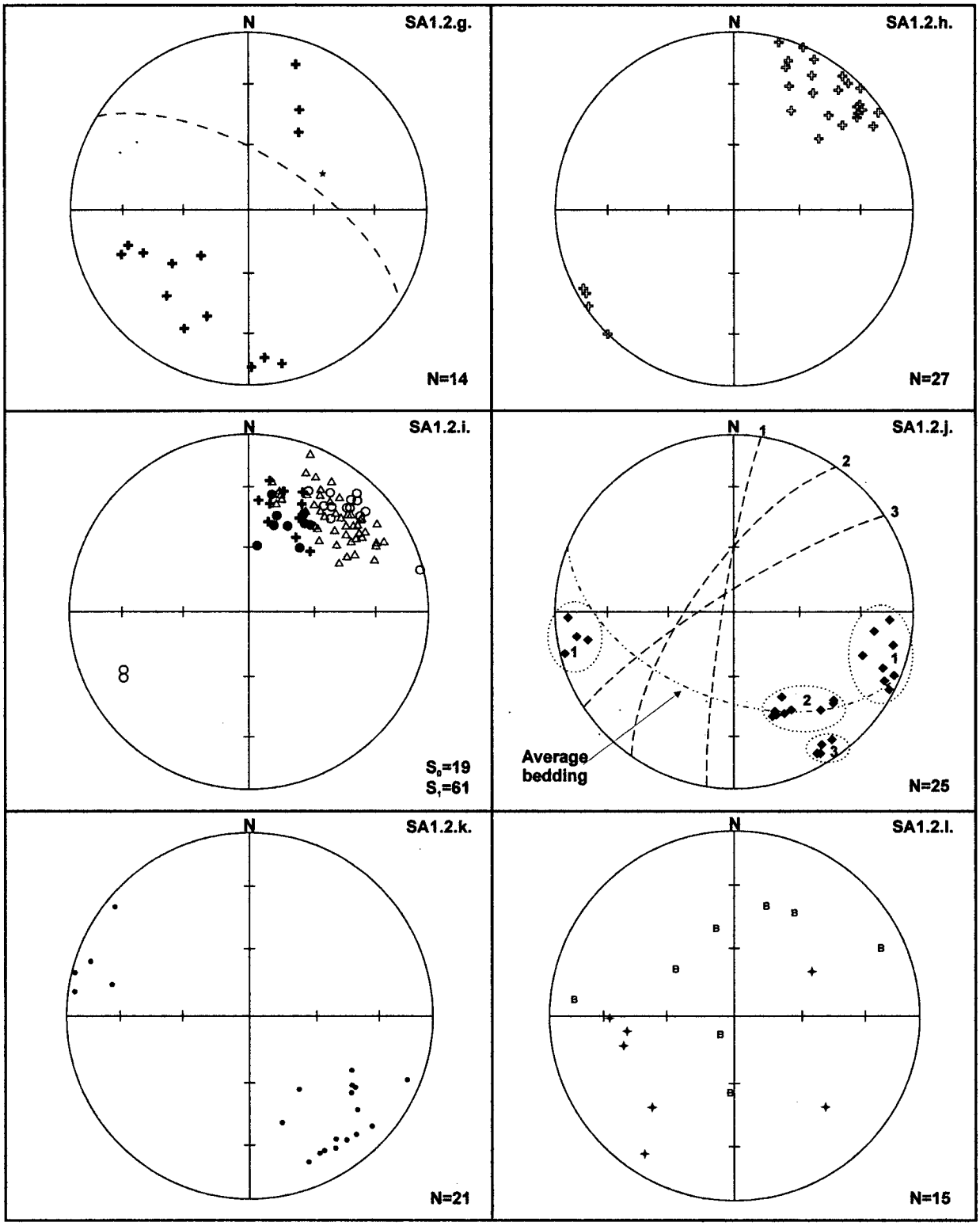

Study Area 1, Domain 2. g-h) Northeast-trending syncline in south-centre of domain, g) bedding, h) cleavage. i-j) Data from east of domain, i) bedding and cleavage, j) fractures. k) Bedding-cleavage intersection lineations for the whole of the domain. l) Fault data for the whole of the domain.

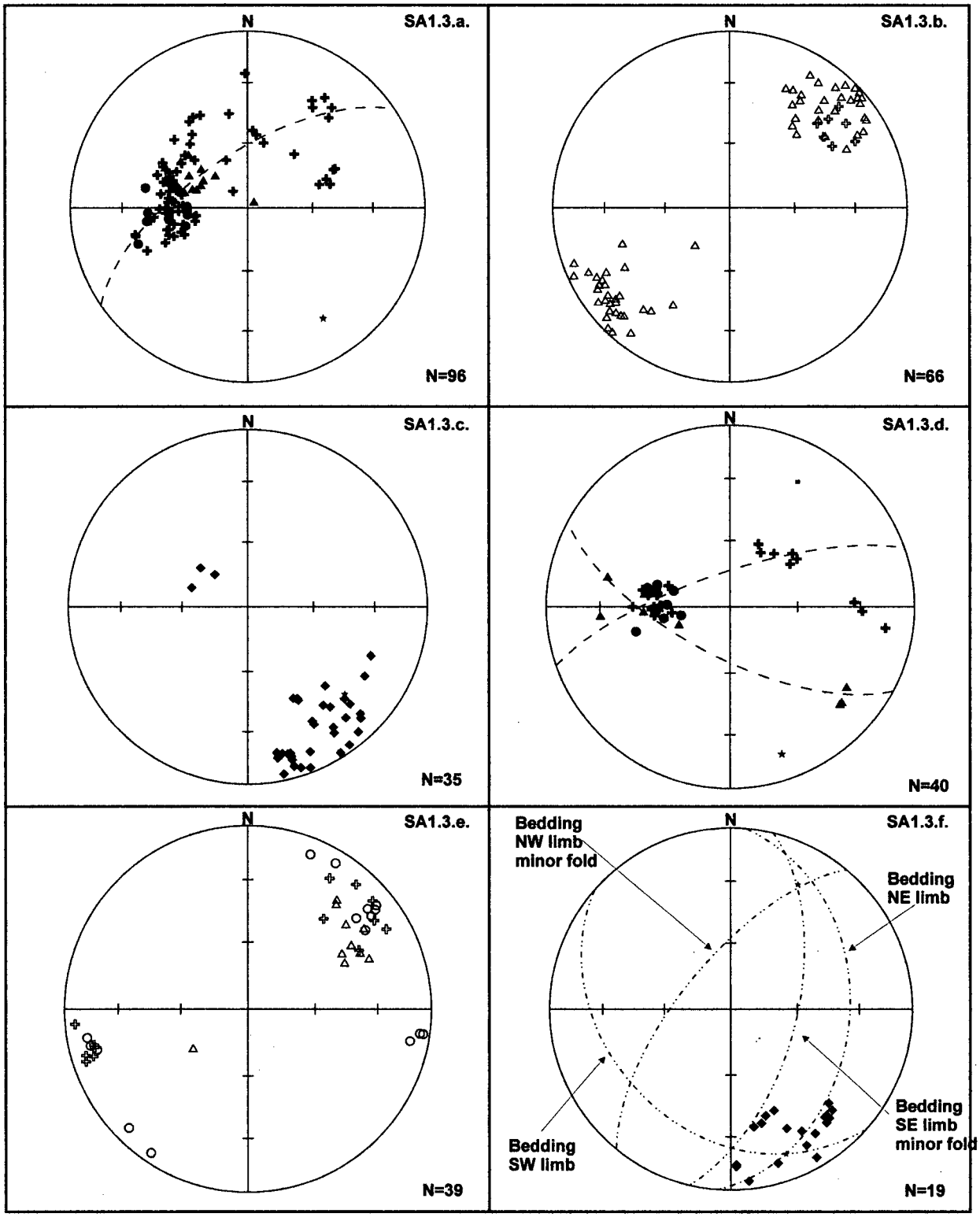

Study Area 1, Domain 3. a-c) Northwest-trending syncline from east-centre of domain, a) bedding, b) cleavage, c) fractures. d-e) Northwest-trending anticline from extreme east of domain, with minor northeast-trending anticline, d) bedding, e) cleavage, f) fractures.

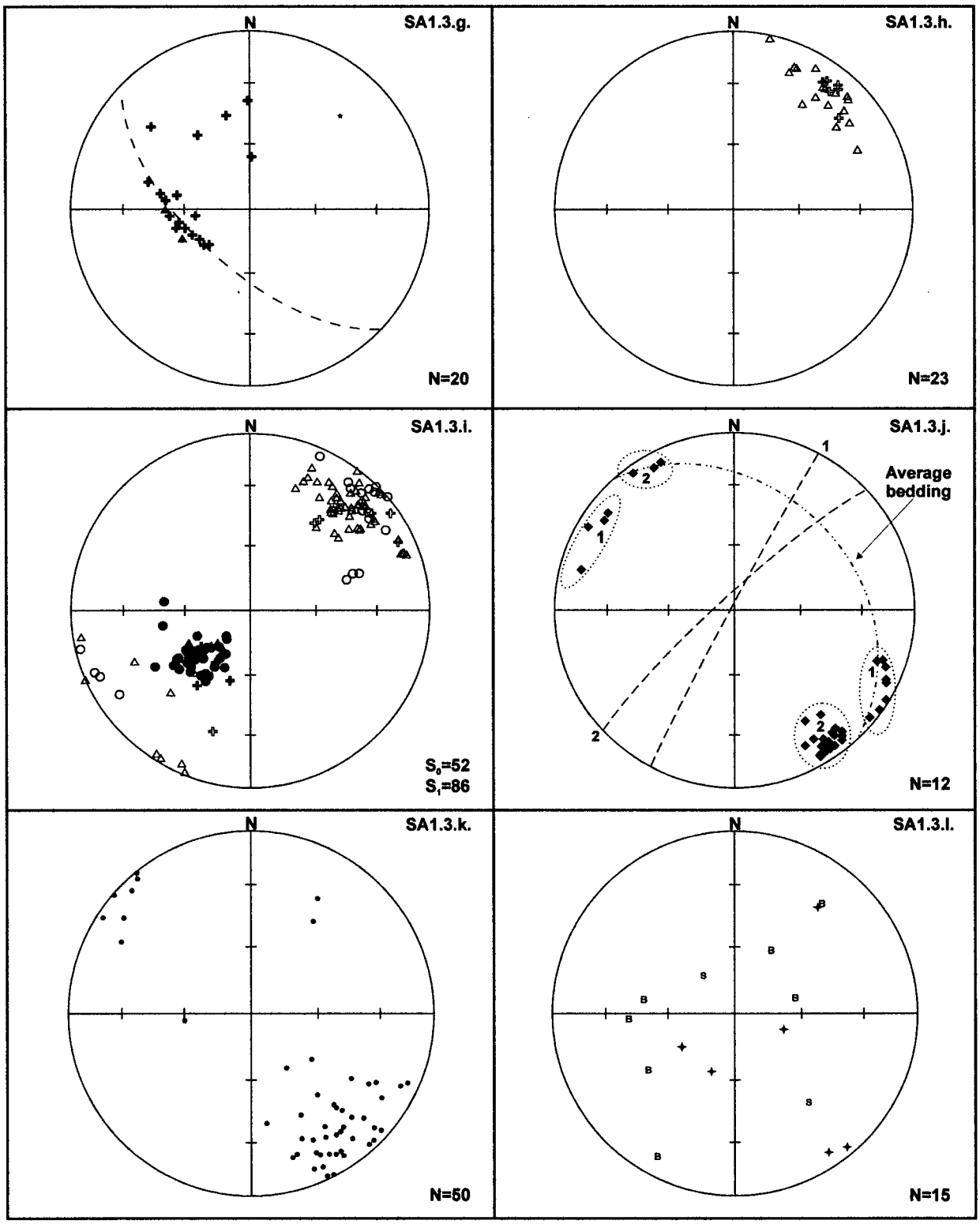

Study Area 1, Domain 3. g-h) Northeast-trending syncline from west-centre of domain, g) bedding, h) cleavage. i-j) Data from the extreme west of the domain, i) bedding and cleavage data, j) fracture data. k) Bedding-cleavage intersection lineations for the domain. l) Fault data for the domain.

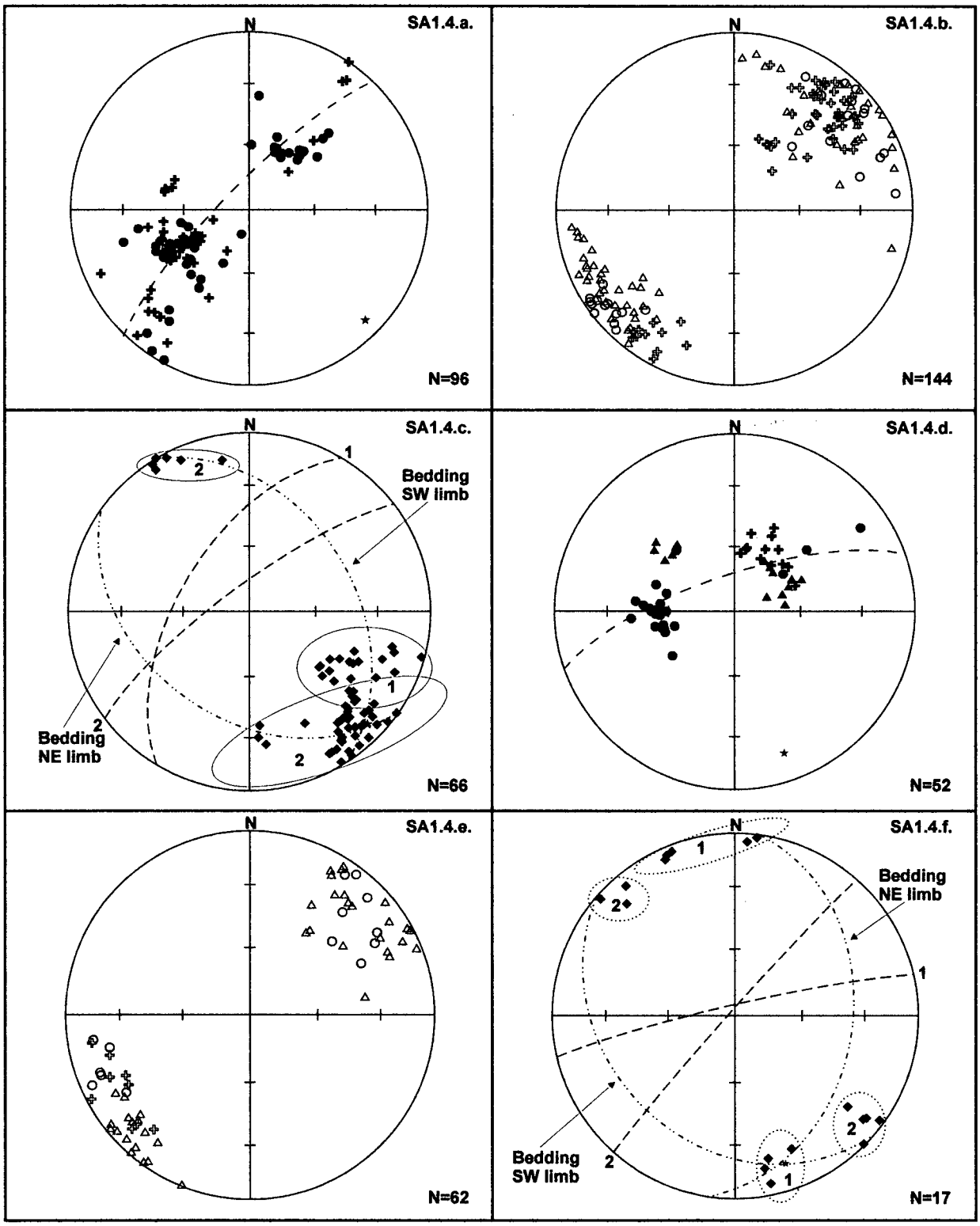

Study Area 1, Domain 4. a-c) Northwest-trending syncline in west of domain, a) bedding, b) cleavage, c) fractures. d-f) Northwest-trending anticline in east of domain, d) bedding, e) cleavage, f) fractures.

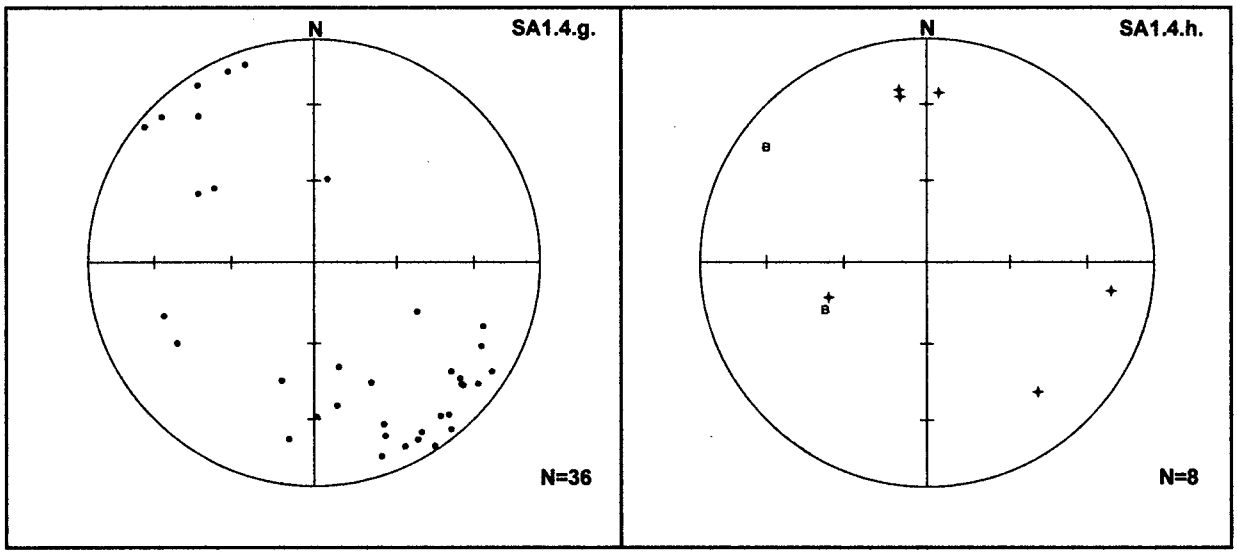

Study Area 1, Domain 4. g) Bedding-cleavage intersection lineations for domain, h) fault and vein data for domain.

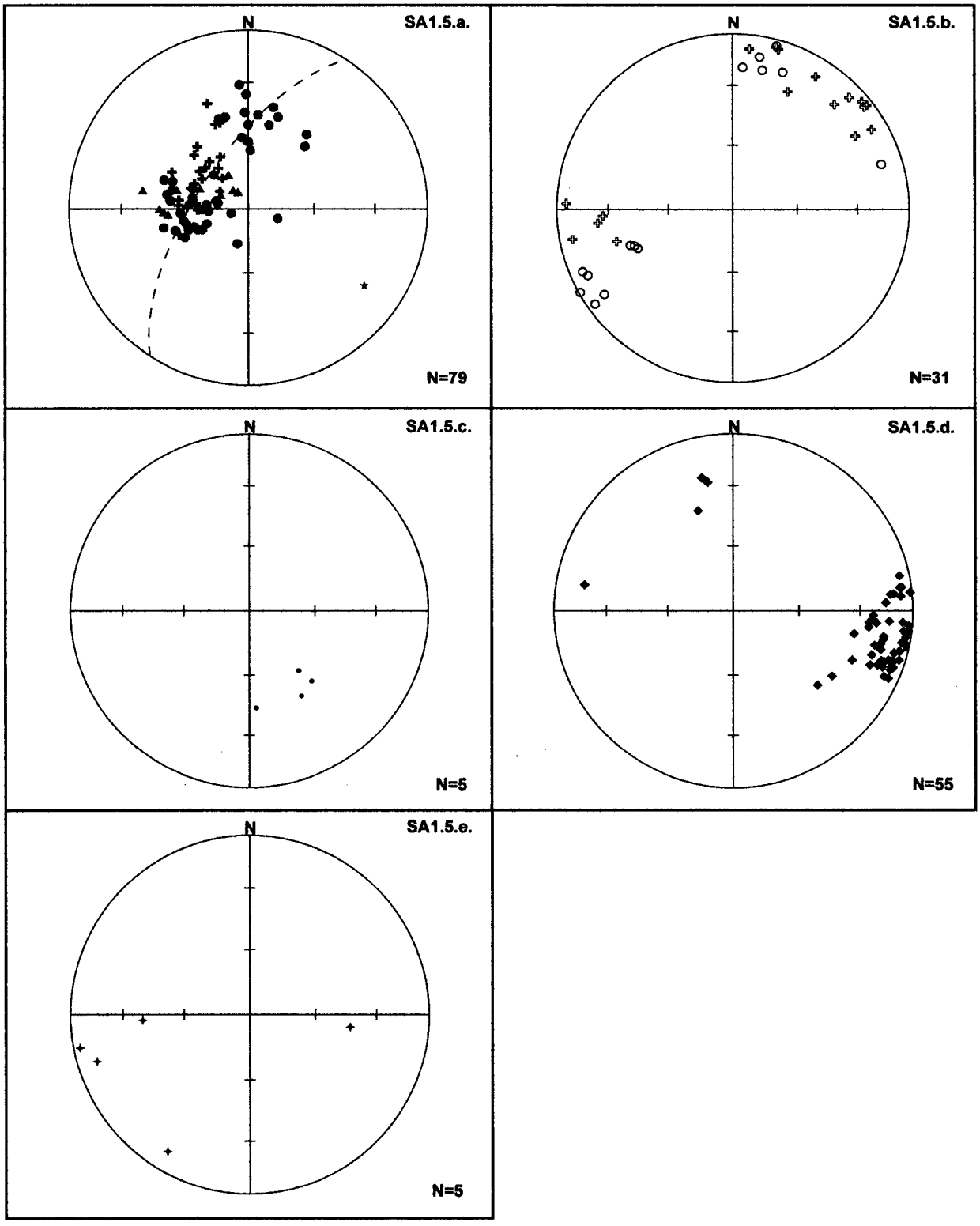

Study Area 1, Domain 5. a) Bedding, b) cleavage, c) bedding-cleavage intersection lineations, d) fractures, e) faults and veins.

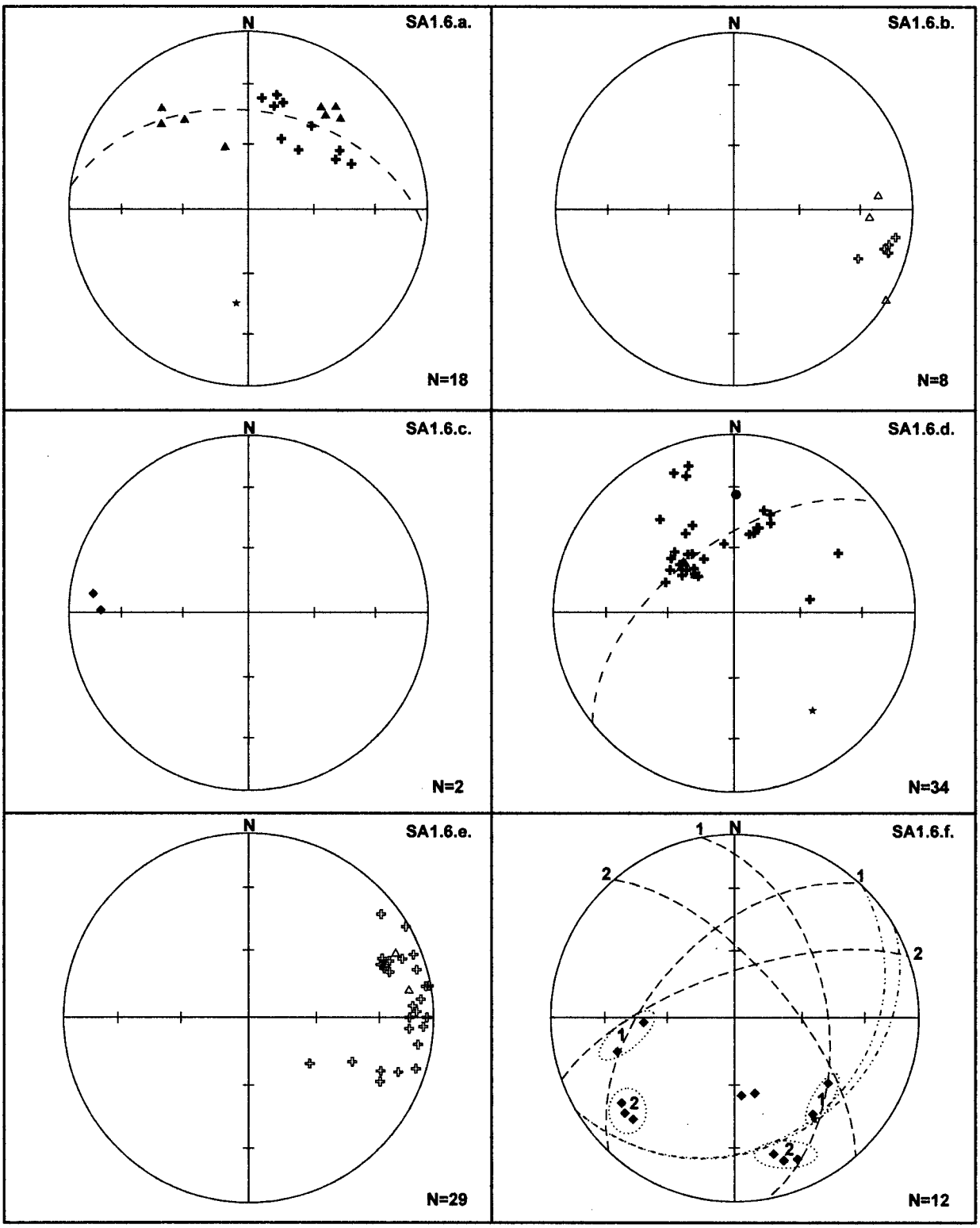

Study Area 1, Domain 6. a-c) Northeast-trending folds from southwest of domain, a) bedding, b) cleavage, c) fractures. d-f) Northwest-trending fold from centre of domain, d) bedding, e) cleavage, f) fractures.

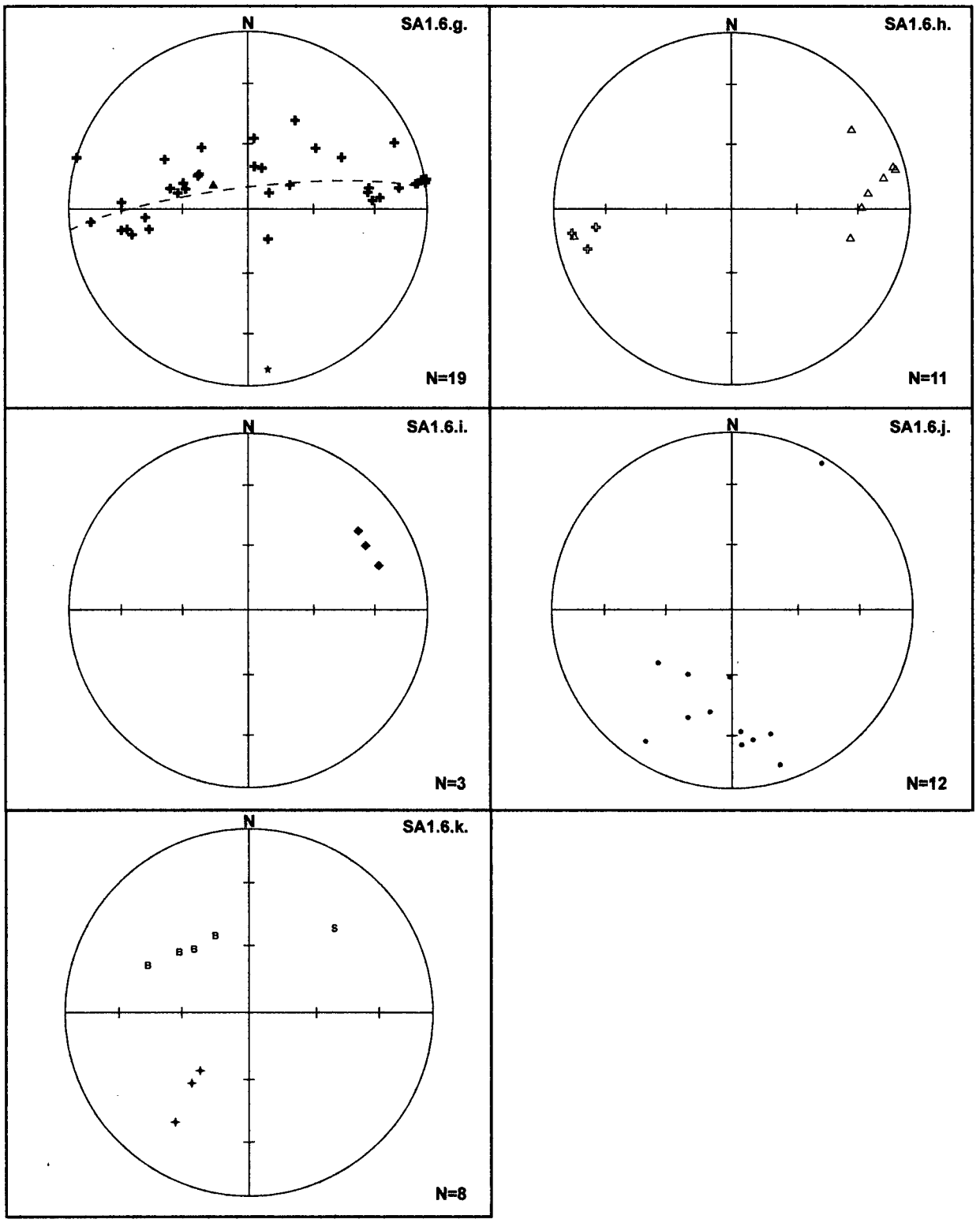

Study Area 1, Domain 6. g-i) North-trending fold in north of domain, g) bedding, h) cleavage, i) fractures. j) Bedding-cleavage intersection lineations for domain. k) Fault data for domain.

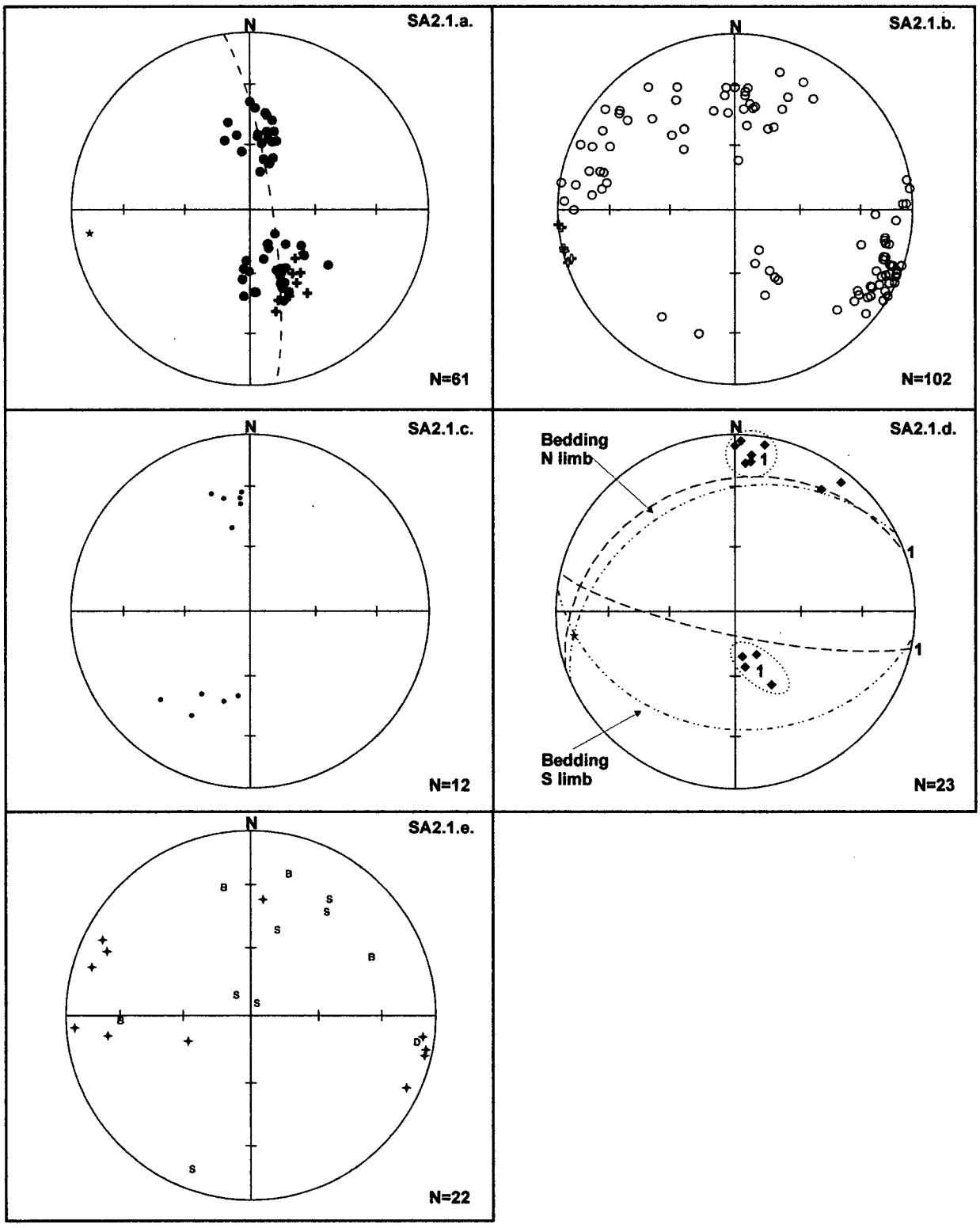

Study Area 2, Domain 1. a) Bedding, b) cleavage, c) bedding-cleavage intersection lineations, d) fractures, e) faults and veins.

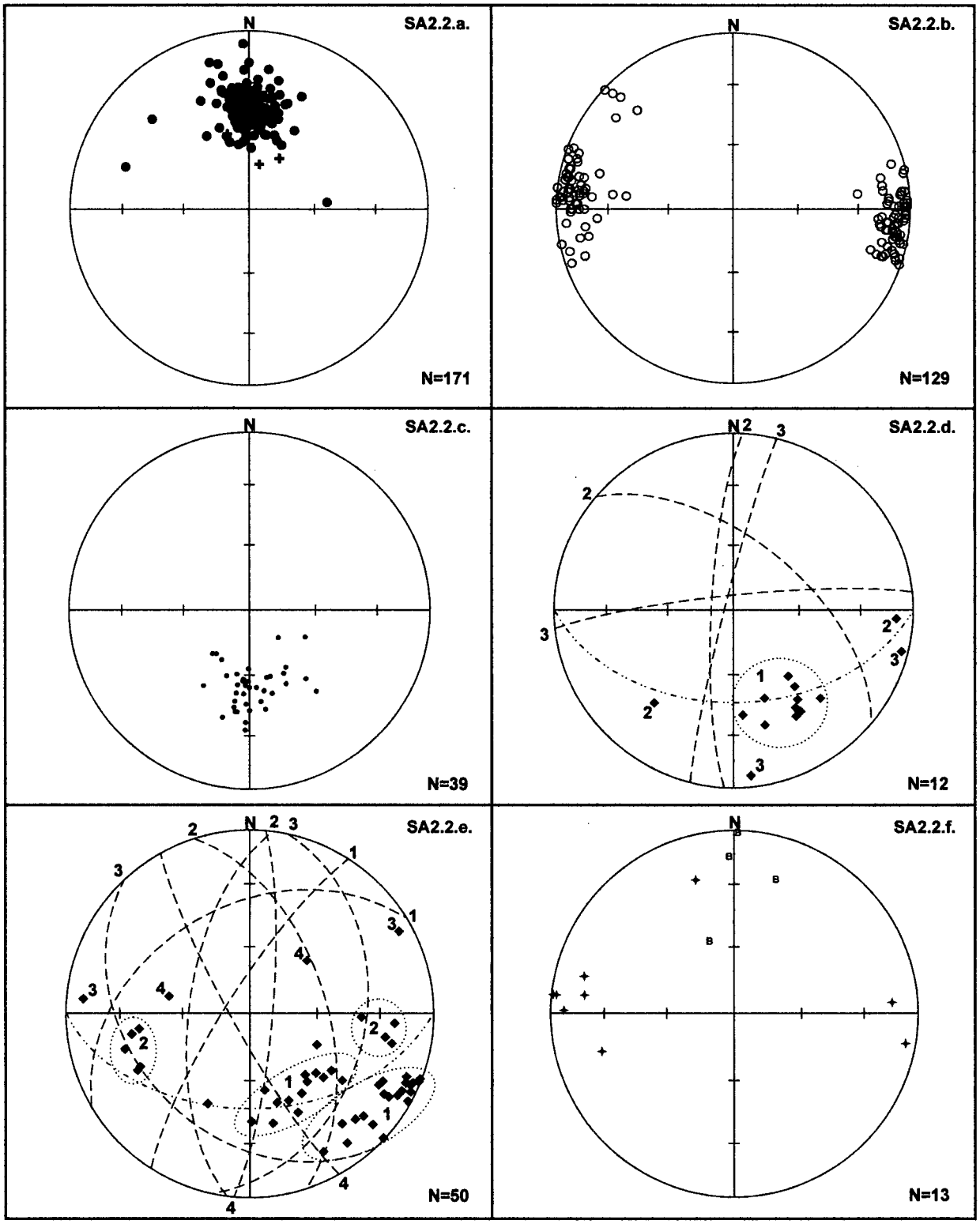

Study Area 2, Domain 2. a) Bedding, b) cleavage, c) bedding-cleavage intersection lineations, d) fracture data from the western third of the domain, e) fracture data from the eastern two thirds of the domain, f) faults and veins.

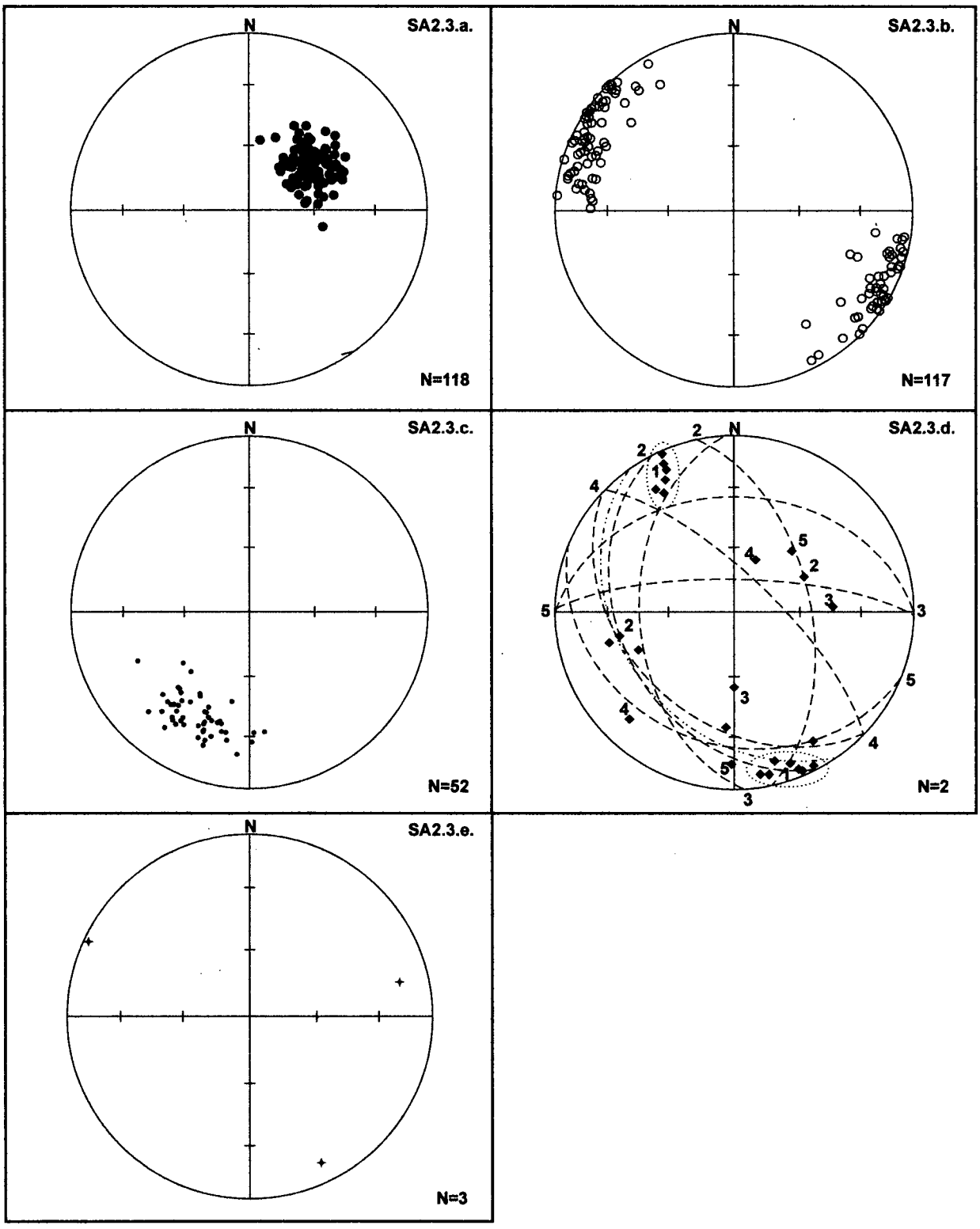

Study Area 2, Domain 3. a-e) Data from northwest corner of domain, a) bedding, b) cleavage, c) bedding-cleavage intersection lineations, d) fractures, e) faults and veins.

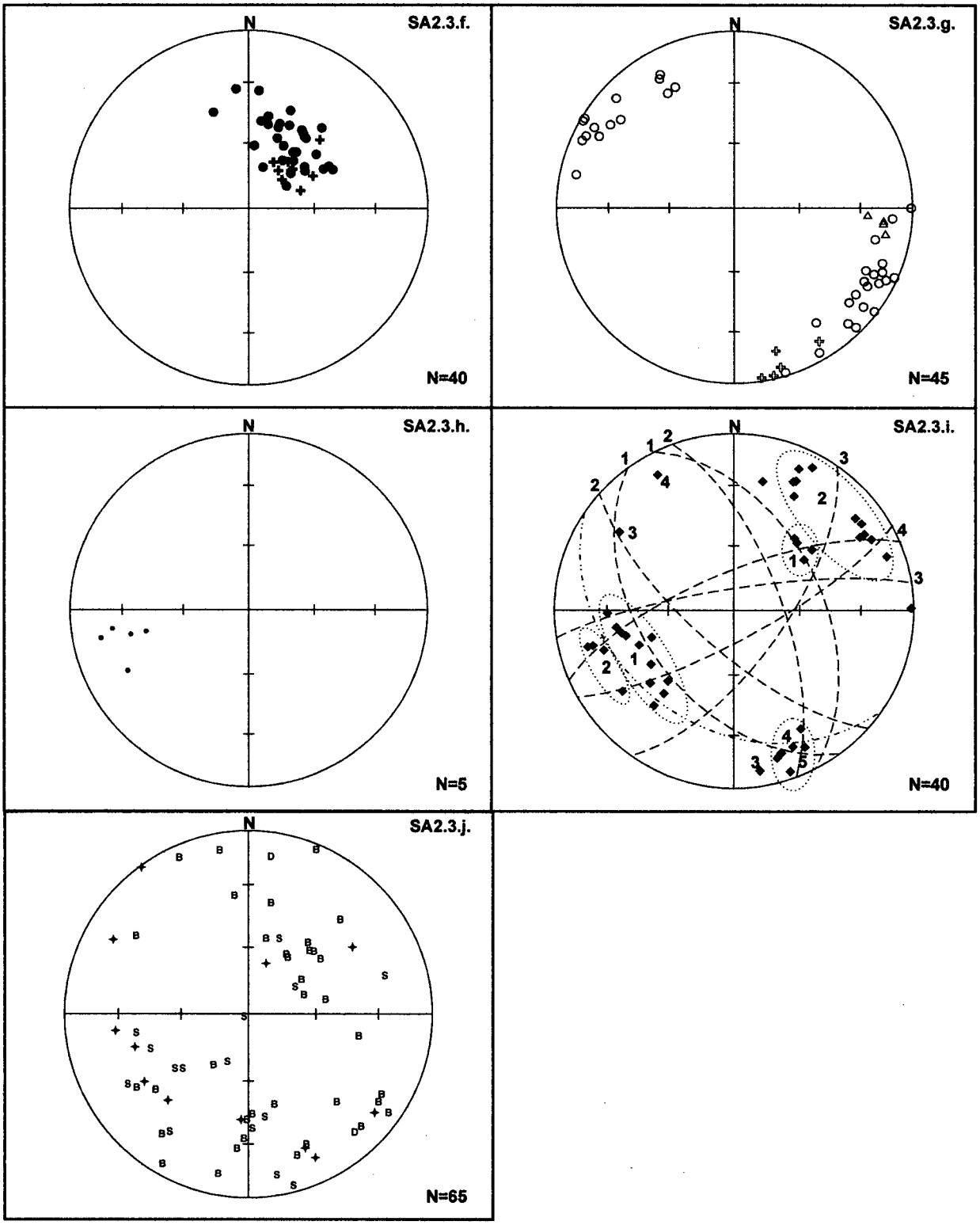

Study Area 2, Domain 3. f-j) Data from north-central area of domain, f) bedding, g) cleavage, h) bedding-cleavage intersection lineations, i) fractures, j) faults and veins.

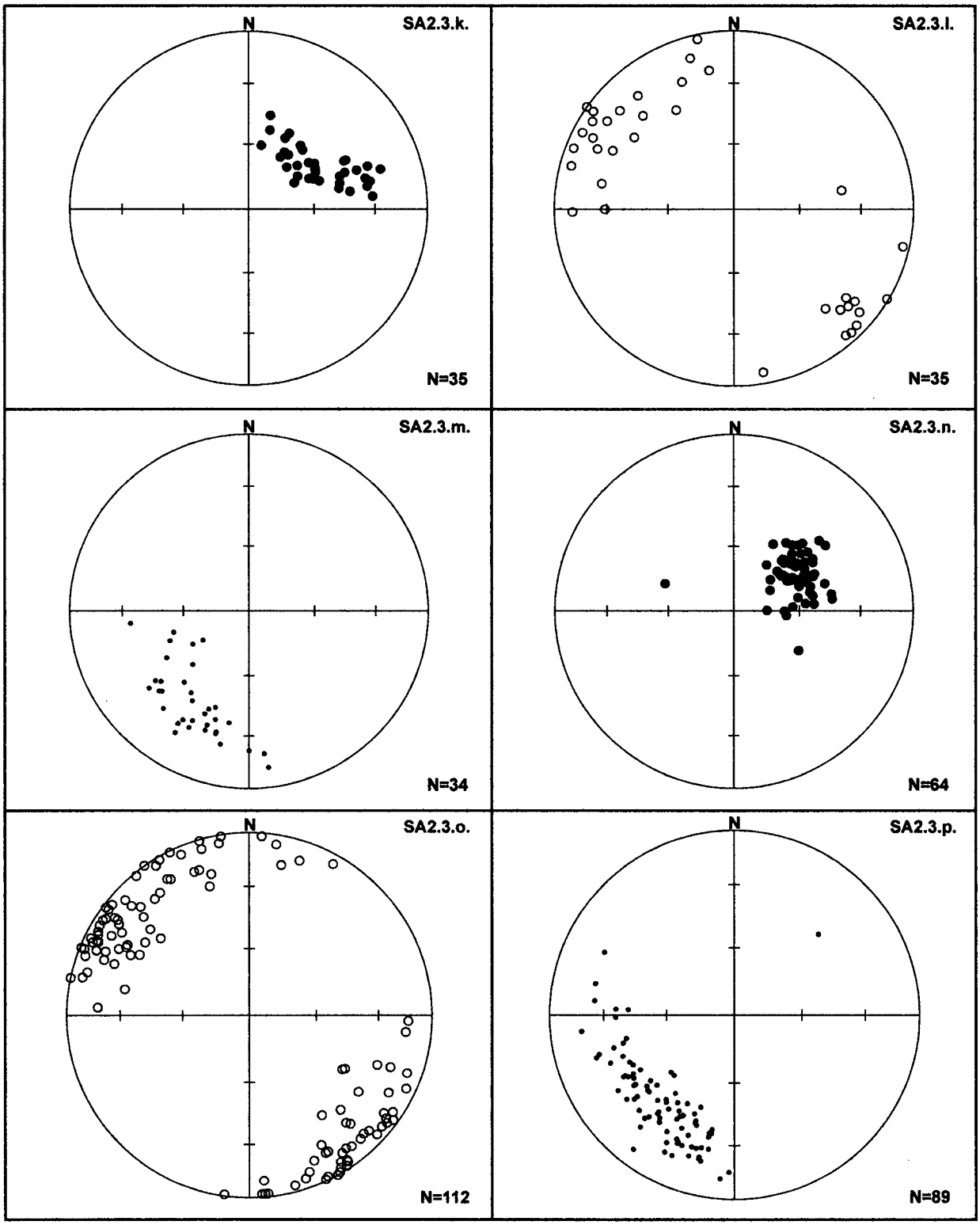

Study Area 2, Domain 3. k-m) Data from central part of domain, k) bedding, l) cleavage, m) bedding -cleavage intersection lineations. n-p) Data from southern part of domain, n) bedding, o) cleavage p) bedding-cleavage intersection lineations.

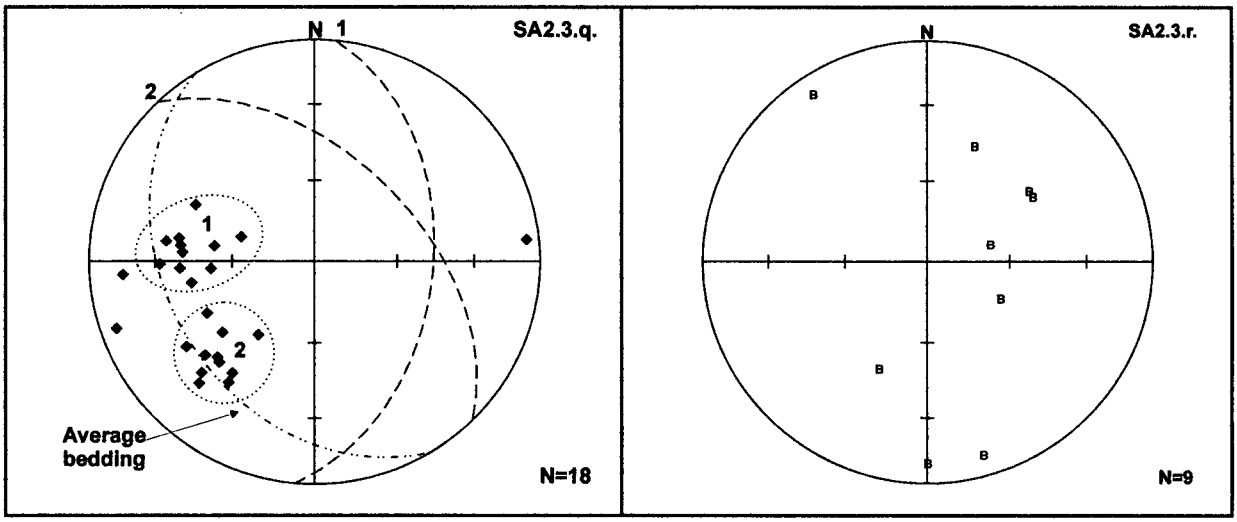

Study Area 2, Domain 3. q) Fracture data from the southern half of the domain, r) fault data from the southern half of the domain.

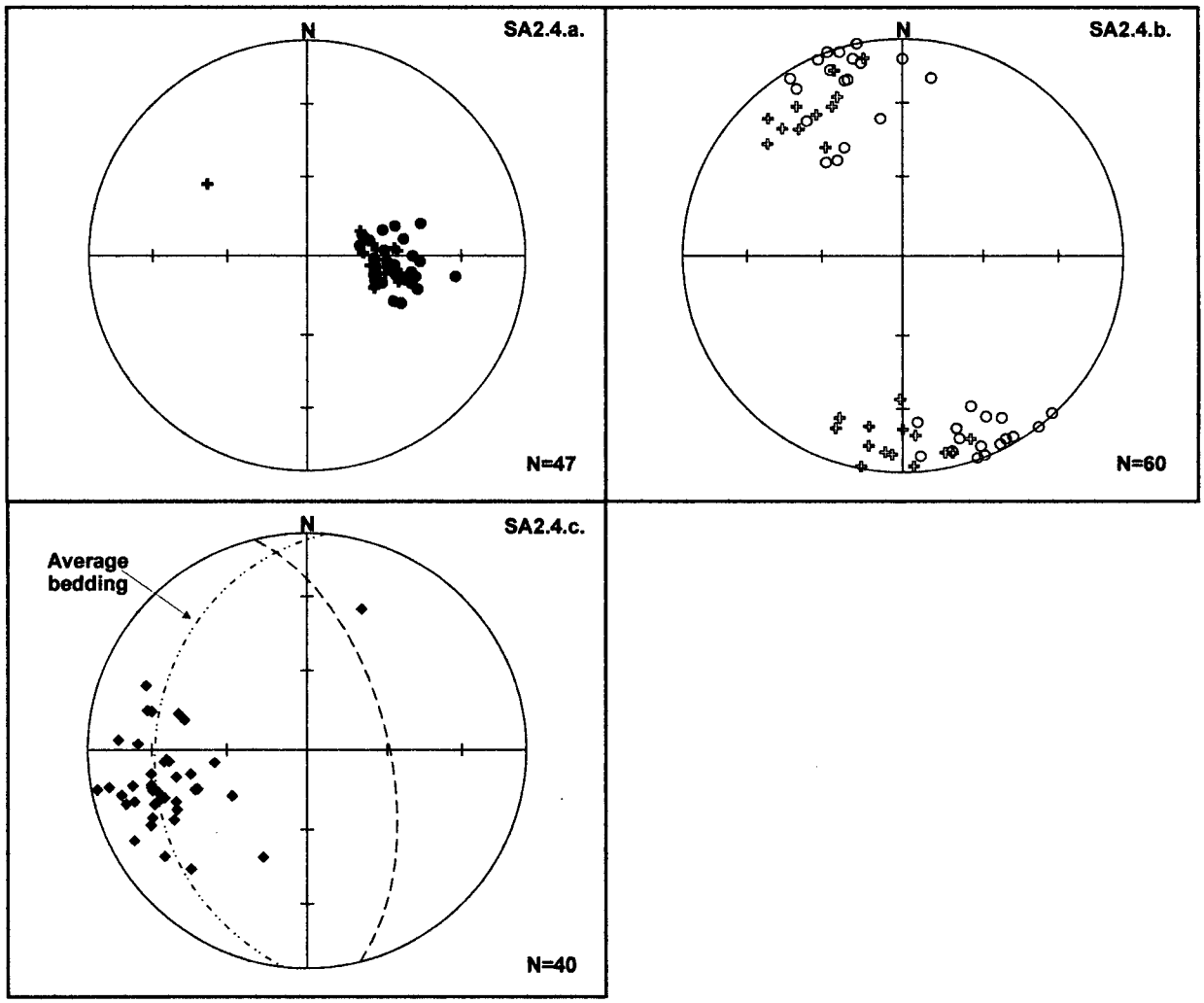

Study Area 2, Domain 4. a) bedding, b) cleavage, c) fractures.

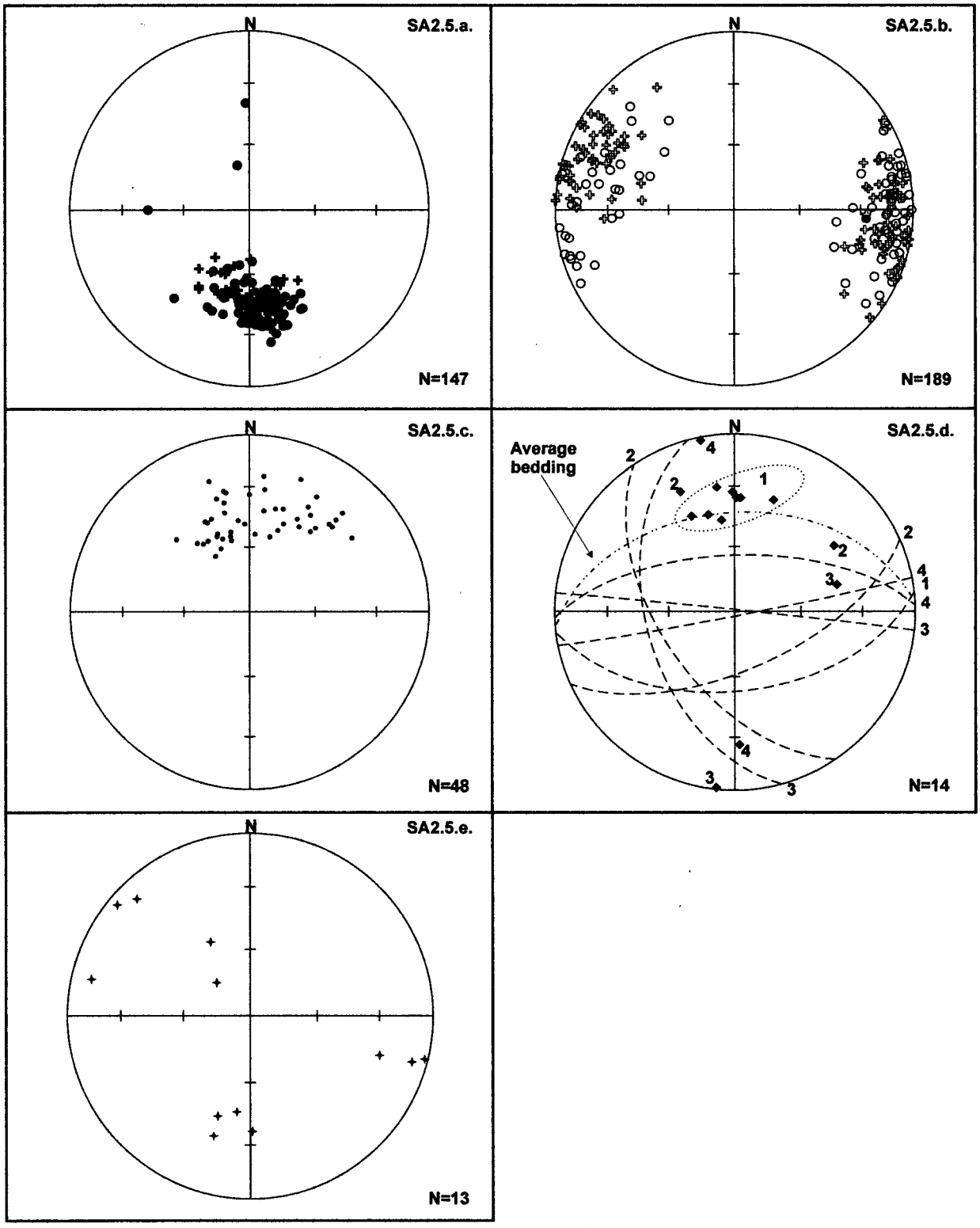

Study Area 2, Domain 5. a) Bedding, b) cleavage, c) bedding-cleavage intersection lineations, d) fractures, e) faults and veins.

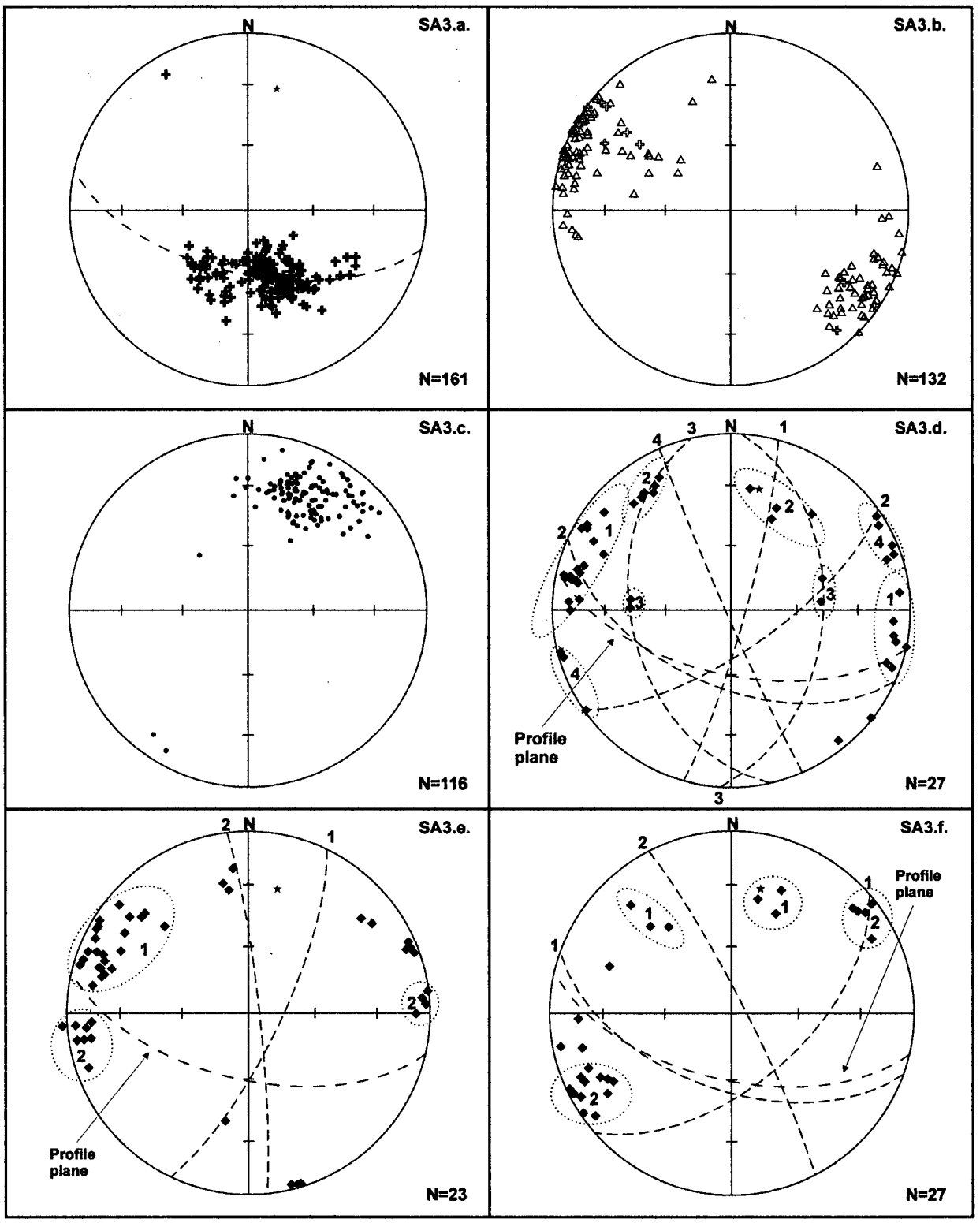

Study Area 3. a) Bedding, b) cleavage, c) bedding-cleavage intersection lineations, d) fractures located in the northwest of the study area, e) fractures located in the northeast of the study area, f) fractures located in the southeast of the domain.

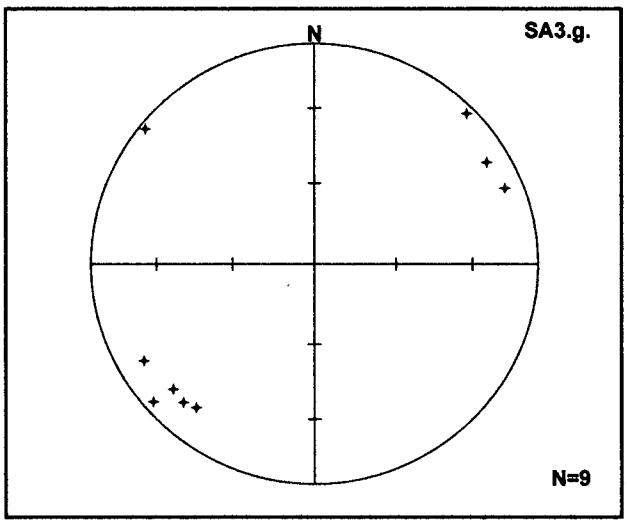

Study Area 3. g) Faults and veins.